PHASE 2 INITIAL BOREHOLE DRILLING AND TESTING, IGNACE AREA

WP04b Data Report - Geomechanical Testing of Core for IG_BH01

APM-REP-01332-0232 **June 2022**

Golder Associates Ltd.

nwmo
NUCLEAR WASTE MANAGEMENT ORGANIZATION
SOCIÉTÉ DE GESTION DES DÉCHETS NUCLÉAIRES

Nuclear Waste Management Organization
22 St. Clair Avenue East, 4th Floor
Toronto, Ontario
M4T 2S3
Canada

Tel: 416-934-9814
Web: www.nwmo.ca

GOLDER
MEMBER OF WSP

REPORT

PHASE 2 INITIAL BOREHOLE DRILLING AND TESTING, IGNACE AREA

WP4b Data Report - Geomechanical Testing of Core for IG_BH01

Submitted to:

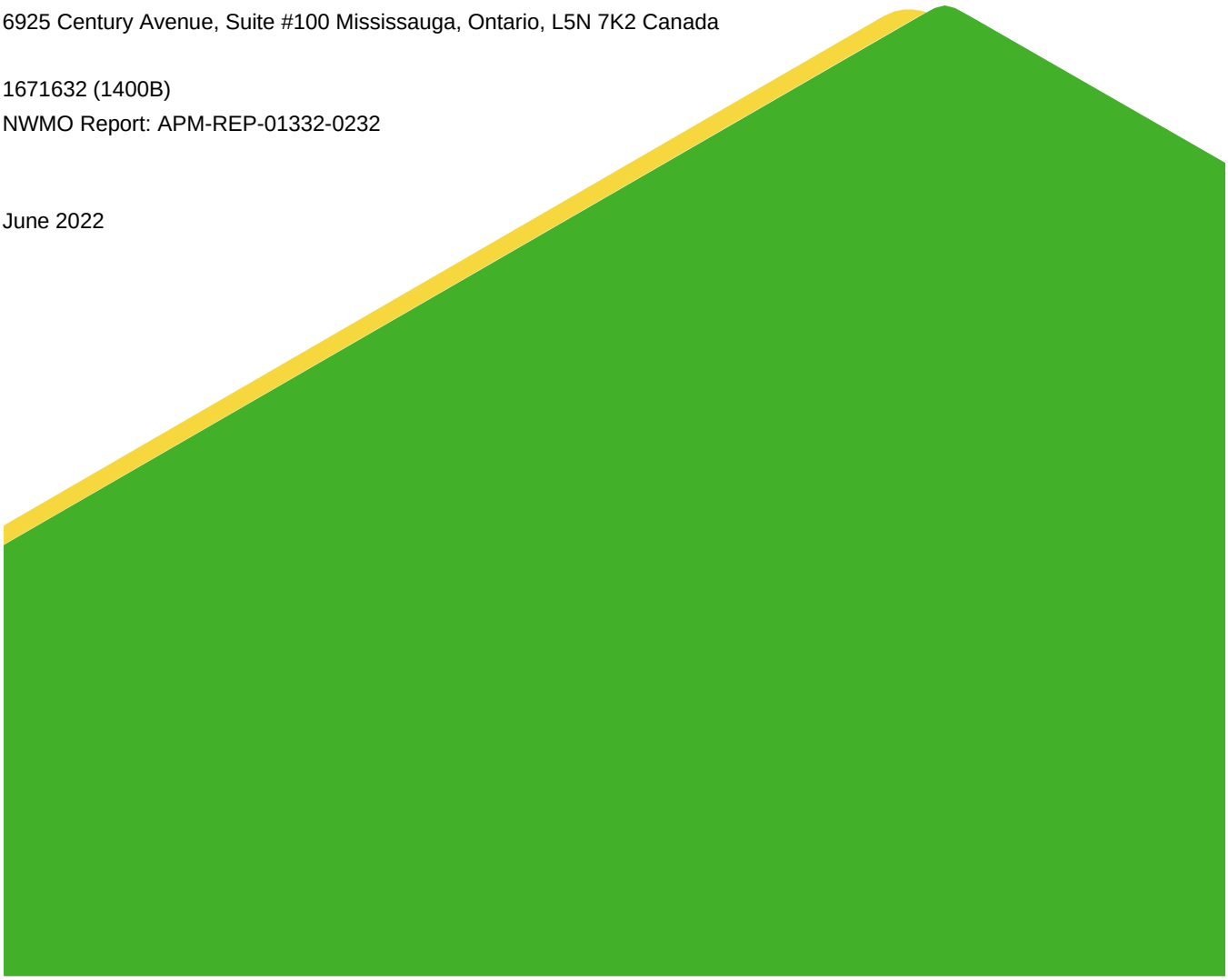
Nuclear Waste Management Organization
4th Floor
22 St. Clair Avenue East
Toronto, Ontario, M4T 2S3

Submitted by:

Golder Associates Ltd.
6925 Century Avenue, Suite #100 Mississauga, Ontario, L5N 7K2 Canada

1671632 (1400B)
NWMO Report: APM-REP-01332-0232

June 2022



Distribution List

NWMO - 1 eCopy

Golder Associates Ltd. - 1 eCopy

WP4B DATA REPORT
GEOMECHANICAL TESTING OF CORE FOR IG_BH01

CLIENT INFORMATION

Project Name: Phase 2 Initial Borehole Drilling and Testing, Ignace Area

Project Number: 1671632

Client PO Number: 2000141 (Formerly 01559 A-TGS)

Document Name: 1671632 (1400B) IG_BH01_WP4B_Report_22Jun2022_r5a_Clean.docx

Client: Nuclear Waste Management Organization (NWMO)
22 St. Clair Avenue East, Fourth Floor
Toronto, Ontario
M4T 2S3

Client Contact: Hossein Kasani and Maria Sánchez-Rico Castejón

Email: hkasani@nwmo.ca and msanchez@nwmo.ca

ISSUE/REVISION INDEX

Issue Code	Revision					Revision Details
	No.	By	Rev'd.	App.	Date	
RR	0	JLC	GWS	GWS	May 14, 2018	Draft released for review and comment
RR	1	JLC	GWS	GWS	July 9, 2018	Final Draft released for review and comment
RR	2	JLC	GWS	GWS	August 1, 2018	Final Draft released for review and comment
RR	3a	JLC	GWS	GWS	October 4, 2018	Final Draft released for review and comment
RR	3b	JLC	GWS	GWS	October 19, 2018	Final Draft released for review and comment
RI	3c	JLC	GWS	GWS	October 25, 2018	Final Report released for Information
RR	4a	JLC	DD	GWS	April 12, 2022	Revised Final Draft released for review and comment – Additional Test Results
RI	5a	JLC	DD	GWS	June 22, 2022	Revised Final released for Information – Additional Test Results

Issue Codes: RR = Released for Review and Comments, RI = Released for Information

SIGNATURES

Prepared by:

Joe Carvalho, Ph.D., P.Eng.
Mining & Rock Engineering - Principal

Reviewed by:

David Dixon, Ph.D., P.Geo.
Senior Geoscientist

Approved by:

George Schneider, M.Sc., P.Geo.
Senior Geoscientist - Principal

Table of Contents

1.0 INTRODUCTION 1

2.0 BACKGROUND INFORMATION 1

2.1 Geological Setting 1

2.2 Technical Objectives 5

2.3 Description of Testing Procedures 6

2.4 Test Apparatus and Procedures 8

2.4.1 Sample Preparation 8

2.4.2 Uniaxial Compressive Strength (UCS) Tests 8

2.4.2.1 Acoustic Emissions (AE) Data Acquisition 8

2.4.3 Indirect Tensile Strength (Brazilian) Tests 8

2.4.4 Water Content and Density Measurements 9

2.4.5 Thermal Conductivity, Volumetric Heat Capacity and Thermal Diffusivity 9

2.4.6 Thermal Expansion 10

2.5 Analysis of Data 11

2.5.1 Zero Pressure P-S Wave Velocity Tests 11

2.5.2 Uniaxial Compressive Strength (UCS) Tests 12

2.5.3 Acoustic Emissions Data 13

2.5.4 Indirect Tensile (Brazilian) Strength Tests 15

2.5.5 Thermal Conductivity, Volumetric Heat Capacity and Thermal Diffusivity 15

2.5.6 Thermal Expansion 16

3.0 LABORATORY RESULTS 17

3.1 Dimensions and Physical Properties of Specimens 17

3.2 Laboratory Testing Results 24

3.2.1 Geomechanical Results 24

3.2.2 Thermal Results 27

4.0 DATA QUALITY 54

4.1 Uncertainties and Limitations 54

5.0 REFERENCES 56

TABLES

Table 1: Target Temperature Schedule for Hot Disk Tests 10

Table 2: Target Temperature Schedule for Thermal Expansion Tests 11

Table 3: Dimensions and Physical Properties of Lab Specimens 18

Table 4: Average strength properties and elastic moduli for Biotite Granodiorite-Tonalite 24

Table 5: Strength and Strain properties determined from UCS tests 25

Table 6: Dynamic properties determined from UCS samples 26

Table 7: Tensile strength determined from Brazilian tests 27

Table 8: Thermal properties determined from the Hot Disk ThermTest TPS 1500 27

Table 9: Summary of equations describing thermal properties Cv, k and κ as a function of temperature for the range ~20°C to 90°C or 100°C 48

Table 10: Coefficient of linear thermal expansion determined from the first and second heating cycles and as a function of temperature (from quadratic fit) for the first heating cycle 49

Table 11: Summary of the coefficient of linear thermal expansion, α, average (from linear regression) and as a function of temperature (from quadratic fit) for the range ~20°C to 90°C 53

FIGURES

Figure 1: Location of IG_BH02 in Relation to the Wabigoon / Ignace Area 3

Figure 2: Geological setting and location of boreholes IG_BH01, IG_BH02 and IG_BH03 in the northern portion of the Revell batholith 4

Figure 3: Cumulative energy (volt·sec) vs axial stress measured during UCS testing of sample IG_BH01_UC001, IG_BH01_UC003 and IG_BH01_UC005. Note that C_i in this figure is the same as σCI discussed in section 2.5.2 in the text. 14

Figure 4: Cumulative energy (in kilovolt.sec) versus axial stress (MPa) measured during UCS testing of sample IG_BH01-UC002 in a log-log scale 15

Figure 5: Schematic of the thermal expansion apparatus and components of the displacement correction. 16

Figure 6: Volumetric heat capacity for saturated samples of Biotite Granodiorite-Tonalite as a function of temperature. 32

Figure 7: Volumetric heat capacity for dry samples of Biotite Granodiorite-Tonalite as a function of temperature. 32

Figure 8: Thermal conductivity for saturated samples of Biotite Granodiorite-Tonalite as a function of temperature 33

Figure 9: Thermal conductivity for dry samples of Biotite Granodiorite-Tonalite as a function of temperature 33

Figure 10: Thermal diffusivity for saturated samples of Biotite Granodiorite-Tonalite as a function of temperature 34
Figure 11: Thermal diffusivity for dry samples of Biotite Granodiorite-Tonalite as a function of temperature 34
Figure 12: Volumetric heat capacity for saturated samples of Biotite Tonalite as a function of temperature. 35
Figure 13: Thermal conductivity for saturated samples of Biotite Tonalite as a function of temperature 36
Figure 14: Thermal diffusivity for saturated samples of Biotite Tonalite as a function of temperature 36
Figure 15: Volumetric heat capacity for saturated sample of Amphibolite as a function of temperature 37
Figure 16: Volumetric heat capacity for dry sample of Amphibolite as a function of temperature 38
Figure 17: Thermal conductivity for saturated sample of Amphibolite as a function of temperature 38
Figure 18: Thermal conductivity for dry sample of Amphibolite as a function of temperature 39
Figure 19: Thermal diffusivity for saturated sample of Amphibolite as a function of temperature 39
Figure 20: Thermal diffusivity for dry sample of Amphibolite as a function of temperature 40
Figure 21: Volumetric heat capacity for saturated sample of Aplite Dyke as a function of temperature 41
Figure 22: Volumetric heat capacity for dry sample of Aplite Dyke as a function of temperature 41
Figure 23: Thermal conductivity for saturated sample of Aplite Dyke as a function of temperature 42
Figure 24: Thermal conductivity for dry sample of Aplite Dyke as a function of temperature 42
Figure 25: Thermal diffusivity for saturated sample of Aplite Dyke as a function of temperature 43
Figure 26: Thermal diffusivity for dry sample of Aplite Dyke as a function of temperature 43
Figure 27: Volumetric heat capacity for saturated sample of Feldspar-phyric Tonalite Dyke as a function of temperature 44
Figure 28: Volumetric heat capacity for dry sample of Feldspar-phyric Tonalite Dyke as a function of temperature 45
Figure 29: Thermal conductivity for saturated sample of Feldspar-phyric Tonalite Dyke as a function of temperature 45
Figure 30: Thermal conductivity for dry sample of Feldspar-phyric Tonalite Dyke as a function of temperature 46
Figure 31: Thermal diffusivity for saturated sample of Feldspar-phyric Tonalite Dyke as a function of temperature 46
Figure 32: Thermal diffusivity for dry sample of Feldspar-phyric Tonalite Dyke as a function of temperature 47
Figure 33: Linear coefficient of thermal expansion as a function of temperature for all samples 52

APPENDICES

APPENDIX A
UCS Tests: Stress-Strain Graphs and Photographs of Intact and Broken Test Specimens

APPENDIX B
Acoustic Emission Data and Graph Report

APPENDIX C
Indirect Tensile (Brazilian) Strength Tests: Load-Time and Stress-Displacement Graphs and Photographs of Intact and Broken Test Specimens

APPENDIX D
Thermal Conductivity, Volumetric Heat Capacity and Thermal Diffusion Tests: Test Data and Graphs

APPENDIX E
Thermal Expansion Tests: Test Data and Graphs

1.0 INTRODUCTION

The Initial Borehole Drilling and Testing project in the Wabigoon and Ignace Area, Ontario is part of Phase 2 Geoscientific Preliminary Field Investigations of the NWMO's Adaptive Phased Management (APM) Site Selection Phase.

This project involves the drilling and testing of the first of three deep boreholes within the northern portion of the Revell batholith. The first drilled borehole, IG_BH01, is located a direct distance of approximately 21 km southeast of the Wabigoon Lake Ojibway Nation and a direct distance of 43 km northwest of the Town of Ignace. Access to the IG_BH01 drill site is via Highway 17 and primary logging roads, as shown on Figure 1.

The project was carried out by a team led by Golder Associates Ltd. (Golder) on behalf of the NWMO. The overall program is described in the Initial Borehole Characterization Plan (Golder 2017). This report describes the testing methodology and results for Work Package 4B (WP4B): Geomechanical Testing of Core for IG_BH01, which includes Uniaxial Compressive Strength tests (w/ elastic constants), Indirect Tensile (Brazilian) Strength tests, P-wave and S-wave ultrasonic pulse velocity, acoustic emissions (AE) measurements (on UCS tests) and Thermal testing comprising Thermal Conductivity, Thermal Diffusivity, Volumetric Heat Capacity, and Thermal Expansion. Wet and dry density and water content were measured for all tested samples.

2.0 BACKGROUND INFORMATION

2.1 Geological Setting

The approximately 2.7 billion year old Revell batholith is located in the western part of the Wabigoon Subprovince of the Archean Superior Province. The batholith is roughly elliptical in shape trending northwest, is approximately 40 km in length, 15 km in width, and covers an area of approximately 455 km^2. Based on geophysical modelling, the batholith is approximately 2 km to 3 km thick through the center of the northern portion (SGL 2015). The batholith is surrounded by supracrustal rocks of the Raleigh Lake (to the north and east) and Bending Lake (to the southwest) greenstone belts (Figure 2).

Borehole IG_BH01 is located within an investigation area of approximately 19 km^2 in size, situated in the northern portion of the Revell batholith. Bedrock exposure in the area is generally very good due to minimal overburden, few water bodies, and relatively recent logging activities. Ground elevations generally range from 400 to 450 m above sea level. The ground surface broadly slopes towards the northwest as indicated by the flow direction of the main rivers in the area. Local water courses tend to flow to the southwest towards Mennin Lake (Figure 1).

Four main rock units are identified in the supracrustal rock group: mafic metavolcanic rocks, intermediate to felsic metavolcanic rocks, metasedimentary rocks, and mafic intrusive rocks (Figure 2). Sedimentation within the supracrustal rock assemblage was largely synvolcanic, although sediment deposition in the Bending Lake area may have continued past the volcanic period (Stone 2009; Stone 2010a; Stone 2010b). All supracrustal rocks are affected, to varying degrees, by penetrative brittle-ductile to ductile deformation under greenschist- to amphibolite-facies metamorphic conditions (Blackburn and Hinz 1996; Stone et al. 1998). In some locations, primary features, such as pillow basalt or bedding in sedimentary rocks are preserved, in other locations, primary relationships are completely masked by penetrative deformation. Uranium-lead (U-Pb) geochronological analysis of the supracrustal rocks produced ages that range between 2734.6 +/-1.1 Ma and 2725 +/-5 Ma (Stone et al. 2010).

Three main suites of plutonic rock are recognized in the Revell batholith, including, from oldest to youngest: a Biotite Tonalite to Granodiorite suite, a Hornblende Tonalite to Granodiorite suite, and a Biotite Granite to Granodiorite suite (Figure 2). Plutonic rocks of the Biotite Tonalite to Granodiorite suite occur along the southwestern and northeastern margins of the Revell batholith. The principal type of rock within this suite is a white to grey, medium-grained, variably massive to foliated or weakly gneissic, biotite tonalite to granodiorite. One sample of foliated and medium-grained biotite tonalite produced a U-Pb age of 2734.2+/-0.8 Ma (Stone et al. 2010). The Hornblende Tonalite to Granodiorite suite occurs in two irregularly-shaped zones surrounding the central core of the Revell batholith. Rocks of the Hornblende Tonalite to Granodiorite suite range compositionally from tonalite through granodiorite to granite and also include significant proportions of quartz diorite and quartz monzodiorite. One sample of coarse-grained grey mesocratic hornblende tonalite produced a U-Pb age of 2732.3+/-0.8 Ma (Stone et al. 2010). Rocks of the Biotite Granite to Granodiorite suite underlie most of the northern, central and southern portions of the Revell batholith. Rocks of this suite are typically coarse-grained, massive to weakly foliated, and white to pink in colour. The Biotite Granite to Granodiorite suite ranges compositionally from granite through granodiorite to tonalite. A distinct potassium (K)-Feldspar Megacrystic Granite phase of the Biotite Granite to Granodiorite suite occurs as an oval-shaped body in the central portion of the Revell batholith (Figure 2). One sample of coarse-grained, pink, massive K-feldspar megacrystic biotite granite produced a U-Pb age of 2694.0+/-0.9 Ma (Stone et al. 2010).

The bedrock surrounding IG_BH01 is composed mainly of massive to weakly foliated felsic intrusive rocks that vary in composition between granodiorite and tonalite, and together form a relatively homogeneous intrusive complex. Bedrock identified as tonalite transitions gradationally into granodiorite and no distinct contact relationships between these two rock types are typically observed (SRK and Golder 2015; Golder and PGW 2017). Massive to weakly foliated granite is identified at the ground surface to the northwest of the feldspar-megacrystic granite. The granite is observed to intrude into the granodiorite-tonalite bedrock, indicating it is distinct from, and younger than, the intrusive complex (Golder and PGW 2017).

West-northwest trending mafic dykes interpreted from aeromagnetic data extend across the northern portion of the Revell batholith and into the surrounding greenstone belts. One mafic dyke occurrence, located to the northwest of IG_BH01, is approximately 15-20 m wide (Figure 2). All of these mafic dykes have a similar character and are interpreted to be part of the Wabigoon dyke swarm. One sample from the same Wabigoon swarm produced a U-Pb age of 1887+/-13 Ma (Stone et al. 2010), indicating that these mafic dykes are Proterozoic in age. It is assumed based on surface measurements that these mafic dykes are sub-vertical (Golder and PGW 2017).

Long, narrow valleys are located along the western and southern limits of the investigation area (Figure 1). These local valleys host creeks and small lakes that drain to the southwest and may represent the surface expression of structural features that extend into the bedrock. A broad valley is located along the eastern limits of the investigation area and hosts a more continuous, un-named water body that flows to the south. The linear and segmented nature of this waterbody’s shorelines may also represent the surface expression of structural features that extend into the bedrock.

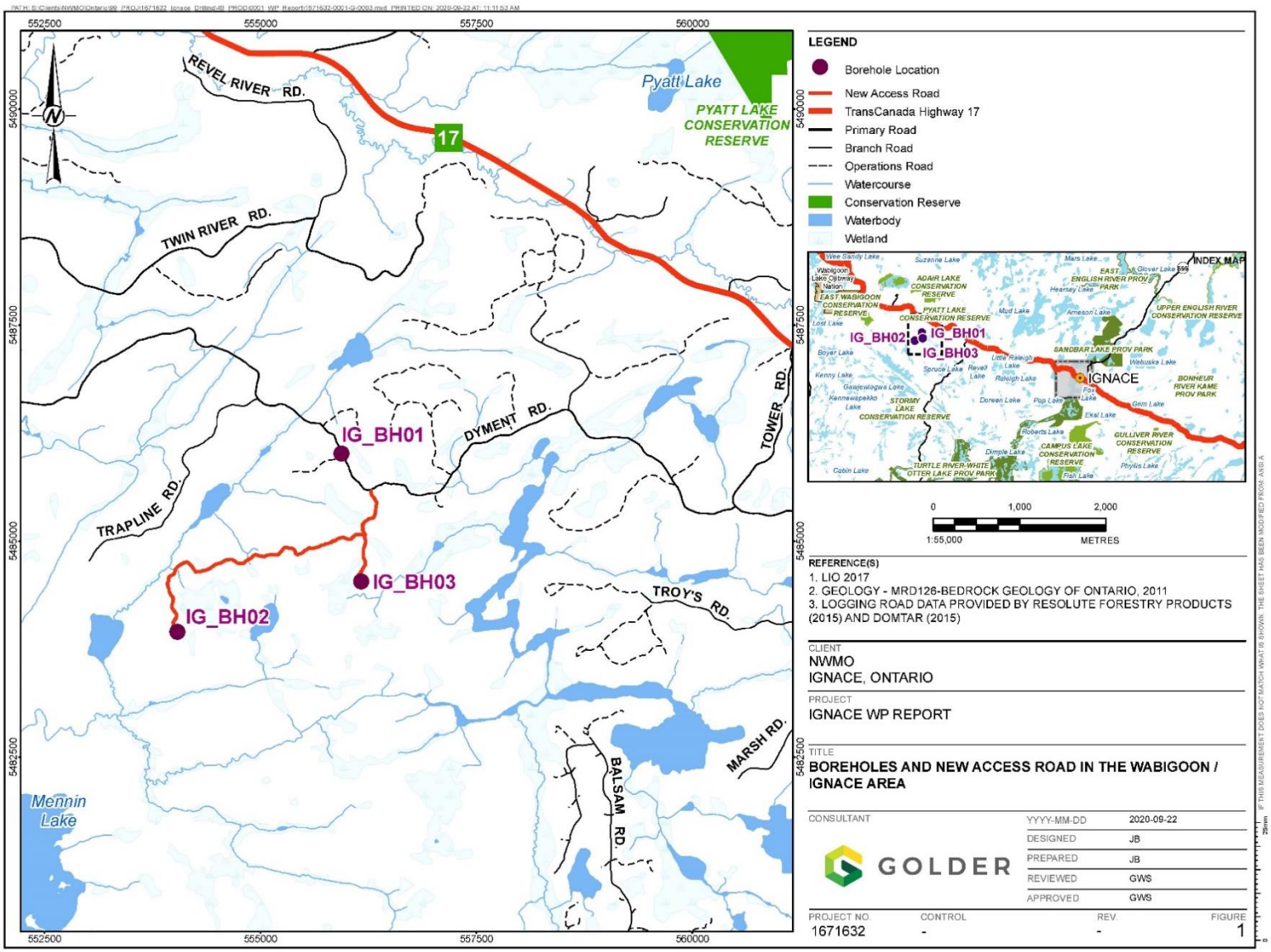


Figure 1: Location of IG_BH02 in Relation to the Wabigoon / Ignace Area

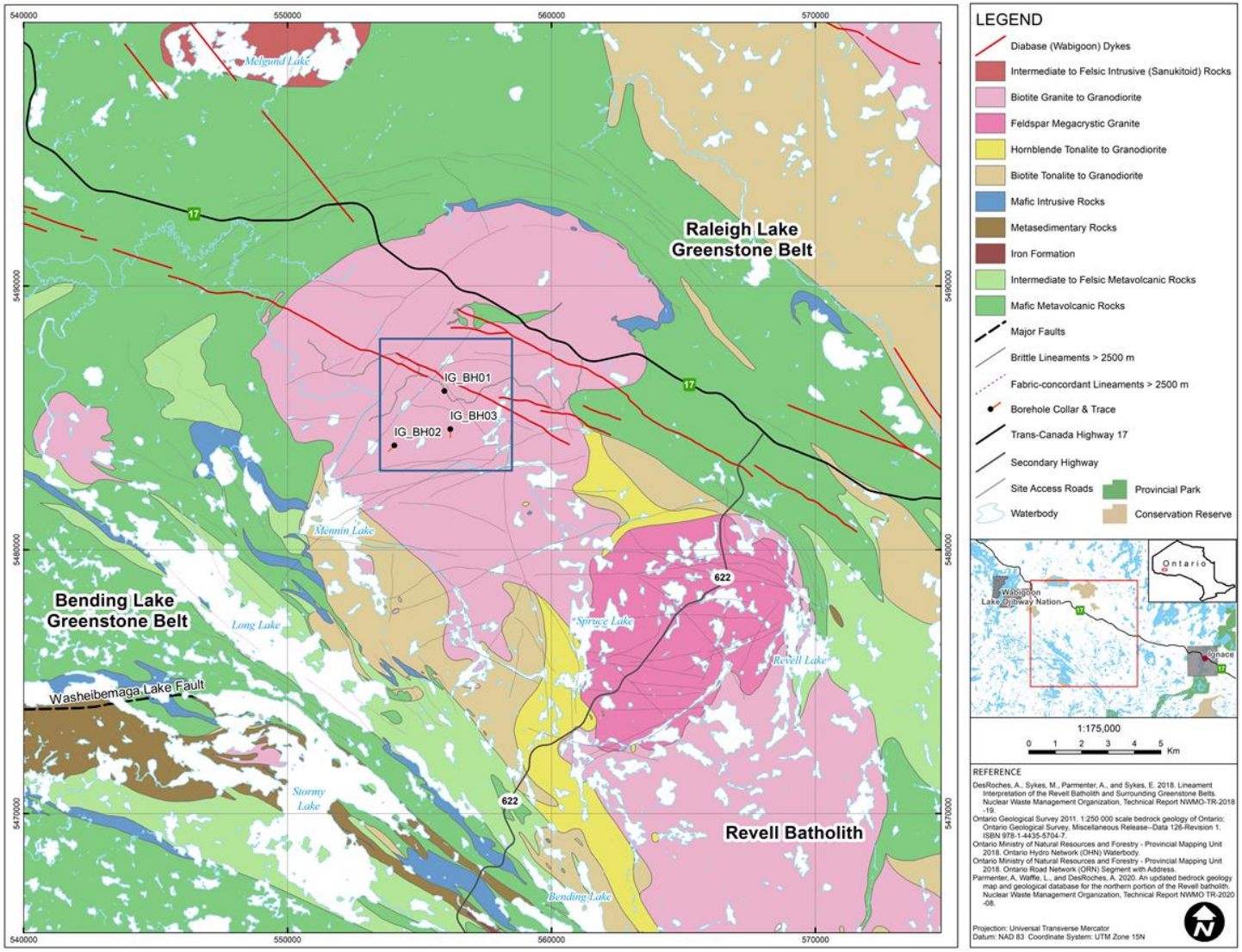


Figure 2: Geological setting and location of boreholes IG_BH01, IG_BH02 and IG_BH03 in the northern portion of the Revell batholith

Regional observations from mapping have indicated that structural features are widely spaced (typical 30 to 500 cm spacing range) and dominantly comprised of sub-vertical joints with two dominant orientations, northeast and northwest trending (Golder and PGW 2017). Interpreted bedrock lineaments generally follow these same dominant orientations in the northern portion of the Revell batholith (Figure 2; DesRoches et al. 2018). Minor sub-horizontal joints have been observed with minimal alteration, suggesting they are younger and perhaps related to glacial unloading. One mapped regional-scale fault, the Washeibemaga Lake fault, trends east and is located to the west of the Revell batholith (Figure 2). Additional details of the lithological units and structures found at surface within the investigation area are reported in Golder and PGW (2017).

2.2 Technical Objectives

The technical objective of the geomechanical laboratory testing and thermal testing program is to assess the key geomechanical and thermal properties of the crystalline host rock mainly within the repository horizon (presently assumed to be between depths of approximately 400 and 600 m) as well as a few samples from outside this horizon.

The testing was undertaken in more than one campaign, as follows:

- Campaign 1: During the drilling of IG_BH01, six (6) samples were collected and preserved for UCS strength testing, of which three (3) were sent to the laboratory for testing and the other three (3) were archived for later testing, if required. Also, six (6) samples were collected and preserved for Indirect Tensile (Brazilian) strength testing, of which three (3) were sent to the laboratory for testing and the other three (3) were archived for later testing. Samples were tested in their natural water content state (as collected and preserved).
- Campaign 2: The three (3) archived (preserved) samples for UCS strength testing and an additional four (4) samples (unpreserved) were selected from the stored rock core boxes for UCS strength testing. The three (3) archived (preserved) samples for Indirect Tensile (Brazilian) strength testing and an additional four (4) samples (unpreserved) were selected from the stored rock core boxes for Indirect Tensile (Brazilian) strength testing. The preserved samples were tested in their natural water content state and the unpreserved samples were re-saturated before testing. In addition, fourteen (14) samples were selected from the stored rock core boxes for thermal testing; however, one sample broke during shipping. The remaining thirteen (13) thermal samples were re-saturated before testing for Thermal Conductivity, Thermal Diffusivity, and Volumetric Heat Capacity. Thermal expansion tests deviated from the test plan and needed to be repeated. The thermal conductivity, thermal diffusivity and volumetric heat capacity samples were tested under re-saturated conditions when they should have been tested in dry conditions, according to the test plan. Therefore, a select few more samples would be also targeted for additional testing under dry conditions.
- Campaign 3: Due to unintentional deviations from the specifications set out in the test plan that were identified following completion of the second testing campaign, an additional thirteen (13) samples were selected for thermal testing. All thirteen (13) samples were tested for thermal expansion in re-saturated conditions, and a select seven (7) samples were tested for thermal conductivity, thermal diffusivity and volumetric heat capacity in dry conditions.

Uniaxial Compressive Strength (UCS) testing of core samples were performed on ten (10) samples, in Campaigns 1 and 2, to determine the intact unconfined compressive strength and elastic properties (elastic moduli and

Poisson's ratio) of the bedrock. Additional non-destructive testing/measurements for each UCS core sample included:

- Determination of water content and rock density;
- Determination of P-wave and S-wave ultrasonic pulse velocities and determination of ultrasonic elastic constants; and
- Monitoring and recording of incremental and cumulative acoustic emissions throughout each test.

Crack Initiation and Crack Damage stress levels were interpreted from the stress-strain curves for each test and compared to interpreted AE results for verification.

Indirect Tensile (Brazilian) Strength testing of core samples were performed on ten (10) samples (selected adjacent to the UCS samples), in Campaigns 1 and 2, to determine the tensile strength of the rock.

Twenty-six (26) samples were also selected for thermal property testing, including:

- Determination of volumetric heat capacity;
- Absolute thermal conductivity;
- Thermal diffusivity;
- Thermal expansion; and
- Determination of water content (as-received or re-saturated), wet (as-received or re-saturated) and dry density;

Initially (Campaign 2), the volumetric heat capacity, thermal conductivity and thermal diffusivity tests were completed on thirteen (13) samples under re-saturated conditions. An additional thirteen samples were selected from the stored core in Campaign 3; seven (7) samples were tested under dry conditions for volumetric heat capacity, thermal conductivity and thermal diffusivity; all additional thirteen (13) samples were tested for thermal expansion under re-saturated conditions. Water content and rock density of test specimens sub-cored from all twenty-six (26) samples were determined.

2.3 Description of Testing Procedures

The geomechanical testing program was carried out at the CANMET-MMSL rock mechanics testing facility located in Bells Corners (Ottawa), Ontario. Laboratory tests were carried out according to CANMET-MMSL's Standard Operating Procedures (SOPs), which follow ASTM standard test methods and ISRM suggested methods:

Preparation and Non-destructive Testing

- ASTM D4543-08 & ASTM D4543-19 Standard Practices for Preparing Rock Core as Cylindrical Test Specimens and Verifying Conformance to Dimensional and Shape Tolerances
- ASTM D2216-10 & ASTM D2216-19 Standard Test Methods for Laboratory Determination of Water (Moisture) Content of Soil and Rock by Mass

- ASTM D7263-09 & ASTM D7263-09 (2018)ε2, Laboratory Determination of Density (Unit Weight) of Soil Specimens

UCS Testing and Elastic Parameters

- ASTM D7012-14ε1 Standard Test Methods for Compressive Strength and Elastic Moduli of Intact Rock Core Specimens under Varying States of Stress and Temperatures
- ASTM D2845-08 Standard Test Method for Laboratory Determination of Pulse Velocities and Ultrasonic Elastic Constants of Rock. Note that ASTM D2845-08 has been withdrawn in 2017 without replacement. however, CANMET-MMSL methodology for this test still followed ASTM D2845-08 despite its withdrawal.

Indirect Tensile Strength Testing

- ASTM D3967-08 & ASTM D3967-16 Standard Test Method for Splitting Tensile Strength of Intact Rock Core Specimens

The thermal testing program was carried out at the RESPEC testing facility located in Rapid City, South Dakota. Laboratory tests were carried out according to RESPEC's Standard Operating Procedures (SOPs), which follow ASTM standard test methods and ISO 22007 standard.

Preparation and Non-destructive Testing

RESPEC follows their internal Test Procedure 02 (TP-02, RSI Standard Procedure for Rock Specimen Preparation, Rev. 5) for sample preparation, which follow ASTM standard test methods:

- ASTM D2216-10 & ASTM D2216-19 Standard Test Methods for Laboratory Determination of Water (Moisture) Content of Soil and Rock by Mass
- ASTM D7263-09 (reapproved 2018)ε2, Laboratory Determination of Density (Unit Weight) of Soil

For the hot disk specimens which had to be stored between drying and testing, they were double bagged using Ziplock bags and were stored in a room subject to year-round air conditioning.

For the thermal expansion specimens which had to be stored between saturating and testing, they were placed in Ziplock bags with excess water. Specimens were periodically checked to ensure that moist surface conditions were maintained.

Thermal Conductivity, Specific Heat and Thermal Diffusivity

Thermal testing was conducted on full-diameter size core (61 mm). The ends of the specimens are either ground flat in the surface grinder or finished in the lathe depending on the type of rock. The following standard applies:

- ISO 22007-2: 2015(E) Determination of thermal conductivity and thermal diffusivity Part 2: Transient plane heat source (hot disc) method.

Thermal Expansion

Thermal expansion testing was conducted on samples sub-cored to 32 mm (1.25'') diameter. Thermal expansion testing was conducted on saturated samples. Re-saturation for all non-preserved samples preceded thermal expansion testing.

- ASTM D4535-13$^{\varepsilon 1}$ & ASTM D4535-13$^{\varepsilon 2}$, Standard Test Methods for Measurement of Thermal Expansion of Rock Using Dilatometer – Method A (unconfined).

2.4 Test Apparatus and Procedures

2.4.1 Sample Preparation

Preparation of cylindrical specimens for UCS tests, and verification of conformance to dimensional and shape tolerances were done according to the ASTM D4543-19 standard test method. Fresh water was used for cutting and end preparation. Specimen ends were ground flat to within 0.025 mm and parallel to each other as specified by the ASTM D4543-19 standard test method for a loading system with fixed platens.

Specimen dimensions, i.e., average length and diameter, were measured to the nearest 0.01 mm. Cross-sectional area and volume were determined. Specimens were weighted to the nearest 0.1 g, and density was computed to the nearest 0.01 g/cm^3 as well. Zero-pressure P- and S-wave velocities were also measured.

Specimens with a nominal thickness-to-diameter ratio of 0.66 were prepared to carry out splitting tensile (Brazilian) tests.

2.4.2 Uniaxial Compressive Strength (UCS) Tests

UCS tests were carried out using a computer-controlled, servo-hydraulic MTS Rock Mechanics Testing System, Model 815, consisting of a 2.6 MN rated capacity load cell, the load frame itself, the hydraulic power supply, and digital controllers and test software to control experiments. Displacements were converted into strains taking into account the specific dimensions of each test specimen. UCS test specimens were covered by a thin Teflon heat shrink jacket prior the beginning of the test to protect the instrumentation and avoid the projection of fragments, especially when testing brittle materials. Test specimens were loaded up to failure at constant axial displacement rate, e.g., controlled strain rate, equal to 0.0009 mm/sec for 60 mm (nominal) OD specimens, with failure expected between 5 and 10 minutes after the beginning of loading for UCS tests, in accordance with the requirements of the ASTM D7012 standard test method for UCS tests. All data, e.g., time, axial load, axial stress, and axial and circumferential displacements, were sampled and recorded every 0.2 second over the whole test duration, and converted into engineering units afterwards, i.e., conversion of loads and displacements into stresses and strains, respectively.

2.4.2.1 Acoustic Emissions (AE) Data Acquisition

Acoustic emissions were recorded during UCS tests. The system used was a Pocket AE-2^{TM} system manufactured by Physical Acoustics Corporation (PAC). This system is a dual channel 18-bit system connected to Pico^{TM} sensors with a frequency range of 200-750 kHz and a sampling rate of 20Ms/sec.

Two sensors were fixed on opposite sides of UCS test specimens, at 180 degrees from each other, one sensor being fixed 3 cm above the specimen mid-section, and the second sensor 3 cm below the mid-section, so these were not interfering with the movement of the MTS chain extensometer. Acoustic emission data were recorded systematically. Main features recorded were the number of emissions (or hits) and the waveform signal.

2.4.3 Indirect Tensile Strength (Brazilian) Tests

Tests were performed on the same system used for the UCS testing, but with a smaller load cell for higher accuracy, e.g., a rated capacity of 500 kN. Test specimens were loaded diametrically at a constant load rate of

0.10 kN/sec, with breakage expected sometime between two and five minutes after the beginning of the test. Tests were carried out in conformity with the requirements of the ASTM D3967-16 standard test method for indirect tensile (Brazilian) strength tests. All test data, i.e., time, diametrical load, tensile stress and vertical displacement (Ram LVDT), were recorded every 0.2 seconds over the whole test duration.

2.4.4 Water Content and Density Measurements

The samples were measured and weighed before testing. After testing, they were weighed and placed in the oven to start the drying process (ASTM D2216-19). Because of the destructive nature of the UCS and Brazilian tests, there is a possibility that some of the sample material may be lost during testing, which will make it difficult to know the exact volume of the sample after the test. Due to the lower porosity of the rock samples from IG_BH01, any loss, however small, can have a significant effect in the determination of the water content and dry density. Therefore, the more precise way to determine the dry density for samples undergoing destructive testing is using the bulk density and the water content measured on sample collected after the destructive testing.

The density of the bulk samples, as received, is calculated as follows:

Volume of the prepared sample = V

Mass of the prepared sample = M

$$\rho_{\text{bulk}} = \frac{M}{V}$$

The water content of the sample is calculated as follows:

Mass of the sample after testing (initial mass before drying) = M_{init}

Mass of the sample after drying = M_{dry}

$$w = \frac{M_{init} - M_{dry}}{M_{dry}}$$

Calculation of the sample dry density:

$$\rho_{\text{dry}} = \frac{\rho_{\text{bulk}}}{1 + w}$$

Note that when no material is lost, and the mass and volume after the test have not changed, the dry density reverts to

$$\rho_{\text{dry}} = \frac{M_{dry}}{V}$$

2.4.5 Thermal Conductivity, Volumetric Heat Capacity and Thermal Diffusivity

Thermal conductivity, volumetric heat capacity and thermal diffusivity were measured both in re-saturated (13 samples) and dry conditions (7 samples). Samples tested in the dry state were dried at temperatures not exceeding 80°C prior to testing; after testing, samples were further dried following the same procedure provided for water content measurements described above to a precision not less than 0.01% of the initial sample weight.

Testing was performed using a Thermtest TPS 1500 that heats and measures the thermal gradient across an area. The Transient Plane Source (TPS) sensor was placed between two pieces of material to be measured, each

with plane surfaces facing the sensor. The solution to the thermal conductivity equation assumes the sensor is in an infinite medium, so the measurement and subsequent analysis of data must account for the limitation created by the outer boundaries of the material. The TPS sensor contains both a heating element and a temperature measuring sensor. A known amount of power is supplied to the heater for a set amount of time. The temperature gradient is measured as it spreads out from the heat source. From these data, the thermal analyzer can determine the thermal conductivity, volumetric heat capacity and thermal diffusivity.

Thermal conductivity, volumetric heat capacity and thermal diffusivity were measured between room temperature (25°C) and 300°C in 10 temperature intervals for the thirteen (13) re-saturated samples (Campaign 2). The first temperature interval was 15°C and the subsequent intervals were 30°C. For the seven (7) samples tested under dry conditions five (5) measurements were made between room temperature and 90°C during heating and a repeat measurement during cooling at 60°C, followed the heating schedule shown in Table 1 (Campaign 3).

Table 1: Target Temperature Schedule for Hot Disk Tests

Data Point	Target Temperature	Comments
1	20 – 25°C	Room temperature
2	40°C	
3	60°C	
4	80°C	
5	90°C	
6	60°C	Repeat measurement during cooling

2.4.6 Thermal Expansion

Thermal expansion was measured using a Unitherm 1054L apparatus that has been updated to allow automatic control and temperatures ranging from 25°C to 300°C. Tests were performed using a push-rod dilatometer and heating element. The dilatometer system is capable of testing two specimens simultaneously. The test setup is described as unconfined and uniaxial because the specimen is subjected only to atmospheric pressure and deformation is only measured in the axial direction of the specimen.

Thermal expansion was measured between room temperature and 90°C for the thirteen (13) re-saturated samples (Campaign 3), following the target temperature schedule shown in Table 2. Two heating-cooling paths were followed with five (5) measurements during heating and a measurement at 60°C during cooling. The rate of heating/cooling between target temperatures did not exceed 1°C/min. A target rate of heating/cooling of 0.5 °C/min was used to ensure that the maximum rate of 1°C/min was not exceeded due to temperature fluctuations. Compliance with this requirement has been demonstrated graphically by plotting temperature rate vs time and included in the metadata deliverable.

Table 2: Target Temperature Schedule for Thermal Expansion Tests

Data Point	Target Temperature	Comments
1	20 – 25°C (room temp)	1st Heating Path
2	40°C	
3	60°C	
4	80°C	
5	90°C	
6	60°C	1st Cooling Path
7	20 – 25°C (room temp)	
8	40°C	2nd Heating Path
9	60°C	
10	80°C	
11	90°C	
12	60°C	2nd Cooling Path
13	20 – 25°C (room temp)	

2.5 Analysis of Data

2.5.1 Zero Pressure P-S Wave Velocity Tests

P (compressive) and S (shear) wave velocities are determined from the time taken by a sinusoidal wave to travel across the test specimen along its longitudinal axis. P and S wave velocities were determined for all UCS specimens prepared for the test program. Dynamic elastic constants are calculated by the following expressions:

$$E_D = \frac{\rho V_S^2 (3V_P^2 - 4V_S^2)}{V_P^2 - V_S^2}$$

$$G_D = \rho V_S^2$$

$$\nu_D = \frac{V_P^2 - 2V_S^2}{2(V_P^2 - V_S^2)}$$

where:

E_D – dynamic Young's modulus
G_D – dynamic shear modulus
ν_D – dynamic Poisson's ratio
V_P – compressive (P) wave velocity
V_S – shear (S) wave velocity
ρ – density

2.5.2 Uniaxial Compressive Strength (UCS) Tests

Raw original data recorded during uniaxial compression tests consist of axial load, and axial and circumferential displacements. Axial displacements are corrected for the compression of steel platens, between which displacements are measured, and the circumferential displacement is corrected for the gap between the measuring chain-extensometer and the specimen side. Engineering stresses and strains are computed using the following formulas:

$$\sigma_1 = \frac{P}{A_0}$$

$$\varepsilon_A = \frac{\Delta L}{L_0}$$

$$\varepsilon_C = \frac{\Delta D}{D_0}$$

where:

σ_1 – axial stress
P – axial load
A_0 – initial cross-sectional area of the specimen
ε_A – axial strain
ε_C – circumferential strain
ΔL – change in specimen length
L_0 – specimen length
ΔD – change in specimen circumference
D_0 – specimen circumference

The volumetric strain (ε_V) is defined by the following expression:

$$\varepsilon_V = \varepsilon_A + 2\varepsilon_C$$

The uniaxial compressive strength (UCS) was determined for all UCS tests carried out during the test program. The Young's modulus (E_{40}) was determined at a nominal stress level of 40% of the UCS, as the slope of the linear regression line through axial stress-axial strain data points over 30-50% of the axial stress interval. The Poisson's ratio (ν_{40}) was determined as negative of the slope of the linear regression line through circumferential strain-axial strain data points, averaged over the same axial stress interval. Strength is given by the following expression:

$$UCS = \frac{P_C}{A_0}$$

where:

UCS – uniaxial compressive strength
P_C – ultimate axial load on the specimen at failure
As mentioned, strain data are obtained from displacements measured with the mechanical sensors, e.g., axial LVDTs and MTS circumferential chain-extensometer.

The crack damage threshold, σ_{CD}, has been interpreted in this report as the stress level at which the volumetric strain, ε_V, reaches its maximum and starts reversing direction, i.e., the inflexion point on the $\sigma_1 - \varepsilon_V$ graph, hence

indicating dilation due to the formation and growth of unstable cracks. Theoretically, it is assumed that the progressive fracturing process starts above the crack damage threshold, leading to the failure of the rock material (Ghazvinian et al., 2012).

The crack initiation threshold, σ_{CI}, has been interpreted in this report as the stress level at which the crack volumetric strain, ε_{VC}, reaches its maximum and starts reversing direction, i.e., the inflexion point on the $\sigma_1 - \varepsilon_{VC}$ graph, hence indicating a departure from elasticity, and the development and growth of stable cracks. The crack volumetric strain, ε_{VC}, is determined by the difference between the volumetric strain, ε_V, and the elastic volumetric strain, ε_{VE}, recorded during UCS tests assuming a perfectly linear elastic material, following these expressions:

$$\varepsilon_{VC} = \varepsilon_V - \varepsilon_{VE}$$

$$\varepsilon_{VE} = \frac{1 - 2\nu_{40}}{E_{40}}\sigma_1$$

2.5.3 Acoustic Emissions Data

The counts per time period and cumulative counts per time period of AE hits, as well as energy per time period and cumulative energy per time period for each specimen are provided in Appendix B. Recording of the acoustic emissions may not start at the same time as the recording of the strains; therefore, the two records (strains and AE) are time-matched at the peak stress in order to compare the time (and stress) of the crack initiation process. Crack initiation is defined at the time that systematic cracking develops (not the first crack) which can be identified as the change in the slope of the cumulative energy graph. Crack damage starts when individual cracks start to coalesce and create a localized feature; this threshold can be more difficult to identify in the AE data. Figure 3 shows the cumulative energy for one or both sensors for samples IG_BH01_UC001/003/005 (vertical scale exaggerated) and the crack initiation stress as interpreted from the stress-strain data. After adjusting for the time lag between the stress-strain record and the AE record, there is reasonable agreement between them.

For the second campaign of testing, the data was also provided in raw digital format, which allowed plotting the graphs for cumulative energy vs axial stress in a log-log scale. Figure 4 shows the log-log plot of cumulative energy vs axial stress for sample IG_BH01-UC002.

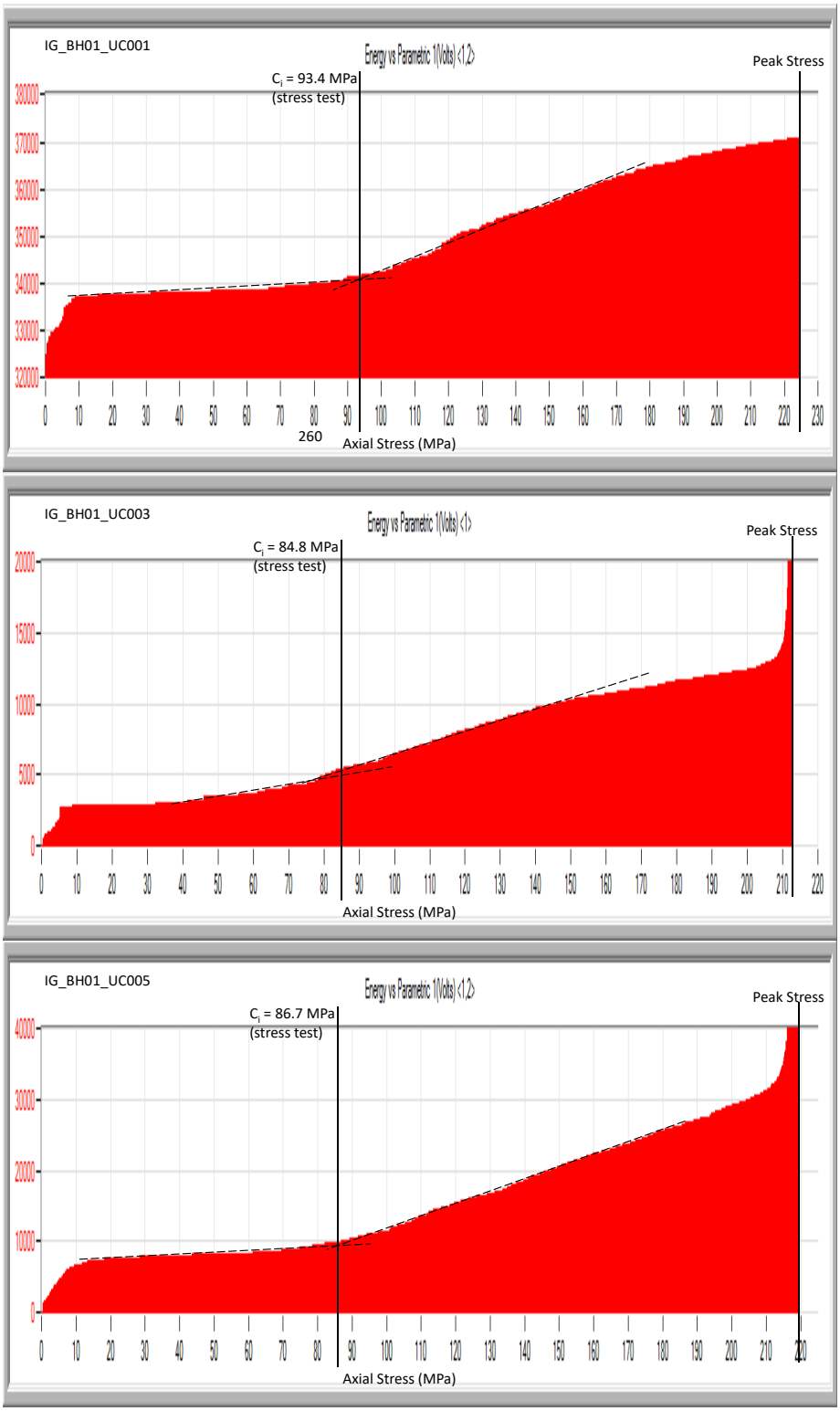


Figure 3: Cumulative energy (volt·sec) vs axial stress measured during UCS testing of sample IG_BH01_UC001, IG_BH01_UC003 and IG_BH01_UC005. Note that C_i in this figure is the same as σ_{CI} discussed in section 2.5.2 in the text.

The AE record seems to suggest a lower C_i value, although the interpretation can be somewhat subjective. For this reason, the interpretation from the UCS crack volumetric strain is more reliable. Plots of cumulative energy vs axial stress for all the samples are included in APPENDIX B.

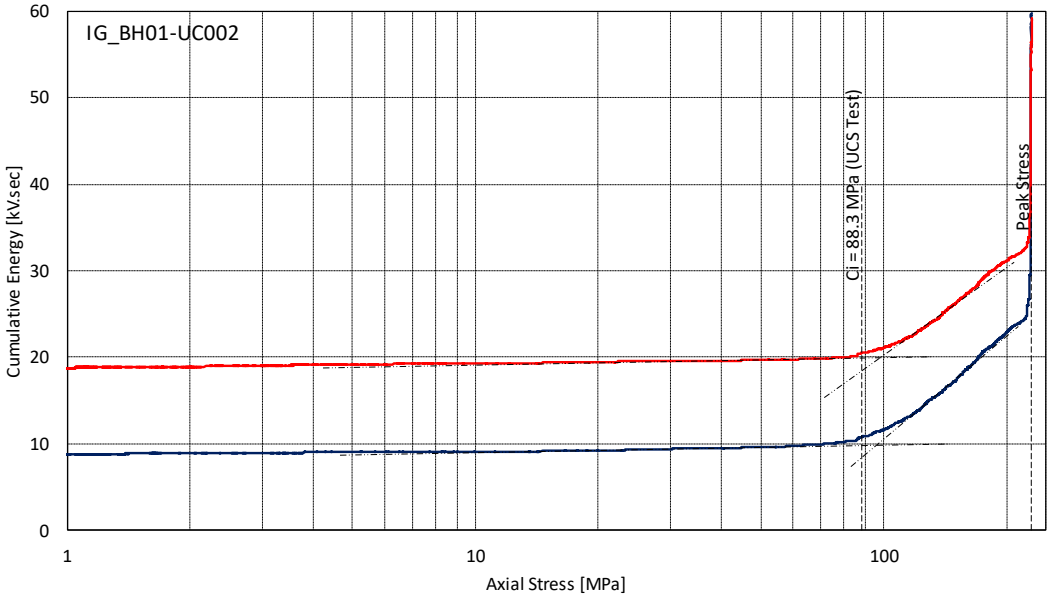


Figure 4: Cumulative energy (in kilovolt.sec) versus axial stress (MPa) measured during UCS testing of sample IG_BH01-UC002 in a log-log scale

2.5.4 Indirect Tensile (Brazilian) Strength Tests

The indirect tensile (Brazilian) strength of a test specimen at failure, σ_T, is given by the following expression:

$$\sigma_T = \frac{2P}{\pi DT}$$

where:

σ_T – tensile strength
P – diametrical load on the specimen at failure
D – diameter of the specimen
T – thickness of the specimen

2.5.5 Thermal Conductivity, Volumetric Heat Capacity and Thermal Diffusivity

The thermal conductivity, k, volumetric heat capacity, C_V, and thermal diffusivity, κ, for each sample were measured at the following 11 temperatures using a Thermtest TPS 1500 for the thirteen (13) re-saturated samples:

25°C, 40°C, 70°C, 100°C, 129°C, 159°C, 188°C, 218°C, 247°C, 277°C, and 295°C.

The seven (7) samples tested in a dry state were subjected to the heating cycle shown in Table 1.

The thermal diffusivity, κ, can be calculated at each temperature from the thermal conductivity, k, and the volumetric heat capacity, C_V, according to the following relationship:

$$\kappa = \frac{k}{C_V}$$

This relationship provides a check on the results reported by the Thermtest TPS 1500.

If the specific heat, c, is required, it can be obtained from the volumetric heat capacity by dividing it by the density, ρ:

$$c = \frac{C_V}{\rho}$$

2.5.6 Thermal Expansion

The coefficient of linear thermal expansion, α for the seven (7) samples tested in a dry state was measured throughout the heating cycles shown in Table 2.

The displacement measured by the LVDT includes the expansion of sample as well as the components of the apparatus; therefore, it needs to be corrected. Primary machine components that affect measurements are the push rods and the specimen holders. Displacement measurements are referenced to the top of the specimen holders (see Figure 5). The lengthening of the specimen holders is greater than the lengthening of the push rods because they are made from the same material, but the holders are longer; therefore, the LVDTs under-register the specimen displacement.

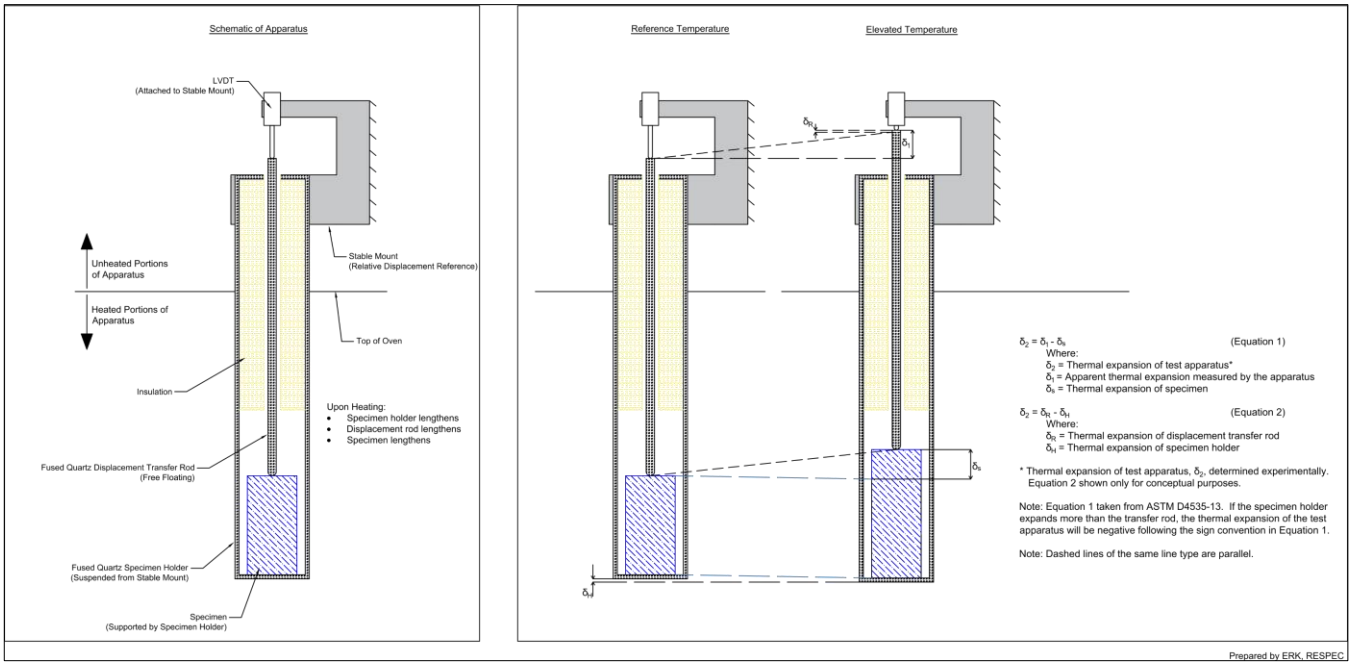


Figure 5: Schematic of the thermal expansion apparatus and components of the displacement correction.

3.0 LABORATORY RESULTS

3.1 Dimensions and Physical Properties of Specimens

The specimen number, top of specimen depth, rock type (according to terminology adopted in WP10 – Golder 2022), specimen dimensions, mass, bulk density (as received), dry density, and water content for all laboratory specimens are shown in Table 3.

Table 3: Dimensions and Physical Properties of Lab Specimens

Sample ID	Depth (mbgs)[1]	Rock Type	Testing Campaign	Diameter (mm)	Length (mm)	L:D Ratio	Wet Mass (g)	Wet Density[2] (g/cm^3)	Dry Density (g/cm^3)	Water Content[2] (%)
IG_BH01_UC001	408.40	Biotite Granodiorite-Tonalite	1	60.69	136.98	2.26	1054.25	2.66	2.66	0.18
IG_BH01_UC002	442.01	Biotite Granodiorite-Tonalite	2	60.73	137.03	2.26	1062.41	2.68	2.67	0.14
IG_BH01_UC003	468.02	Biotite Granodiorite-Tonalite	1	60.37	136.98	2.27	1049.76	2.68	2.67	0.14
IG_BH01_UC004	522.64	Biotite Granodiorite-Tonalite	2	60.66	137.03	2.26	1062.85	2.68	2.68	0.13
IG_BH01_UC005	567.77	Biotite Granodiorite-Tonalite	1	60.75	136.98	2.25	1067.48	2.69	2.69	0.12
IG_BH01_UC006	600.72	Biotite Granodiorite-Tonalite	2	60.97	137.03	2.25	1077.34	2.69	2.69	0.12
IG_BH01_UC007[3]	450.79	Biotite Tonalite	2	60.73	137.03	2.26	1077.19	2.71	2.71	0.11
IG_BH01_UC008[3]	559.94	Feldspar-phyric Tonalite Dyke	2	59.96	137.02	2.29	1041.90	2.69	2.69	0.13
IG_BH01_UC009[3]	655.01	Amphibolite	2	60.83	137.04	2.25	1156.01	2.91	2.91	0.12
IG_BH01_UC010[3]	658.31	Amphibolite	2	60.82	137.03	2.25	1179.03	2.97	2.97	0.03
IG_BH01_BR001	408.61	Biotite Granodiorite-Tonalite	1	60.72	40.00	0.66	307.12	2.65	2.65	0.17
IG_BH01_BR002	442.26	Biotite Granodiorite-Tonalite	2	60.75	39.88	0.66	308.81	2.67	2.67	0.20
IG_BH01_BR003	468.23	Biotite Granodiorite-Tonalite	1	60.38	39.99	0.66	306.30	2.67	2.67	0.15

Sample ID	Depth (mbgs)[1]	Rock Type	Testing Campaign	Diameter (mm)	Length (mm)	L:D Ratio	Wet Mass (g)	Wet Density[2] (g/cm^3)	Dry Density (g/cm^3)	Water Content[2] (%)
IG_BH01_BR004	522.90	Biotite Granodiorite-Tonalite	2	60.67	39.88	0.66	309.39	2.68	2.68	0.21
IG_BH01_BR005	568.04	Biotite Granodiorite-Tonalite	1	60.77	39.99	0.66	311.38	2.68	2.68	0.16
IG_BH01_BR006	601.00	Biotite Granodiorite-Tonalite	2	60.97	39.86	0.65	313.49	2.69	2.69	0.22
IG_BH01_BR007[3]	451.06	Biotite Tonalite	2	60.74	39.90	0.66	313.30	2.71	2.71	0.11
IG_BH01_BR008[3]	560.11	Feldspar-phyric Tonalite Dyke	2	59.95	39.86	0.66	303.04	2.69	2.68	0.14
IG_BH01_BR009[3]	655.46	Amphibolite	2	60.86	39.86	0.65	337.49	2.95	2.94	0.12
IG_BH01_BR010[3]	658.55	Amphibolite	2	60.80	39.87	0.66	338.28	2.90	2.90	0.05
IG_BH01_TH001[3,4,7]	299.74 299.78	Biotite Granodiorite-Tonalite	2	60.96 60.95	35.27 39.20	N/A	275.96 306.72	2.68 2.68	2.68 2.68	0.11 0.11
IG_BH01_TH002[3,4,7]			2		Broken in transit					
IG_BH01_TH003[3,4,7]	352.98 353.01	Biotite Granodiorite-Tonalite	2	60.64 60.63	34.34 34.57	N/A	263.92 265.48	2.66 2.66	2.66 2.65	0.18 0.20
IG_BH01_TH004[3,4,7]	401.71 401.75	Aplite Dyke	2	60.69 60.69	37.13 36.25	N/A	280.29 273.43	2.61 2.61	2.61 2.60	0.15 0.15
IG_BH01_TH005[3,4,7]	421.80 421.84	Biotite Granodiorite-Tonalite	2	60.67 60.68	36.93 35.36	N/A	282.93 270.85	2.65 2.65	2.65 2.64	0.15 0.15
IG_BH01_TH006[3,4,7]	448.64 448.66	Biotite Tonalite	2	60.87 60.87	30.12 29.47	N/A	236.54 231.70	2.70 2.70	2.70 2.70	0.11 0.12
IG_BH01_TH007[3,4,7]	450.50 450.54	Biotite Tonalite	2	60.86 60.85	33.83 35.43	N/A	266.10 278.59	2.70 2.70	2.70 2.70	0.13 0.12

Sample ID	Depth (mbgs)[1]	Rock Type	Testing Campaign	Diameter (mm)	Length (mm)	L:D Ratio	Wet Mass (g)	Wet Density[2] (g/cm^3)	Dry Density (g/cm^3)	Water Content[2] (%)
IG_BH01_TH008[3,4,7]	456.85 456.89	Biotite Granodiorite-Tonalite	2	60.69 60.67	28.84 30.07	N/A	222.30 231.88	2.66 2.67	2.66 2.66	0.12 0.13
IG_BH01_TH009[3,4,7]	501.76 501.80	Biotite Granodiorite-Tonalite	2	60.70 60.71	30.15 30.14	N/A	232.99 232.38	2.67 2.66	2.67 2.66	0.14 0.12
IG_BH01_TH010[3,4,7]	530.30 530.33	Biotite Granodiorite-Tonalite	2	60.69 60.69	36.10 35.03	N/A	280.00 271.77	2.68 2.68	2.68 2.68	0.10 0.11
IG_BH01_TH011[3,4,7]	555.97 556.00	Biotite Granodiorite-Tonalite	2	60.45 60.45	32.02 33.61	N/A	245.84 257.96	2.68 2.67	2.67 2.67	0.13 0.13
IG_BH01_TH012[3,4,7]	560.36 560.40	Feldspar-phyric Tonalite Dyke	2	59.91 59.92	31.49 31.25	N/A	234.23 235.94	2.64 2.68	2.63 2.67	0.18 0.17
IG_BH01_TH013[3,4,7]	603.56 603.60	Biotite Granodiorite-Tonalite	2	61.06 61.06	30.45 31.29	N/A	239.17 245.78	2.68 2.68	2.68 2.68	0.13 0.13
IG_BH01_TH014[3,4,7]	657.97 658.00	Amphibolite	2	60.90 60.93	31.94 29.55	N/A	273.31 251.87	2.94 2.92	2.93 2.92	0.09 0.10
IG_BH01_TH017[4,6]	402.05 402.09	Aplite Dyke	3	60.70 60.70	35.00 35.57	N/A	263.68[8] 268.29[8]	-	2.60 2.61	-
IG_BH01_TH020[4,6]	451.68 451.72	Biotite Tonalite	3	60.88 60.88	34.64 33.79	N/A	271.97[8] 265.47[8]	-	2.70 2.70	-
IG_BH01_TH021[4,6]	457.17 457.21	Biotite Granodiorite-Tonalite	3	60.70 60.70	33.22 34.14	N/A	255.99[8] 262.93[8]	-	2.66 2.66	-
IG_BH01_TH024[4,6]	556.28 556.32	Biotite Granodiorite-Tonalite	3	60.47 60.48	34.57 33.67	N/A	265.64[8] 258.65[8]	-	2.68 2.67	-
IG_BH01_TH025[4,6]	561.31 561.35	Feldspar-phyric Tonalite Dyke	3	60.08 60.13	32.87 34.54	N/A	249.11[8] 262.63[8]	-	2.67 2.68	-
IG_BH01_TH026[4,6]	603.95 603.99	Biotite Granodiorite-Tonalite	3	61.09 61.08	34.51 34.04	N/A	270.96[8] 267.18[8]	-	2.68 2.68	-

Sample ID	Depth (mbgs)[1]	Rock Type	Testing Campaign	Diameter (mm)	Length (mm)	L:D Ratio	Wet Mass (g)	Wet Density[2] (g/cm^3)	Dry Density (g/cm^3)	Water Content[2] (%)
IG_BH01_TH027[4,6]	657.67 657.71	Amphibolite	3	60.88 60.93	35.45 36.35	N/A	302.81[8] 309.33[8]	-	2.93 2.92	-
IG_BH01_TH001[3]	299.82	Biotite Granodiorite-Tonalite	2	30.00	79.25	N/A	150.14	2.68	2.68	0.11
IG_BH01_TH002[3]			2		Broken in transit					
IG_BH01_TH003[3]	353.06	Biotite Granodiorite-Tonalite	2	29.94	79.11	N/A	148.01	2.66	2.65	0.14
IG_BH01_TH004[3]	401.83	Aplite Dyke	2	37.85	79.38	N/A	233.22	2.61	2.61	0.15
IG_BH01_TH005[3]	421.87	Biotite Granodiorite-Tonalite	2	30.01	78.22	N/A	146.37	2.65	2.64	0.15
IG_BH01_TH006[3]	448.77	Biotite Tonalite	2	37.78	79.16	N/A	238.87	2.69	2.69	0.14
IG_BH01_TH007[3]	450.58	Biotite Tonalite	2	29.85	79.30	N/A	150.11	2.70	2.70	0.14
IG_BH01_TH008[3]	456.94	Biotite Granodiorite-Tonalite	2	30.05	79.19	N/A	149.58	2.66	2.66	0.12
IG_BH01_TH009[3]	501.67	Biotite Granodiorite-Tonalite	2	29.46	79.06	N/A	143.84	2.67	2.67	0.13
IG_BH01_TH010[3]	530.37	Biotite Granodiorite-Tonalite	2	29.66	79.13	N/A	146.77	2.68	2.68	0.12
IG_BH01_TH011[3]	556.04	Biotite Granodiorite-Tonalite	2	29.92	78.82	N/A	148.34	2.68	2.67	0.14
IG_BH01_TH012[3]	560.43	Feldspar-phyric Tonalite Dyke	2	29.95	80.00	N/A	151.23	2.68	2.68	0.16
IG_BH01_TH013[3]	603.63	Biotite Granodiorite-Tonalite	2	29.27	77.52	N/A	140.00	2.68	2.68	0.15
IG_BH01_TH014[3]	658.03	Amphibolite	2	30.00	78.66	N/A	162.36	2.92	2.92	0.13

Sample ID	Depth (mbgs)[1]	Rock Type	Testing Campaign	Diameter (mm)	Length (mm)	L:D Ratio	Wet Mass (g)	Wet Density[2] (g/cm^3)	Dry Density (g/cm^3)	Water Content[2] (%)
IG_BH01_TH015[3,5]	299.43	Biotite Granodiorite-Tonalite	3	31.46	79.19	N/A	164.98	2.68	2.68	0.10
IG_BH01_TH016[3,5]	353.54	Biotite Granodiorite-Tonalite	3	31.29	79.69	N/A	162.85	2.66	2.65	0.12
IG_BH01_TH017[3,5]	401.95	Aplite Dyke	3	31.35	79.56	N/A	160.27	2.61	2.61	0.16
IG_BH01_TH018[3,5]	422.33	Biotite Granodiorite-Tonalite	3	31.33	78.96	N/A	160.81	2.64	2.64	0.12
IG_BH01_TH019[3,5]	448.22	Biotite Tonalite	3	31.37	78.89	N/A	164.62	2.70	2.70	0.11
IG_BH01_TH020[3,5]	451.57	Biotite Tonalite	3	31.24	79.84	N/A	165.28	2.70	2.70	0.12
IG_BH01_TH021[3,5]	457.06	Biotite Granodiorite-Tonalite	3	31.40	79.38	N/A	163.76	2.66	2.66	0.12
IG_BH01_TH022[3,5]	501.98	Biotite Granodiorite-Tonalite	3	31.32	79.33	N/A	163.37	2.67	2.67	0.11
IG_BH01_TH023[3,5]	529.63	Biotite Granodiorite-Tonalite	3	31.39	79.29	N/A	164.31	2.68	2.68	0.10
IG_BH01_TH024[3,5]	556.17	Biotite Granodiorite-Tonalite	3	31.36	79.36	N/A	164.50	2.68	2.68	0.09
IG_BH01_TH025[3,5]	561.20	Feldspar-phyric Tonalite Dyke	3	31.43	79.44	N/A	165.40	2.68	2.68	0.17
IG_BH01_TH026[3,5]	603.84	Biotite Granodiorite-Tonalite	3	31.29	79.37	N/A	163.63	2.68	2.68	0.10
IG_BH01_TH027[3,5]	657.79	Amphibolite	3	31.41	79.38	N/A	179.31	2.91	2.91	0.07

[1]Top depth of prepared sub-sample (depth along borehole)

[2]Water Content represents as-received water content for preserved samples and re-saturated water content for unpreserved samples. Specimens were oven-dried in accordance with ASTM D2216-10 & ASTM D2216-19.

[3]Unpreserved samples. Samples were saturated before testing. Saturated mass reported. Bulk density represents saturated density. Water content represents saturated water content.
[4]Samples for thermal diffusivity, thermal conductivity, and heat capacity (two disks).
[5]Samples for thermal expansion.
[6]Unpreserved samples. Samples were dried at 80°C before testing and at 110°C after testing.
[7]Samples were heated to about 300°C during testing.
[8]Dry mass reported.

3.2 Laboratory Testing Results

3.2.1 Geomechanical Results

Table 4 shows a summary of the average strength properties for the Biotite Granodiorite-Tonalite determined from all testing programs. Table 5 presents the results of the UCS testing. P and S wave velocities are shown in Table 6 along the derived dynamic elastic moduli. Table 7 presents the results of the Brazilian testing.

Table 4: Average strength properties and elastic moduli for Biotite Granodiorite-Tonalite

Rock Type	UCS (MPa)	σ_{CI} (MPa)	σ_{CD} (MPa)	σ_T (MPa)	E_{40} (GPa)	ν_{40}
Average	220.5	87.5	172.8	10.6	71.9	0.197
Std. Dev.	6.3	3.1	8.4	1.2	1.5	0.020

The results of the six UCS tests on Biotite Granodiorite-Tonalite are very consistent and within the range of expected values. The average value for the UCS is 220 MPa (min = 214 MPa; max = 230 MPa). All specimens reached peak strength at an axial strain between 0.36% and 0.39%. Stress-strain graphs and photographs of intact and broken test specimens are shown in APPENDIX A.

Crack Damage (CD) and Crack Initiation (CI) thresholds, or stress levels, determined for all UCS tests carried out during the test program are shown in Table 5. Both crack initiation and crack damage thresholds (σ_{CI} and σ_{CD}) are well correlated with the UCS. Volumetric strain graphs were plotted against the axial stress, σ_1. These are presented in APPENDIX A, adjacent to stress-strain graphs and photographs of all intact and broken test specimens.

The following average relationships were obtained for the Biotite Granodiorite-Tonalite:

$$\sigma_{CI} = 0.40 \times UCS$$

$$\sigma_{CD} = 0.78 \times UCS$$

The results of the indirect tensile (Brazilian) strength tests on Biotite Granodiorite-Tonalite are also quite consistent, with an average value for the tensile strength (σ_T) of 10.6 MPa. Load-time and stress-displacement graphs, and photographs of all intact and broken test specimens are shown in APPENDIX C. The relationship between the Brazilian tensile strength and the UCS is as follows:

$$\sigma_T = 0.048 \times UCS$$

The correlation observed between the Young's modulus (E_{40}) and the UCS, both expressed in MPa, is as follows:

$$E_{40} = 326 \times UCS$$

This relationship fits in well with the expected values for granitic rocks (Hoek and Diederichs, 2006). The estimates of elastic moduli from the bench top dynamic testing are about 20% lower than those obtained from the UCS testing. This can be explained by the fact that the samples are in a stress-free state and open micro cracks would yield slower velocities than under a compressed state.

Table 5: Strength and Strain properties determined from UCS tests

Sample ID	Depth (m)[1]	Date Tested	UCS (MPa)	Young's Modulus (GPa)	Poisson's ratio	Axial Strain @ peak (%)	Max. Vol. Strain (%)	Crack Initiation Threshold (MPa)	Crack Damage Threshold (MPa)	Description of Failure Mode
IG_BH01_UC001	408.40	Mar-05-18	225.8	73.3	0.215	0.374	0.170	93.4	173.0	Massive[2], general shear over whole specimen length, vertical splitting
IG_BH01_UC002	442.01	Aug-16-19	230.2	70.5	0.208	0.393	0.186	88.3	186.9	Massive[2], general shear over whole specimen length, vertical splitting
IG_BH01_UC003	468.02	Mar-05-18	214.3	72.4	0.188	0.368	0.175	84.8	161.3	Massive[2], general shear over whole specimen length, vertical splitting
IG_BH01_UC004	522.64	Aug-19-19	214.6	70.5	0.161	0.362	0.185	86.0	173.4	Massive[2], general shear over whole specimen length, vertical splitting
IG_BH01_UC005	567.77	Mar-05-18	219.6	73.8	0.214	0.360	0.165	86.7	173.9	Massive[2], general shear over whole specimen length, vertical splitting
IG_BH01_UC006	600.72	Aug-19-19	218.4	70.7	0.198	0.379	0.180	85.8	168.3	Massive[2], general shear over whole specimen length, vertical splitting
IG_BH01_UC007[3]	450.79	Aug-27-19	208.9	64.4	0.154	0.400	0.204	85.7	162.2	Massive[2], general shear over whole specimen length, vertical splitting
IG_BH01_UC008[3]	559.94	Aug-27-19	242.4	59.1	0.299	0.505	0.196	100.7	165.6	Massive[2], shear band (60°), vertical splitting

Sample ID	Depth (m)[1]	Date Tested	UCS (MPa)	Young's Modulus (GPa)	Poisson's ratio	Axial Strain @ peak (%)	Max. Vol. Strain (%)	Crack Initiation Threshold (MPa)	Crack Damage Threshold (MPa)	Description of Failure Mode
IG_BH01_UC009[3]	655.01	Aug-27-19	83.4	47.4	0.098	0.212	0.160	N/A	N/A	Structural failure along discontinuity (62°)
IG_BH01_UC010[3]	658.31	Aug-28-19	194.3	74.5	0.136	0.337	0.184	82.8	167.4	Vertical splitting, secondary shear plane (70°) from bottom

[1]Top depth of prepared sub-sample

[2]Massive Failure indicates failure through intact rock

[3]Unpreserved samples. Samples were saturated before testing.

Table 6: Dynamic properties determined from UCS samples

Sample ID	Depth (m)[1]	Date Tested	P-wave Velocity (km/sec)	S-wave Velocity (km/sec)	Dynamic Young's Modulus (GPa)	Dynamic Shear Modulus (GPa)	Dynamic Poisson's ratio
IG_BH01_UC001	408.40	Mar-05-18	5.11	2.96	58.3	23.4	0.246
IG_BH01_UC002	442.01	Aug-16-19	4.49	2.71	47.8	19.7	0.213
IG_BH01_UC003	468.02	Mar-05-18	5.00	2.88	55.5	22.2	0.252
IG_BH01_UC004	522.64	Aug-19-19	4.78	2.87	53.9	22.2	0.216
IG_BH01_UC005	567.77	Mar-05-18	4.96	2.96	57.8	23.6	0.223
IG_BH01_UC006	600.72	Aug-19-19	4.41	2.70	47.1	19.7	0.198
IG_BH01_UC007[2]	450.79	Aug-27-19	4.27	2.65	45.2	19.1	0.186
IG_BH01_UC008[2]	559.94	Aug-27-19	4.09	2.42	38.7	15.7	0.232
IG_BH01_UC009[2]	655.01	Aug-27-19	5.06	2.93	62.3	25.0	0.246
IG_BH01_UC010[2]	658.31	Aug-28-19	5.93	3.33	83.6	32.9	0.269

[1]Top depth of prepared sub-sample

[2]Unpreserved samples. Samples were saturated before testing.

Table 7: Tensile strength determined from Brazilian tests

Sample ID	Depth (m)[1]	Date Tested	Failure Load (kN)	Tensile Strength (MPa)	Description of Failure Mode
IG_BH01_BR001	408.61	Mar-02-18	33.08	8.67	Perfectly diametral tensile splitting
IG_BH01_BR002	442.26	Aug-15-19	40.13	10.54	Perfectly diametral tensile splitting
IG_BH01_BR003	468.23	Mar-02-18	45.74	12.06	Perfectly diametral tensile splitting
IG_BH01_BR004	522.90	Aug-15-19	44.01	11.58	Perfectly diametral tensile splitting
IG_BH01_BR005	568.04	Mar-02-18	38.91	10.20	Perfectly diametral tensile splitting
IG_BH01_BR006	601.00	Aug-15-19	41.18	10.79	Perfectly diametral tensile splitting
IG_BH01_BR007[2]	451.06	Aug-28-19	40.97	10.76	Perfectly diametral tensile splitting
IG_BH01_BR008[2]	560.11	Aug-28-19	56.00	14.92	Perfectly diametral tensile splitting
IG_BH01_BR009[2]	655.46	Aug-28-19	40.59	10.65	Perfectly diametral tensile splitting
IG_BH01_BR010[2]	658.55	Aug-28-19	68.60	18.02	Perfectly diametral tensile splitting

[1]Top depth of prepared sub-sample

[2]Unpreserved samples. Samples were saturated before testing.

3.2.2 Thermal Results

Table 8 shows a summary of the average thermal properties between room temperature and 90°C or 100°C for each sample measured in the Hot Disk ThermTest TPS 1500, determined from all testing programs. Data for the individual tests and the full range of temperatures are included in APPENDIX D. Figure 6 through Figure 32 show plots of the results for the samples grouped by Biotite Granodiorite-Tonalite, Biotite Tonalite, Amphibolite, Aplite Dyke, and the Feldspar-phyric Tonalite Dyke. Results from the Hot Disk ThermTest TPS 1500 tests are within the ranges expected for the tested rock types and follow the expected trends with temperature (Robertson, 1988).

Table 8: Thermal properties determined from the Hot Disk ThermTest TPS 1500

Sample ID	Depth (m)[1]	Date Tested	Average Temperature (°C)	Average Volumetric Heat Capacity (MJ/m³°K)	Average Thermal Conductivity (W/m°K)	Average Thermal Diffusivity (mm²/sec)
IG_BH01_TH001[2]	299.74	Oct-02-19 to Oct-03-19	25.39	2.00	3.92	1.96
			40.19	2.11	3.75	1.78
			69.78	2.33	3.54	1.52
			99.38	2.38	3.32	1.40
IG_BH01_TH003[2]	352.98	Sep-30-19 to Oct-02-19	25.66	2.14	3.54	1.65
			40.16	2.17	3.37	1.55
			69.77	2.33	3.20	1.37
			99.37	2.49	2.98	1.20

Sample ID	Depth (m)[1]	Date Tested	Average Temperature (°C)	Average Volumetric Heat Capacity (MJ/m³°K)	Average Thermal Conductivity (W/m°K)	Average Thermal Diffusivity (mm²/sec)
IG_BH01_TH004[2]	401.71	Nov-27-19 to Nov-28-19	26.35	1.85	3.14	1.70
			40.17	1.88	3.09	1.65
			69.76	2.28	2.96	1.30
			99.36	2.18	2.82	1.30
IG_BH01_TH005[2]	421.80	Sep-13-19 to Sep-14-19	25.53	1.87	3.20	1.71
			40.17	1.98	3.16	1.59
			69.77	2.20	3.04	1.38
			99.37	2.26	2.94	1.30
IG_BH01_TH006[2]	448.64	Sep-19-19 to Sep-20-19	25.42	2.10	2.84	1.35
			40.17	2.13	2.75	1.29
			69.76	2.39	2.66	1.11
			99.36	2.36	2.56	1.08
IG_BH01_TH007[2]	450.50	Sep-20-19 to Sep-21-19	25.41	2.05	2.81	1.37
			40.17	2.12	2.75	1.30
			69.79	2.36	2.65	1.13
			99.36	2.36	2.54	1.08
IG_BH01_TH008[2]	456.86	Nov-25-19 to Nov-26-19	26.46	1.68	3.34	1.99
			40.17	1.70	3.23	1.90
			69.78	1.98	3.15	1.59
			99.37	2.02	3.01	1.49
IG_BH01_TH009[2]	501.76	Sep-23-19 to Sep-24-19	25.40	1.86	3.42	1.84
			40.17	2.03	3.37	1.67
			69.78	2.26	3.25	1.44
			99.37	2.33	3.11	1.34
IG_BH01_TH010[2]	530.30	Oct-04-19 to Oct-05-19	25.42	2.08	3.74	1.80
			40.18	2.17	3.53	1.63
			69.76	2.38	3.32	1.40
			99.38	2.45	3.18	1.30
IG_BH01_TH011[2]	555.97	Sep-16-19 to Sep-17-19	25.46	2.14	3.72	1.74
			40.18	2.19	3.59	1.64
			69.76	2.34	3.41	1.45
			99.37	2.35	3.24	1.38

Sample ID	Depth (m)[1]	Date Tested	Average Temperature (°C)	Average Volumetric Heat Capacity (MJ/m³°K)	Average Thermal Conductivity (W/m°K)	Average Thermal Diffusivity (mm²/sec)
IG_BH01_TH012[2]	560.36	Sep-27-19 to Sep-28-19	25.59	2.09	2.59	1.24
			40.17	2.21	2.56	1.16
			69.77	2.22	2.38	1.07
			99.37	2.34	2.28	0.98
IG_BH01_TH013[2]	603.56	Sep-25-19 to Sep-26-19	25.39	1.97	3.49	1.77
			40.17	2.06	3.38	1.64
			69.77	2.31	3.23	1.40
			99.37	2.27	3.07	1.36
IG_BH01_TH014[2]	657.97	Nov-07-19 to Nov-08-19	26.36	2.15	2.50	1.17
			40.16	2.28	2.49	1.09
			69.76	2.32	2.47	1.07
			99.35	2.48	2.44	0.98
IG_BH01_TH017[3]	402.05	Apr-26-21	20.01	2.01	3.08	1.53
			40.01	2.06	3.03	1.47
			60.04	2.21	3.03	1.37
			79.95	2.29	2.99	1.30
			90.02	2.29	2.97	1.30
			60.05[4]	2.20	3.01	1.37
IG_BH01_TH020[3]	451.68	May-14-21	20.01	2.04	2.53	1.24
			40.01	2.15	2.51	1.17
			60.05	2.28	2.52	1.10
			79.94	2.33	2.52	1.08
			90.02	2.35	2.51	1.07
			60.03[4]	2.29	2.51	1.10
IG_BH01_TH021[3]	457.17	May-17-21	20.00	2.08	3.32	1.60
			40.00	2.15	3.28	1.53
			60.05	2.33	3.26	1.40
			79.94	2.37	3.22	1.36
			90.04	2.45	3.18	1.30
			60.07[4]	2.31	3.24	1.41
IG_BH01_TH024[3]	556.28	May-19-21	20.00	1.85	3.10	1.68
			40.01	1.94	3.06	1.57

Sample ID	Depth (m)[1]	Date Tested	Average Temperature (°C)	Average Volumetric Heat Capacity (MJ/m³°K)	Average Thermal Conductivity (W/m°K)	Average Thermal Diffusivity (mm²/sec)
			60.05	2.06	3.04	1.47
			79.94	2.12	3.01	1.42
			90.03	2.20	2.98	1.36
			60.07[4]	2.09	3.02	1.44
IG_BH01_TH025[3]	561.31	May-21-21	20.00	2.09	2.23	1.07
			40.01	2.19	2.22	1.01
			60.06	2.31	2.23	0.97
			79.94	2.36	2.22	0.94
			90.04	2.46	2.21	0.90
			60.04[4]	2.34	2.20	0.94
IG_BH01_TH026[3]	603.95	May-24-21	20.00	2.18	3.35	1.54
			39.99	2.28	3.29	1.44
			60.05	2.41	3.26	1.36
			79.95	2.50	3.21	1.28
			90.03	2.51	3.19	1.27
			60.05[4]	2.39	3.26	1.37
IG_BH01_TH027[3]	657.67	May-26-21	20.00	2.27	2.80	1.24
			40.01	2.38	2.78	1.17
			60.05	2.51	2.78	1.11
			79.96	2.58	2.74	1.06
			90.04	2.66	2.74	1.03
			60.05[4]	2.48	2.77	1.12

[1]Top depth of prepared sub-sample

[2]Unpreserved samples. Samples were saturated before testing

[3]Unpreserved samples. Samples were dried at 80°C before testing

[4]Measurement to check hysteresis taken at 60°C while cooling; not used for the curve fitting of individual tests

In general, it is observed that:

- The Volumetric Heat Capacity (C_v) data show that the values increase with an increase in temperature but not in a purely linear manner. There appears to be a slightly decreasing rate of change in C_v with increasing temperature, but the data can be described reasonably using a simple linear regression plot.
- The Thermal Conductivity (k) data shows that the values decrease with an increase in temperature, also not in a purely linear fashion. For the purpose of predicting thermal behaviour a linear fit, which provides a reasonable approximation, can be used for this temperature range.

- The Thermal Diffusivity (κ) (parameter derived from the conductivity and heat capacity), shows that the values decrease with an increase in temperature, which is a result of a combination of the trends in the conductivity and heat capacity. A linear fit, which provides a reasonable approximation for this temperature range, can be used.

Best fits for the measurements grouped by rock type included measurement at 60°C while cooling.

Specifically for the Biotite Granodiorite-Tonalite rock:

The Volumetric Heat Capacity (C_v) data collected for eight (8) water-saturated and four (4) dry specimens all show that C_v values increase with an increase in temperature (θ) but not in a purely linear manner (Figure 6 and Figure 7), There appears to be a slightly decreasing rate of change in C_v with increasing temperature, but the data can be described reasonably using a simple linear regression plot. Seven of the eight tests completed on water-saturated samples shown in Figure 6 show very consistent C_v versus temperature results and can be described to within approximately 10% by a single regression line. The data for dry specimens was essentially identical to that obtained for the water-saturated specimens.

The Thermal Conductivity (k) data for the eight (8) water-saturated specimens (Figure 8) shows that the values decrease with an increase in temperature, also not in a purely linear fashion. Dry specimens show a similar trend but much less marked and exhibit notably lower k values than observed for saturated materials from similar depth (Figure 9). The data for dry rock specimens shows a lower k than for the saturated materials and also a very limited effect of temperature on the k, indicating the importance of porewater on the thermal transport properties (conductivity and diffusivity). For the purpose of predicting thermal behaviour a linear fit, which provides a reasonable approximation, is provided in the graphs.

The Thermal Diffusivity (κ) for Biotite Granodiorite-Tonalite rock is a parameter measured concurrent with the conductivity and heat capacity data presented in Figure 6 through Figure 9. The κ values show a decrease with an increase in temperature, which is a result of a combination of the trends in the conductivity and heat capacity. The data also shows a lower κ for the dry samples than for the saturated samples from similar depth, which is a direct consequence of the lower k values for the dry samples. A linear fit is shown in the graphs, which provides a reasonable approximation for this temperature range.

Note that the sample depths in the graph legends refer to the depth of the original sample as collected (part of the id), not the depth of the sub-samples.

A summary of the equations describing Cv, k and κ are provided in Table 9.

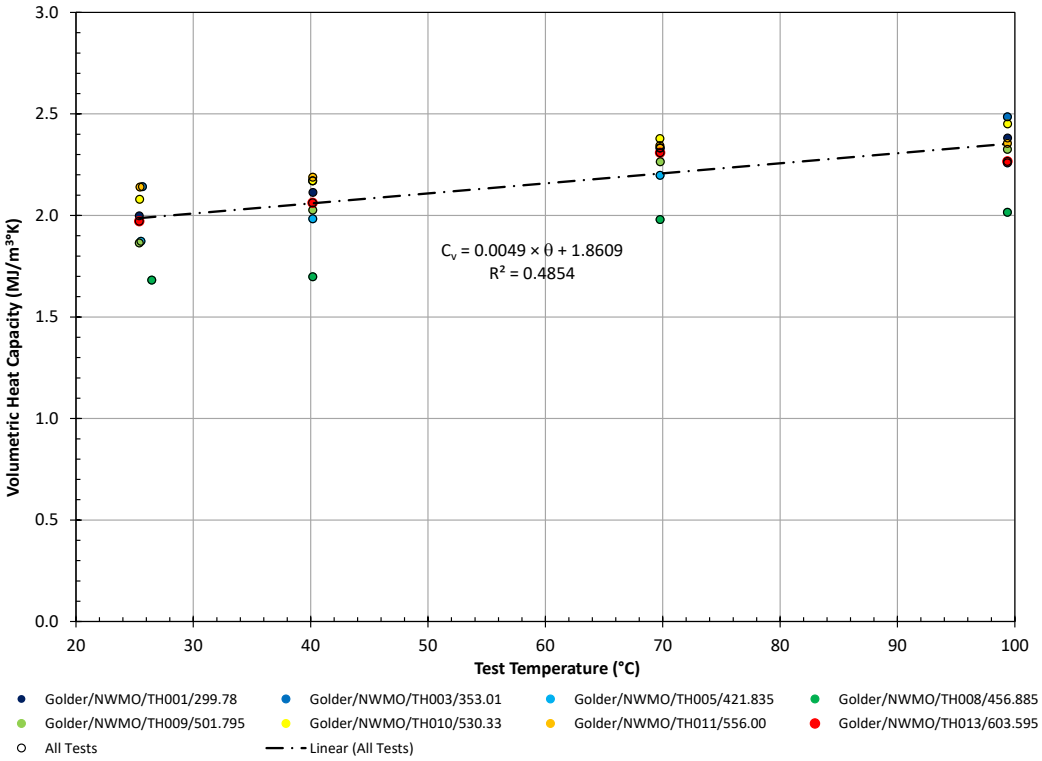


Figure 6: Volumetric heat capacity for saturated samples of Biotite Granodiorite-Tonalite as a function of temperature.

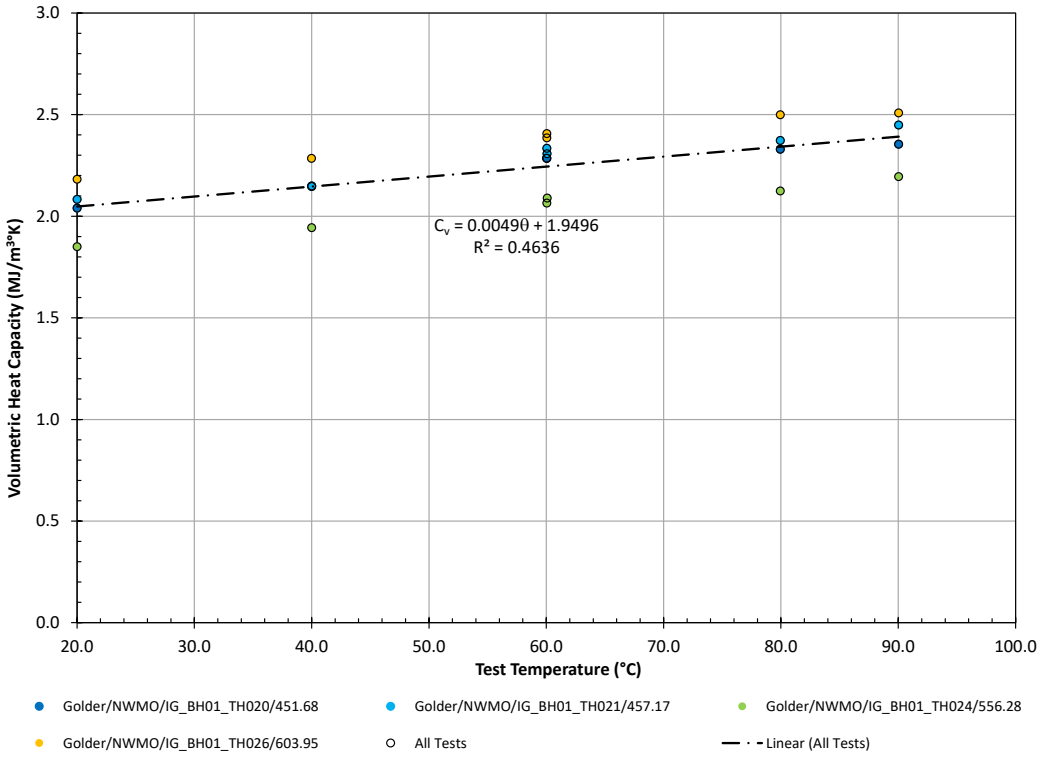


Figure 7: Volumetric heat capacity for dry samples of Biotite Granodiorite-Tonalite as a function of temperature.

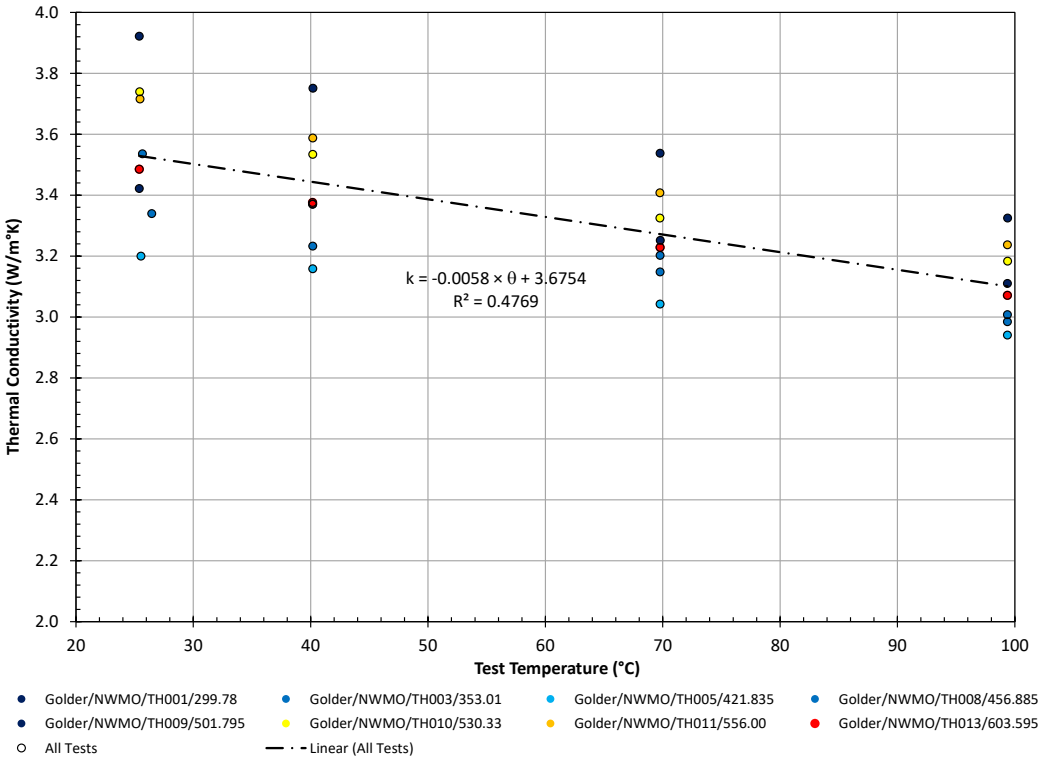


Figure 8: Thermal conductivity for saturated samples of Biotite Granodiorite-Tonalite as a function of temperature

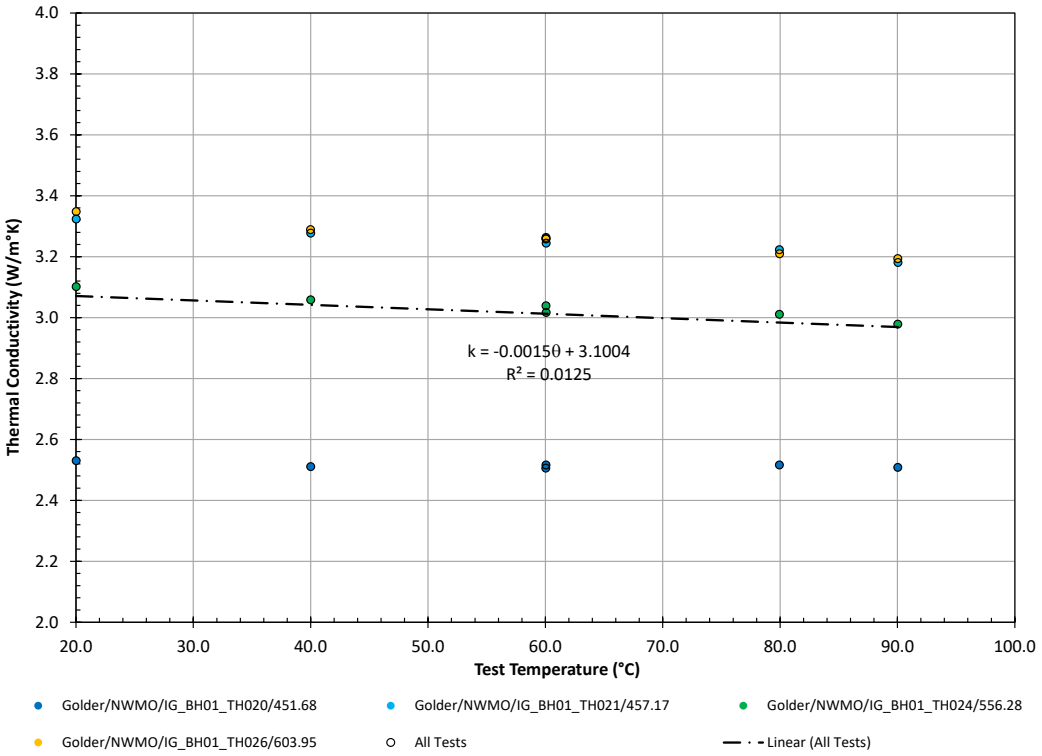


Figure 9: Thermal conductivity for dry samples of Biotite Granodiorite-Tonalite as a function of temperature

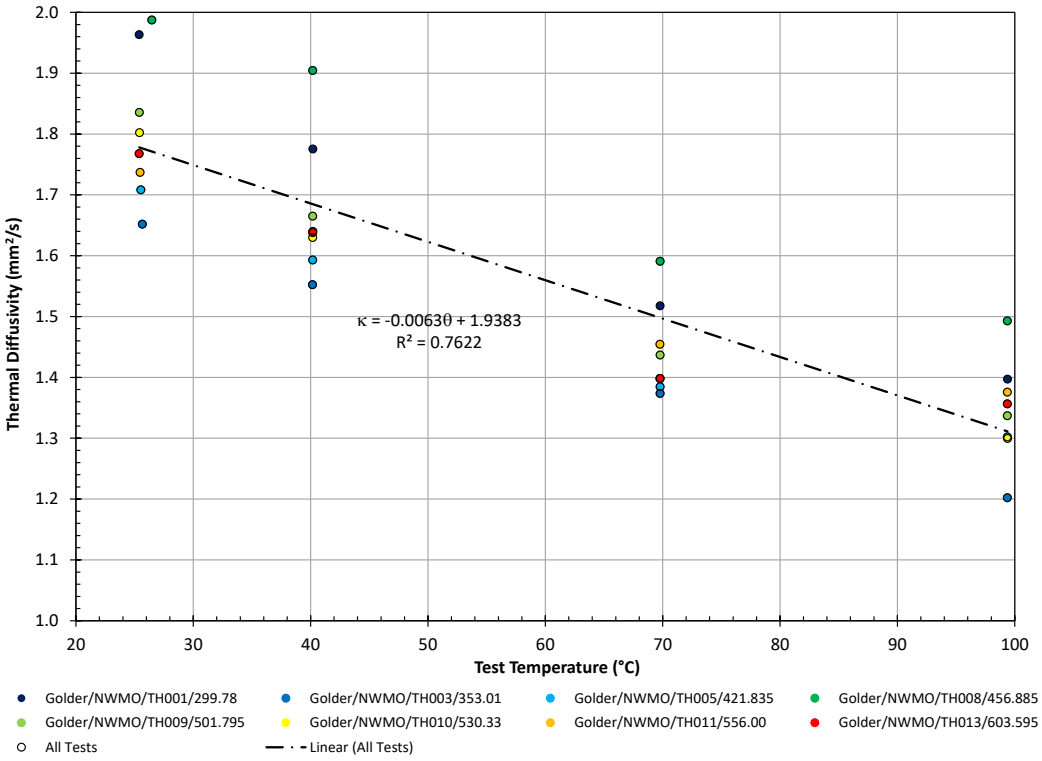


Figure 10: Thermal diffusivity for saturated samples of Biotite Granodiorite-Tonalite as a function of temperature

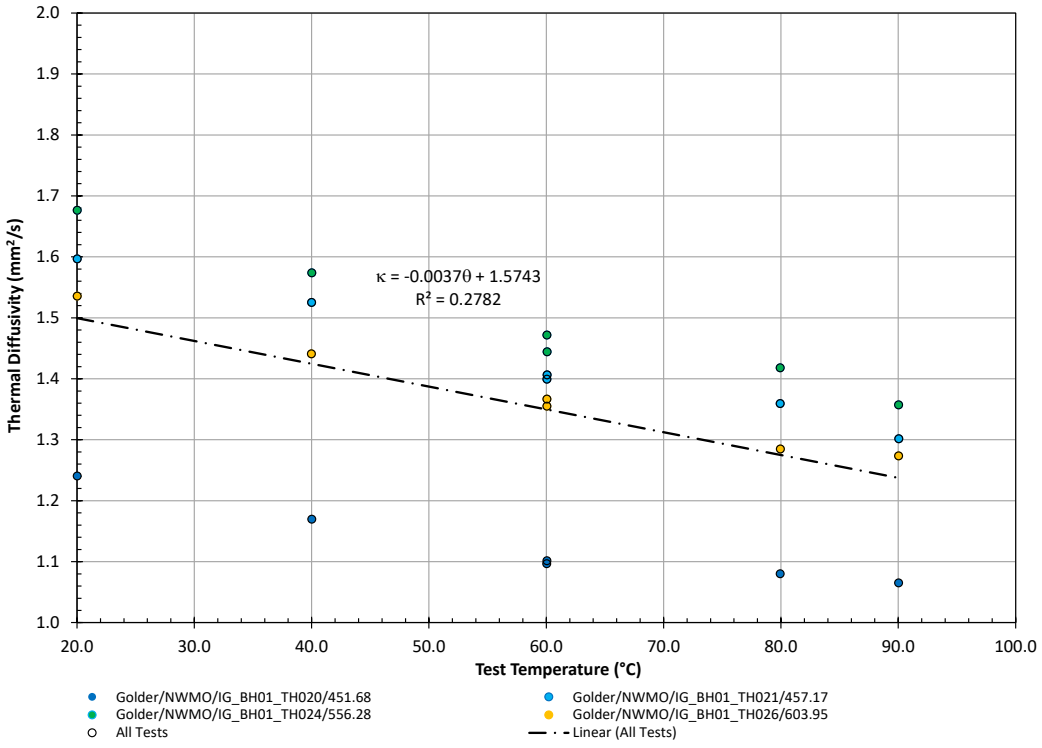


Figure 11: Thermal diffusivity for dry samples of Biotite Granodiorite-Tonalite as a function of temperature

Specifically for Biotite Tonalite

The rock termed Biotite-rich Tonalite is described in the WP3 Data Report – Geological and Geotechnical Core Logging, Photography and Sampling for IG_BH01 (Golder, 2018) and, as it is discernibly different from the Biotite Tonalite, its thermal properties are discussed separately. Two water-saturated samples of the Biotite Tonalite were tested to determine the thermal properties of this material.

The Volumetric Heat Capacity (C_v) for saturated rock shown in Figure 12 is essentially identical to that observed for the Biotite Granodiorite-Tonalite samples.

The Thermal Conductivity (k) for saturated rock shown in Figure 13 is notably higher than was observed for the Biotite Tonalite samples.

The Thermal Diffusivity (κ) for saturated rock shown in Figure 14 is notably lower than was observed for the Biotite Tonalite samples.

The thermal properties of the water-saturated Biotite Granodiorite Tonalite (Figure 6, Figure 8 and Figure 10) and the water-saturated Biotite Tonalite (Figure 12 through Figure 14) are notably different. While their volumetric heat capacities are essentially identical, their k and κ properties are different (lower for a given temperature).

Note that the sample depths in the graph legends refer to the depth of the original sample as collected (part of the id), not the sub-samples.

A summary of the equations describing Cv, k and κ are provided in Table 9.

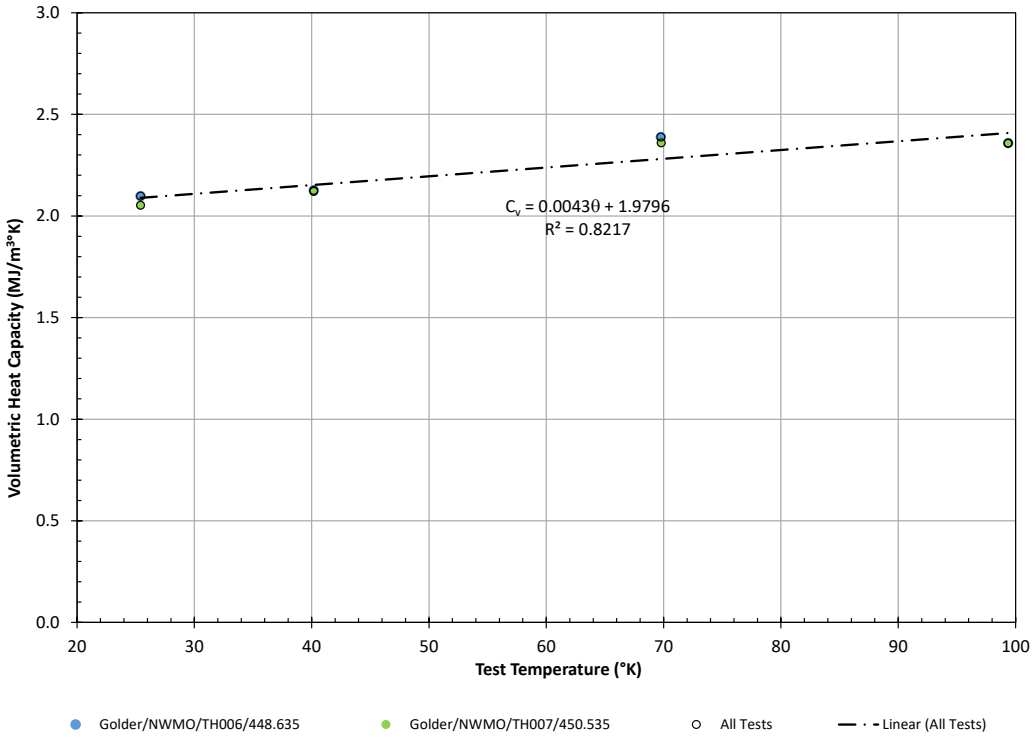


Figure 12: Volumetric heat capacity for saturated samples of Biotite Tonalite as a function of temperature.

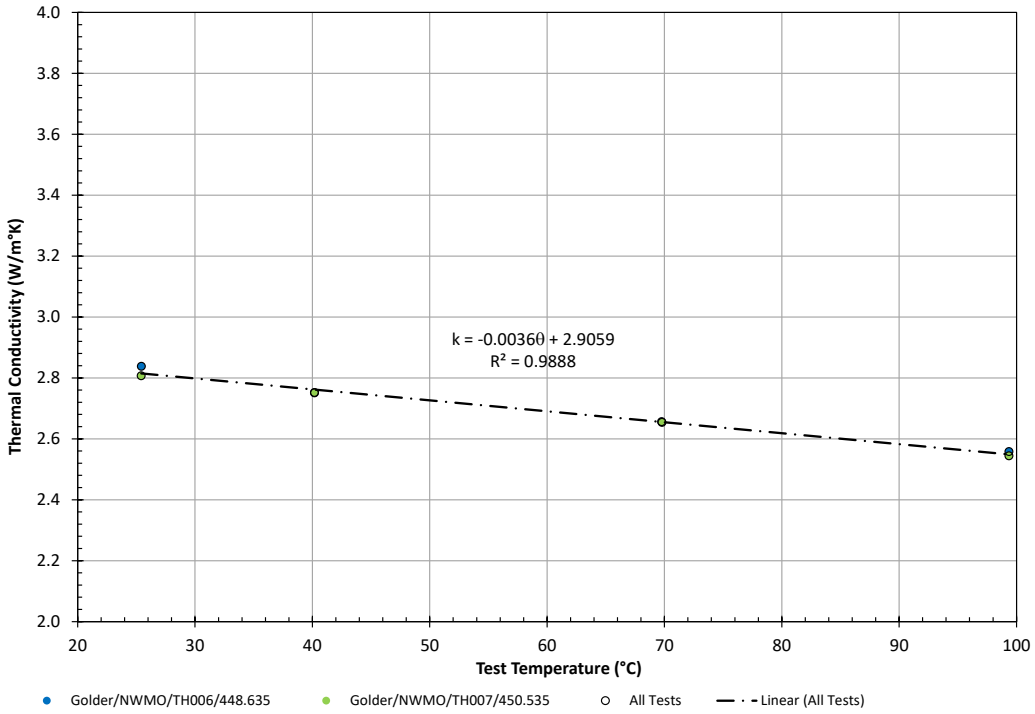


Figure 13: Thermal conductivity for saturated samples of Biotite Tonalite as a function of temperature

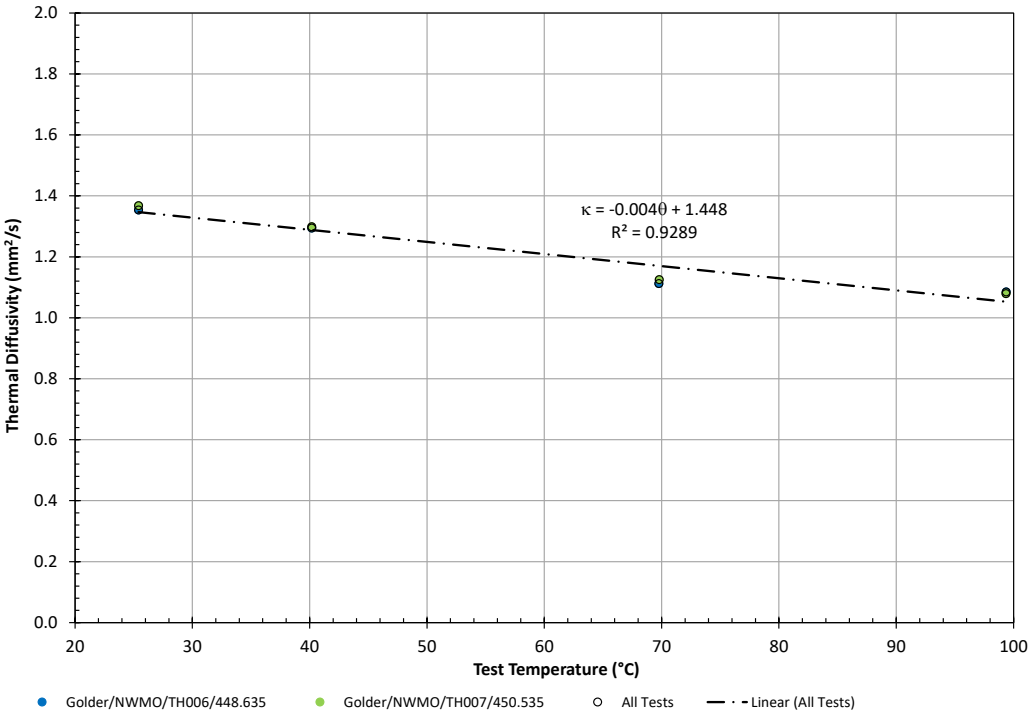


Figure 14: Thermal diffusivity for saturated samples of Biotite Tonalite as a function of temperature

Specifically for Amphibolite

The rock termed Amphibolite is described in the WP3 Data Report – Geological and Geotechnical Core Logging, Photography and Sampling for IG_BH01 (Golder, 2018). One water-saturated and one dry sample of the Amphibolite rock were tested to determine the thermal properties of this material.

The Volumetric Heat Capacity (C_v) of saturated and dry sample are presented in Figure 15 and Figure 16, respectively.

The Thermal Conductivity (k) of saturated and dry sample are presented in Figure 17 and Figure 18, respectively.

The Thermal Diffusivity (κ) of saturated and dry sample are presented in Figure 19 and Figure 20, respectively.

Note that the sample depths in the graph legends refer to the depth of the original sample as collected (part of the id), not the sub-samples.

The equations describing the thermal properties of the Amphibolite are summarized in Table 9.

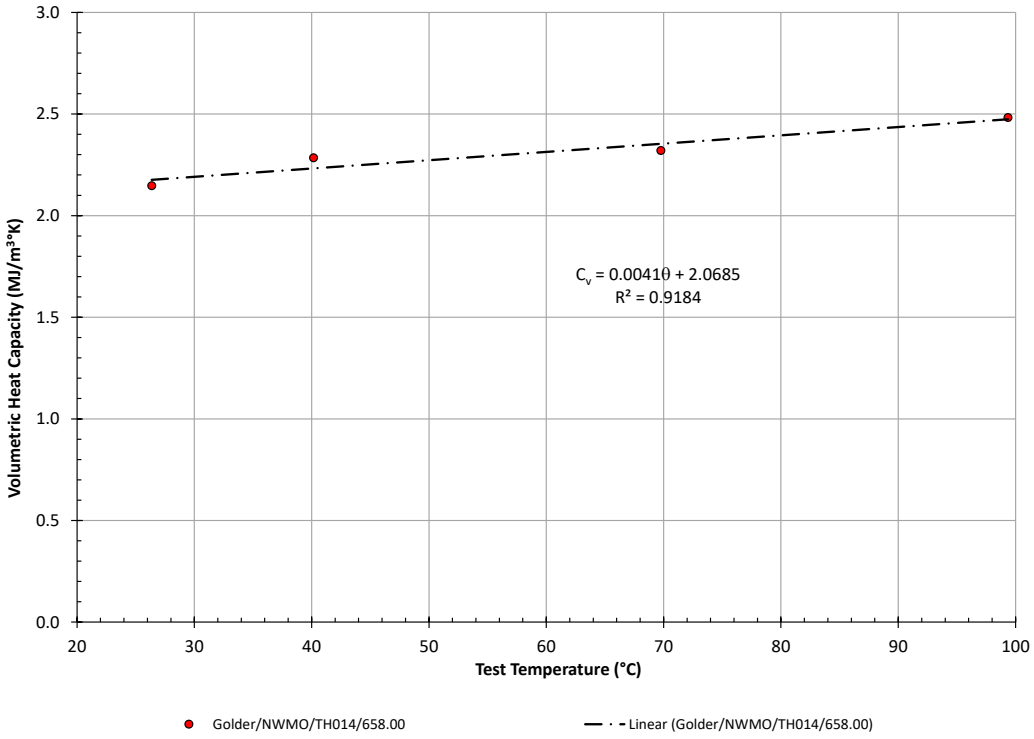


Figure 15: Volumetric heat capacity for saturated sample of Amphibolite as a function of temperature

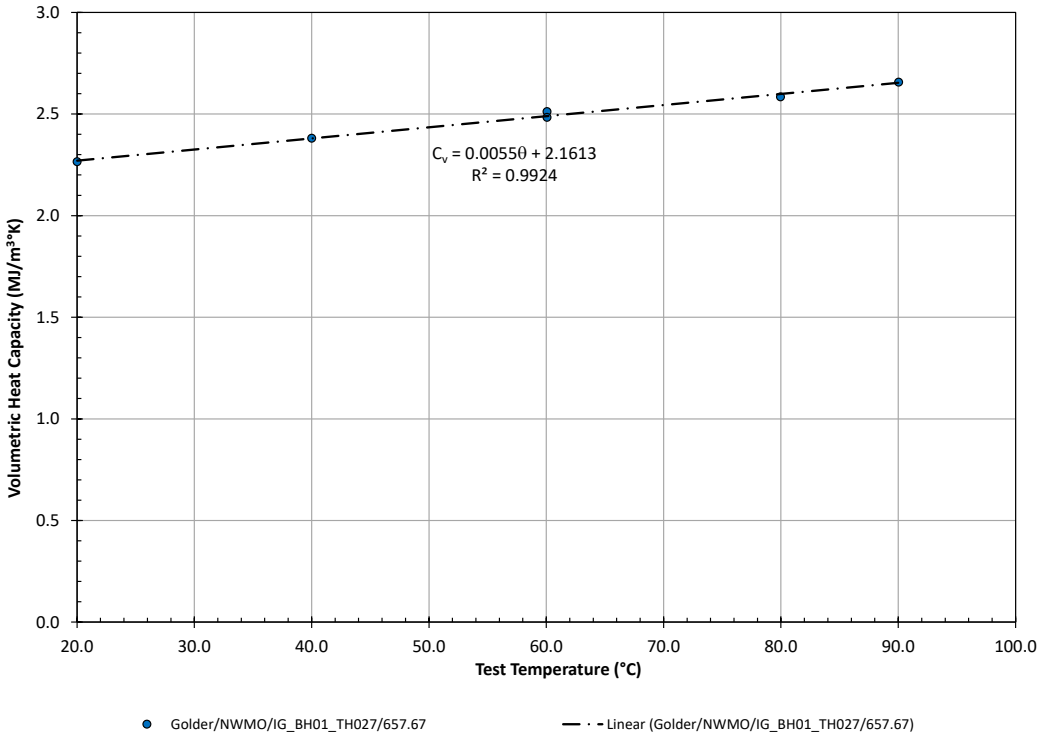


Figure 16: Volumetric heat capacity for dry sample of Amphibolite as a function of temperature

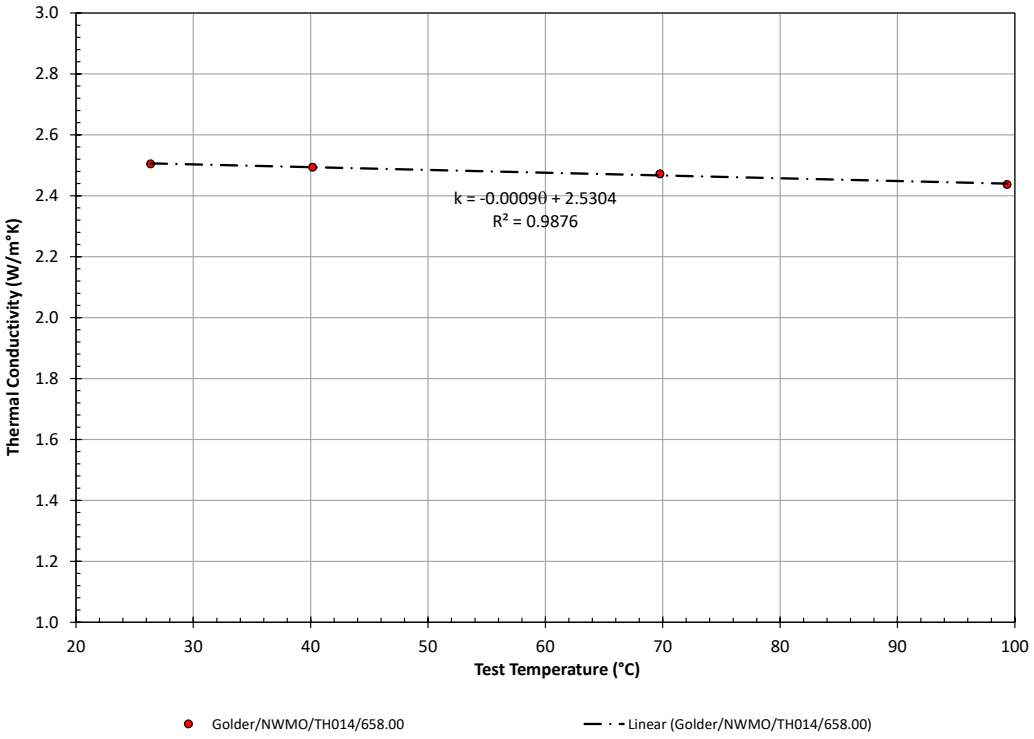


Figure 17: Thermal conductivity for saturated sample of Amphibolite as a function of temperature

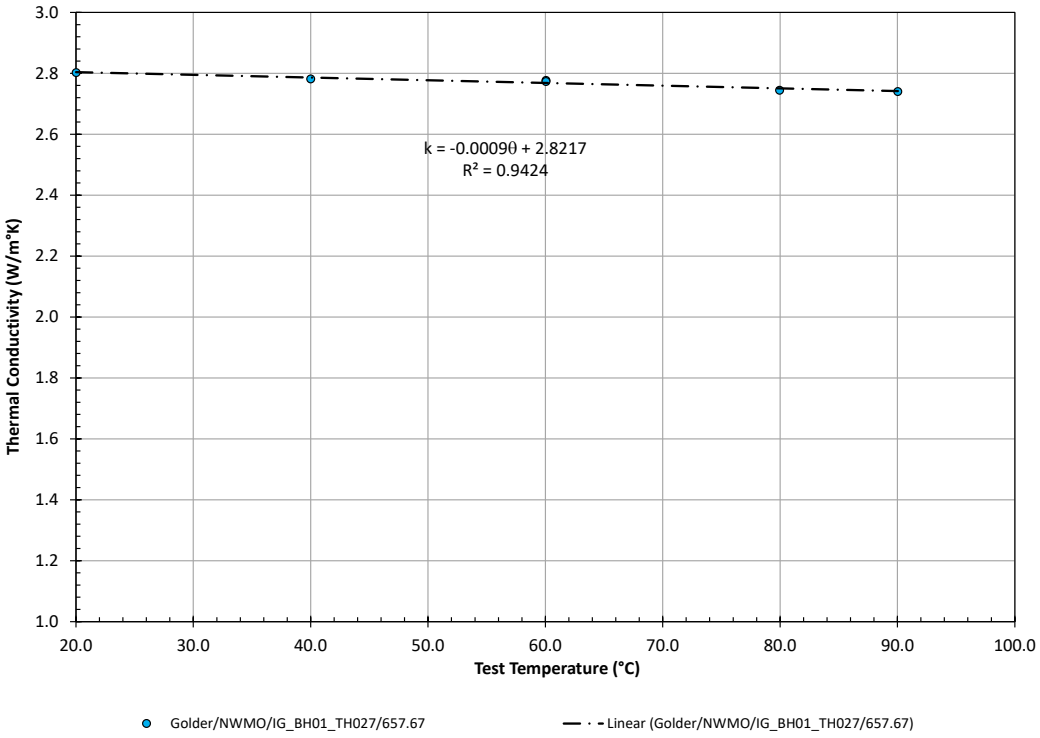


Figure 18: Thermal conductivity for dry sample of Amphibolite as a function of temperature

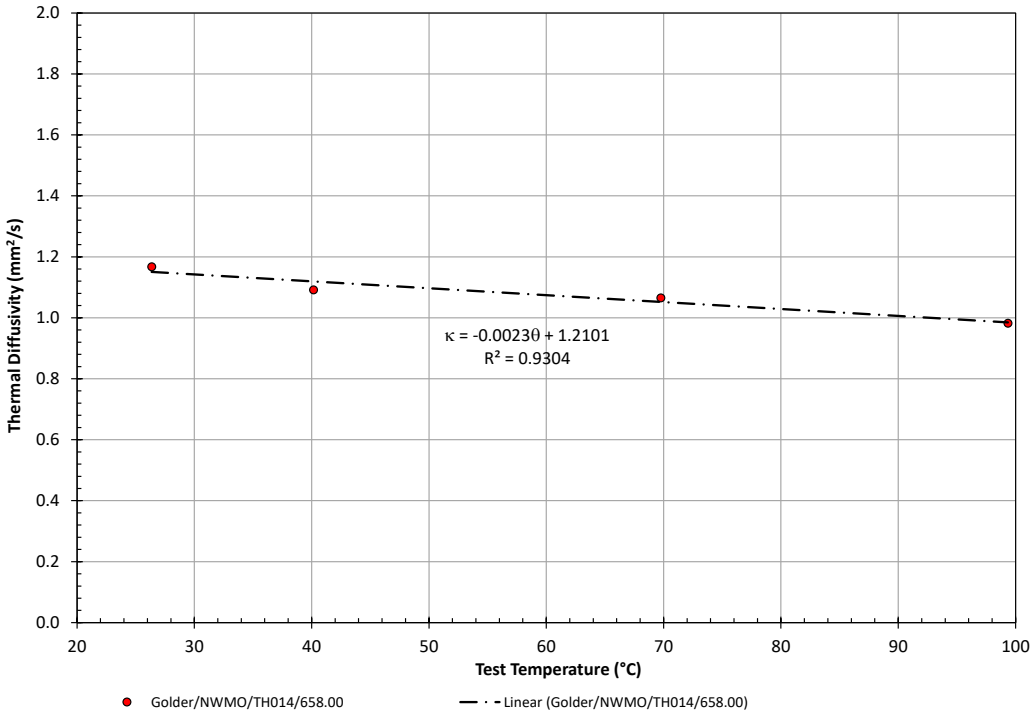


Figure 19: Thermal diffusivity for saturated sample of Amphibolite as a function of temperature

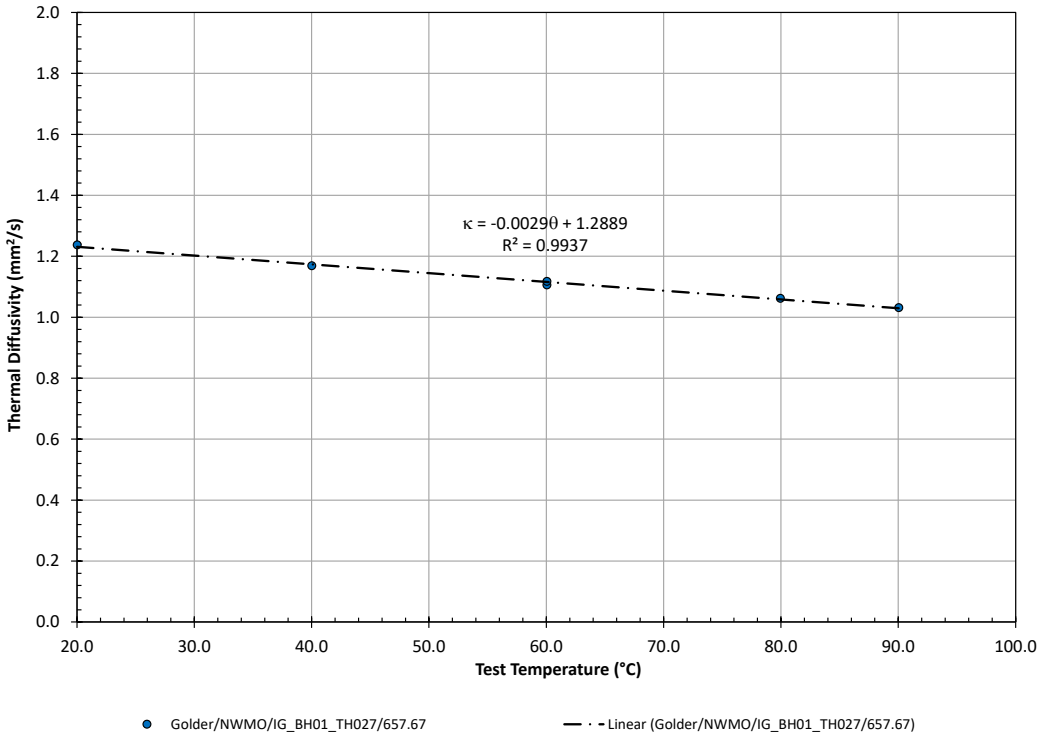


Figure 20: Thermal diffusivity for dry sample of Amphibolite as a function of temperature

Specifically for Aplite Dyke

The rock termed Aplite Dyke is described in the WP3 Data Report – Geological and Geotechnical Core Logging, Photography and Sampling for IG_BH01 (Golder, 2018) and as it is discernibly different than the other rock types described previously. One water-saturated and one dry sample of the Aplite Dyke rock were tested to determine the thermal properties of this material.

The Volumetric Heat Capacity (C_v) of saturated and dry sample are presented in Figure 21 and Figure 22, respectively.

The Thermal Conductivity (k) of saturated and dry sample are presented in Figure 23 and Figure 24, respectively.

The Thermal Diffusivity (κ) of saturated and dry sample are presented in Figure 25 and Figure 26, respectively.

Note that the sample depths in the graph legends refer to the depth of the original sample as collected (part of the id), not the sub-samples.

The equations describing the thermal properties of the Aplite Dyke rock are provided in Table 9.

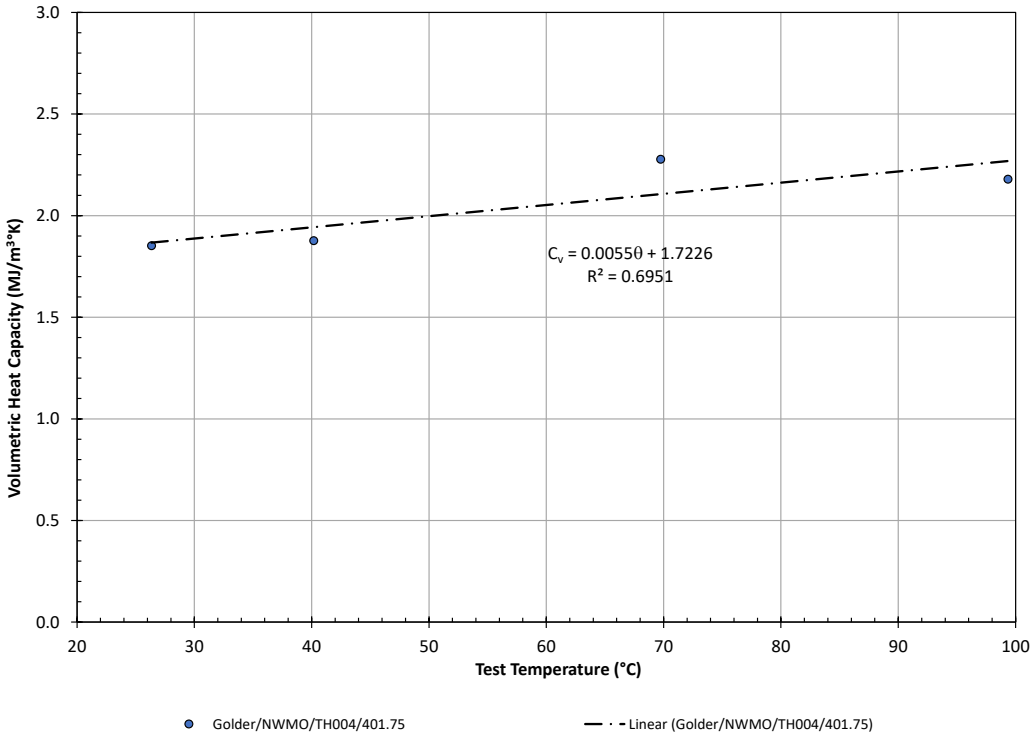


Figure 21: Volumetric heat capacity for saturated sample of Aplite Dyke as a function of temperature

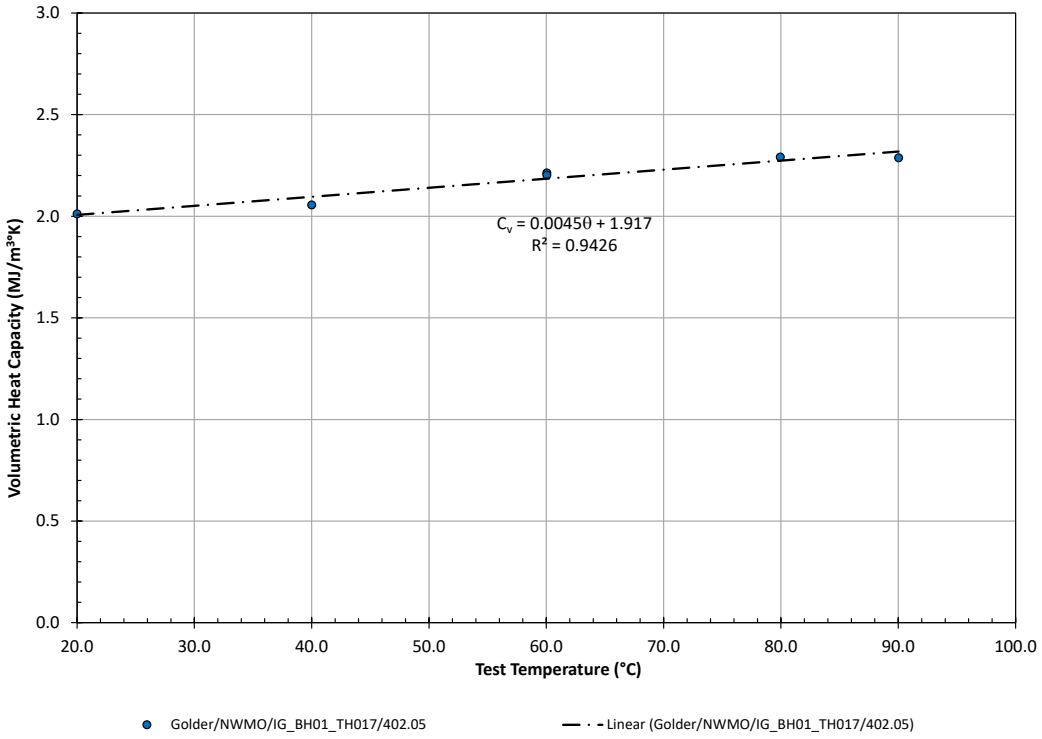


Figure 22: Volumetric heat capacity for dry sample of Aplite Dyke as a function of temperature

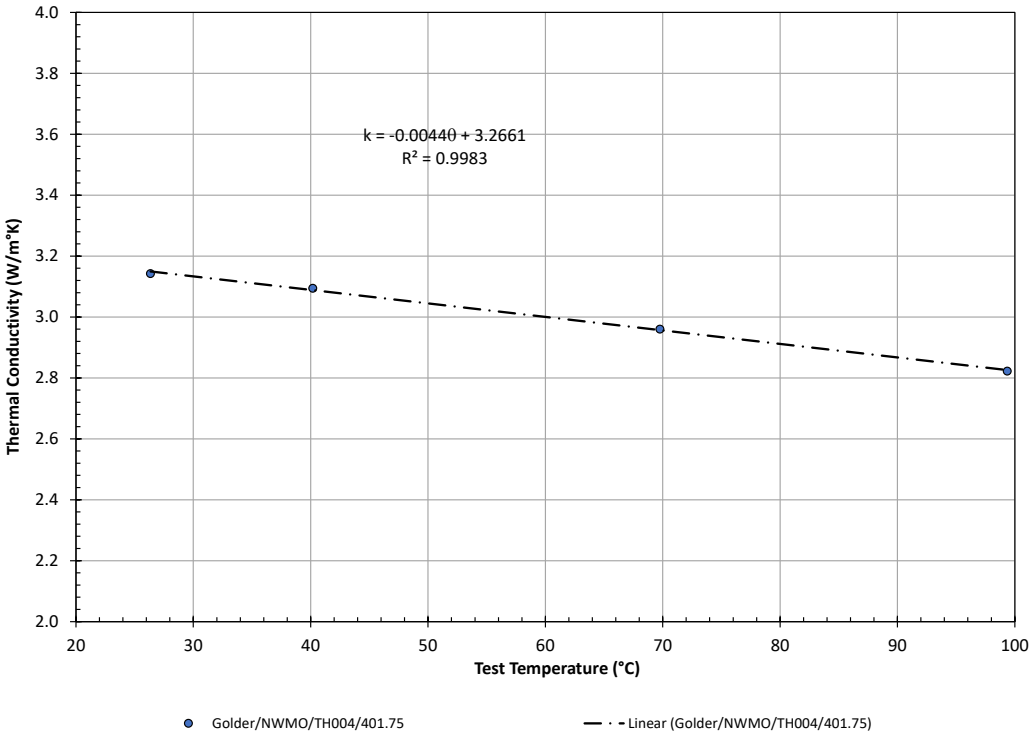


Figure 23: Thermal conductivity for saturated sample of Aplite Dyke as a function of temperature

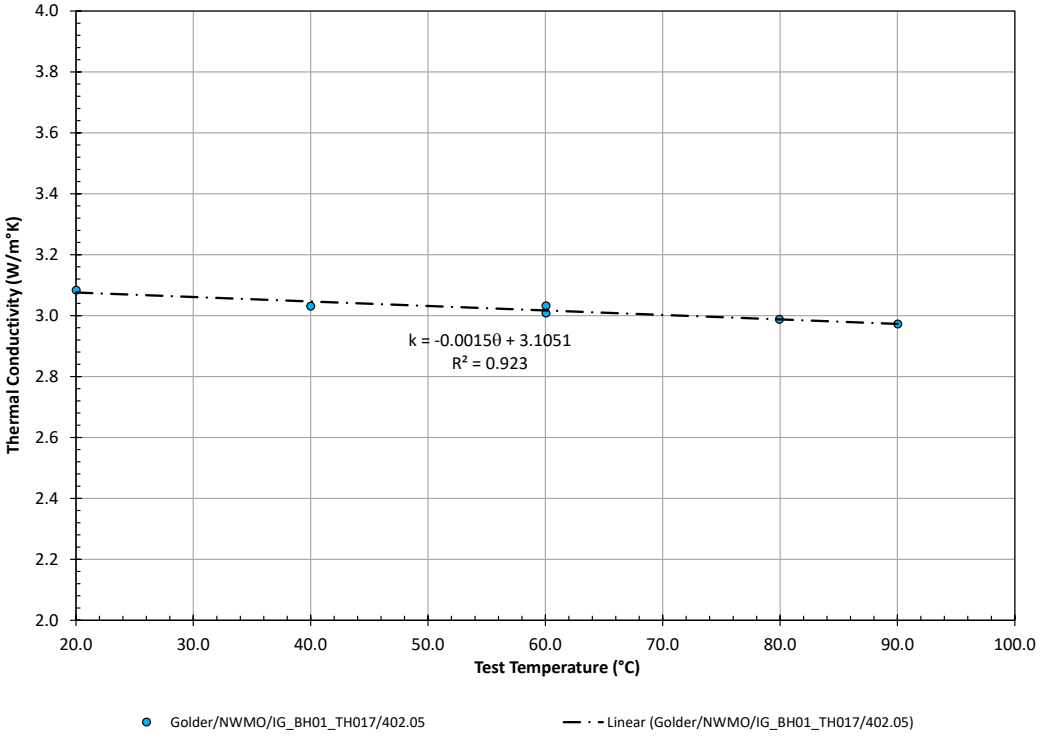


Figure 24: Thermal conductivity for dry sample of Aplite Dyke as a function of temperature

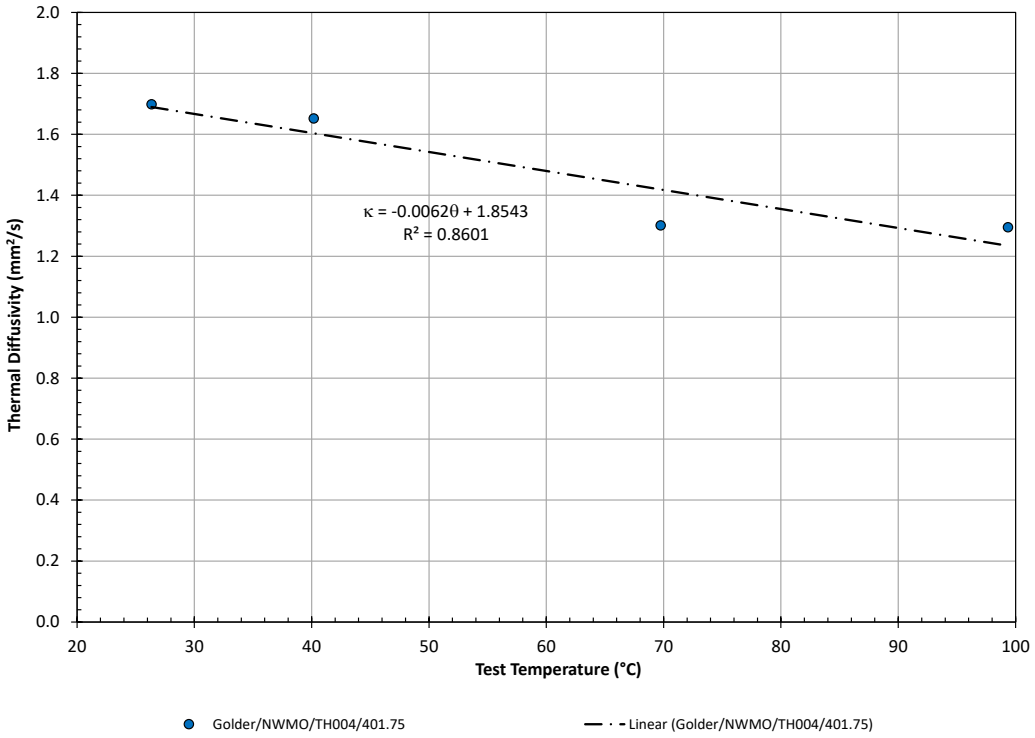


Figure 25: Thermal diffusivity for saturated sample of Aplite Dyke as a function of temperature

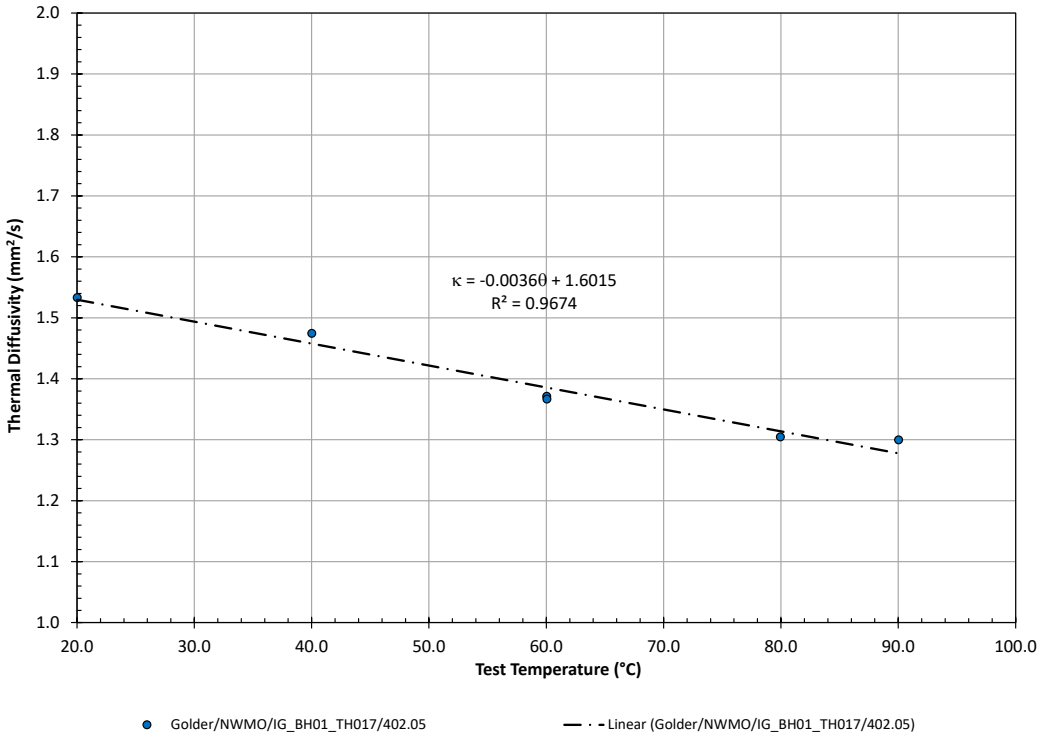


Figure 26: Thermal diffusivity for dry sample of Aplite Dyke as a function of temperature

Specifically for Feldspar-phyric Tonalite Dyke rock

The rock termed Feldspar-phyric Tonalite Dyke is described in the WP3 Data Report – Geological and Geotechnical Core Logging, Photography and Sampling for IG_BH01 (Golder, 2018) and as it is discernibly different than the other rock types described previously. One water-saturated and one dry sample of the Feldspar-phyric Tonalite Dyke rock were tested to determine the thermal properties of this material.

The Volumetric Heat Capacity (C_v) of saturated and dry sample are presented in Figure 27 and Figure 28, respectively.

The Thermal Conductivity (k) of saturated and dry sample are presented in Figure 29 and Figure 30, respectively.

The Thermal Diffusivity (κ) of saturated and dry sample are presented in Figure 31 and Figure 32, respectively.

Note that the sample depths in the graph legends refer to the depth of the original sample as collected (part of the id), not the sub-samples.

The equations describing the thermal properties of the Feldspar-phyric Tonalite Dyke rock are provided in Table 9.

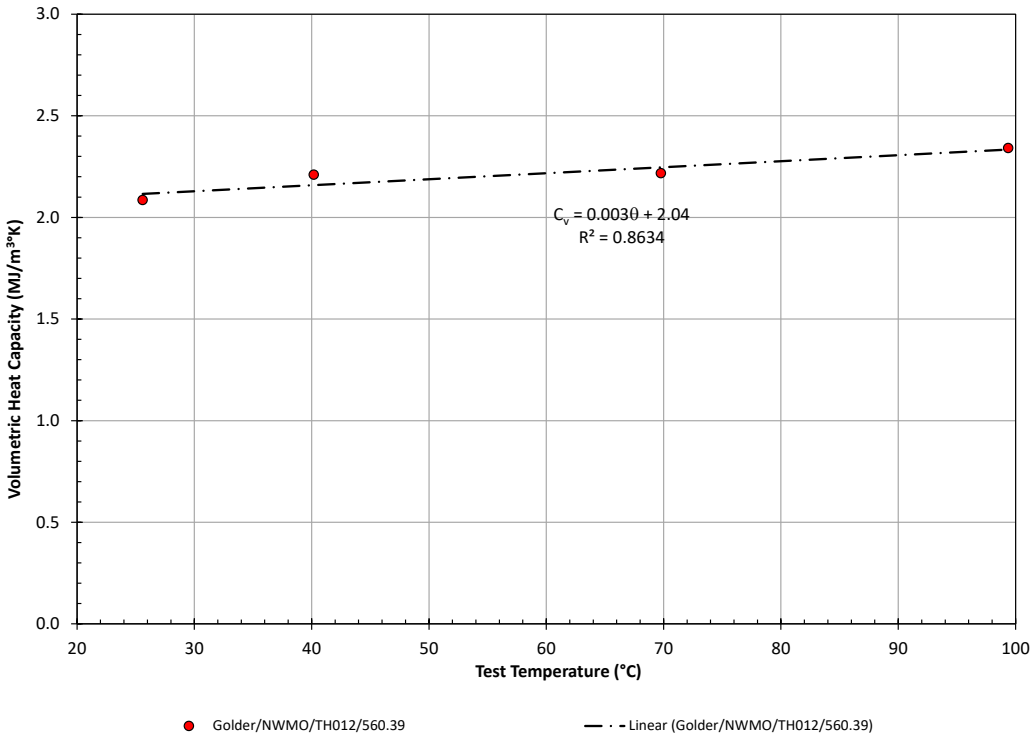


Figure 27: Volumetric heat capacity for saturated sample of Feldspar-phyric Tonalite Dyke as a function of temperature

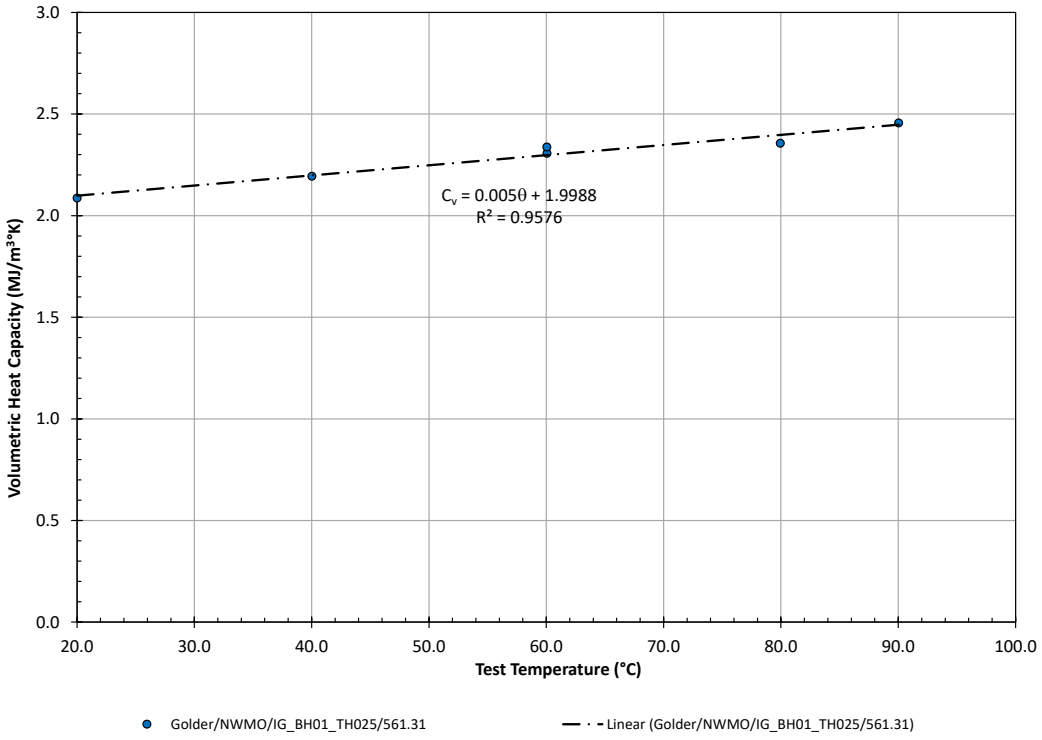


Figure 28: Volumetric heat capacity for dry sample of Feldspar-phyric Tonalite Dyke as a function of temperature

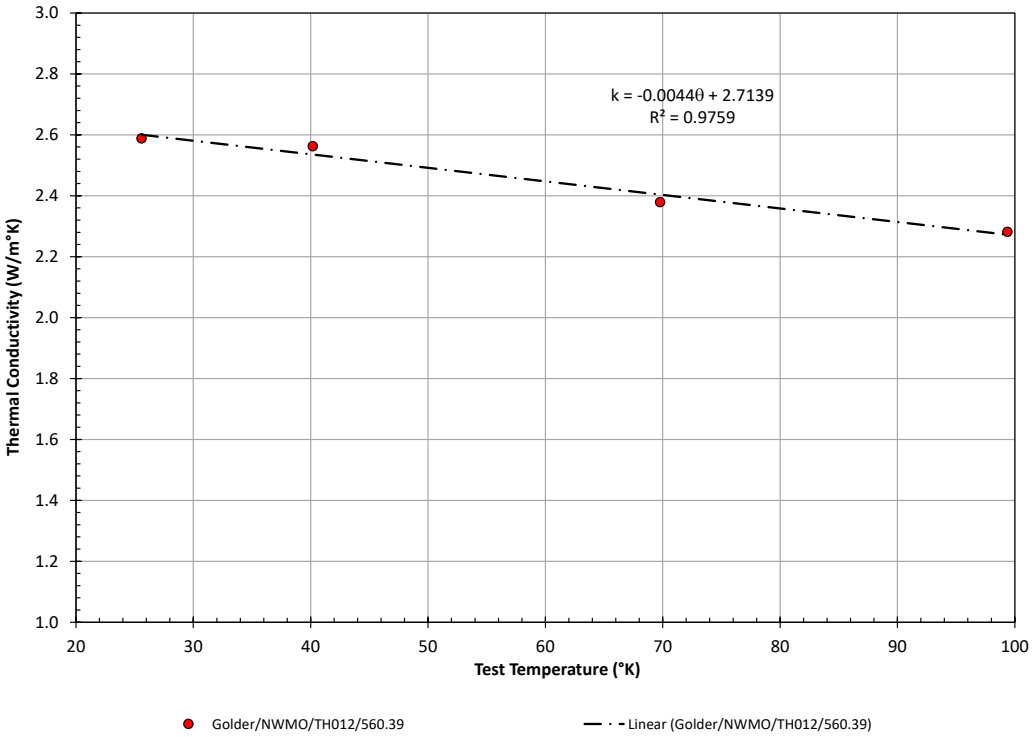


Figure 29: Thermal conductivity for saturated sample of Feldspar-phyric Tonalite Dyke as a function of temperature

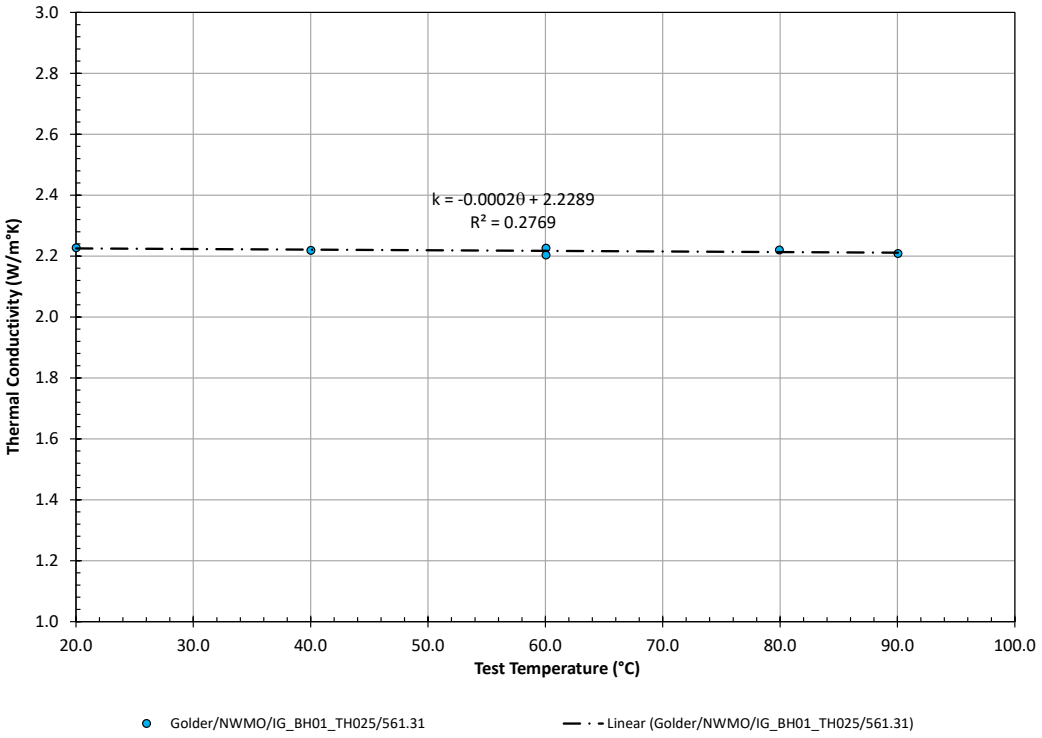


Figure 30: Thermal conductivity for dry sample of Feldspar-phyric Tonalite Dyke as a function of temperature

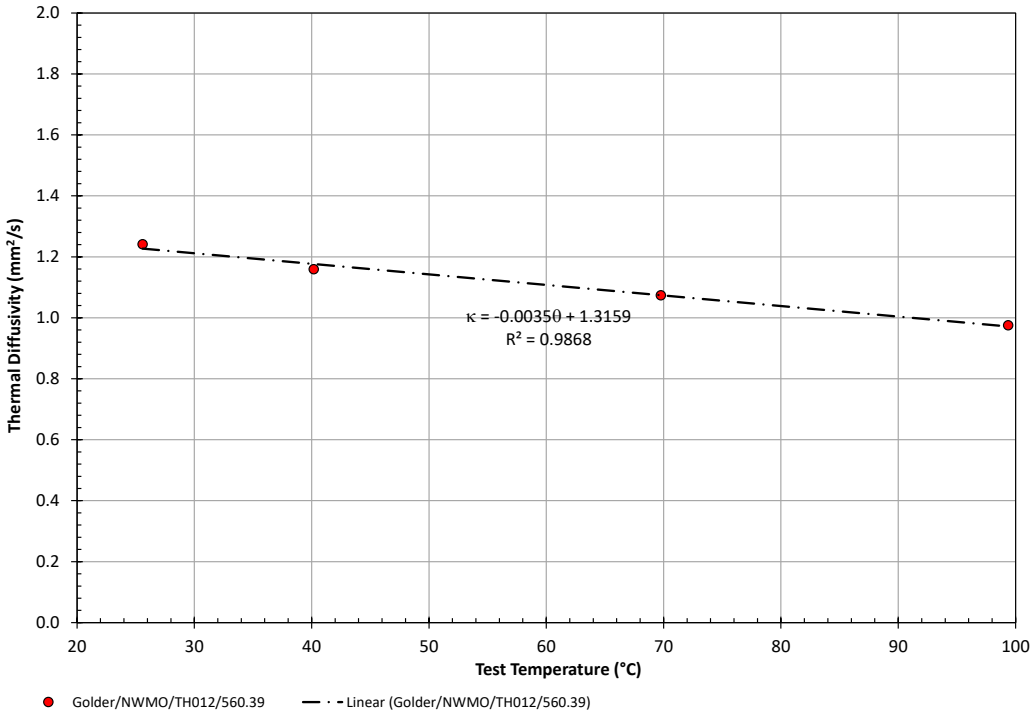


Figure 31: Thermal diffusivity for saturated sample of Feldspar-phyric Tonalite Dyke as a function of temperature

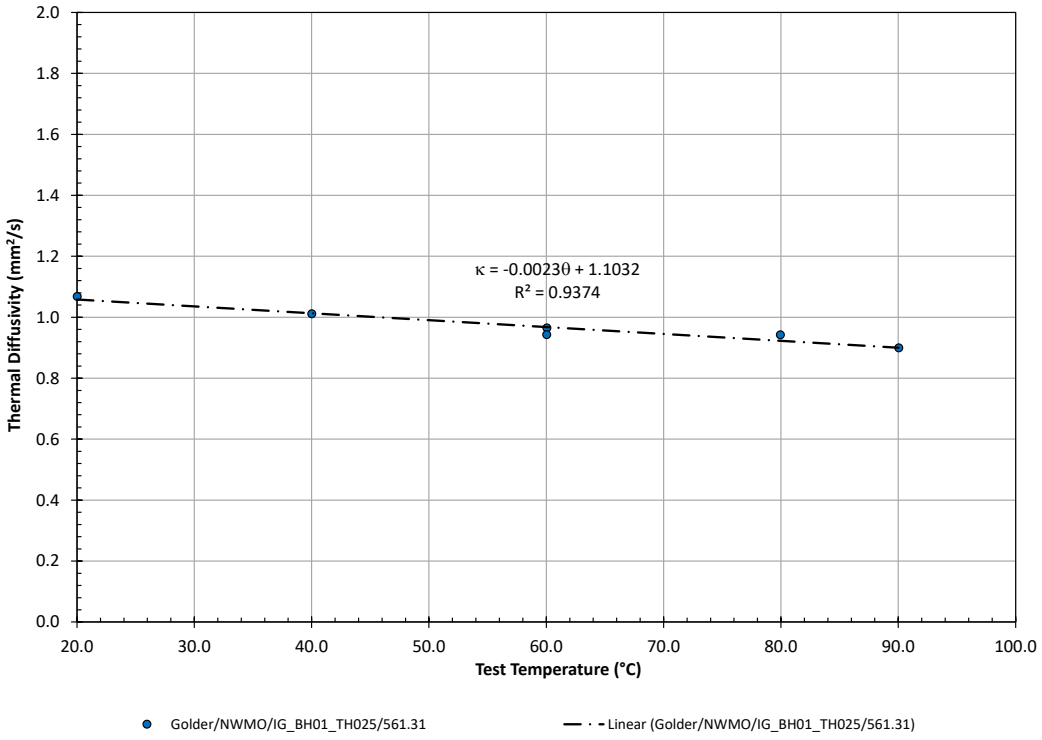


Figure 32: Thermal diffusivity for dry sample of Feldspar-phyric Tonalite Dyke as a function of temperature

Summary of equations for thermal transport properties as a function of temperature by rock type

The equations describing volumetric heat capacity, thermal conductivity and thermal diffusivity as a function of temperature for different rock types and for wet and dry conditions are provided in Table 9.

Table 9: Summary of equations describing thermal properties Cv, k and κ as a function of temperature for the range ~20°C to 90°C or 100°C

Rock Type	No. of Samples	C_v (wet) [MJ/(m^3.°K)]	C_v (dry) [MJ/(m^3.°K)]	k (wet) [W/(m.°K)]	k (dry) [W/(m.°K)]	κ (wet) [mm^2/sec]	κ (dry) [mm^2/sec]
Biotite Granodiorite-Tonalite	8(wet)/4(dry)	$C_v = 0.0049\,\theta + 1.86$	$C_v = 0.0049\,\theta + 1.95$	$k = -0.0058\,\theta + 3.68$	$k = -0.0015\,\theta + 3.10$	$\kappa = -0.0063\,\theta + 1.94$	$\kappa = -0.0037\,\theta + 1.57$
Biotite Tonalite	2(wet)	$C_v = 0.0043\,\theta + 1.98$	-	$k = -0.0036\,\theta + 2.91$	-	$\kappa = -0.0040\,\theta + 1.45$	-
Amphibolite	1(wet)/1(dry)	$C_v = 0.0041\,\theta + 2.07$	$C_v = 0.0055\,\theta + 2.16$	$k = -0.0009\,\theta + 2.53$	$k = -0.0009\,\theta + 2.82$	$\kappa = -0.0023\,\theta + 1.21$	$\kappa = -0.0029\,\theta + 1.29$
Aplite Dyke	1(wet)/1(dry)	$C_v = 0.0055\,\theta + 1.72$	$C_v = 0.0045\,\theta + 1.92$	$k = -0.0044\,\theta + 3.27$	$k = -0.0015\,\theta + 3.11$	$\kappa = -0.0062\,\theta + 1.85$	$\kappa = -0.0036\,\theta + 1.60$
Feldspar-phyric Tonalite Dyke	1(wet)/1(dry)	$C_v = 0.0030\,\theta + 2.04$	$C_v = 0.0050\,\theta + 2.00$	$k = -0.0044\,\theta + 2.71$	$k = -0.0002\,\theta + 2.23$	$\kappa = -0.0035\,\theta + 1.32$	$\kappa = -0.0023\,\theta + 1.10$

θ – temperature in °C

Coefficient of linear thermal expansion

Table 10 shows a summary of the coefficient of linear thermal expansion between room temperature and 90°C for each sample measured in the Unitherm 1054L dilatometer, determined from the current testing program (Campaign 3). The coefficient of linear thermal expansion was calculated from thermal strain vs temperature data points by two methods: 1) as the slope of the linear regression line through the data points and 2) fitting a second order polynomial to the same data and deriving the slope of the polynomial at the target temperatures. Determining coefficient of linear thermal expansion from the linear regression (α_L) seems sufficient given the near linear trend of the data points for the tested temperature range (Table 9). However, the temperature-dependent coefficients of linear thermal expansion ($\alpha_L(\theta)$) were also determined from approach 2 and are summarized in Table 9. Data for the individual tests are included in APPENDIX E. Figure 33 shows plots of the variation of the coefficient of linear thermal expansion with temperature for the Biotite Tonalite, Biotite-rich Tonalite, Amphibolite and the Aplite Dyke. There was only one sample, therefore one curve in Figure 32, for each rock type except for Biotite Tonalite which there were ten (10) samples. For the latter, an average curve was determined which is shown in black dashed line in this figure. Results from the Unitherm 1054L dilatometer tests are within the ranges for the tested rock types and follow the expected trends with temperature. The average α_L values as well as the equations describing the coefficient of linear thermal expansion versus temperature ($\alpha_L(\theta)$) are provided for the first and second heating cycles, by rock type, in Table 11.

Table 10: **Coefficient of linear thermal expansion determined from the first and second heating cycles and as a function of temperature (from quadratic fit) for the first heating cycle**

Sample ID	Depth (m)[1]	Date Tested	Linear fit (range: 20°C - 90°C)		Quadratic fit[3] (range: 20°C - 90°C)	
			α_L (1st heating cycle) (1/°K)	α_L (2nd heating cycle) (1/°K)	Temperature (°C)	$\alpha_L(\theta)$ (1st heating cycle) (1/°K)
IG_BH01_TH015[2]	299.43	Apr-20-21 to Apr-23-21	8.97E-06	8.98E-06	20	7.11E-06
					40	8.13E-06
					60	9.16E-06
					80	1.02E-05
					90	1.07E-05
IG_BH01_TH016[2]	353.54	May-03-21 to May-06-21	7.98E-06	7.87E-06	20	5.82E-06
					40	7.01E-06
					60	8.20E-06
					80	9.39E-06
					90	9.98E-06
IG_BH01_TH017[2]	401.95	May-03-21 to May-06-21	5.88E-06	5.76E-06	20	4.88E-06
					40	5.43E-06
					60	5.99E-06
					80	6.54E-06
					90	6.82E-06

Sample ID	Depth (m)[1]	Date Tested	Linear fit (range: 20°C - 90°C)		Quadratic fit[3] (range: 20°C - 90°C)	
			α_L (1st heating cycle) (1/°K)	α_L (2nd heating cycle) (1/°K)	Temperature (°C)	$\alpha_L(\theta)$ (1st heating cycle) (1/°K)
IG_BH01_TH018[2]	422.33	May-10-21 to May-13-21	6.52E-06	6.45E-06	20	5.52E-06
					40	6.07E-06
					60	6.63E-06
					80	7.18E-06
					90	7.46E-06
IG_BH01_TH019[2]	448.22	May-10-21 to May-13-21	7.06E-06	7.08E-06	20	6.51E-06
					40	6.82E-06
					60	7.12E-06
					80	7.43E-06
					90	7.58E-06
IG_BH01_TH020[2]	451.57	May-14-21 to May-17-21	7.03E-06	6.97E-06	20	6.64E-06
					40	6.85E-06
					60	7.06E-06
					80	7.27E-06
					90	7.38E-06
IG_BH01_TH021[2]	457.06	May-14-21 to May-17-21	7.69E-06	7.33E-06	20	6.23E-06
					40	7.03E-06
					60	7.82E-06
					80	8.62E-06
					90	9.02E-06
IG_BH01_TH022[2]	501.98	May-19-21 to May-22-21	7.35E-06	7.14E-06	20	5.93E-06
					40	6.72E-06
					60	7.52E-06
					80	8.31E-06
					90	8.71E-06
IG_BH01_TH023[2]	529.63	May-19-21 to May-22-21	7.60E-06	7.47E-06	20	6.37E-06
					40	7.06E-06
					60	7.74E-06
					80	8.43E-06
					90	8.77E-06
IG_BH01_TH024[2]	556.17	May-24-21	7.67E-06	7.58E-06	20	6.37E-06

Sample ID	Depth (m)[1]	Date Tested	Linear fit (range: 20°C - 90°C)		Quadratic fit[3] (range: 20°C - 90°C)	
			α_L (1st heating cycle) (1/°K)	α_L (2nd heating cycle) (1/°K)	Temperature (°C)	$\alpha_L(\theta)$ (1st heating cycle) (1/°K)
		to May-27-21			40	7.09E-06
					60	7.81E-06
					80	8.53E-06
					90	8.89E-06
IG_BH01_TH025[2]	561.20	May-24-21 to May-27-21	6.45E-06	6.41E-06	20	6.24E-06
					40	6.36E-06
					60	6.47E-06
					80	6.58E-06
					90	6.64E-06
IG_BH01_TH026[2]	603.84	May-28-21 to May-31-21	7.56E-06	7.44E-06	20	6.29E-06
					40	6.99E-06
					60	7.70E-06
					80	8.40E-06
					90	8.75E-06
IG_BH01_TH027[2]	657.79	May-28-21 to May-31-21	8.10E-06	8.75E-06	20	7.58E-06
					40	7.87E-06
					60	8.16E-06
					80	8.45E-06
					90	8.60E-06

[1]Top depth of prepared sub-sample

[2] Unpreserved samples. Samples were saturated before testing

[3] Appendix E reports the quadratic fit coefficients for both the 1st and 2nd cycles

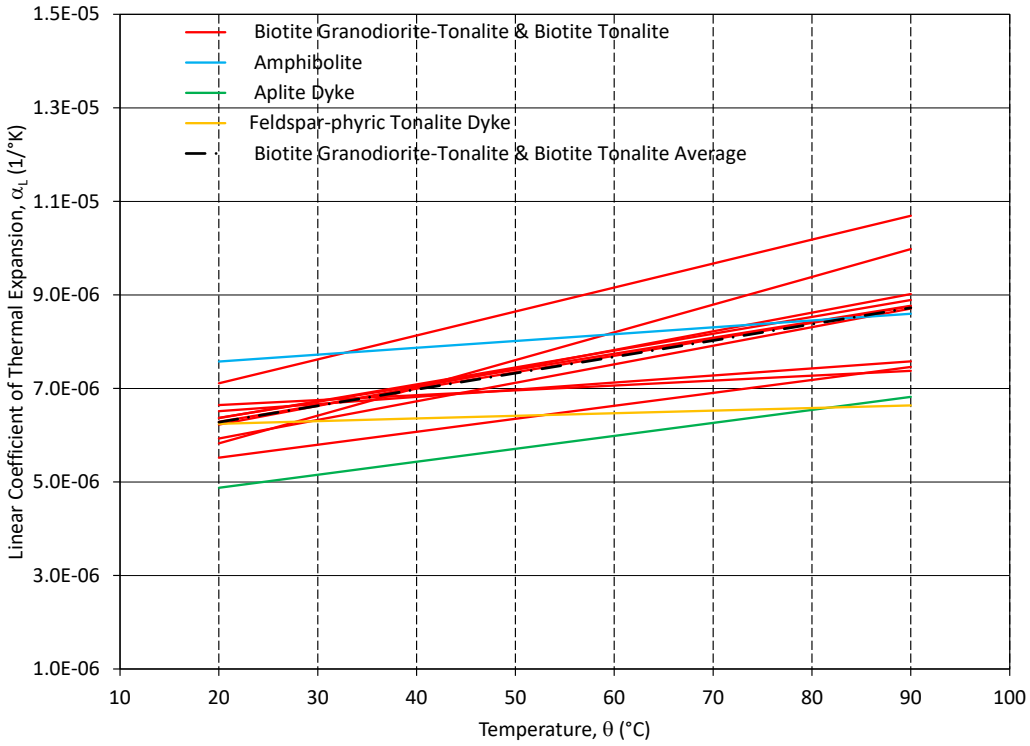


Figure 33: Linear coefficient of thermal expansion as a function of temperature for all samples

Table 11: Summary of the coefficient of linear thermal expansion, α, average (from linear regression) and as a function of temperature (from quadratic fit) for the range ~20°C to 90°C

Rock Type	No. of Samples	Average α_L (1st heating cycle) [1/°K]	$\alpha_L(\theta)$ (1st cycle) [1/°K]	Average α_L (2nd heating cycle) [1/°K]	$\alpha_L(\theta)$ (2nd cycle) [1/°K]
Biotite Tonalite	10	7.54E-06	α_L = 3.49E-08 θ + 5.58E-06	7.43E-06	α_L = 2.50E-08 θ + 6.02E-06
Amphibolite	1	8.10E-06	α_L = 1.46E-08 θ + 7.28E-06	8.75E-06	α_L = 7.52E-09 θ + 8.32E-06
Aplite Dyke	1	5.88E-06	α_L = 2.77E-08 θ + 4.32E-06	5.76E-06	α_L = 2.67E-08 θ + 4.26E-06
Feldspar-phyric Felsic Dyke	1	6.45E-06	α_L = 5.58E-09 θ + 6.13E-06	6.41E-06	α_L = 5.99E-09 θ + 6.07E-06

θ – temperature in °C

4.0 DATA QUALITY

All samples sent to the CANMET laboratory were accounted for and raw testing data were sent back in digital format. The results were checked against expected values and were deemed reasonable. In addition, ratios of moduli to UCS and tensile strength to UCS were within the expected ranges for this rock type. Photographs of the samples before and after testing were also delivered (APPENDIX A). The failure mode confirms that the UCS values are representative of the intact rock strength.

The water content for the Brazilian samples is generally higher than for the UCS samples. It is conceivable that for rocks with very low and poorly connected porosity, such as the Biotite Tonalite, the drying process will only eliminate surface or near-surface water and the results are affected by the surface area to volume ratios. The surface area to volume ratio for the Brazilian samples is higher than that for the UCS samples, thus resulting in higher water content measurements.

All samples sent to the RESPEC laboratory to conduct thermal characterizations were accounted for and raw testing data were sent back in digital format. The thermal expansion tests for the first fourteen (14) samples were heated at a higher rate than that recommended by the testing standards, and therefore they were discarded. A second set of samples were collected and tested. The hot disk tests for the first fourteen (14) samples were tested beyond the target range of room temperature to 90°C. They were also tested in a saturated state instead of a dry state. Therefore, a smaller set of samples were selected for additional testing. The results were checked against expected values and were deemed reasonable. The volumetric heat capacity does not seem to be affected by the degree of saturation, although it should be noted that the porosities of all tested rocks are very low (generally less than 1%).

4.1 Uncertainties and Limitations

At this point in the program, the number of samples tested is limited. Although the results of the UCS tests and the Brazilian tests for Biotite Tonalite were very consistent, the sample population is too small to establish statistical data and confidence limits. The number of samples for the other rock types encountered in the borehole is even more limited than that of the Biotite Tonalite. As the program evolves and data from all boreholes becomes available, statistical analyses of the data will provide more information on the degree of confidence.

In the measurement of water content, the samples were weighed before testing and placed in the oven after completion of the test to start the drying process. It has been observed that because of the destructive nature of the UCS and Brazilian tests, some of the sample material may have been lost during testing. Due to the lower porosity of the tonalite, any loss, however small, can have a significant effect in the determination of the water content and dry density. As a result, a more reliable alternative approach to the determination of the water content and dry density was used.

In this report, the interpretation of Crack Initiation (CI) and Crack Damage (CD) stresses have been based on the maximum crack volumetric strain and the volumetric strain reversal, respectively. A better reported method of interpreting the crack initiation is to follow the Tangent Lateral Stiffness method (Ghazvinian et al., 2012), which considers the same raw data but amplifies the change in lateral strain making identification of systematic diversion more defined. It is recommended this method be used in future work.

Crack damage (CD) is defined as the onset of significant and sustained deviation from linear axial stress vs axial strain behaviour preceding sample failure (Diederichs et al 2004). Volumetric strain reversal may or may not

correspond to CD in uniaxial conditions depending on the internal damage mechanisms; therefore, it is recommended that the deviation from the linear section of the stress strain curve be determined by plotting the tangent modulus (slope of the stress-strain curve) to identify the onset of the deviation. Alternatively, similar to the method to determine CI, the Tangent Axial Stiffness can be used to interpret CD. It is recommended that one of these two methods be used in future work.

The number of samples in the thermal testing program are also limited at this time. Samples of Biotite Tonalite were grouped to establish preliminary trends with temperature, while the other rock types were reported by individual tests. As the program evolves and data from all boreholes becomes available, statistical analyses of the data will provide more information on the degree of confidence.

5.0 REFERENCES

ASTM D4543-08, 2008. Standard Practices for Preparing Rock Core as Cylindrical Test Specimens and Verifying Conformance to Dimensional and Shape Tolerances

ASTM D4543-19, 2019. Standard Practices for Preparing Rock Core as Cylindrical Test Specimens and Verifying Conformance to Dimensional and Shape Tolerances

ASTM D2216-10, 2010. Standard Test Methods for Laboratory Determination of Water (Moisture) Content of Soil and Rock by Mass

ASTM D2216-19, 2019. Standard Test Methods for Laboratory Determination of Water (Moisture) Content of Soil and Rock by Mass

ASTM D7263-09, Laboratory Determination of Density (Unit Weight) of Soil Specimens

ASTM D7263-09 (2018)$^{\varepsilon 2}$, 2018. Laboratory Determination of Density (Unit Weight) of Soil Specimens

ASTM D7012-14$^{\varepsilon 1}$, 2014. Standard Test Methods for Compressive Strength and Elastic Moduli of Intact Rock Core Specimens under Varying States of Stress and Temperatures

ASTM D3967-08, 2008. Standard Test Method for Splitting Tensile Strength of Intact Rock Core Specimens

ASTM D3967-16, 2016. Standard Test Method for Splitting Tensile Strength of Intact Rock Core Specimens

ASTM D4535-13$^{\varepsilon 2}$ Standard Test Methods for Measurement of Thermal Expansion of Rock Using Dilatometer

ASTM D6026-13, 2013 Standard Practice for Using Significant Digits in Geotechnical Data

ASTM D6026-21 Standard Practice for Using Significant Digits in Geotechnical Data

ASTM D2845-08 Standard Test Method for Laboratory Determination of Pulse Velocities and Ultrasonic Elastic

Constants of Rock

Blackburn, C.E. and Hinz, P., 1996. Gold and base metal potential of the northwest part of the Raleigh Lake greenstone belt, northwestern Ontario-Kenora Resident Geologist's District; in Summary of Field Work and Other Activities 1996, Ontario Geological Survey, Miscellaneous Paper 166, p.113-115.

DesRoches, A., Sykes, M., Parmenter, A. and Sykes, E., 2018. Lineament Interpretation of the Revell Batholith and Surrounding Greenstone Belts (Nuclear Waste Management Organization. No. NWMO-TR-2018-19).

Diederichs, M.S., Kaiser, P.K., Eberhardt, E., 2004. Damage initiation and propagation in hard rock during tunnelling and the influence of near-face stress rotation. Int. J. Rock Mech. Min. Sci. 41, 785–812.

Ghazvinian, E., Diederichs, M. and Martin, C.D., 2012. Identification of crack damage thresholds in crystalline rock. Proceedings of the Eurock 2012 International Symposium, Stockholm (Sweden), May 2012, Taylor & Francis Group: 14 p.

Golder (Golder Associates Ltd.), 2017. Phase 2 Initial Borehole Drilling and Testing, Ignace Area - Initial Borehole Characterization Plan for IG_BH01.

Golder and PGW (Paterson Grant and Watson Ltd.), 2017. Phase 2 Geoscientific Preliminary Assessment, Geological Mapping, Township of Ignace and Area, Ontario: APM-REP-01332-0225.

Golder, 2022. WP10 – Phase 2 Initial Borehole Drilling and Testing, Ignace Area - Rock Mass Classification for IG_BH01

Hoek., E. and Diederichs, M.S, 2006. Empirical estimation of rock mass modulus. Int. J. Rock Mech. Min. Sci. 43, 203–215.

ISO 22007-2:2015 (E) Plastics – Determination of thermal conductivity and thermal diffusivity, Part 2: Transient plane heat source (hot disc) method

Robertson, E. C., 1988. Thermal Properties of Rocks, U. S. Geological Survey Open-File Report 88-441, 106 p.

SGL (Sander Geophysics Limited), 2015. Phase 2 Geoscientific Preliminary Assessment, Acquisition, Processing and Interpretation of High-Resolution Airborne Geophysical Data, Township of Ignace, Ontario. Prepared for Nuclear Waste Management Organization (NWMO). NWMO Report Number: APM-REP-06145-0002.

SRK (SRK Consulting, Inc.) and Golder, 2015. Phase 2 Geoscientific Preliminary Assessment, Observation of General Geological Features, Township of Ignace, Ontario. Prepared for Nuclear Waste Management Organization. NWMO Report Number: APM-REP-06145-0004.

Stone, D., 2009. Geology of the Bending Lake Area, Northwestern Ontario; *in* Summary of Field Work and Other Activities 2009. Ontario Geological Survey. Open File Report 6240.

Stone, D., 2010a. Geology of the Stormy Lake Area, Northwestern Ontario; *in* Summary of Field Work and Other Activities 2010. Ontario Geological Survey, Open File Report 6260.

Stone, D., 2010b. Precambrian geology of the central Wabigoon Subprovince area, northwestern Ontario. Ontario Geological Survey, Open File Report 5422.

Stone, D., Halle, J. and Chaloux, E., 1998. Geology of the Ignace and Pekagoning Lake Areas, Central Wabigoon Subprovince; *in* Summary of Field Work and Other Activities 1998, Ontario Geological Survey, Misc. Paper 169.

Stone, D., Davis, D.W., Hamilton, M.A. and Falcon, A., 2010. Interpretation of 2009 Geochronology in the Central Wabigoon Subprovince and Bending Lake Areas, Northwestern Ontario, *in* Summary of Field Work and Other Activities 2010, Ontario Geological Survey, Open File Report 6260.

APPENDIX A

UCS Tests: Stress-Strain Graphs and Photographs of Intact and Broken Test Specimens

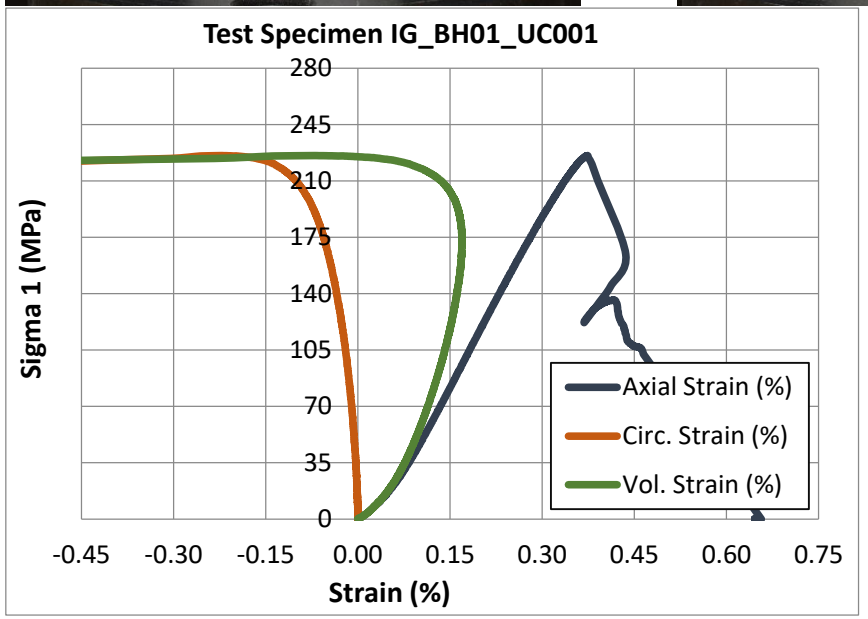
Table A-1: List of uniaxial compression test specimens

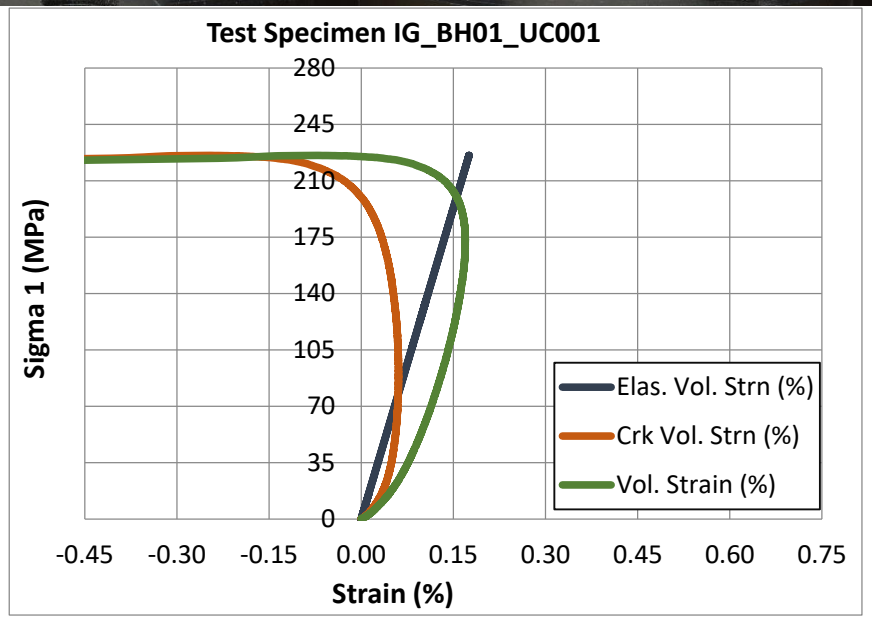
Specimen No.	Depth (m)[1]	Rock Type	Page
IG_BH01_UC001	408.40	Biotite Granodiorite-Tonalite	A-2
IG_BH01_UC002	442.01	Biotite Granodiorite-Tonalite	A-3
IG_BH01_UC003	468.02	Biotite Granodiorite-Tonalite	A-4
IG_BH01_UC004	522.64	Biotite Granodiorite-Tonalite	A-5
IG_BH01_UC005	567.77	Biotite Granodiorite-Tonalite	A-6
IG_BH01_UC006	600.72	Biotite Granodiorite-Tonalite	A-7
IG_BH01_UC007	450.79	Biotite Tonalite	A-8
IG_BH01_UC008	559.94	Feldspar-phyric Tonalite Dyke	A-9
IG_BH01_UC009	655.01	Amphibolite	A-10
IG_BH01_UC010	658.31	Amphibolite	A-11

[1]Top depth of prepared sub-sample





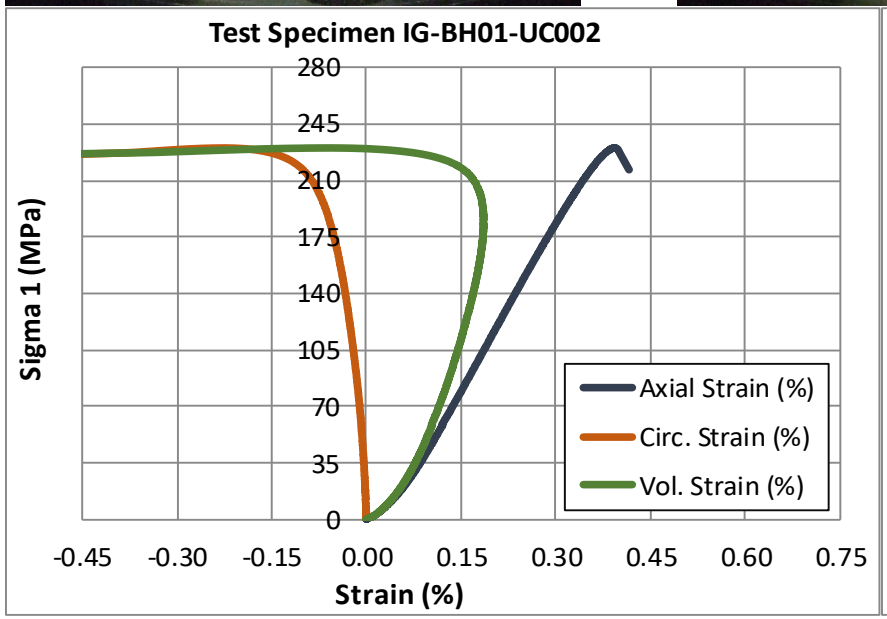


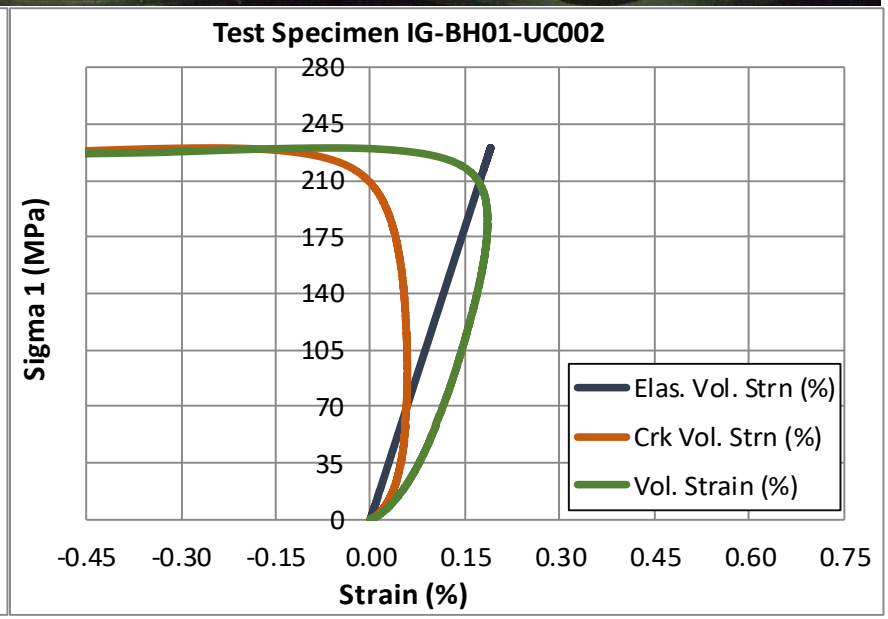


Test Specimen IG_BH01_UC001 – Depth = 408.40 m: Intact and broken specimen photographs and stress-strain curves





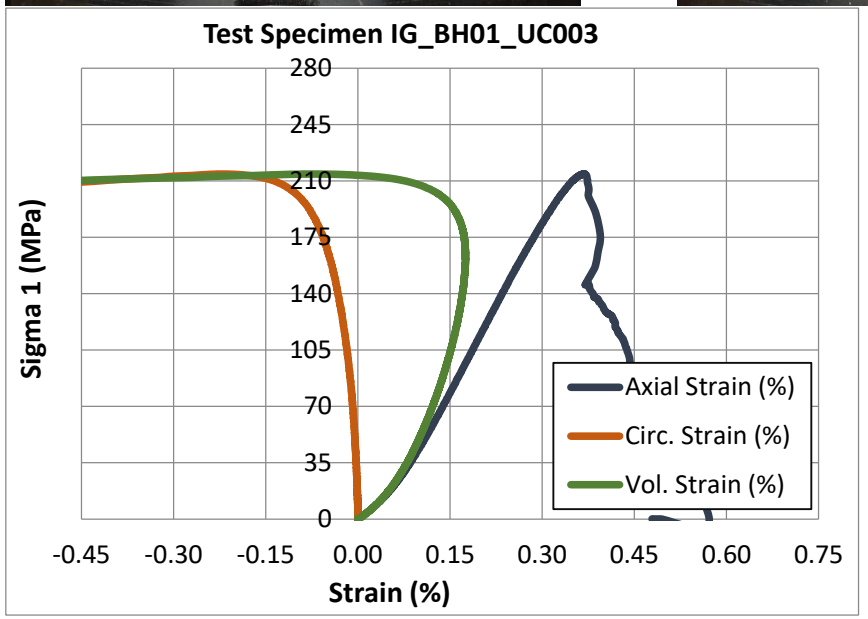


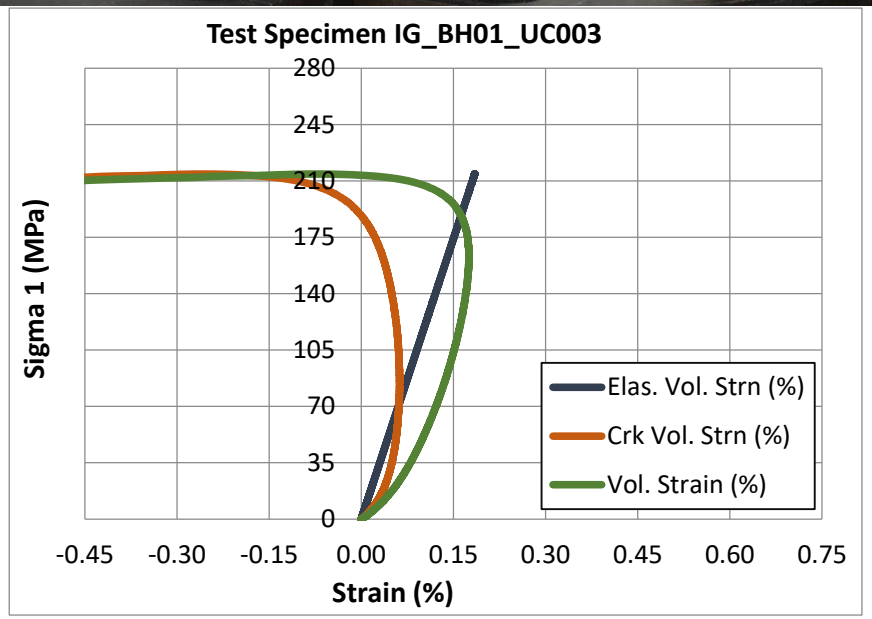


Test Specimen IG_BH01_UC002 – Depth = 442.01 m: Intact and broken specimen photographs and stress-strain curves





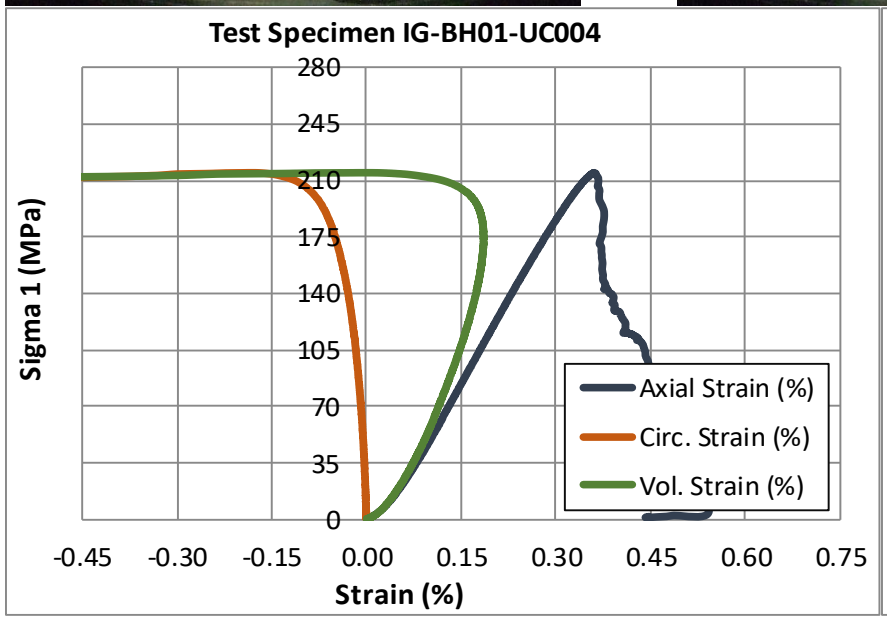


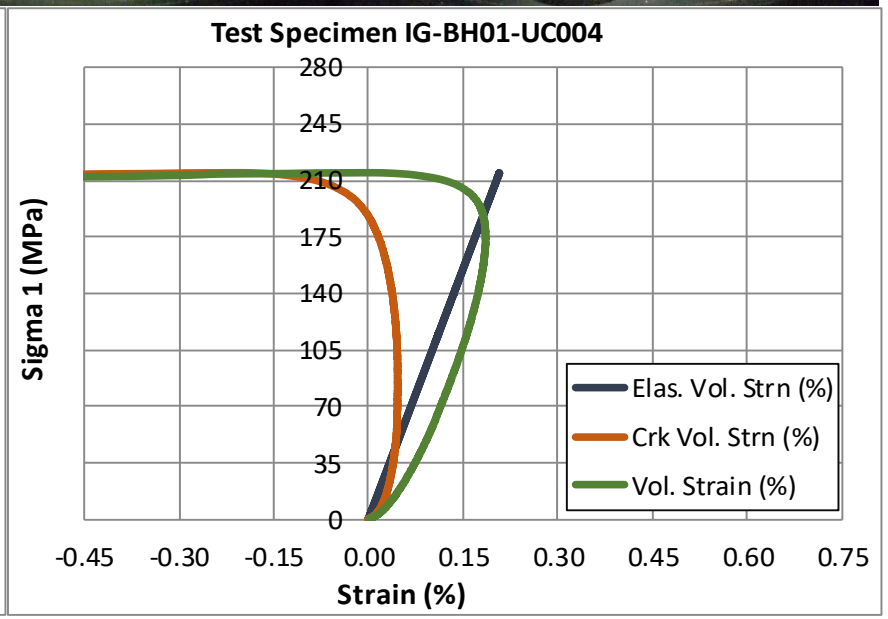


Test Specimen IG_BH01_UC003 – Depth = 468.02 m: Intact and broken specimen photographs and stress-strain curves

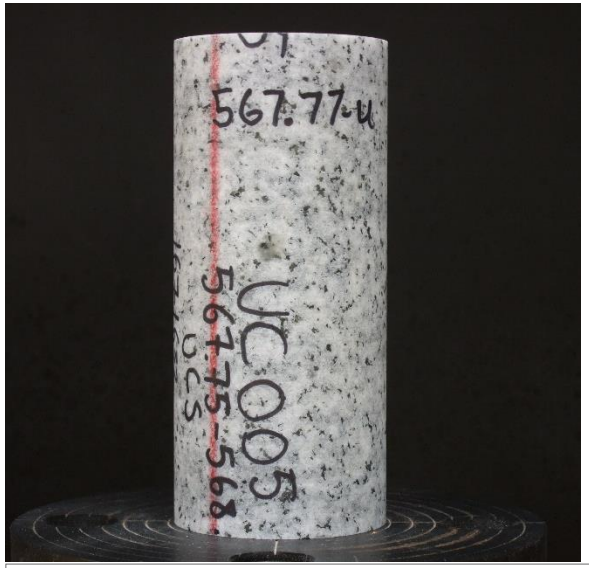




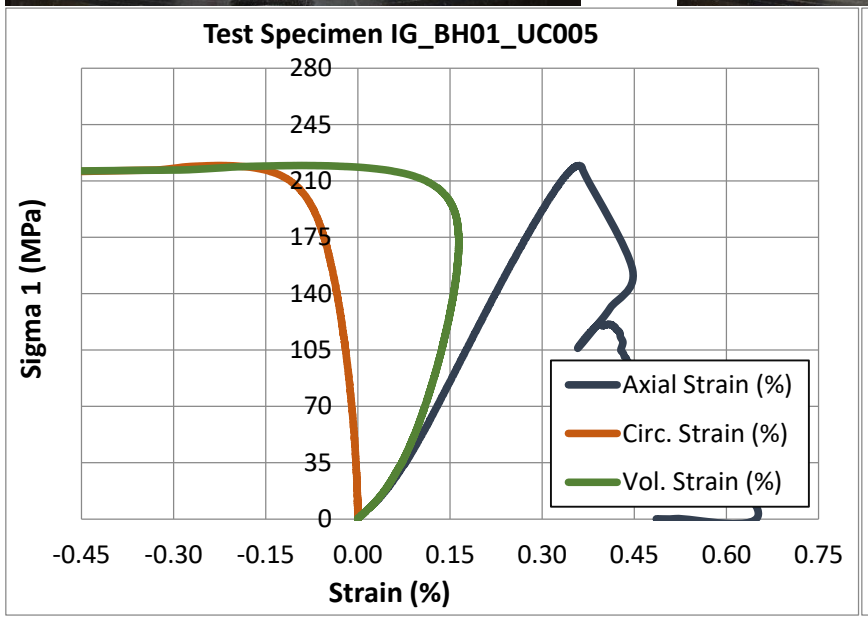


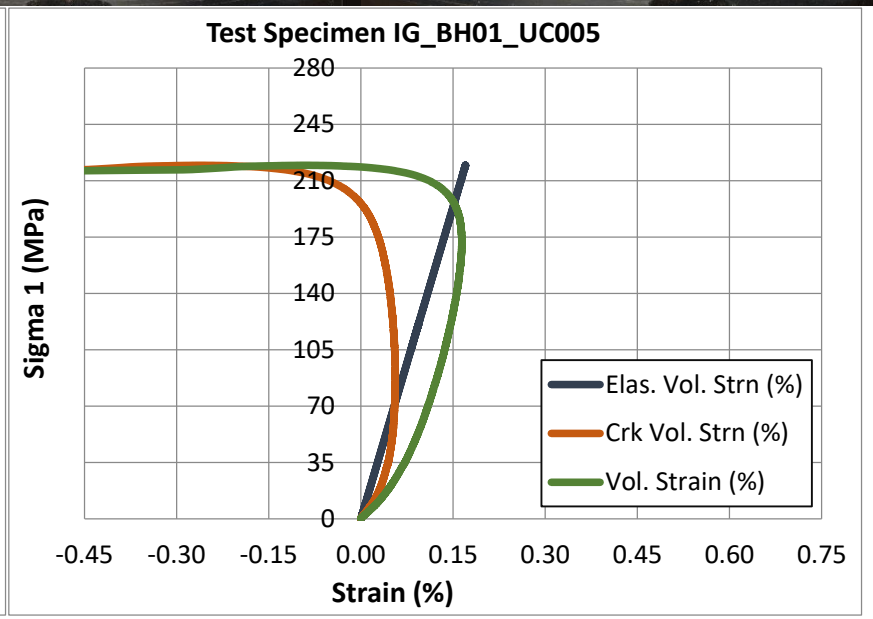


Test Specimen IG_BH01_UC004 – Depth = 522.64 m: Intact and broken specimen photographs and stress-strain curves





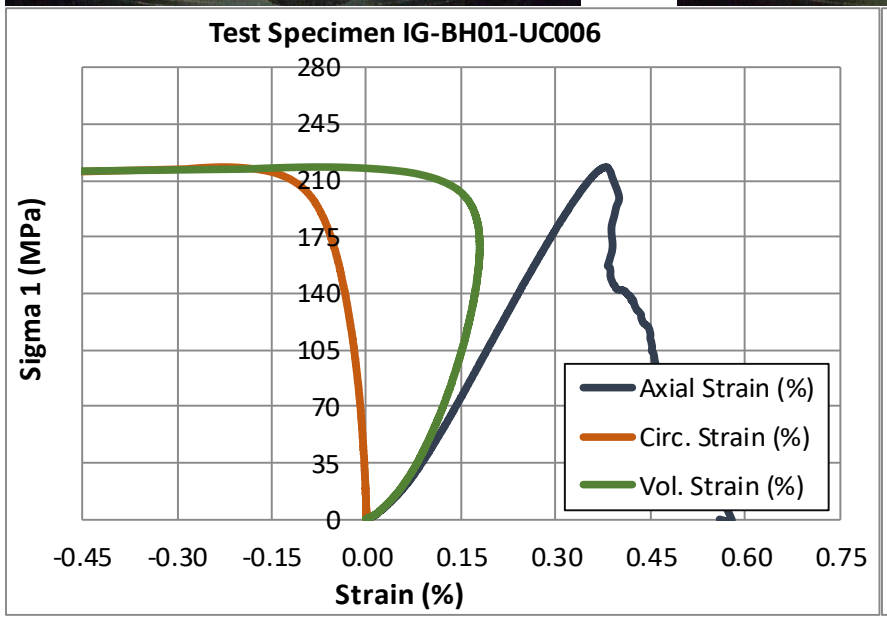


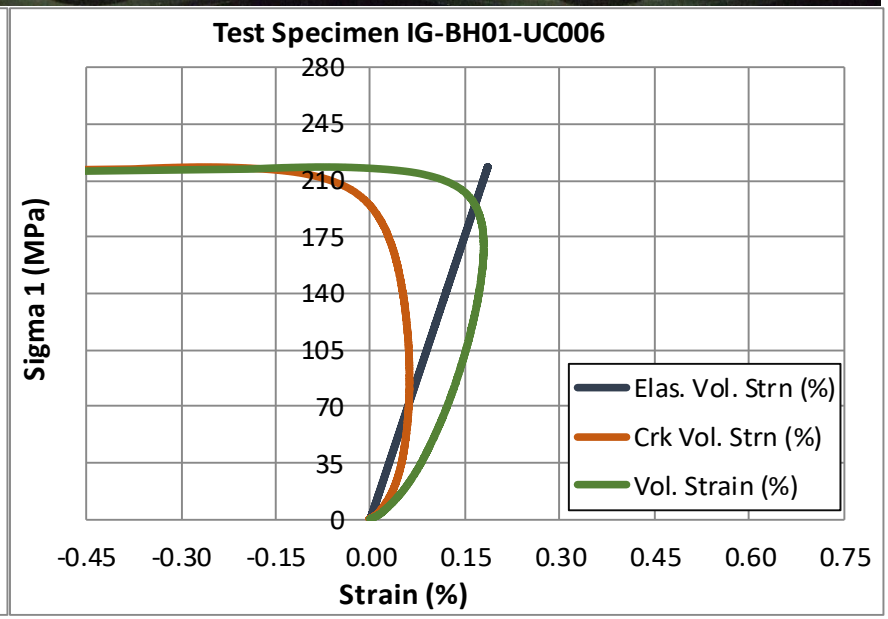


Test Specimen IG_BH01_UC005 – Depth = 567.77 m: Intact and broken specimen photographs and stress-strain curves





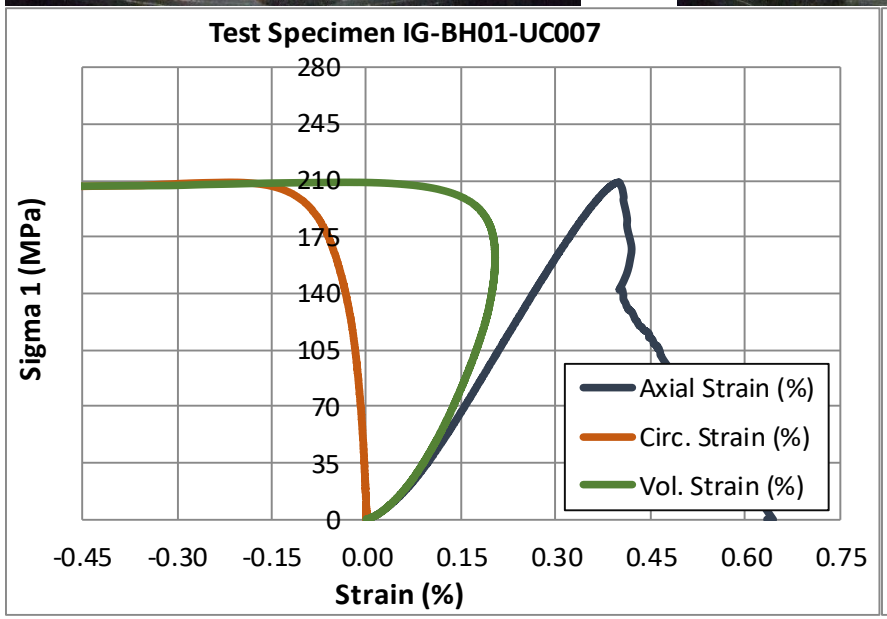


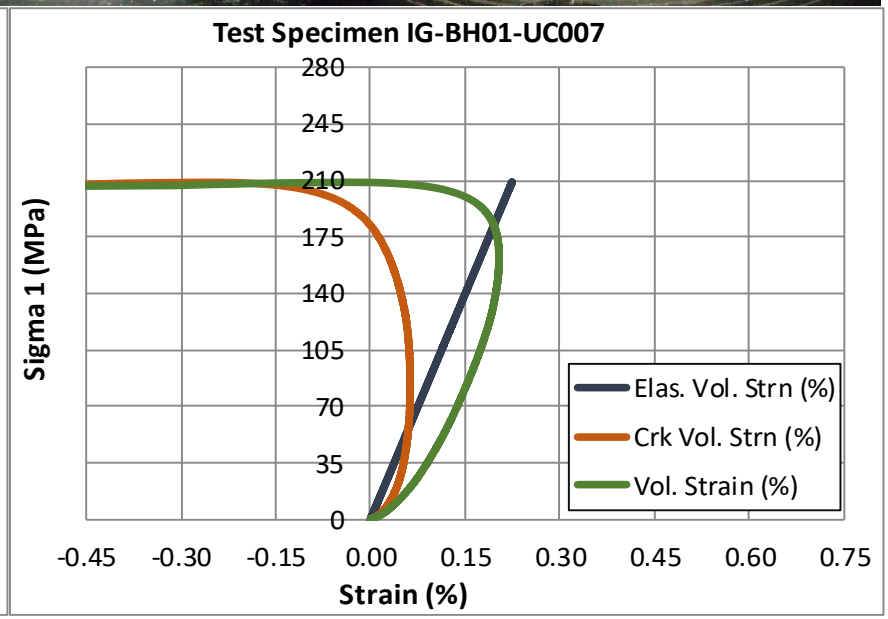


Test Specimen IG_BH01_UC006 – Depth = 600.72 m: Intact and broken specimen photographs and stress-strain curves



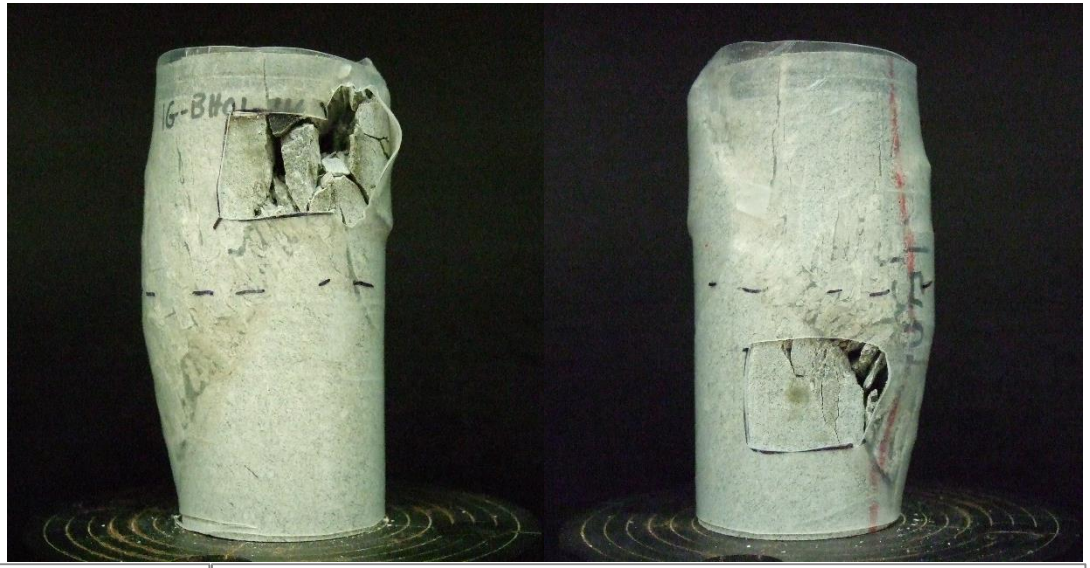


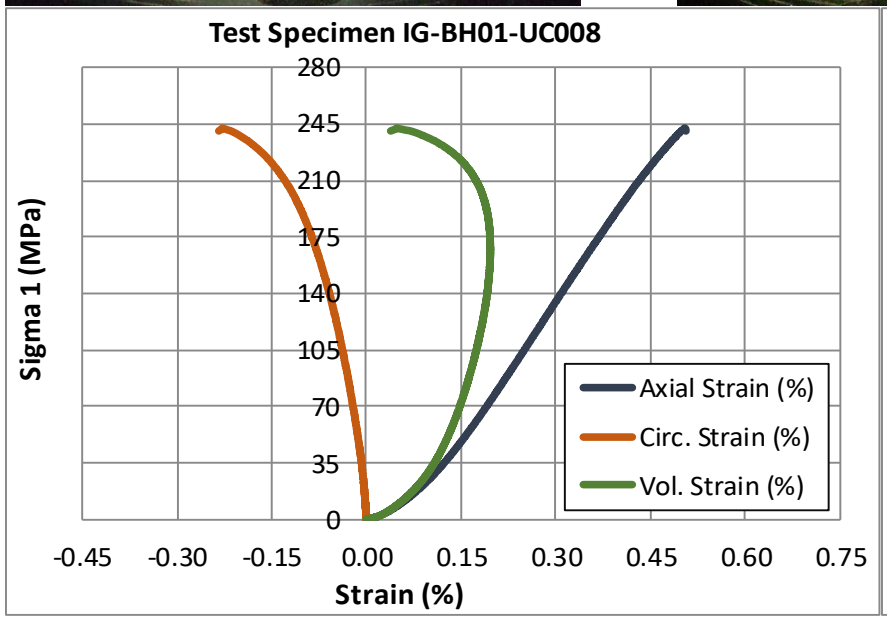


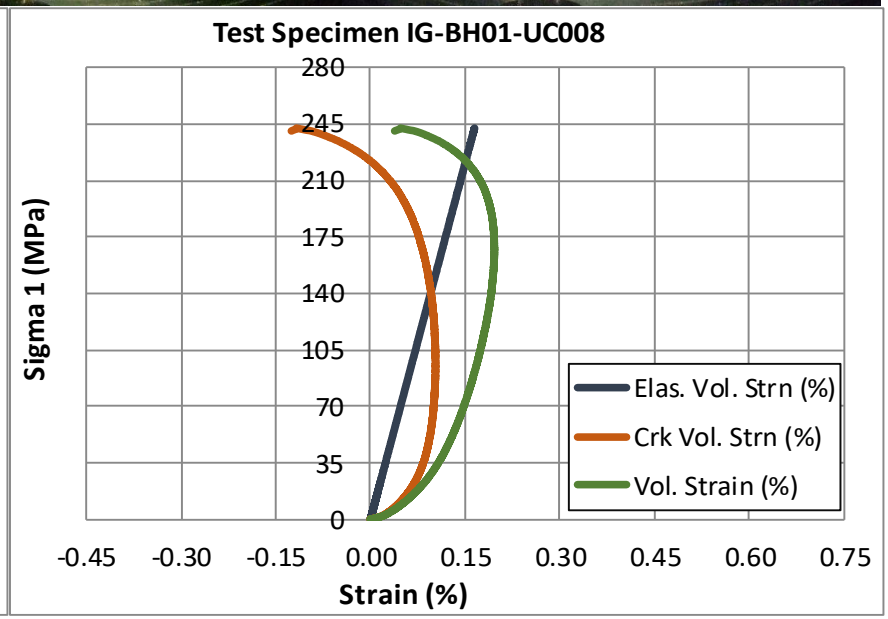


Test Specimen IG_BH01_UC007 – Depth = 450.79 m: Intact and broken specimen photographs and stress-strain curves

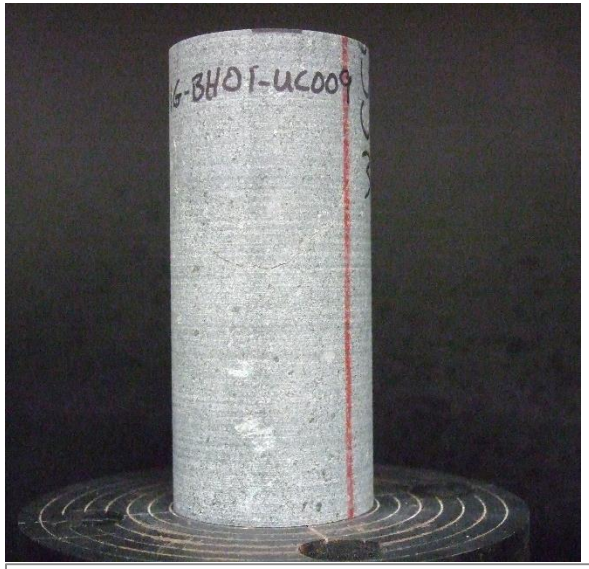


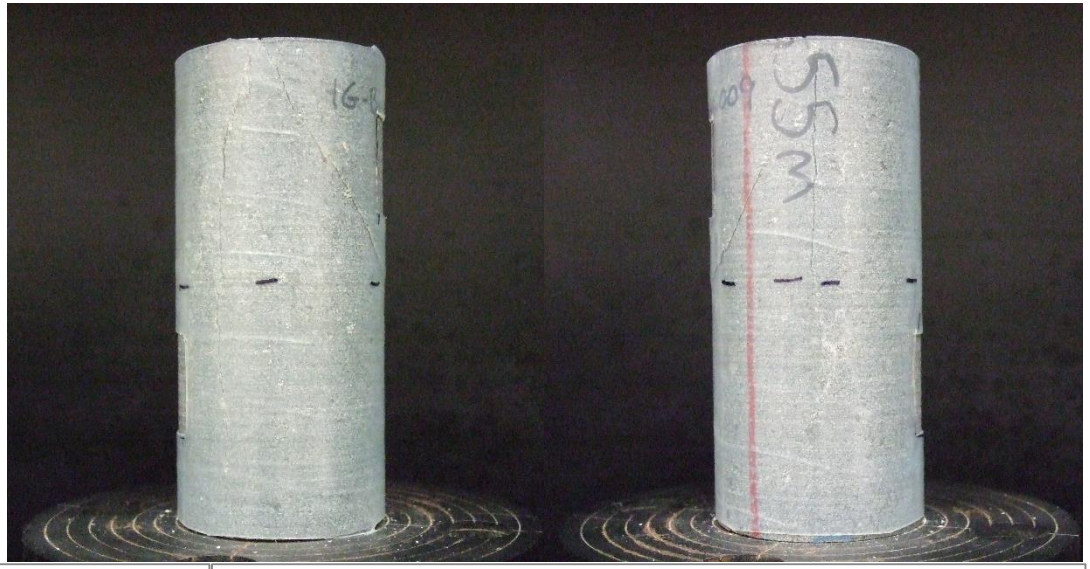


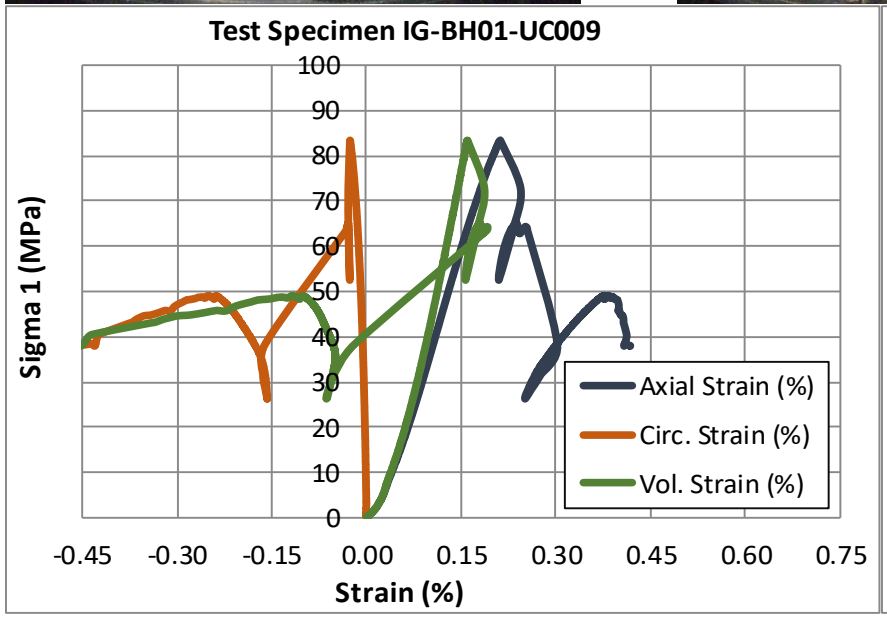


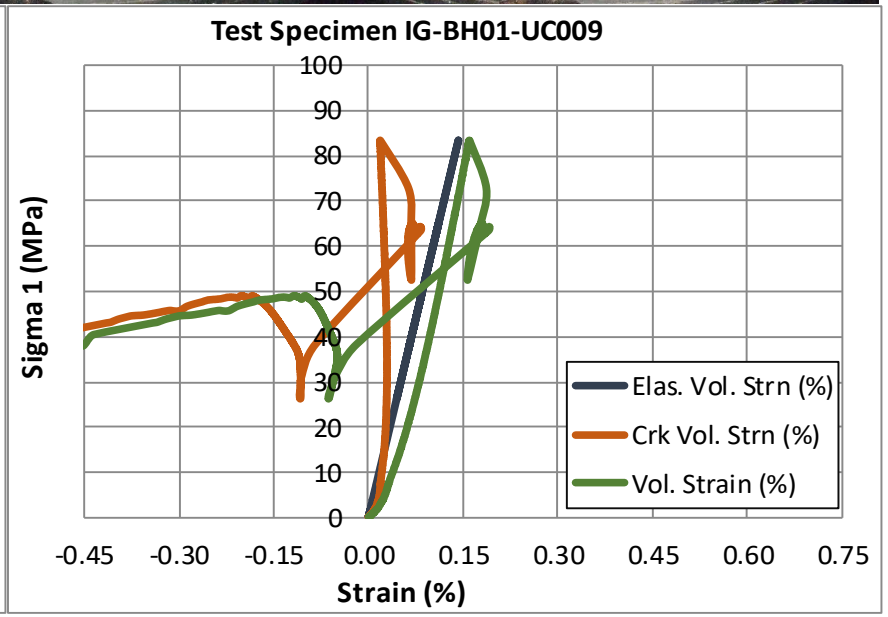


Test Specimen IG_BH01_UC008 – Depth = 559.94 m: Intact and broken specimen photographs and stress-strain curves

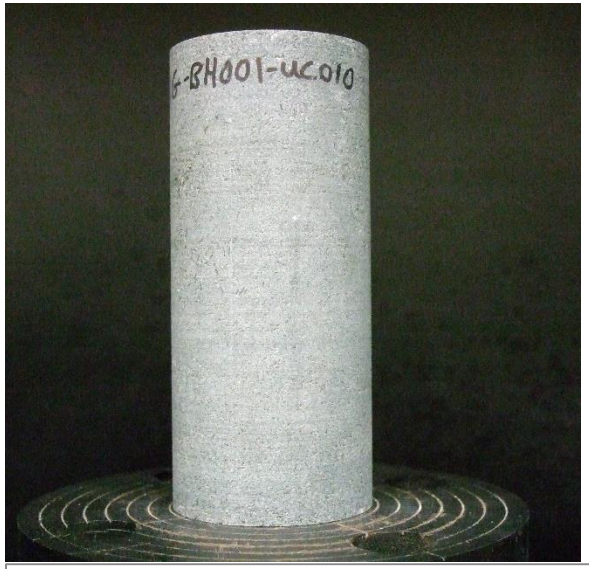


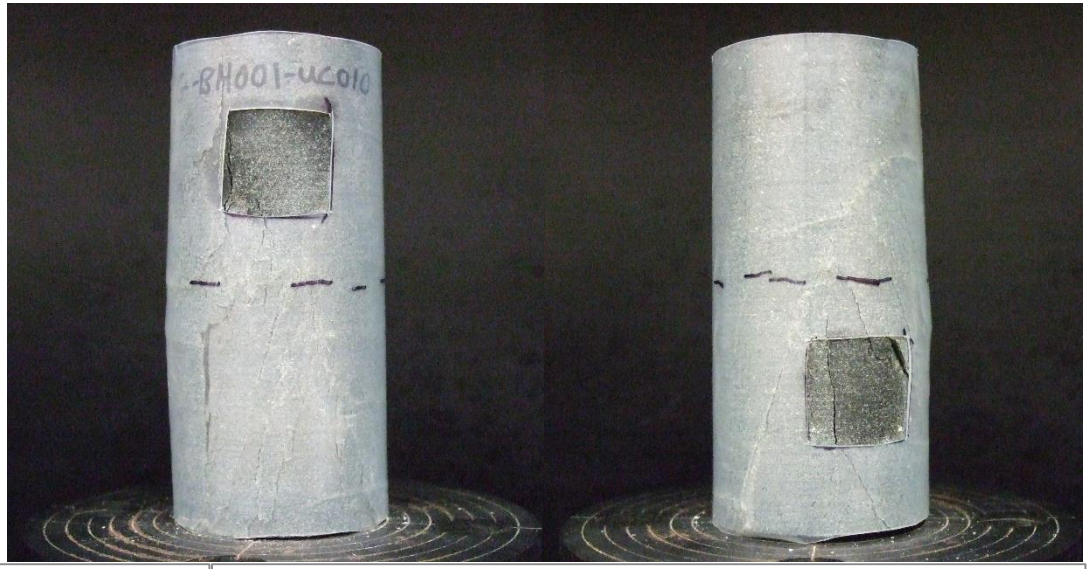


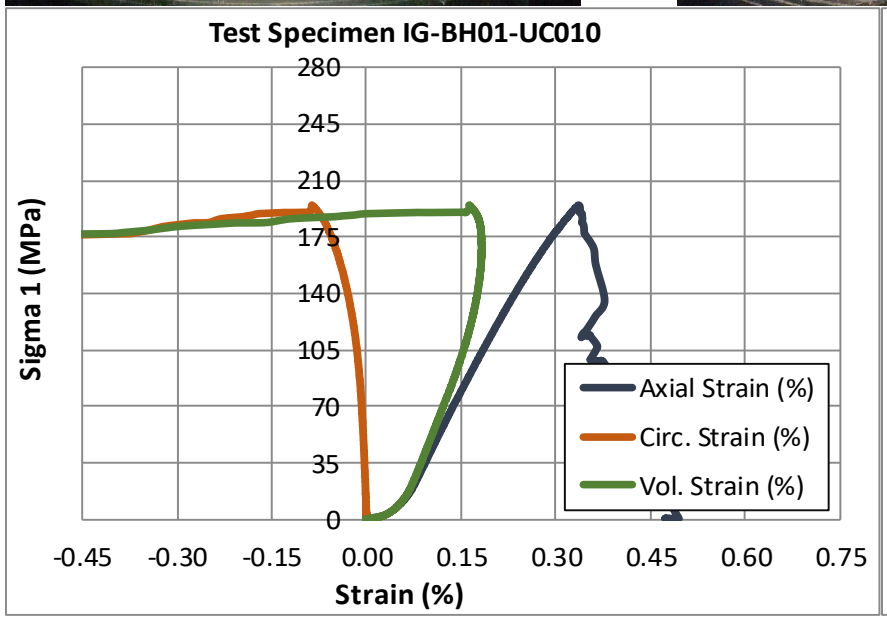


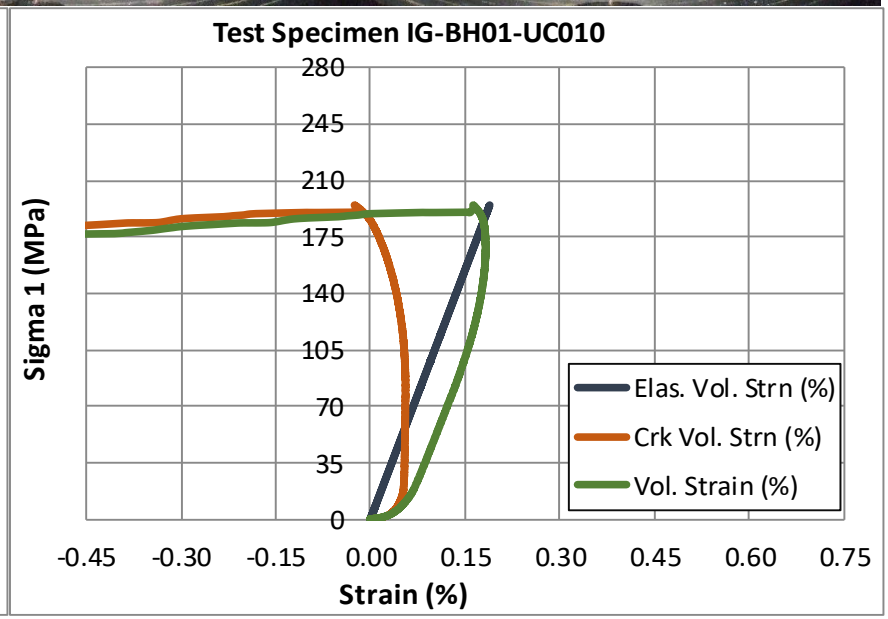


Test Specimen IG_BH01_UC009 – Depth = 655.01 m: Intact and broken specimen photographs and stress-strain curves









Test Specimen IG_BH01_UC010 – Depth = 658.31 m: Intact and broken specimen photographs and stress-strain curves

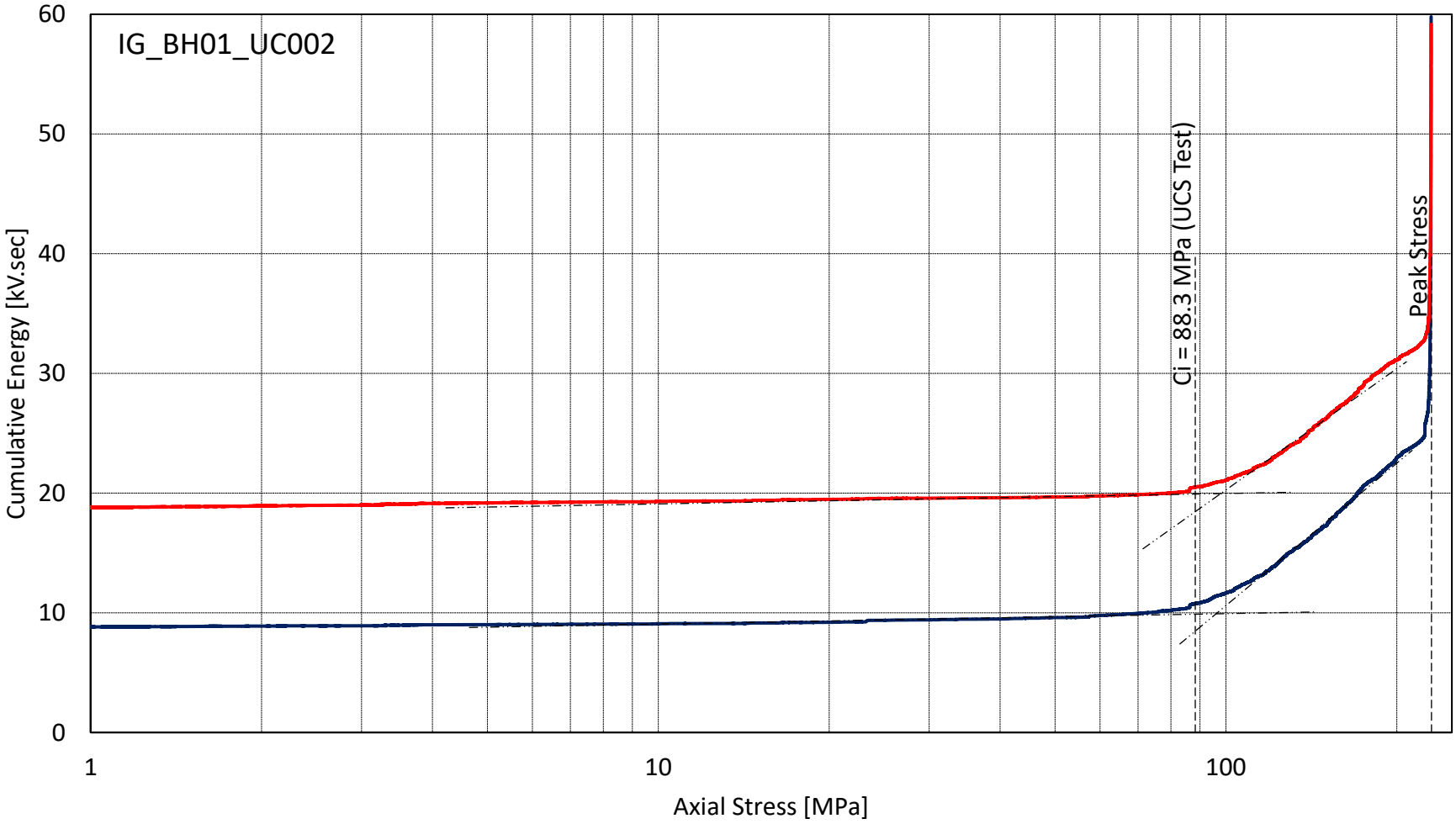
APPENDIX B

Acoustic Emission Data and Graph Report

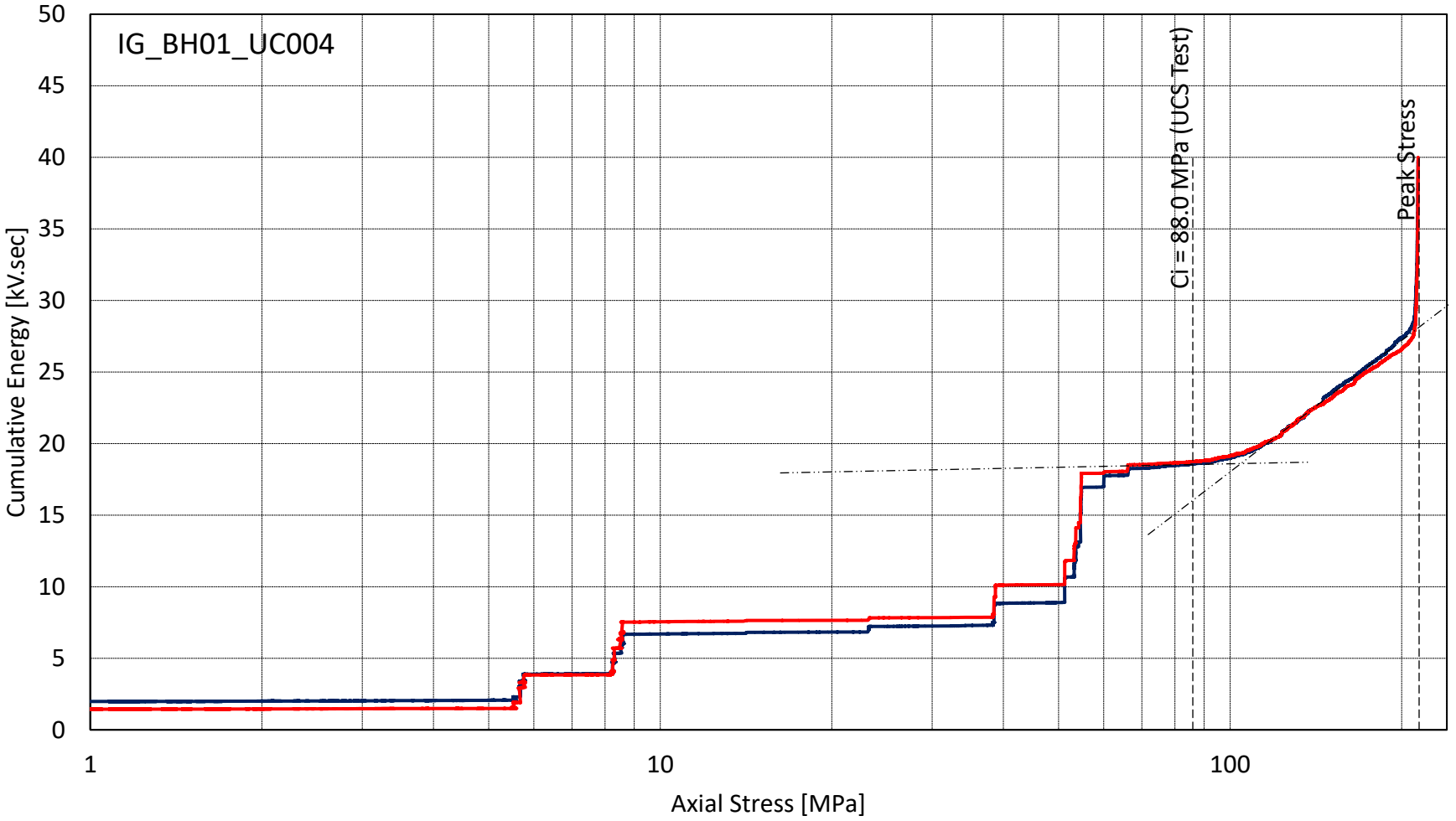
Table B-1: List of uniaxial compression test specimens

Specimen No.	Depth (m)[1]	Rock Type	Page
IG_BH01_UC002	442.26	Biotite Granodiorite-Tonalite	B-2
IG_BH01_UC004	522.90	Biotite Granodiorite-Tonalite	B-3
IG_BH01_UC006	601.00	Biotite Granodiorite-Tonalite	B-4
IG_BH01_UC007	451.06	Biotite Tonalite	B-5
IG_BH01_UC008	560.11	Feldspar-phyric Tonalite Dyke	B-6
IG_BH01_UC009	655.46	Amphibolite	B-7
IG_BH01_UC010	658.55	Amphibolite	B-8

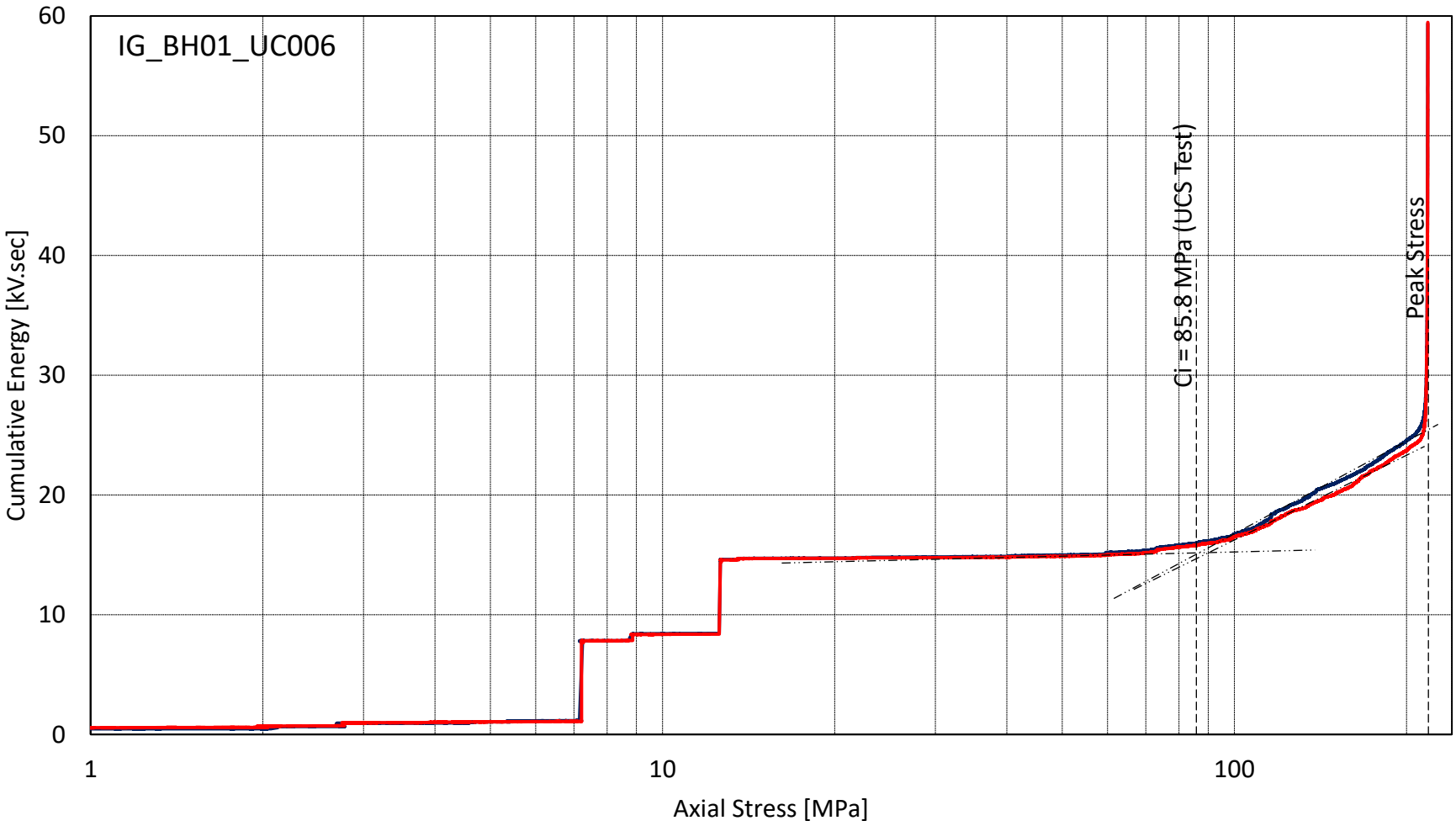
[1]Top depth of prepared sub-sample



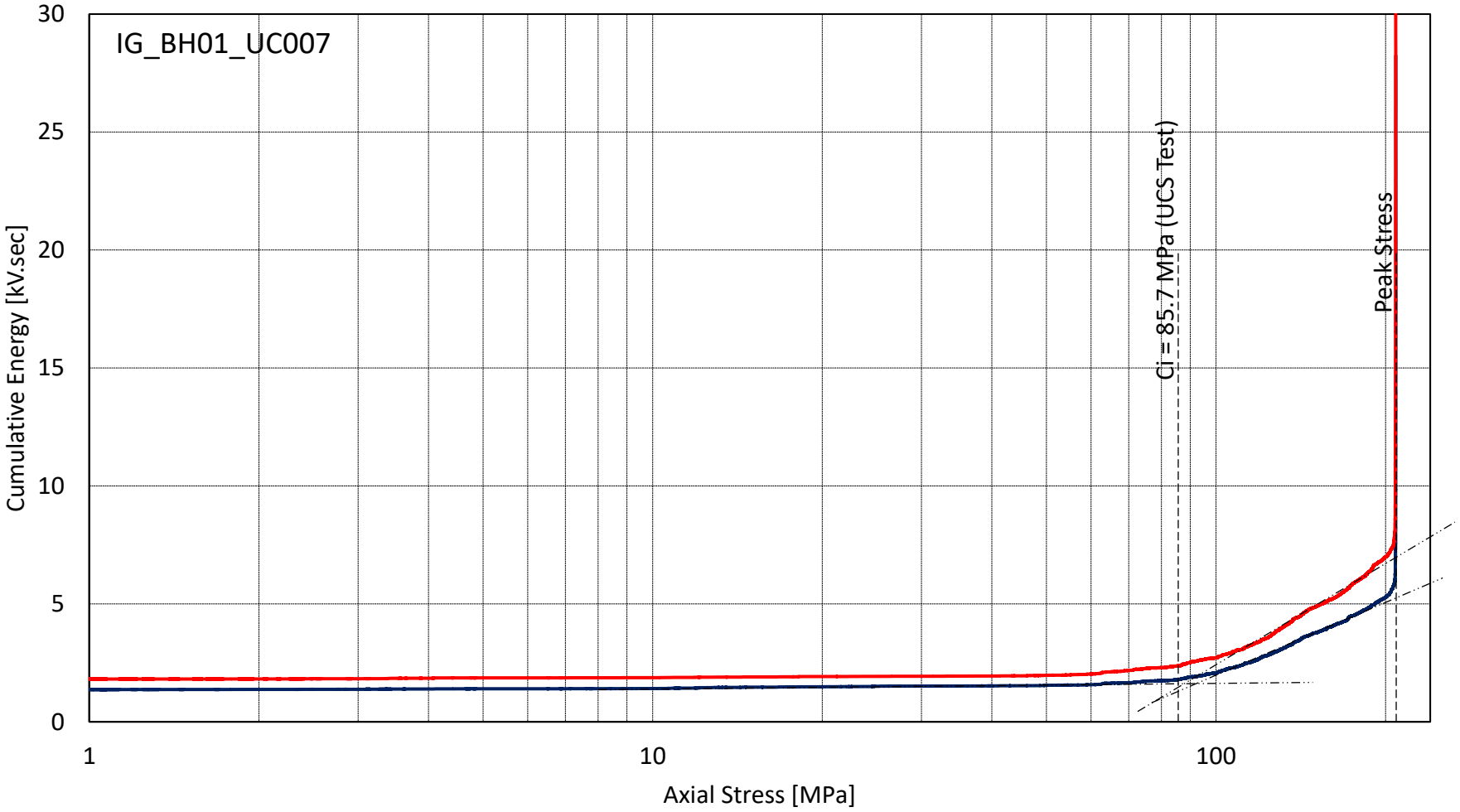
Test Specimen IG_BH01_UC002 – Depth = 442.01 m: Cumulative Energy vs Axial Stress



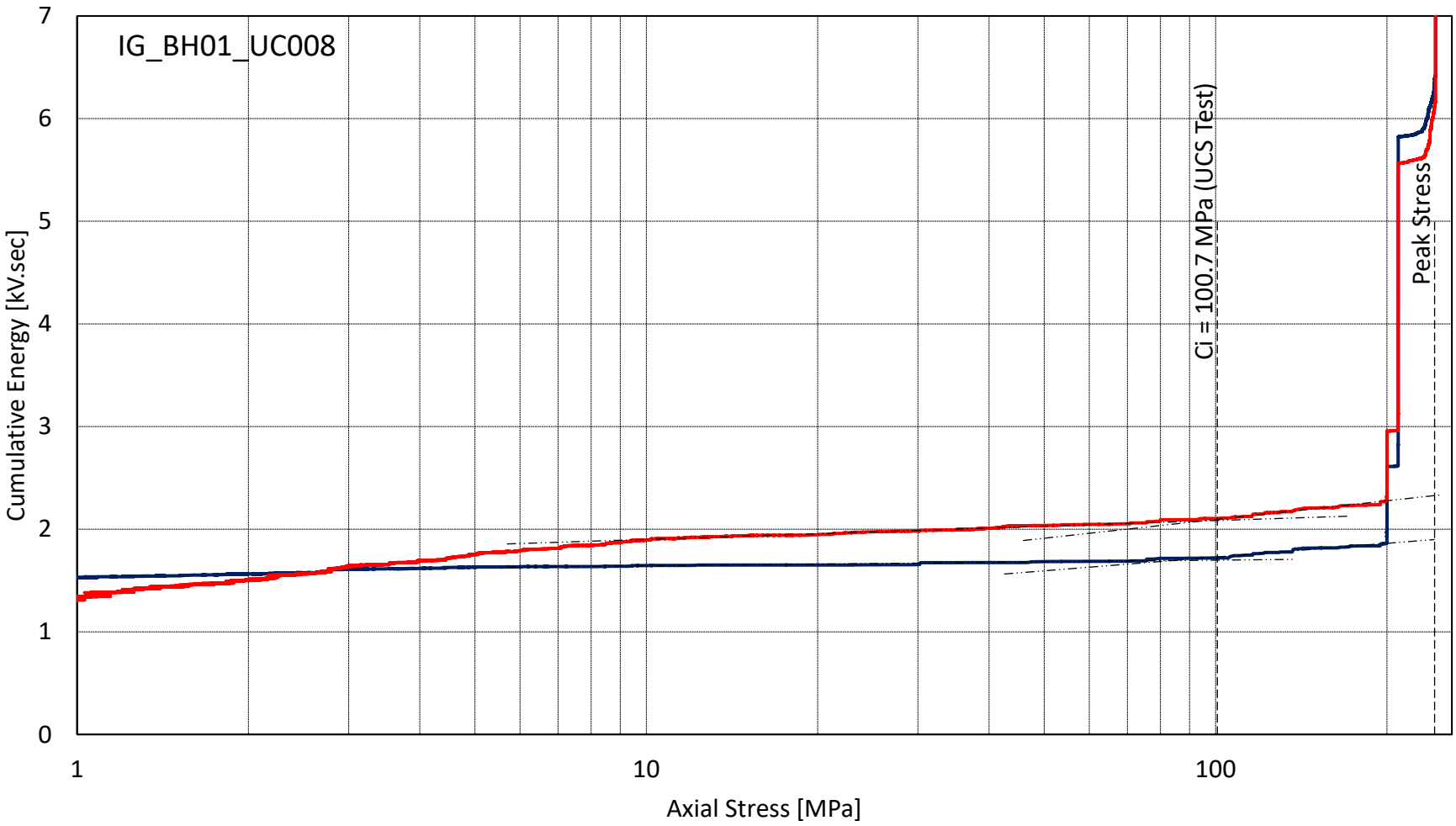
Test Specimen IG_BH01_UC004 – Depth = 522.64 m: Cumulative Energy vs Axial Stress



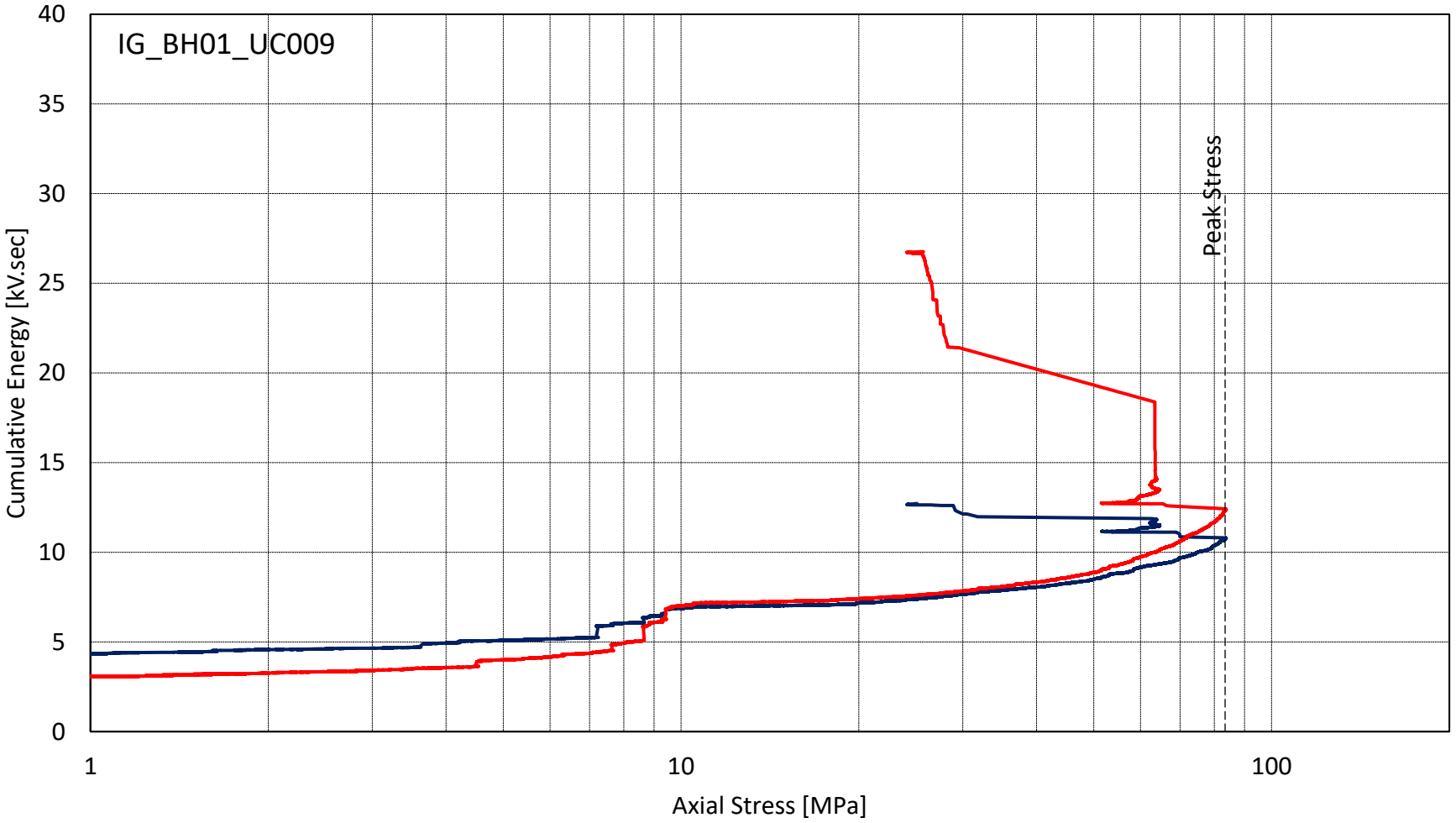
Test Specimen IG_BH01_UC006 – Depth = 600.72 m: Cumulative Energy vs Axial Stress



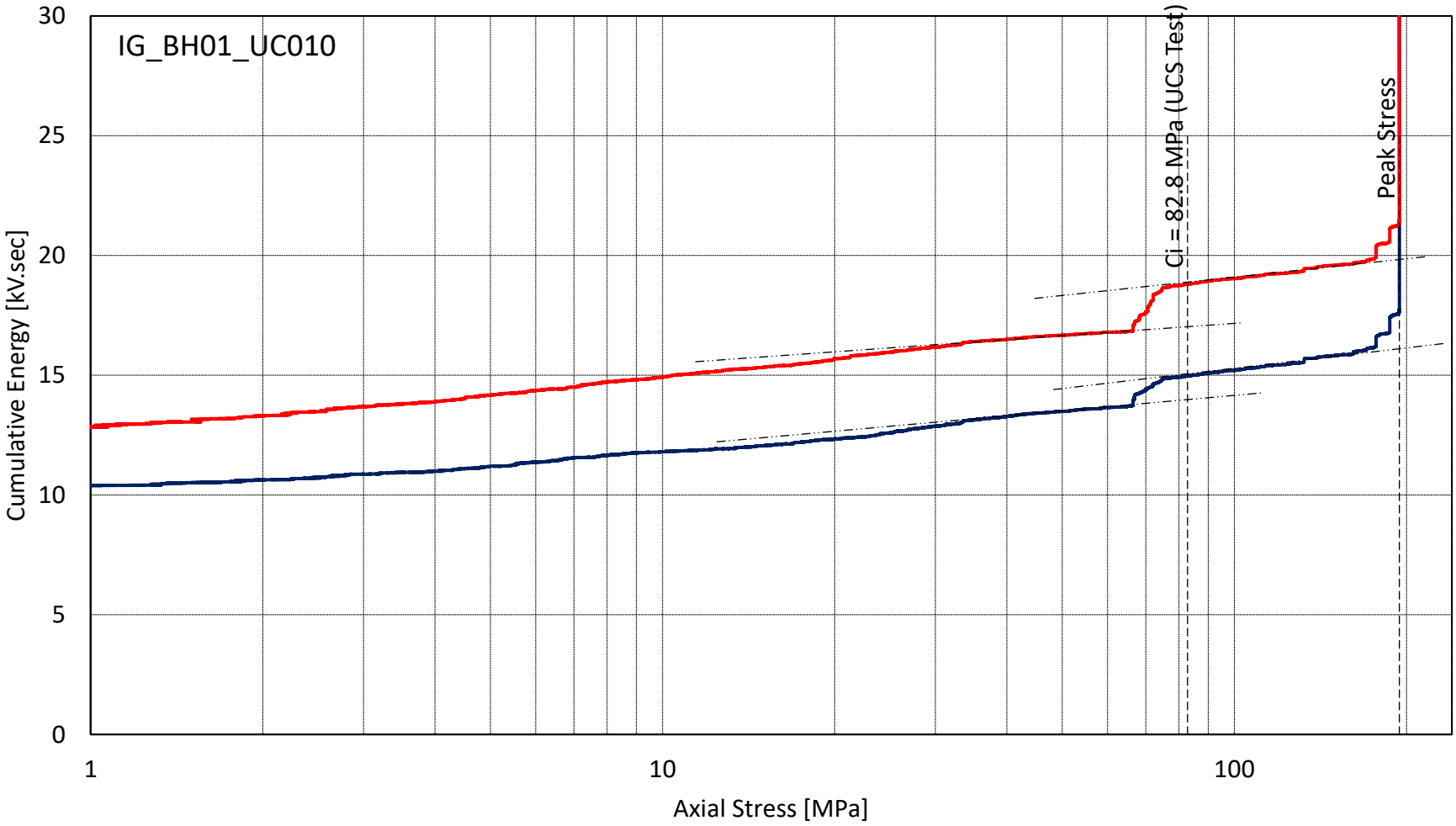
Test Specimen IG_BH01_UC007 – Depth = 450.79 m: Cumulative Energy vs Axial Stress



Test Specimen IG_BH01_UC008 – Depth = 559.94 m: Cumulative Energy vs Axial Stress



Test Specimen IG_BH01_UC009 – Depth = 655.01 m: Cumulative Energy vs Axial Stress



Test Specimen IG_BH01_UC010 – Depth = 658.31 m: Cumulative Energy vs Axial Stress

AE Data and Graph Report

by Denis Labrie, Senior Research-Engineer, **and Ted Anderson,** Senior Technologist
CanmetMINING, Natural Resources Canada, Ottawa, Canada

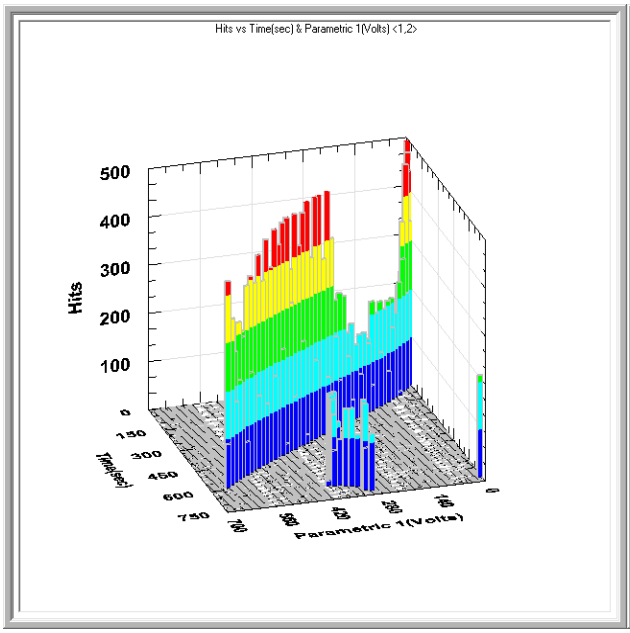
P:\lab data\D Labrie\Golder Associates\P-002797.001 - NWMO - Winter 2018\Test Data\AE\Data\408.dta

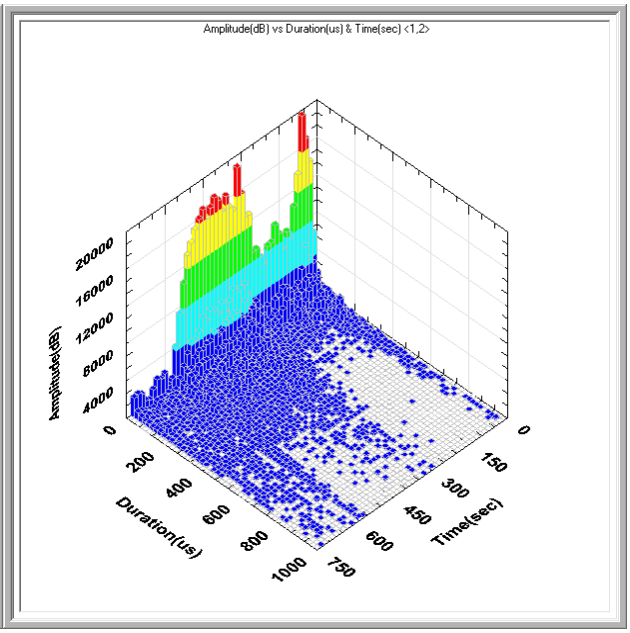
Total AEHits :	31377
Total TDDs :	72
Total Waveforms:	31377
Total Resumes :	2
Total Pauses :	2
Total TimeMarks:	0

Channel	AEHits
1	11886
2	19491

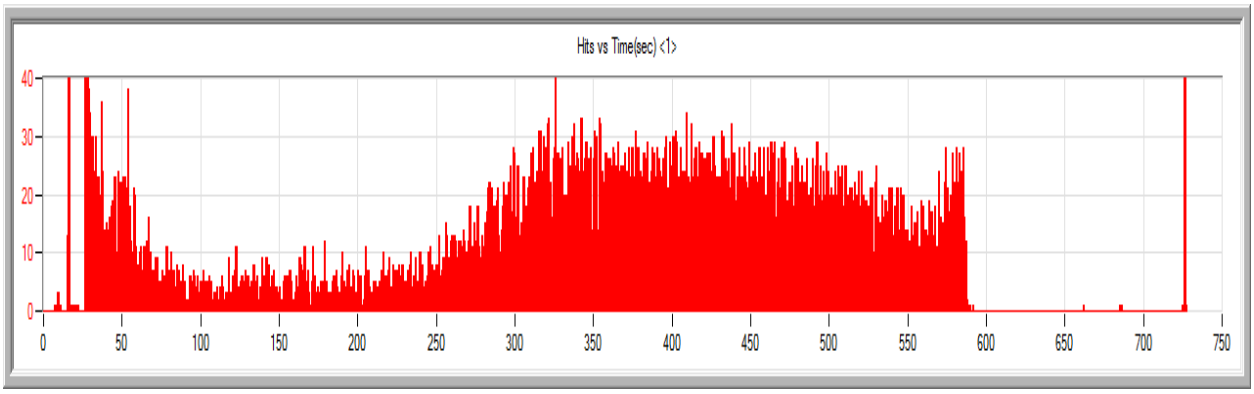
HIT DRIVEN DATA:

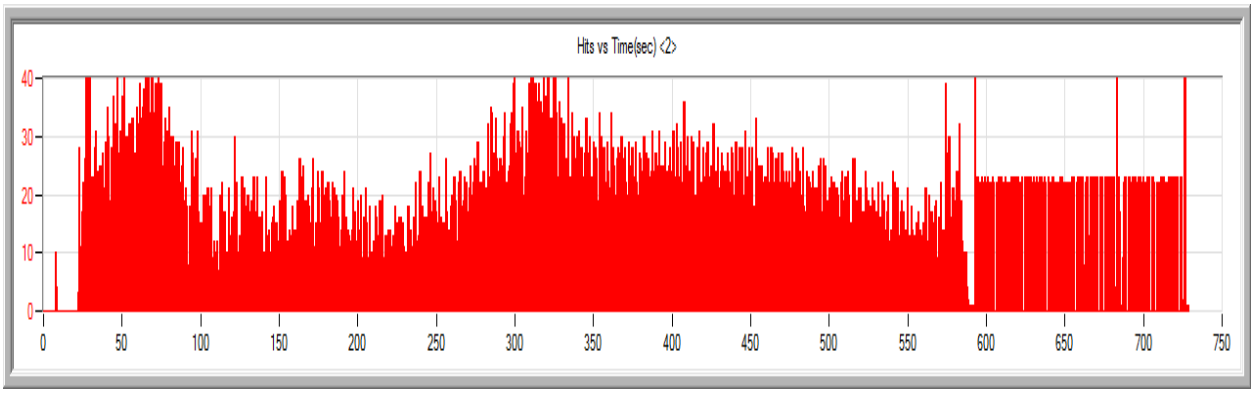
Feature	Chan	Minimum	Maximum	Average	Std Dev
Risetime	1	0.0000	13083.0000	110.3401	681.8783
Counts	1	1.0000	30612.0000	62.0603	829.5817
Energy	1	0.0000	65535.0000	87.4179	1955.1498
Duration	1	0.0000	1000000.0000	2022.5957	39099.4999
Amplitude	1	40.0000	100.0000	46.7353	7.5155
Threshold	1	40.0000	40.0000	40.0000	-1.#IND
SigStrength	1	0.0000	8808158208.0000	1422348.0000	83675408.8717
AbsEnergy	1	0.0000	37712961536.0000	3966316.0000	349787861.2215
Parametric1	1	-0.0009	2.5190	1.4449	0.7563
Risetime	2	0.0000	13007.0000	131.7818	786.9697
Counts	2	1.0000	31722.0000	59.0887	768.2369
Energy	2	0.0000	65535.0000	40.8327	1189.2097
Duration	2	0.0000	1000000.0000	1050.4120	20274.3130
Amplitude	2	40.0000	100.0000	47.2387	7.9845
Threshold	2	40.0000	40.0000	40.0000	-1.#IND
SigStrength	2	0.0000	7931543040.0000	816696.6875	60258850.5439
AbsEnergy	2	0.0000	27801759744.0000	1983122.0000	203059726.3438
Parametric1	2	-0.0006	2.5178	1.2140	0.7335

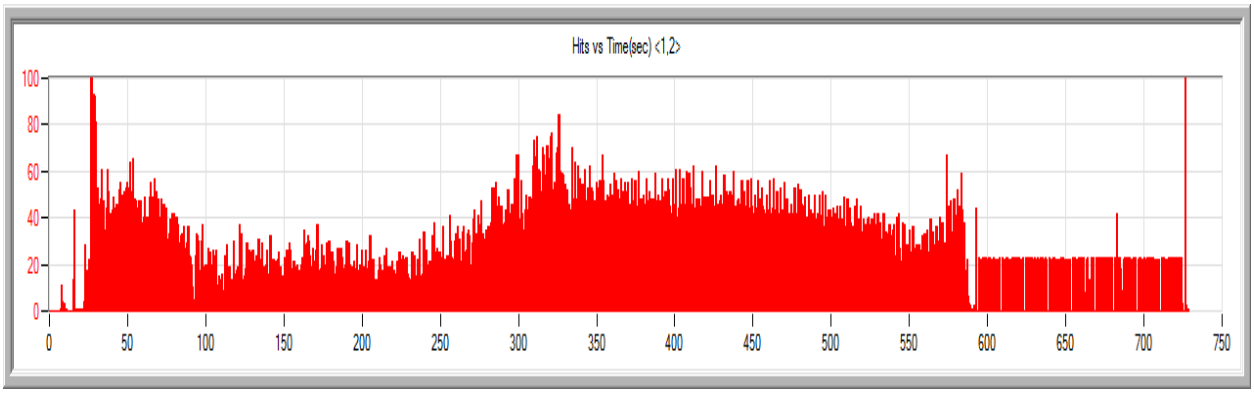




Test Specimen BH01-UC001-408.40-U





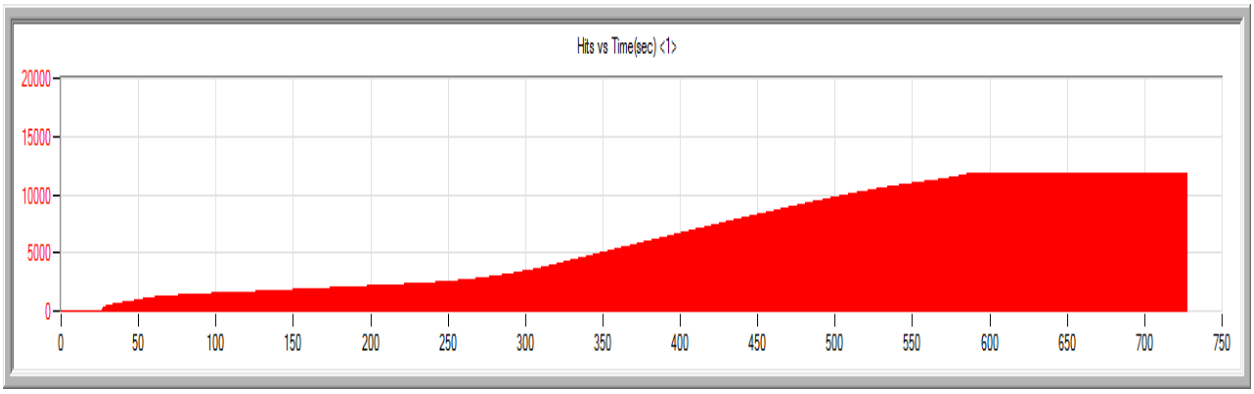


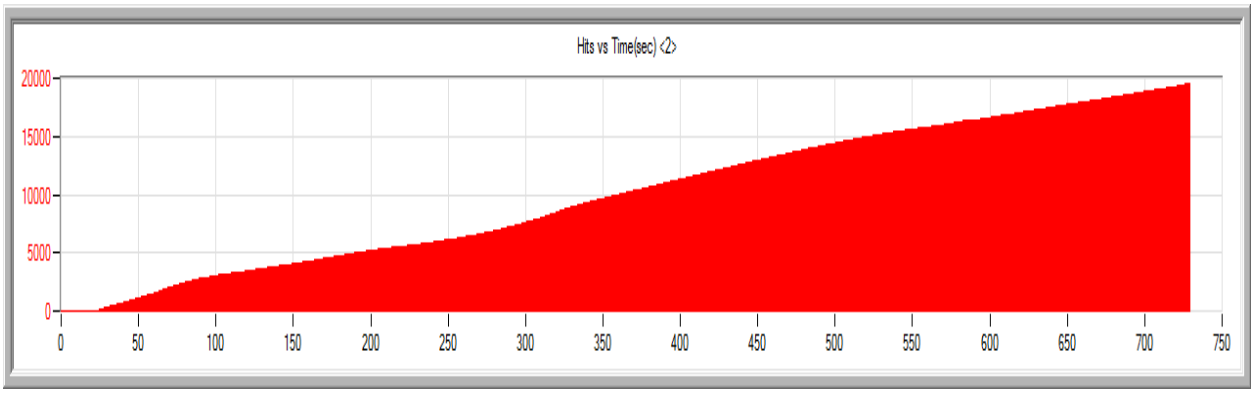
Legend – Page 1: Statistics and Isometric Views

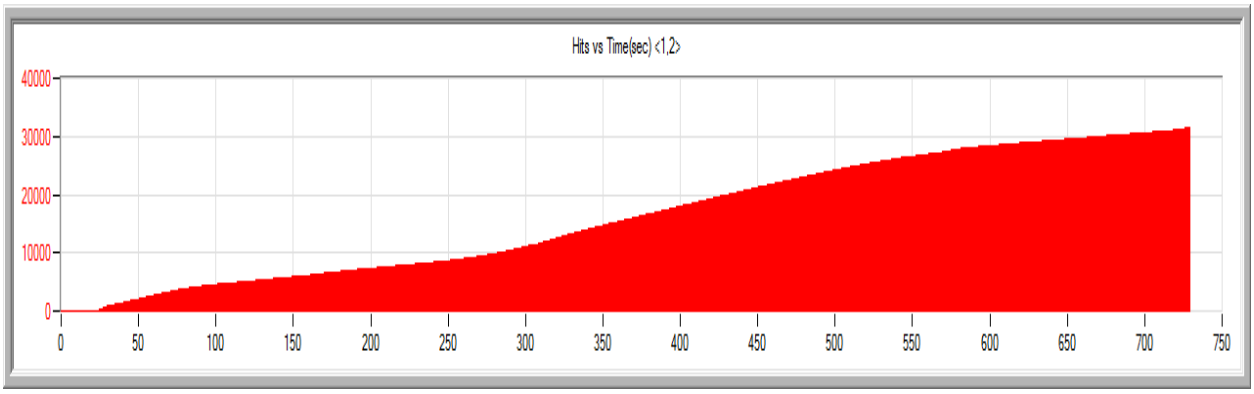
- Statistics of Test BH01-UC001-408.40-U (Top of page)
- Isometric View: (1) Hits vs Time (sec) vs Load (Parametric, in kN) (Bottom of page, left)
- Isometric View: (2) Amplitude (dB) vs Duration (µsec) vs Time (sec) (Bottom of page, right)

Legend – Page 2: Hits Count vs Time (sec) – Per Time Period

- Hits vs Time (sec) – Channel 1 (Top of page)
- Hits vs Time (sec) – Channel 2 (Middle of page)
- Hits vs Time (sec) – Channels 1 and 2, combined (Bottom of page)

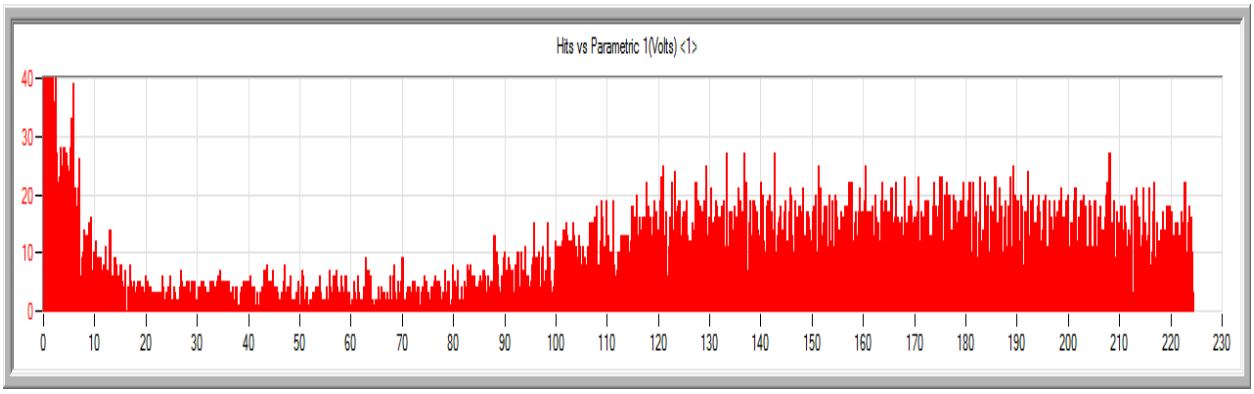


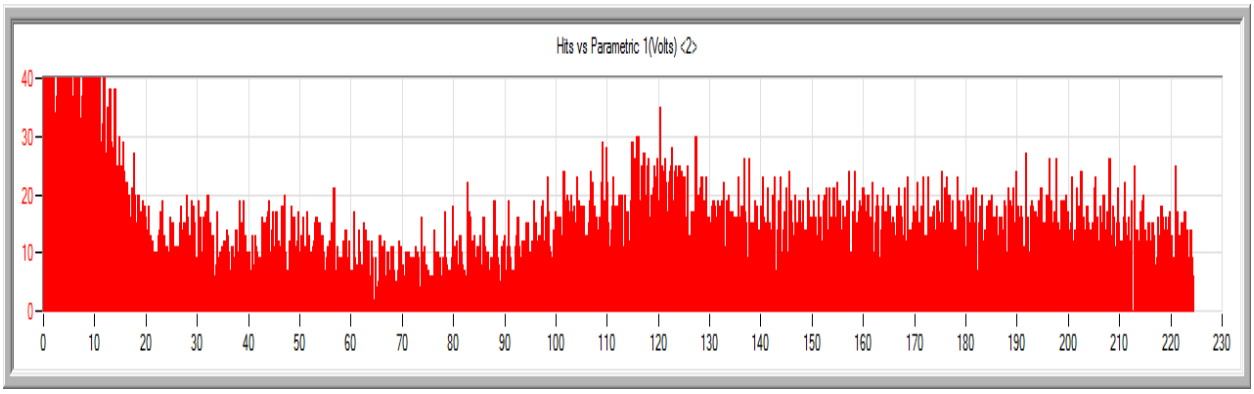


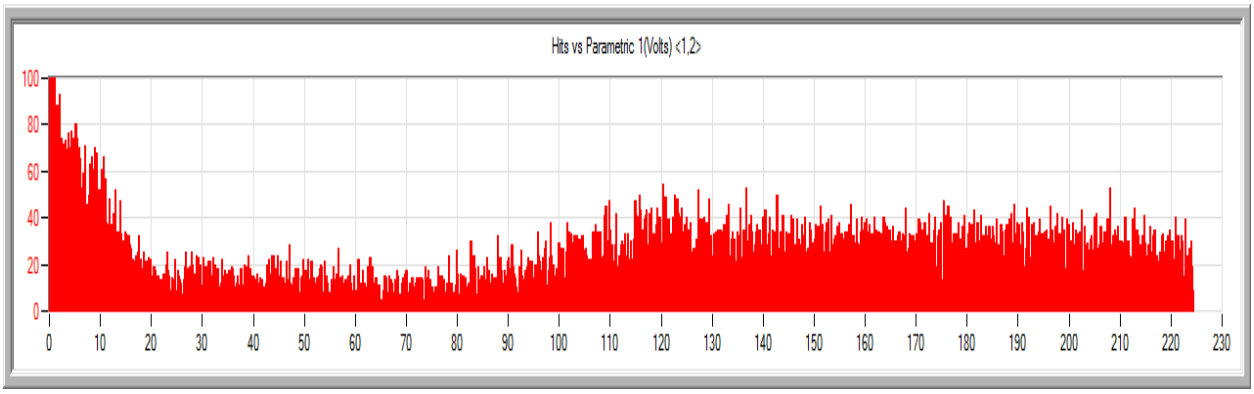


Legend – Page 3: Hits Count vs Time (sec) - Cumulative

- Hits vs Time (sec) – Channel 1 (Top of page)
- Hits vs Time (sec) – Channel 2 (Middle of page)
- Hits vs Time (sec) – Channels 1 and 2, combined (Bottom of page)

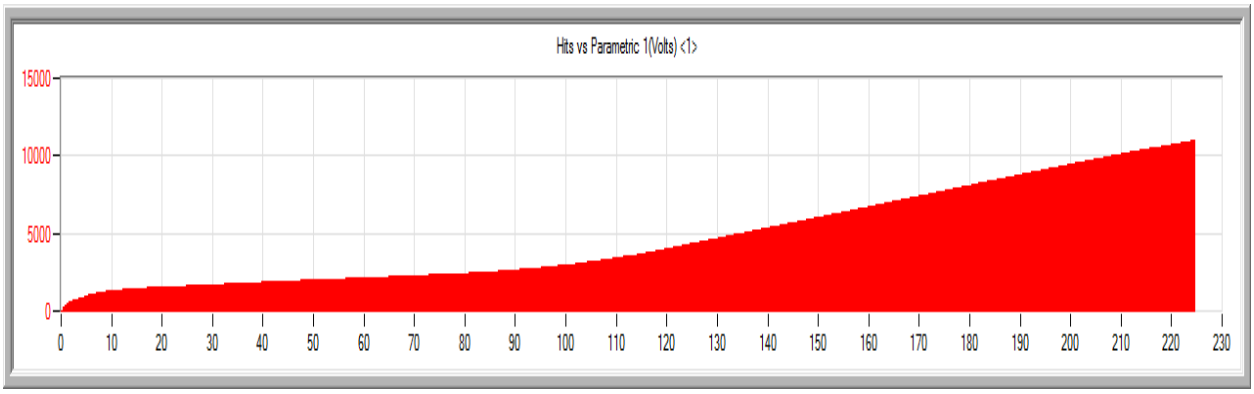


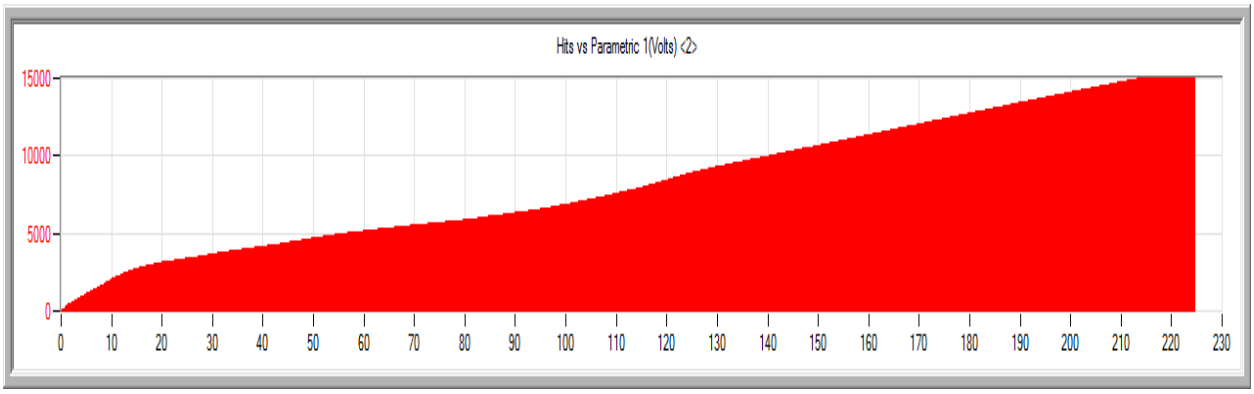


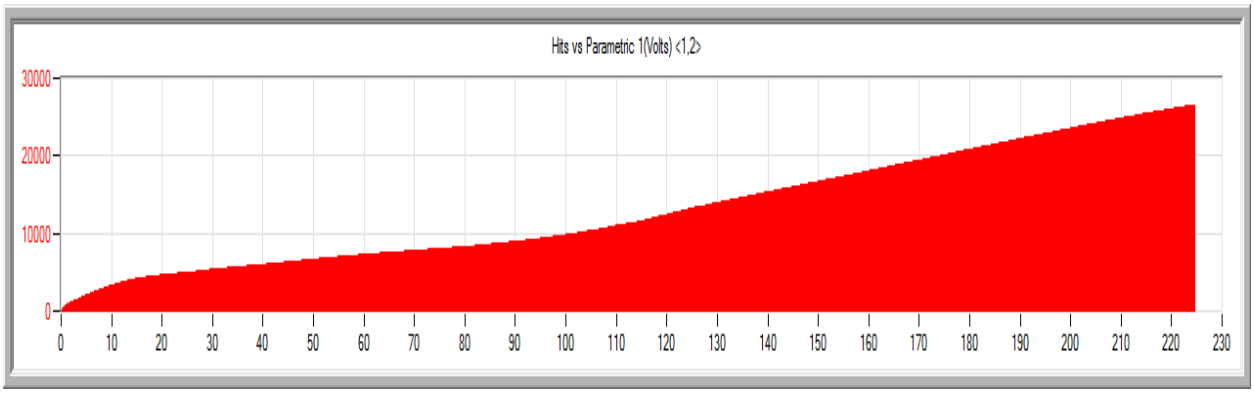


Legend – Page 4: Hits Count vs Stress (MPa) – Per Time Period

- Hits vs Stress (MPa) – Channel 1 (Top of page)
- Hits vs Stress (MPa) – Channel 2 (Middle of page)
- Hits vs Stress (MPa) – Channels 1 and 2, combined (Bottom of page)

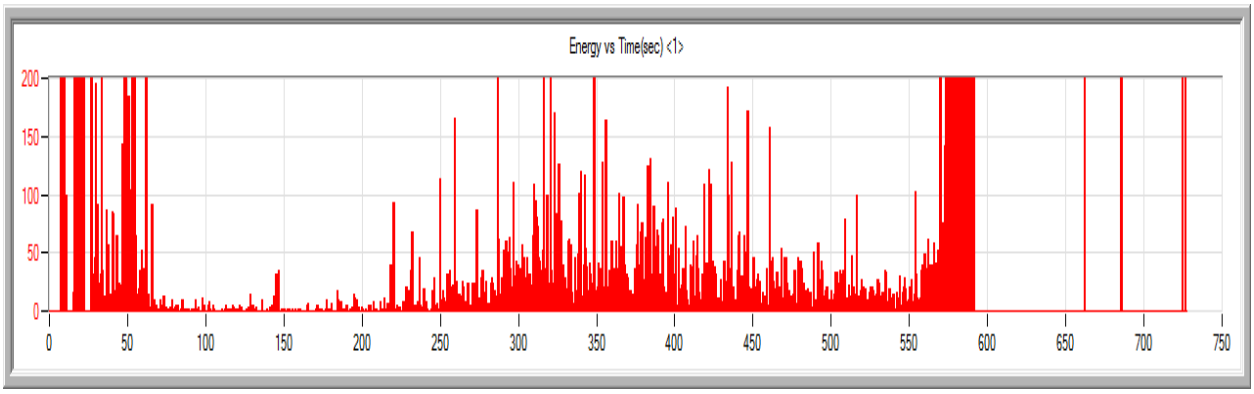


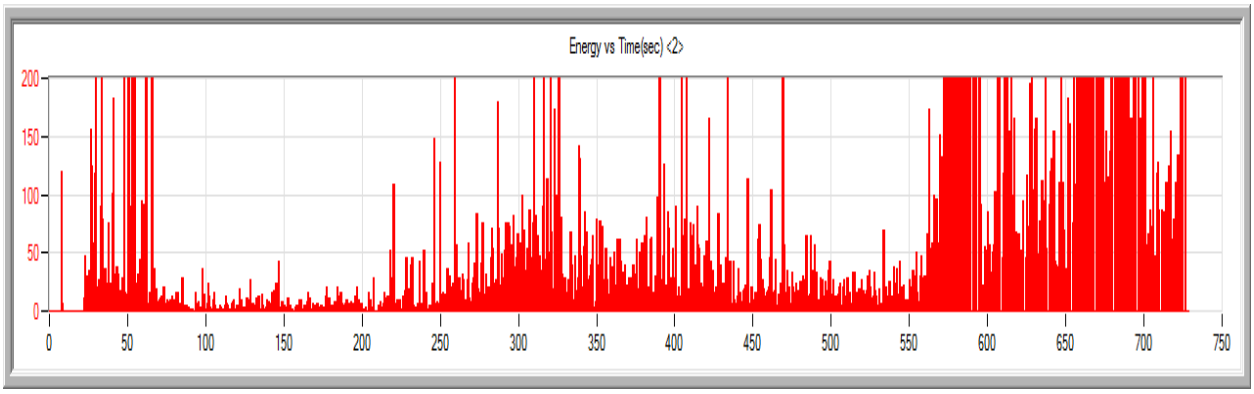


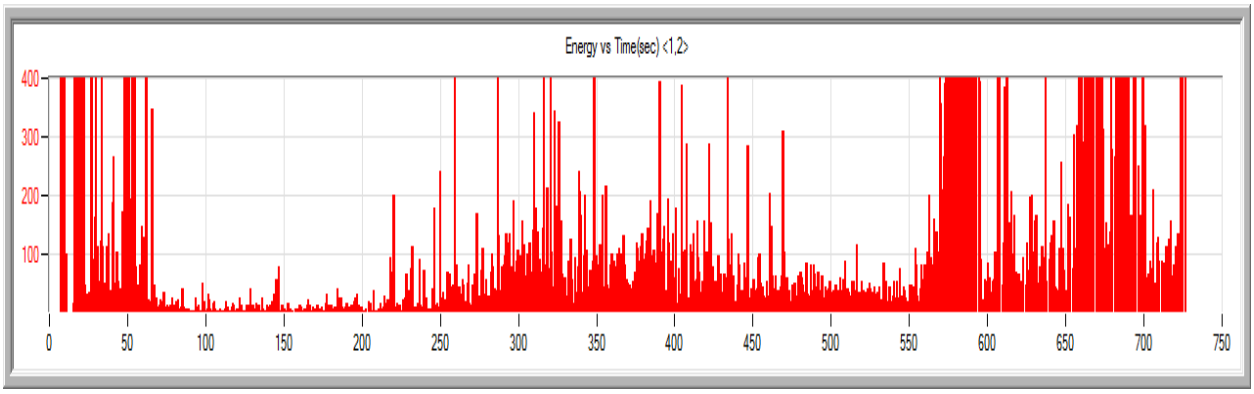


Legend – Page 5: Hits Count vs Stress (MPa) – Cumulative

- Hits vs Stress (MPa) – Channel 1 (Top of page)
- Hits vs Stress (MPa) – Channel 2 (Middle of page)
- Hits vs Stress (MPa) – Channels 1 and 2, combined (Bottom of page)

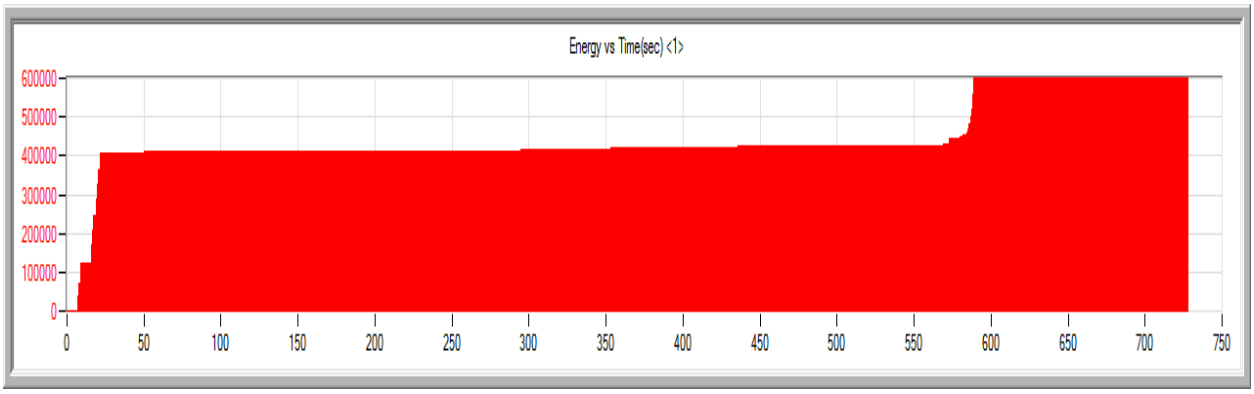


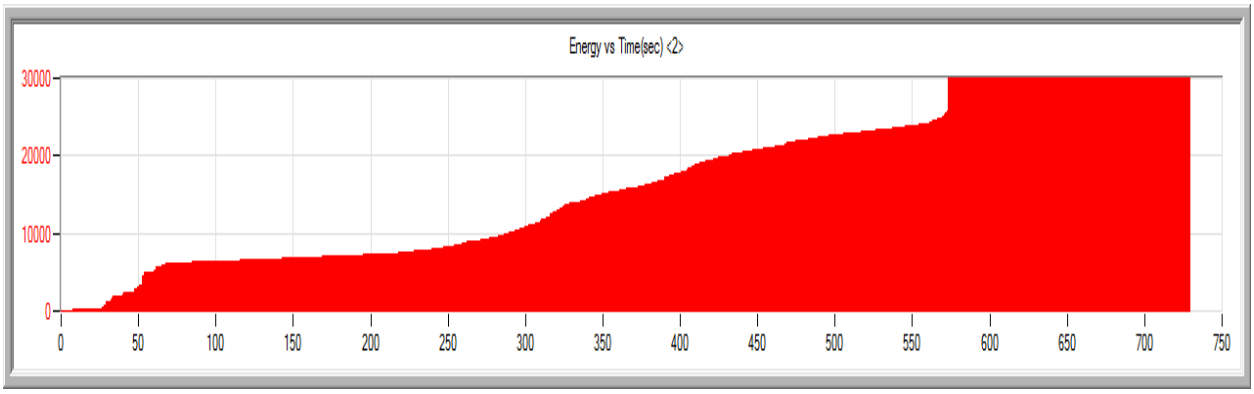


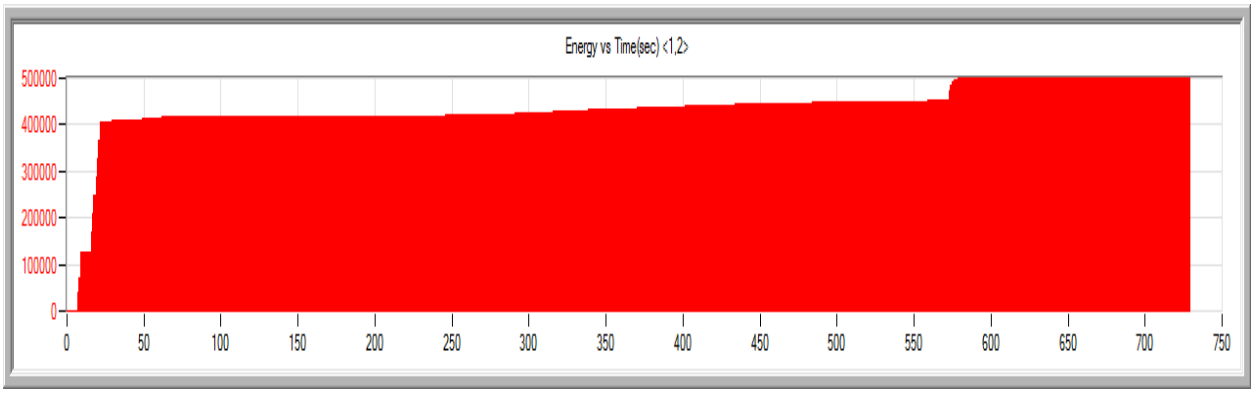


Legend – Page 6: Energy vs Time (sec) – Per Time Period

- Energy vs Time (sec) – Channel 1 (Top of page)
- Energy vs Time (sec) – Channel 2 (Middle of page)
- Energy vs Time (sec) – Channels 1 and 2, combined (Bottom of page)

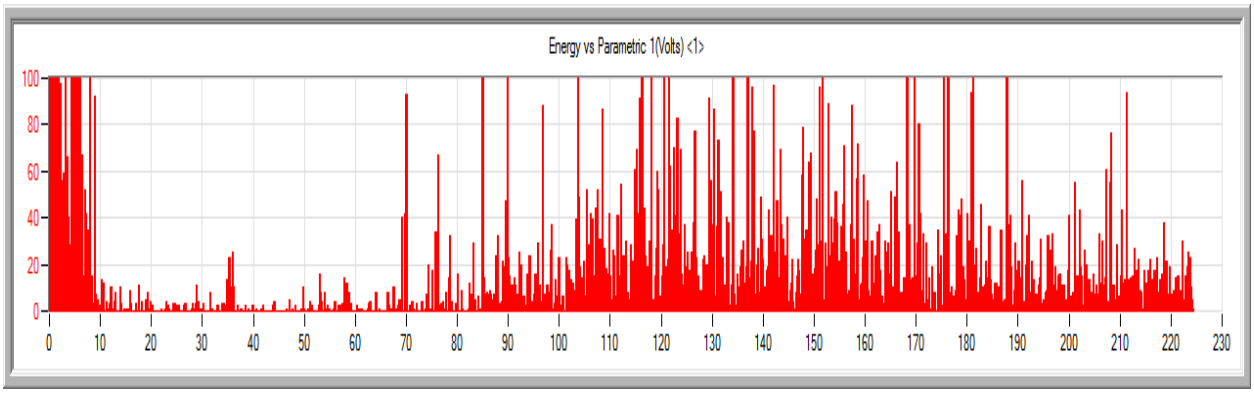


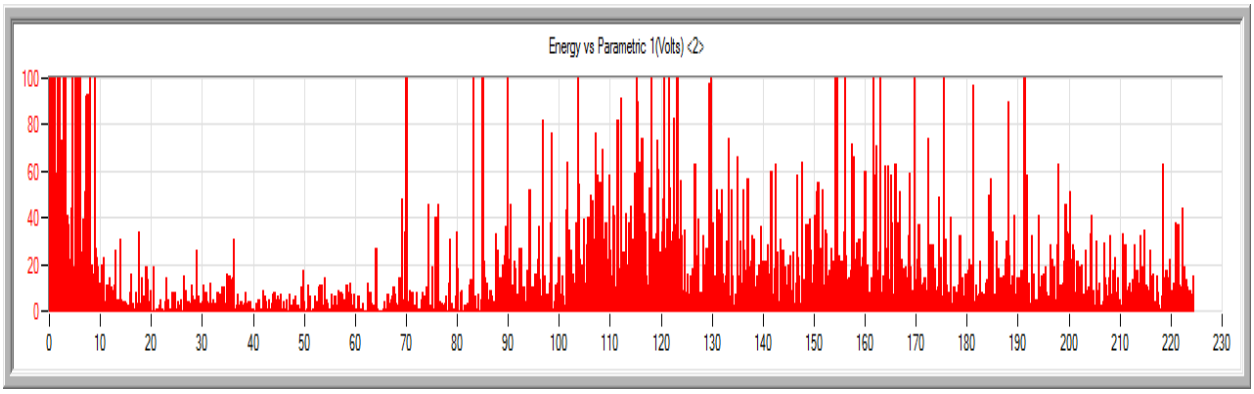


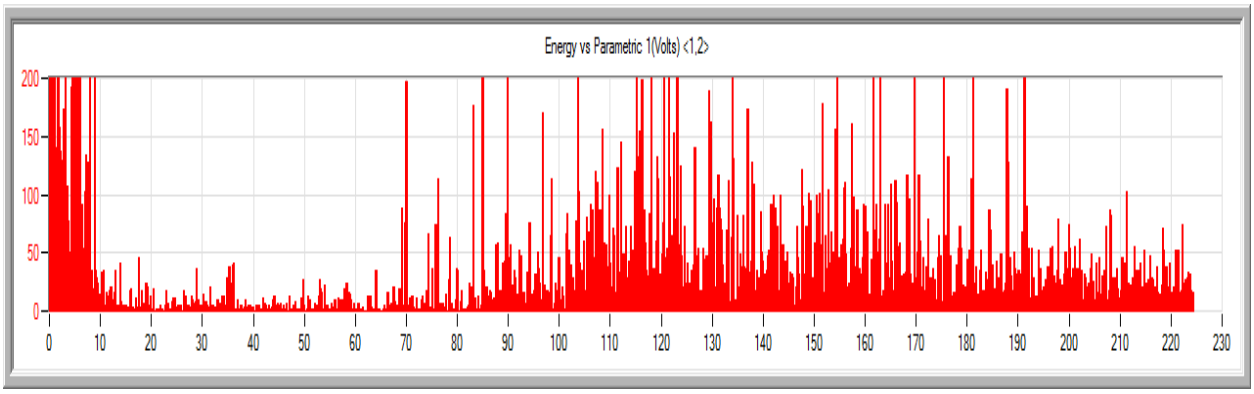


Legend – Page 7: Energy vs Time (sec) - Cumulative

- Energy vs Time (sec) – Channel 1 (Top of page)
- Energy vs Time (sec) – Channel 2 (Middle of page)
- Energy vs Time (sec) – Channels 1 and 2, combined (Bottom of page)

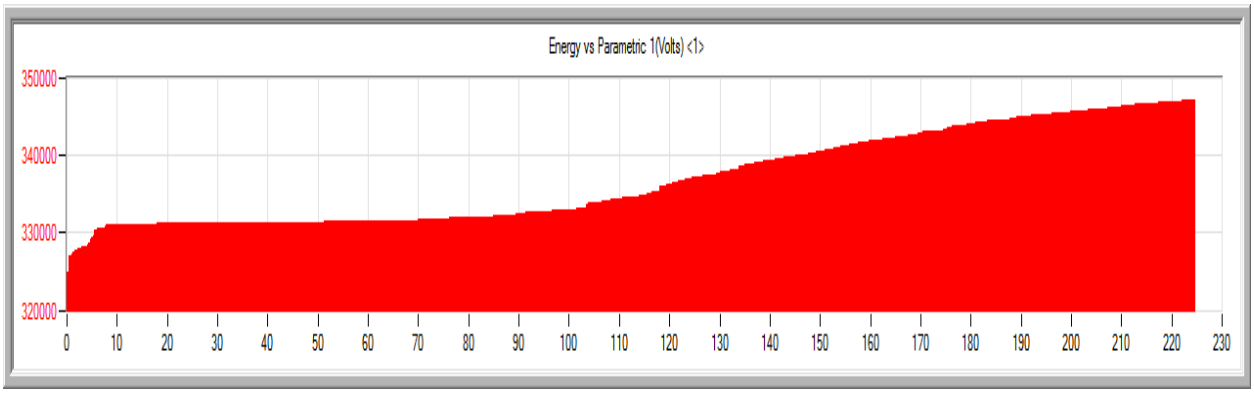


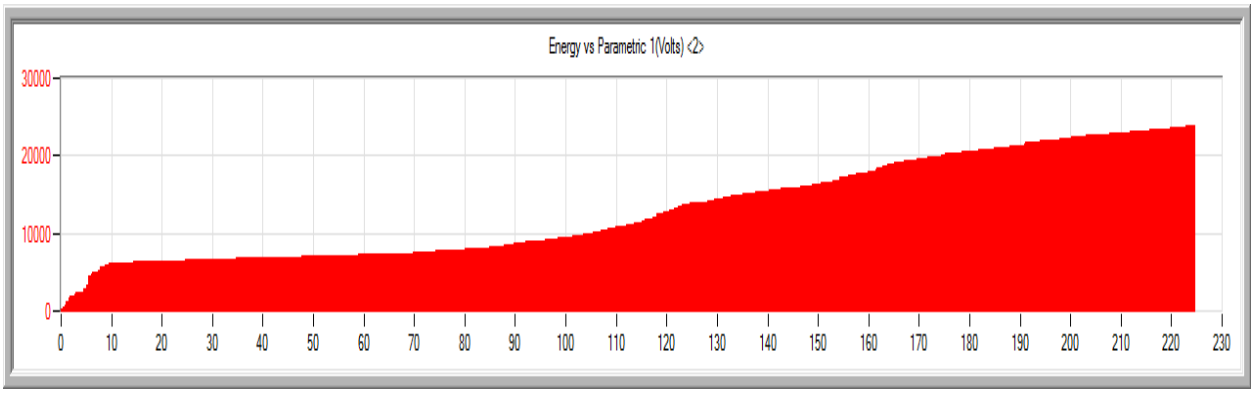


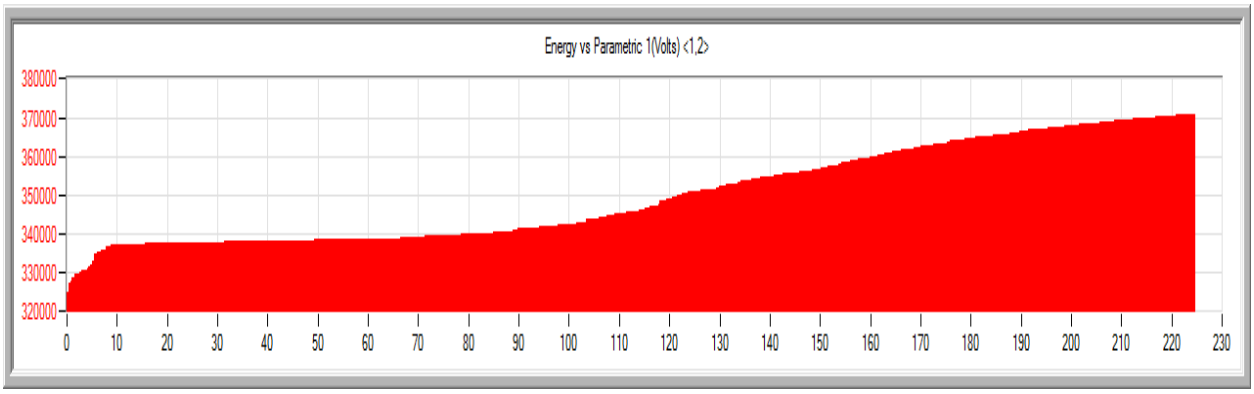


Legend – Page 8: Energy vs Stress (MPa) – Per Time Period

- Energy vs Stress (MPa) – Channel 1 (Top of page)
- Energy vs Stress (MPa) – Channel 2 (Middle of page)
- Energy vs Stress (MPa) – Channels 1 and 2, combined (Bottom of page)







Legend – Page 9: Energy vs Stress (MPa) - Cumulative

- Energy vs Stress (MPa) – Channel 1 (Top of page)
- Energy vs Stress (MPa) – Channel 2 (Middle of page)
- Energy vs Stress (MPa) – Channels 1 and 2, combined (Bottom of page)

Test Specimen BH01-UC003-468.02-U

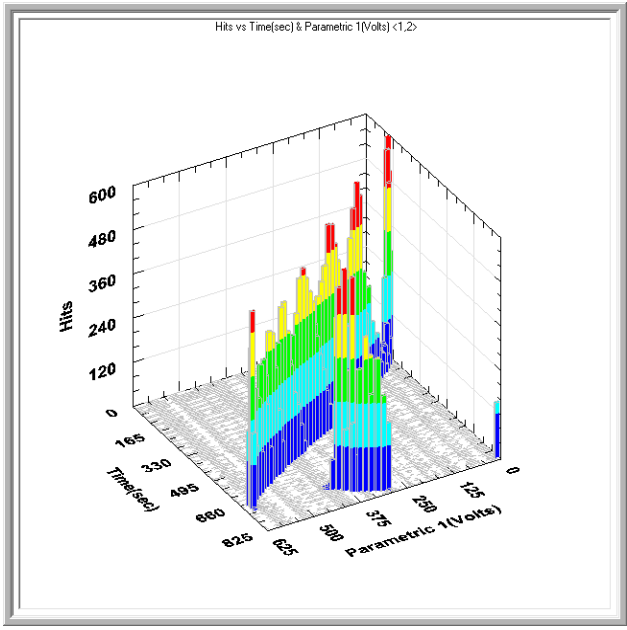
P:\lab data\D Labrie\Golder Associates\P-002797.001 - NWMO - Winter 2018\Test Data\AE\Data\4 02.dta

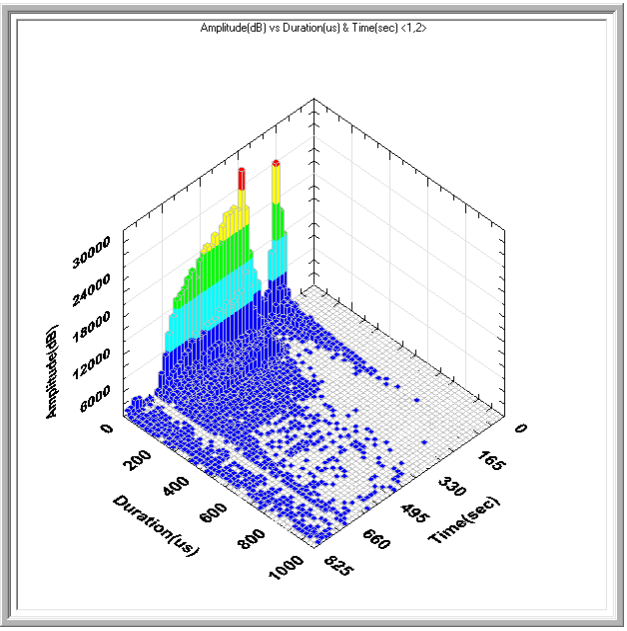
Total AEHits	33819
Total TDDs	68
Total Waveforms	33819
Total Resumes	2
Total Pauses	2
Total TimeMarks	0

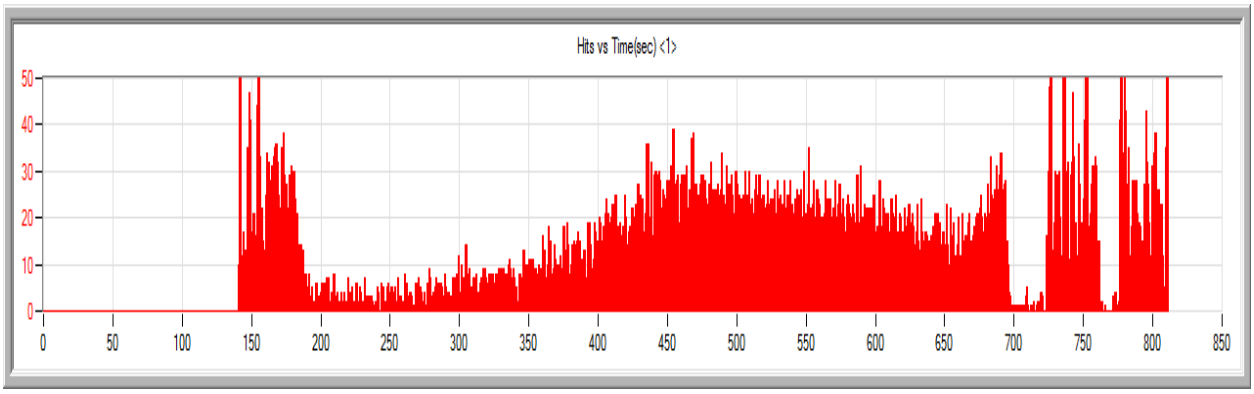
Channel	AEHits
1	13121
2	20698

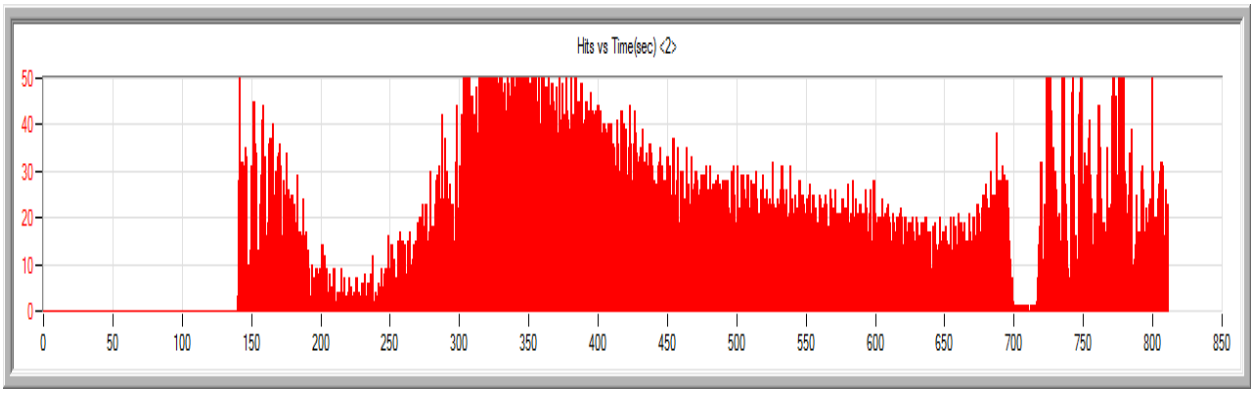
HIT DRIVEN DATA:

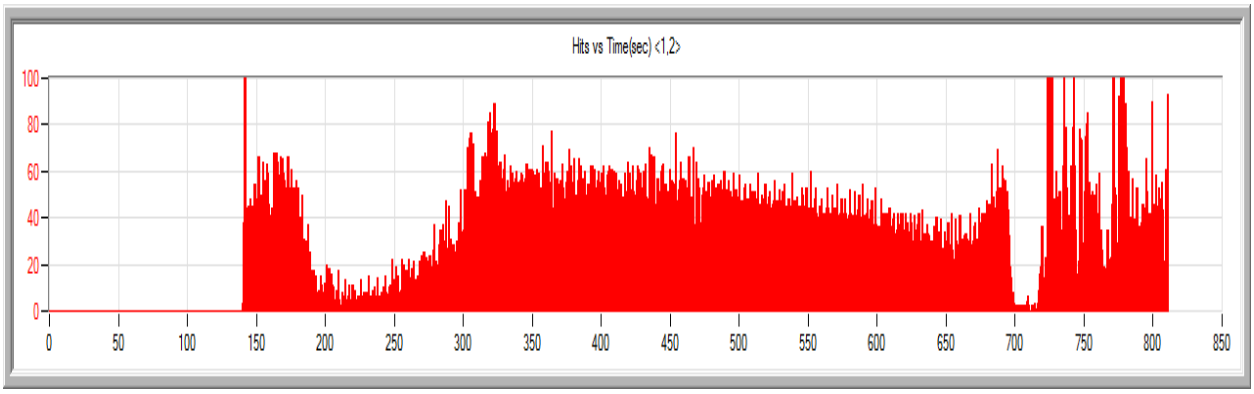
Feature	Chan	Minimum	Maximum	Average	Std Dev
Risetime	1	0.0000	13107.0000	664.1018	1987.7227
Counts	1	1.0000	32335.0000	327.2007	1669.9434
Energy	1	0.0000	65535.0000	201.4070	2544.9102
Duration	1	0.0000	1000000.0000	5464.7090	46373.6792
Amplitude	1	40.0000	100.0000	49.9158	11.5837
Threshold	1	40.0000	40.0000	40.0000	0.0075
SigStrength	1	0.0000	11320305664.0000	3186685.5000	125018656.4413
AbsEnergy	1	0.0000	46020136960.0000	7002710.5000	457243475.3419
Parametric1	1	0.0043	2.3676	1.3406	0.6810
Risetime	2	0.0000	13096.0000	433.7014	1516.4518
Counts	2	1.0000	32316.0000	142.6457	1024.7828
Energy	2	0.0000	65535.0000	99.9596	1800.3890
Duration	2	0.0000	1000000.0000	2834.0923	31915.7535
Amplitude	2	40.0000	100.0000	46.2148	9.9086
Threshold	2	40.0000	40.0000	40.0000	0.0062
SigStrength	2	0.0000	9905671168.0000	1686894.0000	85345698.9844
AbsEnergy	2	0.0000	33616805888.0000	3271833.0000	262900130.6638
Parametric1	2	0.0034	2.3682	1.1587	0.6299









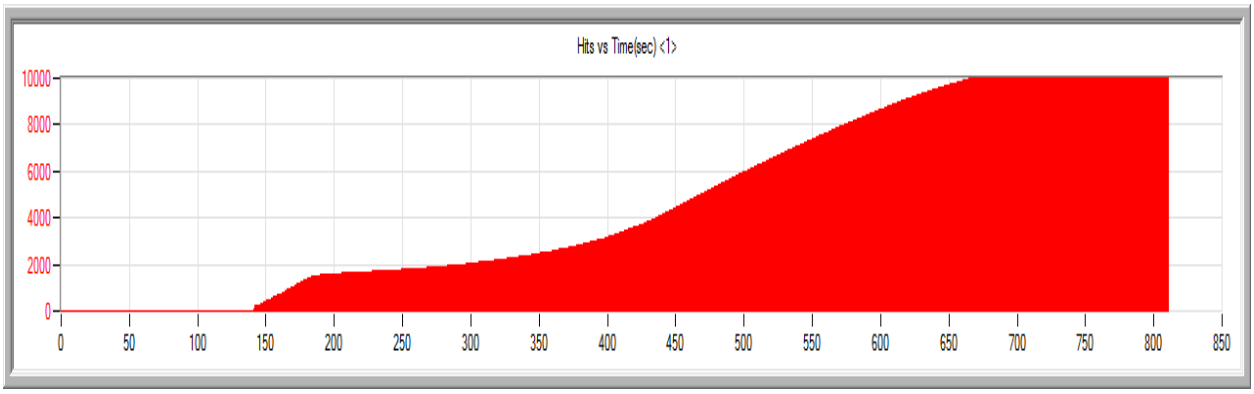


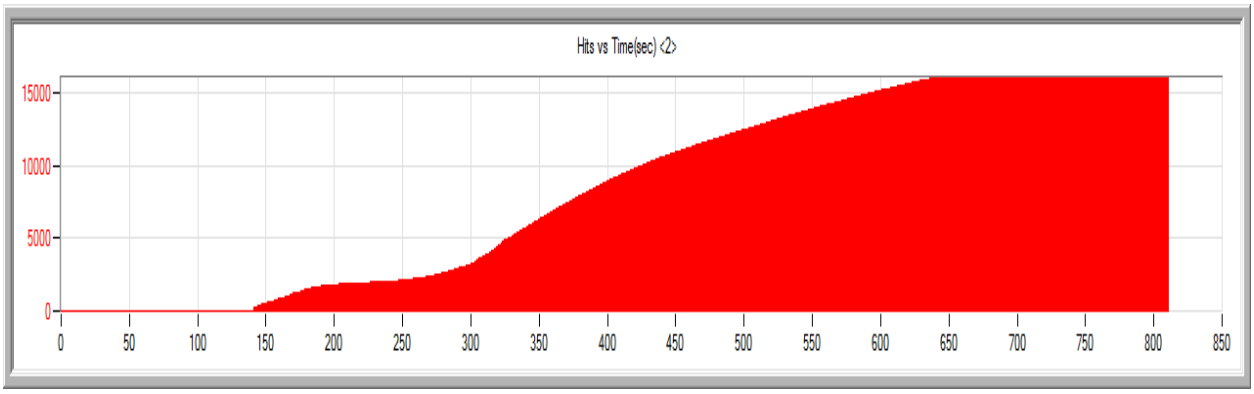
Legend – Page 10: Statistics and Isometric Views

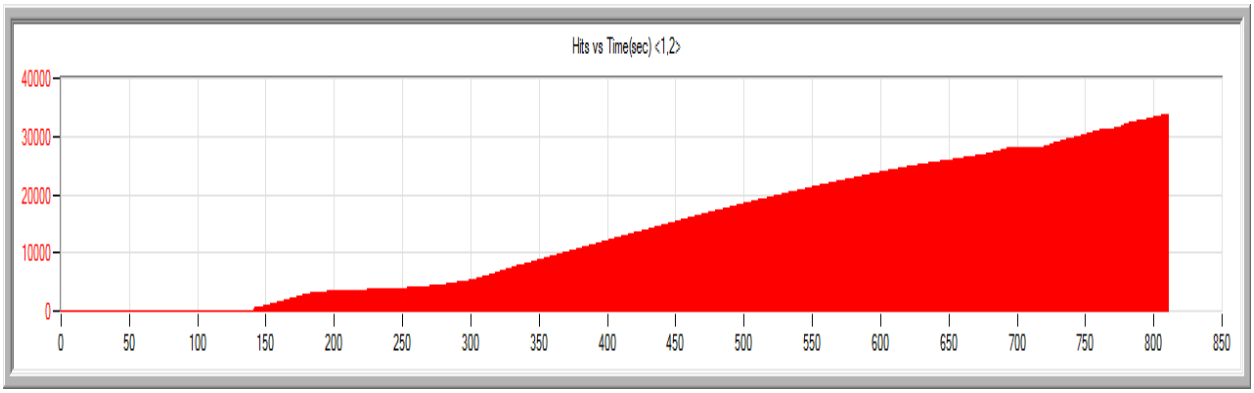
- Statistics of Test BH01-UC003-468.02-U (Top of page)
- Isometric View: (1) Hits vs Time (sec) vs Load (Parametric, in kN) (Bottom of page, left)
- Isometric View: (2) Amplitude (dB) vs Duration (µsec) vs Time (sec) (Bottom of page, right)

Legend – Page 11: Hits Count vs Time (sec) – Per Time Period

- Hits vs Time (sec) – Channel 1 (Top of page)
- Hits vs Time (sec) – Channel 2 (Middle of page)
- Hits vs Time (sec) – Channels 1 and 2, combined (Bottom of page)

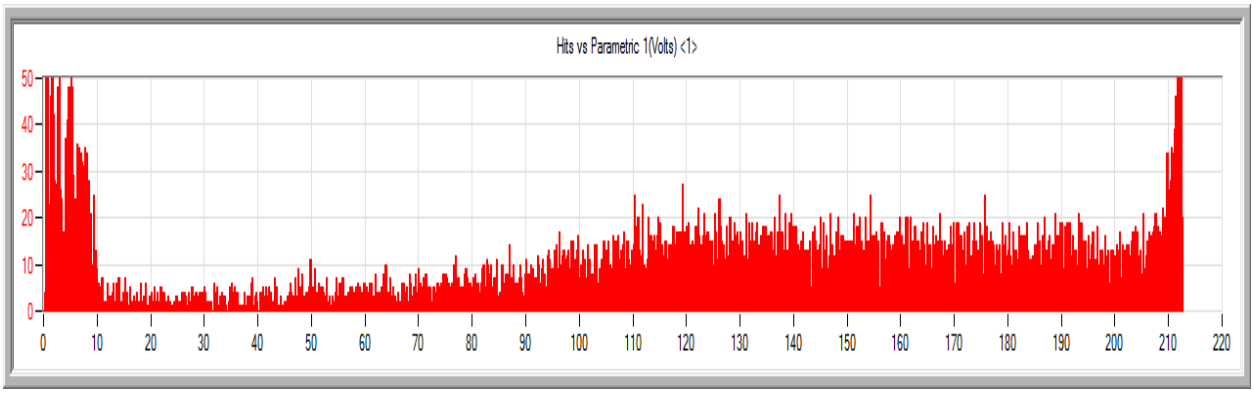


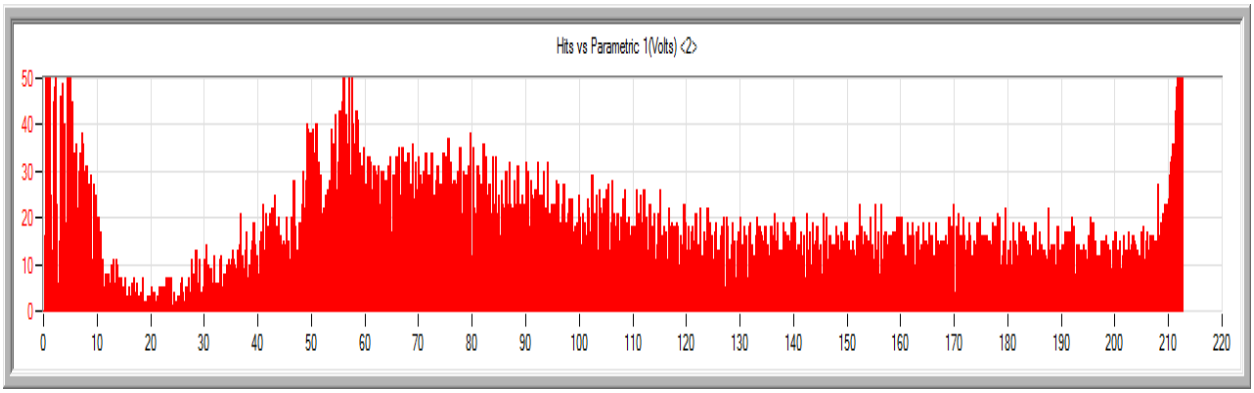


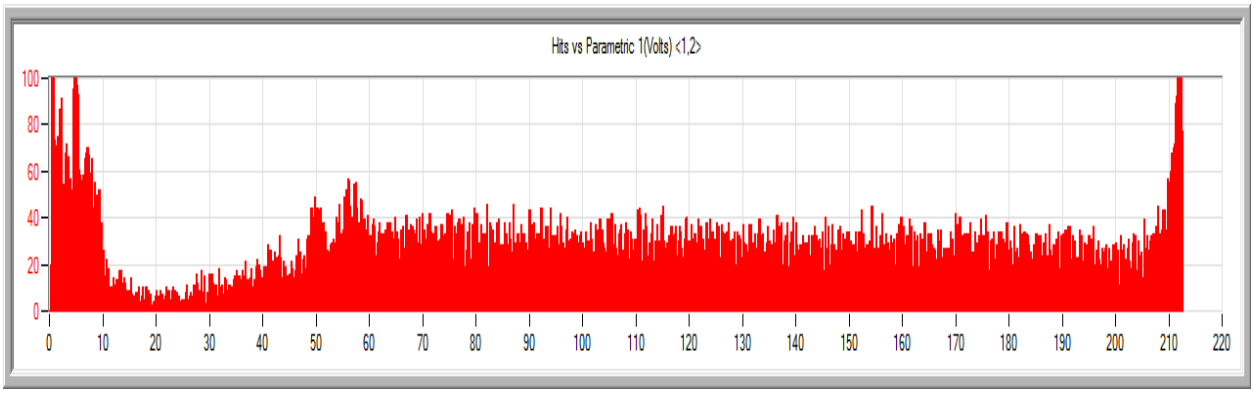


Legend – Page 12: Hits Count vs Time (sec) – Cumulative

- Hits vs Time (sec) – Channel 1 (Top of page)
- Hits vs Time (sec) – Channel 2 (Middle of page)
- Hits vs Time (sec) – Channels 1 and 2, combined (Bottom of page)

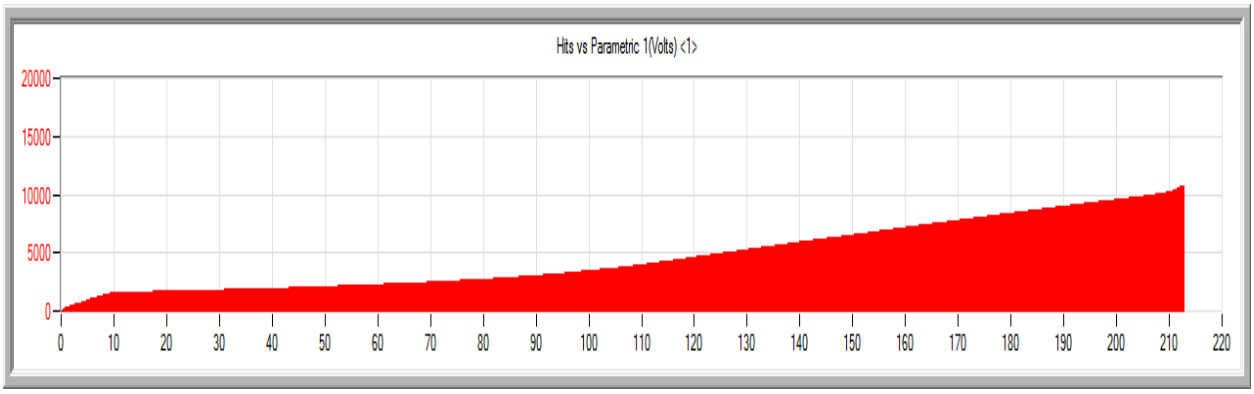


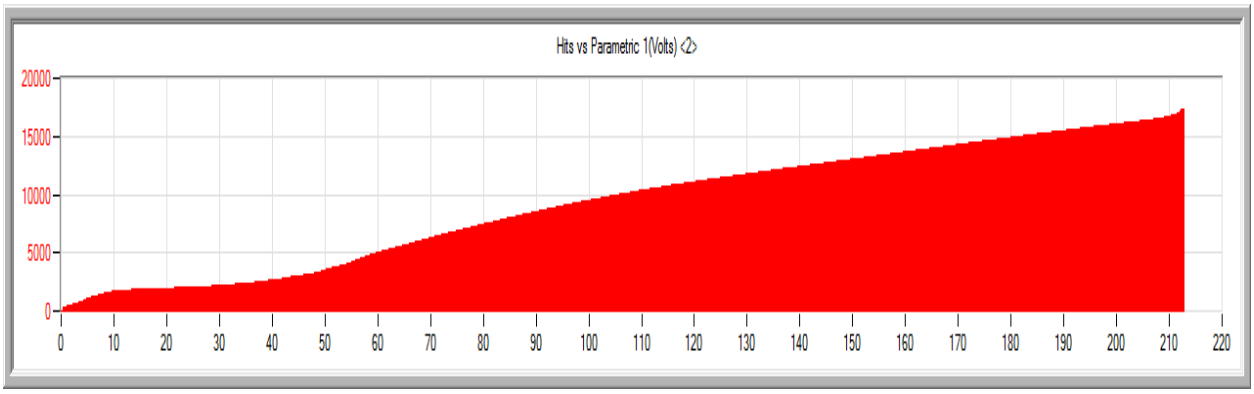


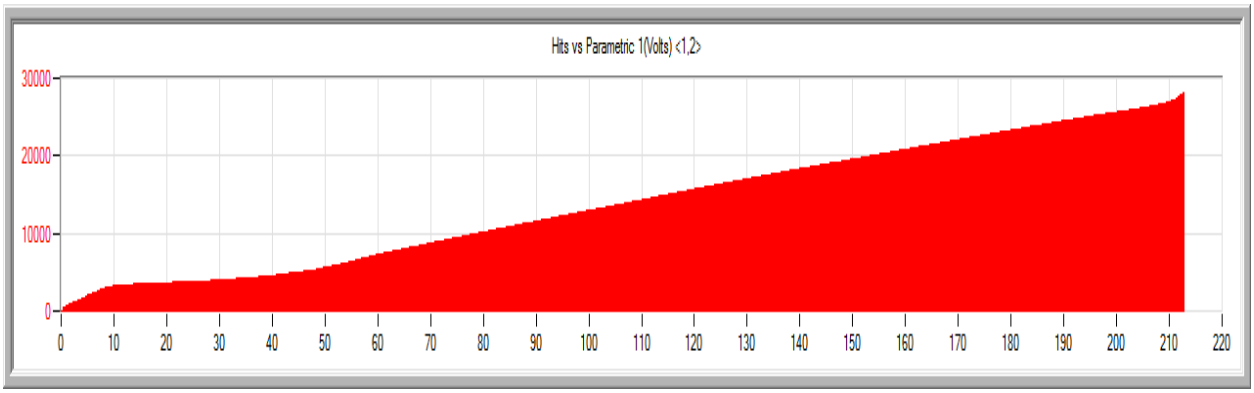


Legend – Page 13: Hits Count vs Stress (MPa) – Per Time Period

- Hits vs Stress (MPa) – Channel 1 (Top of page)
- Hits vs Stress (MPa) – Channel 2 (Middle of page)
- Hits vs Stress (MPa) – Channels 1 and 2, combined (Bottom of page)

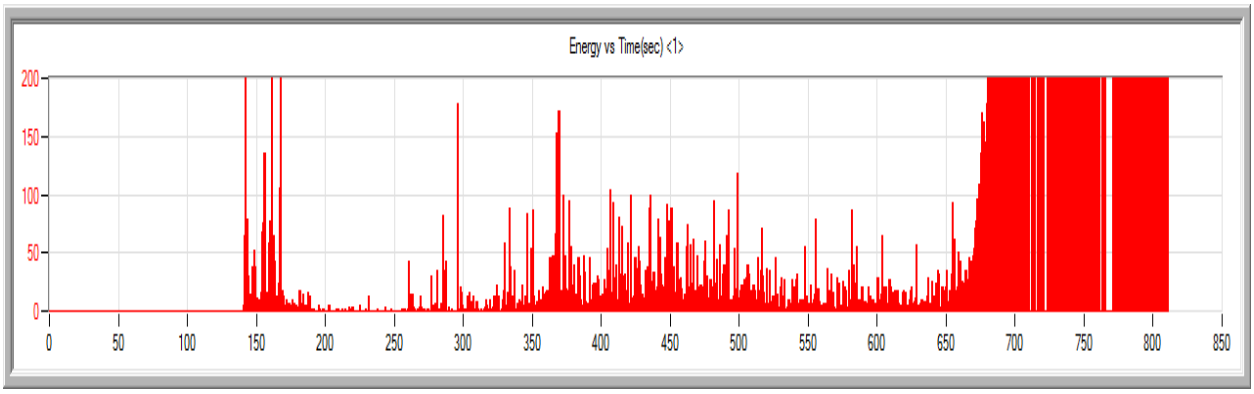


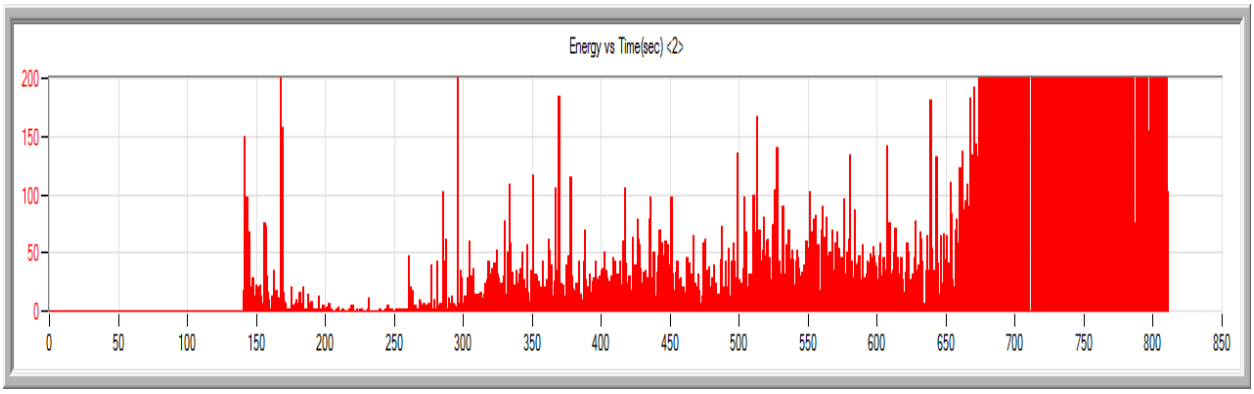


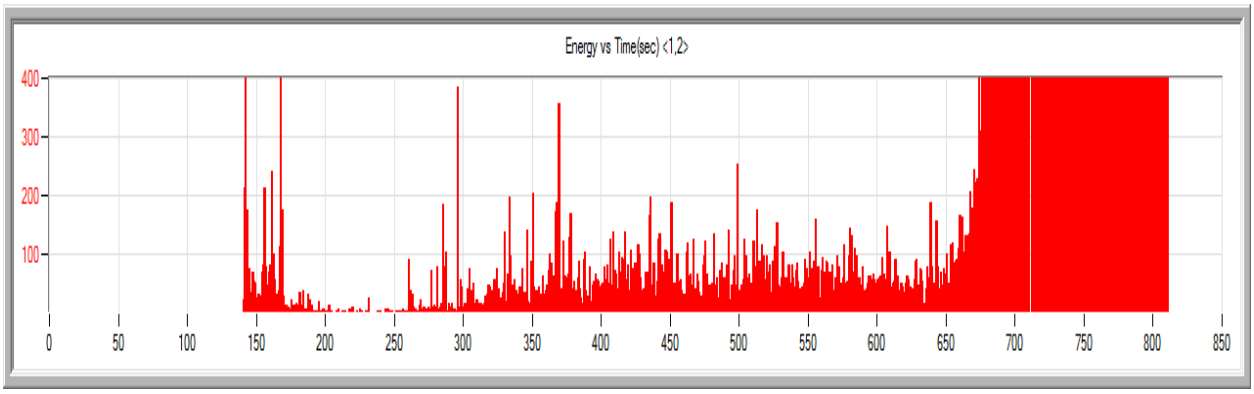


Legend – Page 14: Hits Count vs Stress (MPa) – Cumulative

- Hits vs Stress (MPa) – Channel 1 (Top of page)
- Hits vs Stress (MPa) – Channel 2 (Middle of page)
- Hits vs Stress (MPa) – Channels 1 and 2, combined (Bottom of page)

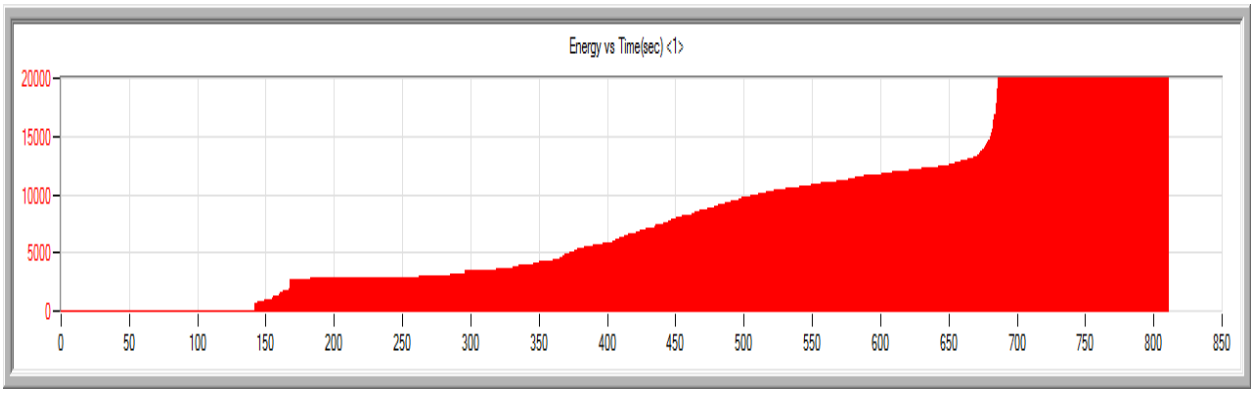


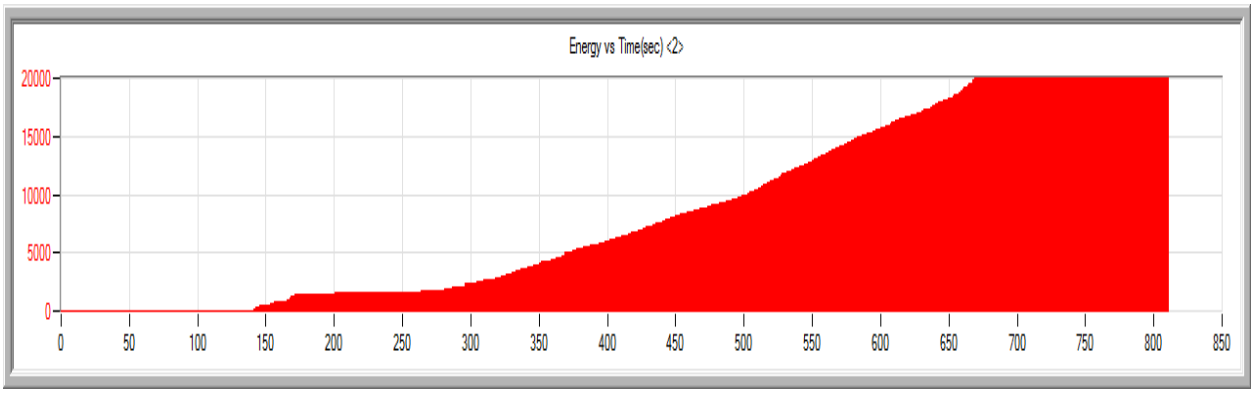


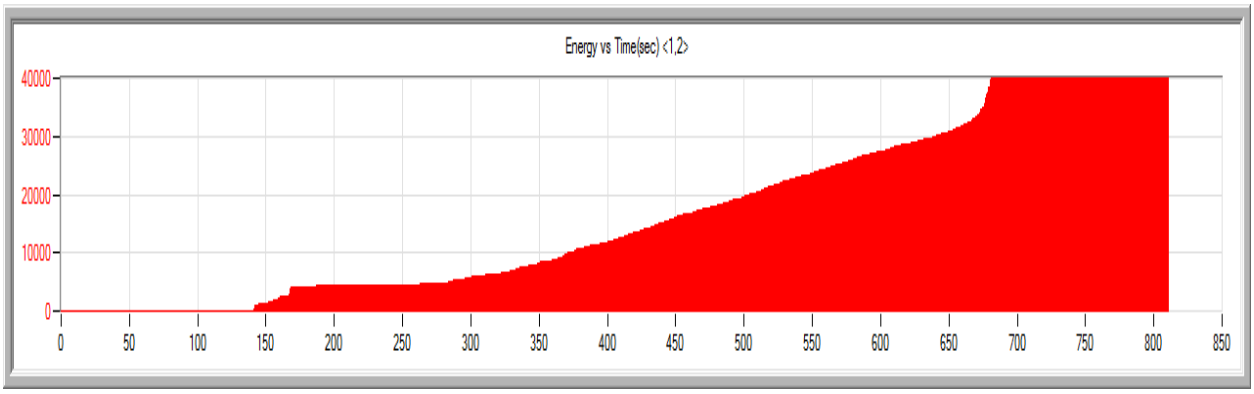


Legend – Page 15: Energy vs Time (sec) – Per Time Period

- Energy vs Time (sec) – Channel 1 (Top of page)
- Energy vs Time (sec) – Channel 2 (Middle of page)
- Energy vs Time (sec) – Channels 1 and 2, combined (Bottom of page)

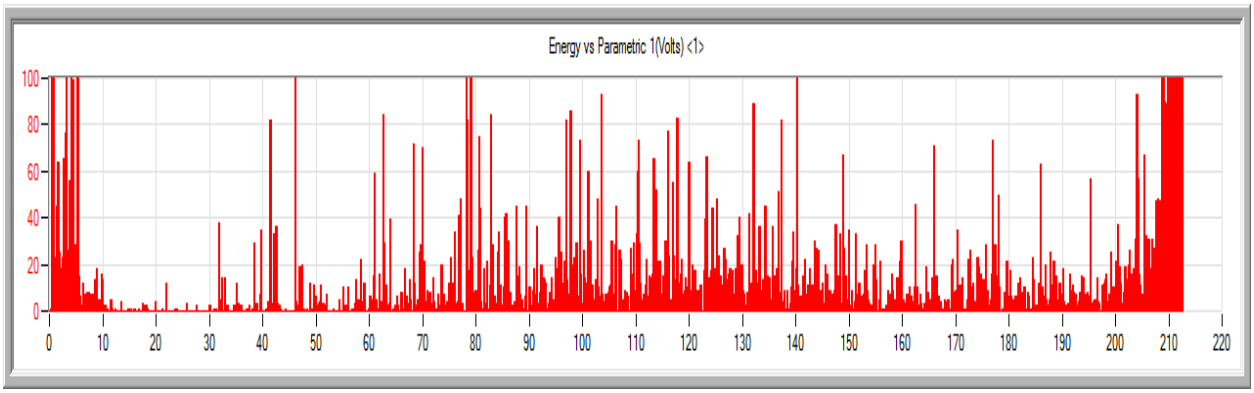


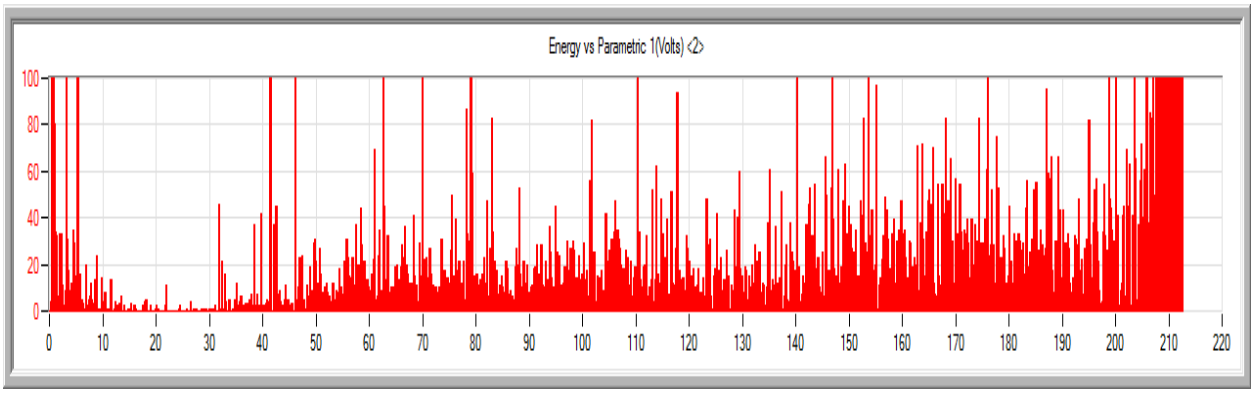


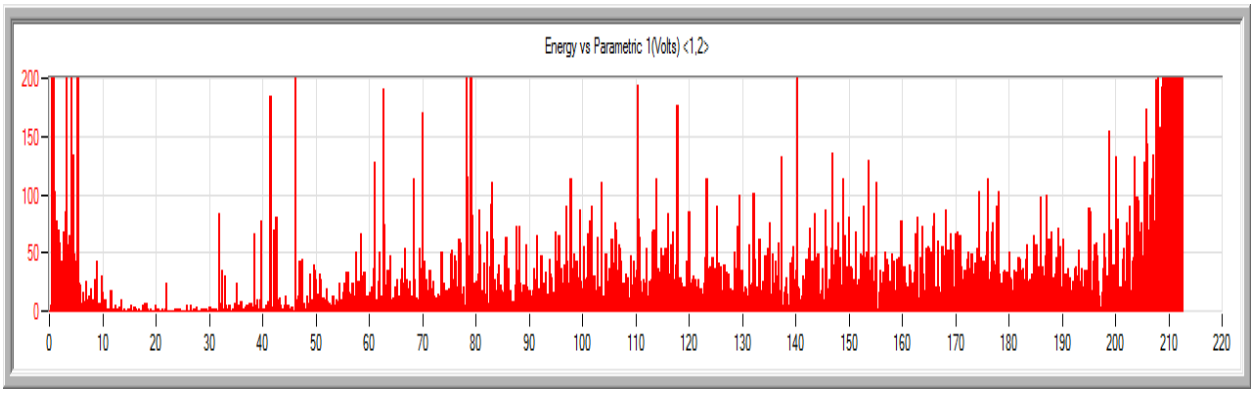


Legend – Page 16: Energy vs Time (sec) - Cumulative

- Energy vs Time (sec) – Channel 1 (Top of page)
- Energy vs Time (sec) – Channel 2 (Middle of page)
- Energy vs Time (sec) – Channels 1 and 2, combined (Bottom of page)

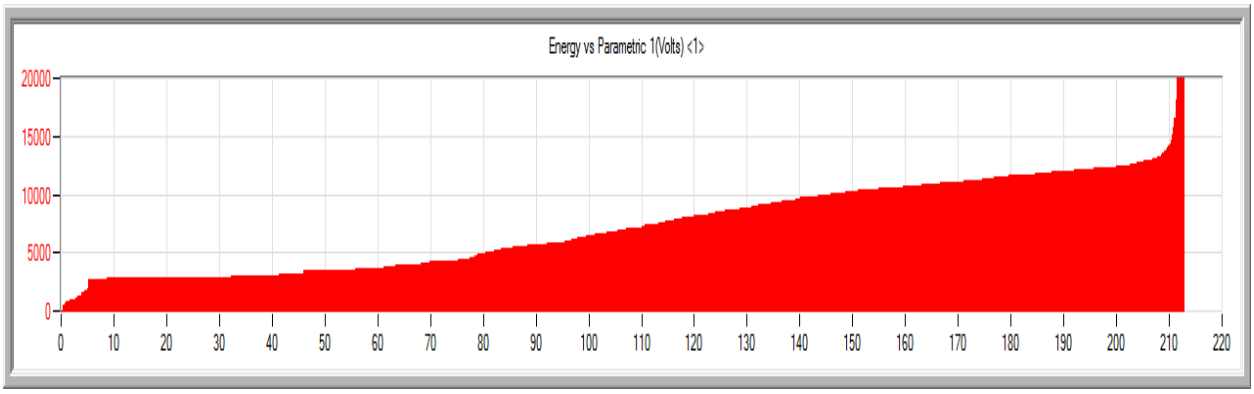


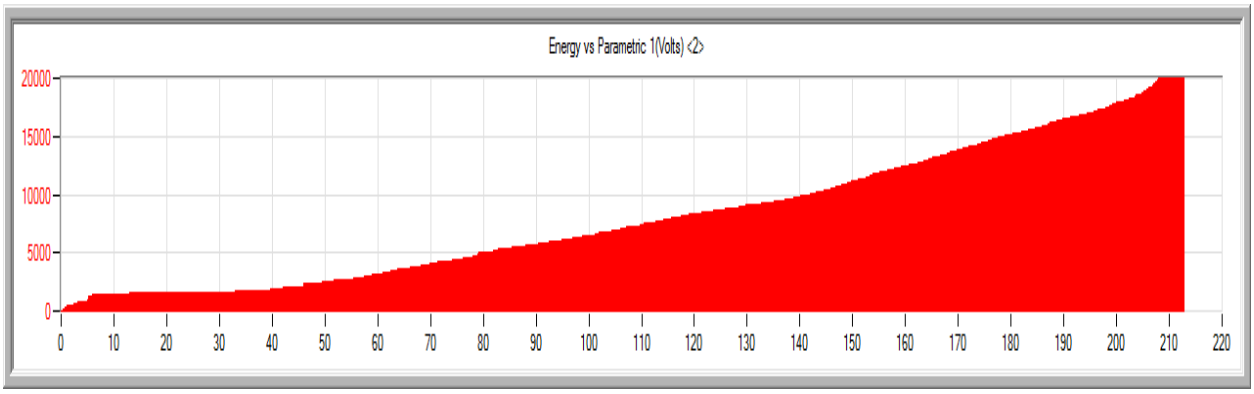


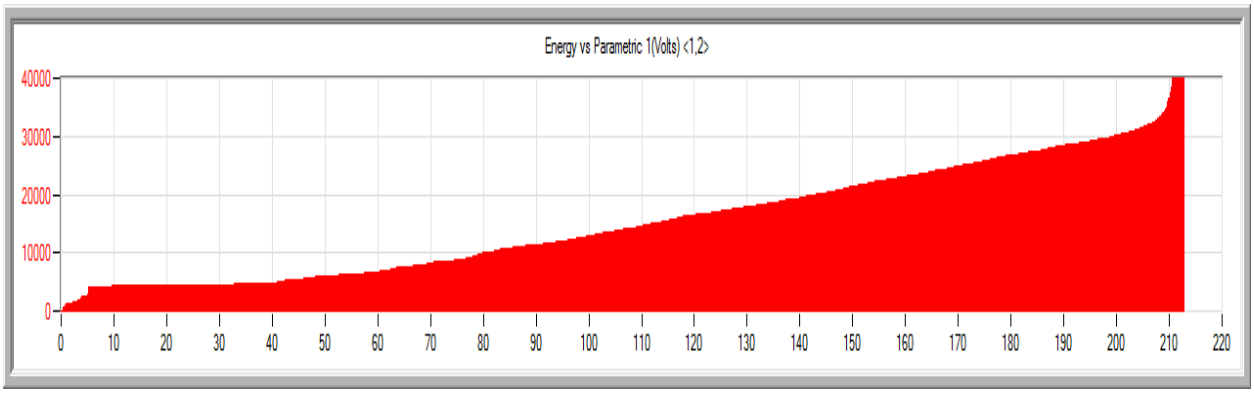


Legend – Page 17: Energy vs Stress (MPa) – Per Time Period

- Energy vs Stress (MPa) – Channel 1 (Top of page)
- Energy vs Stress (MPa) – Channel 2 (Middle of page)
- Energy vs Stress (MPa) – Channels 1 and 2, combined (Bottom of page)







Legend – Page 18: Energy vs Stress (MPa) - Cumulative

- Energy vs Stress (MPa) – Channel 1 (Top of page)
- Energy vs Stress (MPa) – Channel 2 (Middle of page)
- Energy vs Stress (MPa) – Channels 1 and 2, combined (Bottom of page)

Test Specimen BH01-UC005-567.77-U

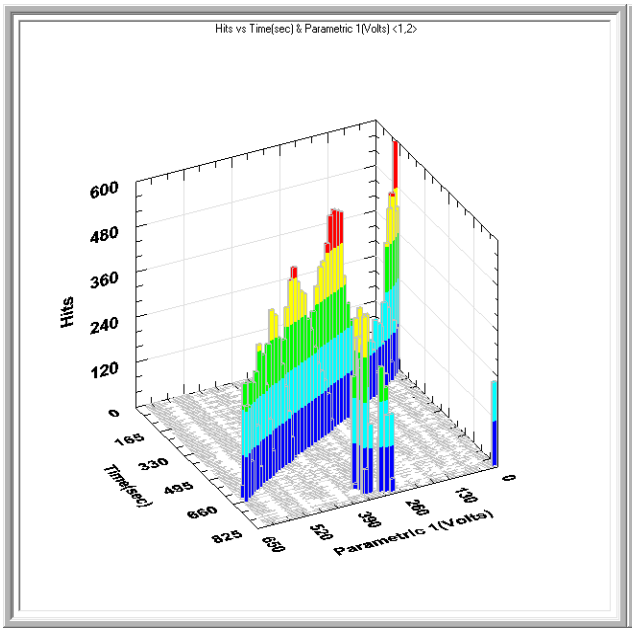
P:\lab data\D Labrie\Golder Associates\P-002797.001 - NWMO - Winter 2018\Test Data\AE\Data\567.dta

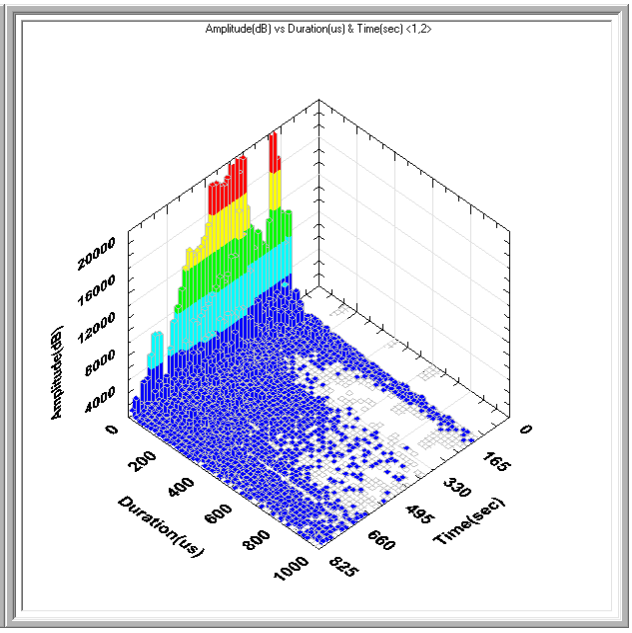
Total AEHits :	34117
Total TDDs :	68
Total Waveforms:	34117
Total Resumes :	2
Total Pauses :	2
Total TimeMarks:	0

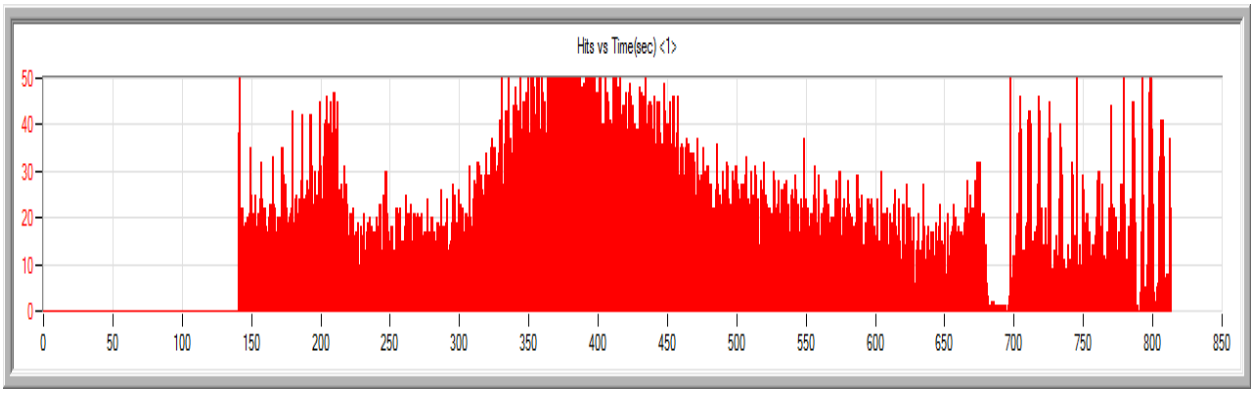
Channel	AEHits
1	21017
2	13100

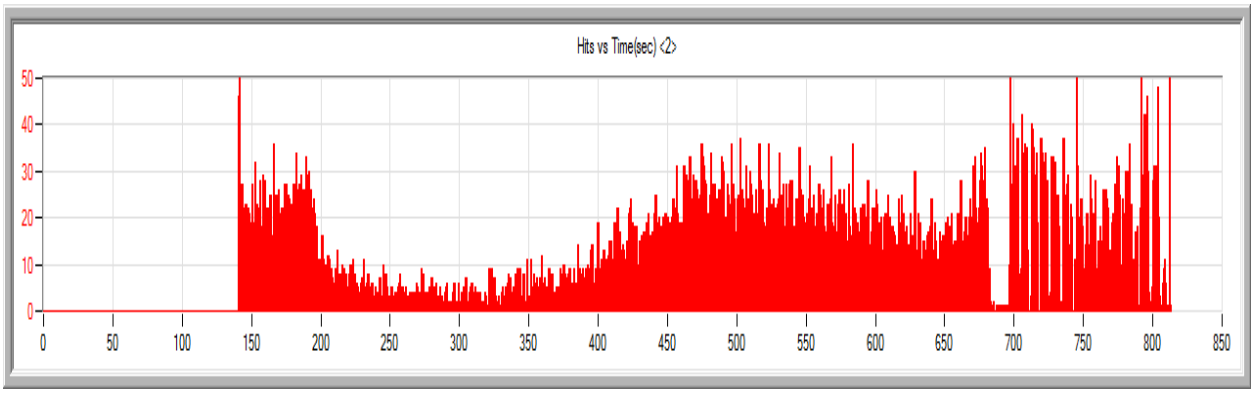
HIT DRIVEN DATA:

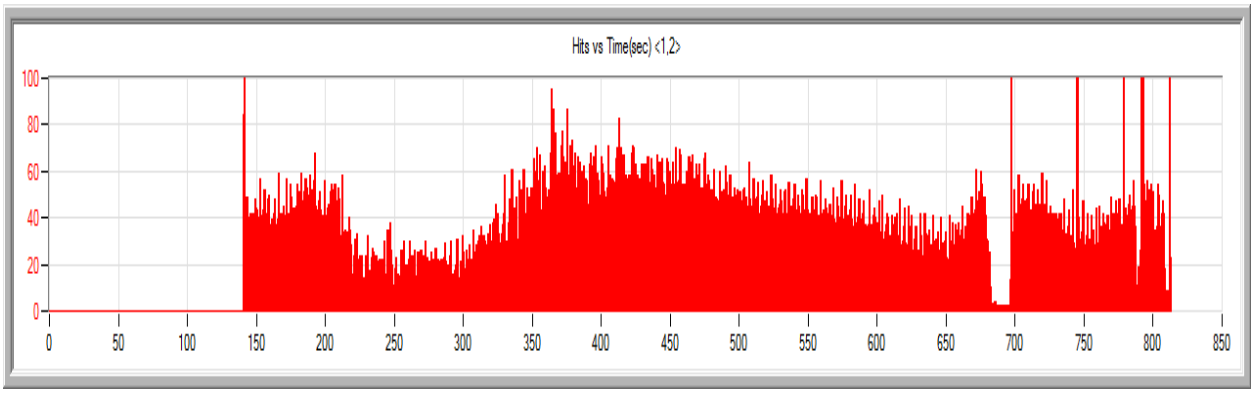
Feature	Chan	Minimum	Maximum	Average	Std Dev
Risetime	1	0.0000	13076.0000	231.0978	1077.5280
Counts	1	1.0000	32571.0000	88.3833	910.2859
Energy	1	0.0000	65535.0000	74.4561	1674.9940
Duration	1	0.0000	1000000.0000	1969.5073	31272.2399
Amplitude	1	40.0000	100.0000	45.4693	8.2820
Threshold	1	40.0000	40.0000	40.0000	0.0062
SigStrength	1	0.0000	6724104192.0000	963679.0625	51387855.5917
AbsEnergy	1	0.0000	21003296768.0000	1504183.5000	148425053.0400
Parametric1	1	0.0040	2.4574	1.1575	0.6363
Risetime	2	0.0000	13100.0000	266.5669	1137.6782
Counts	2	1.0000	32764.0000	112.2092	1038.5751
Energy	2	0.0000	65535.0000	98.8968	2040.8226
Duration	2	0.0000	1000000.0000	2519.4199	37262.8462
Amplitude	2	40.0000	100.0000	48.4093	9.0734
Threshold	2	40.0000	40.0000	40.0000	0.0024
SigStrength	2	0.0000	8609354752.0000	1770749.0000	85538581.0123
AbsEnergy	2	0.0000	46527361024.0000	5164167.5000	418936252.4106
Parametric1	2	0.0040	2.4574	1.3403	0.7148









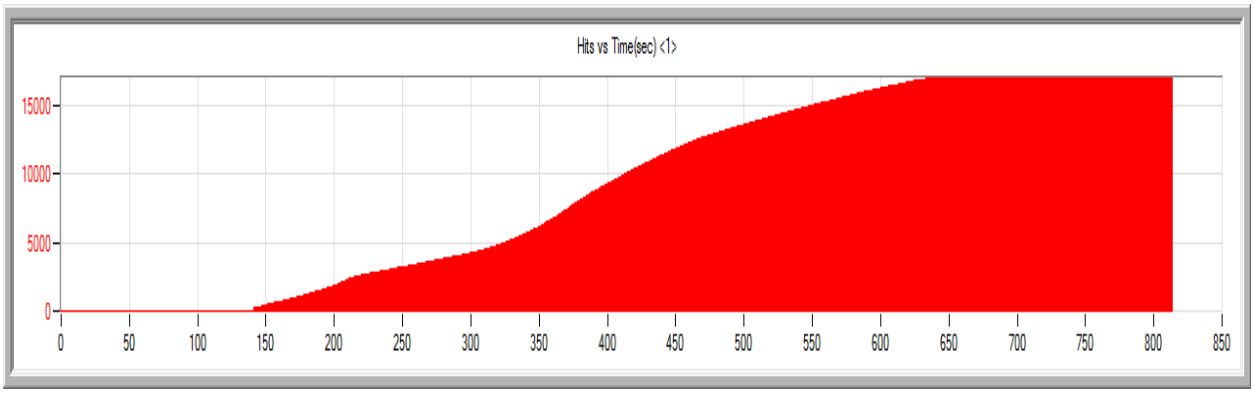


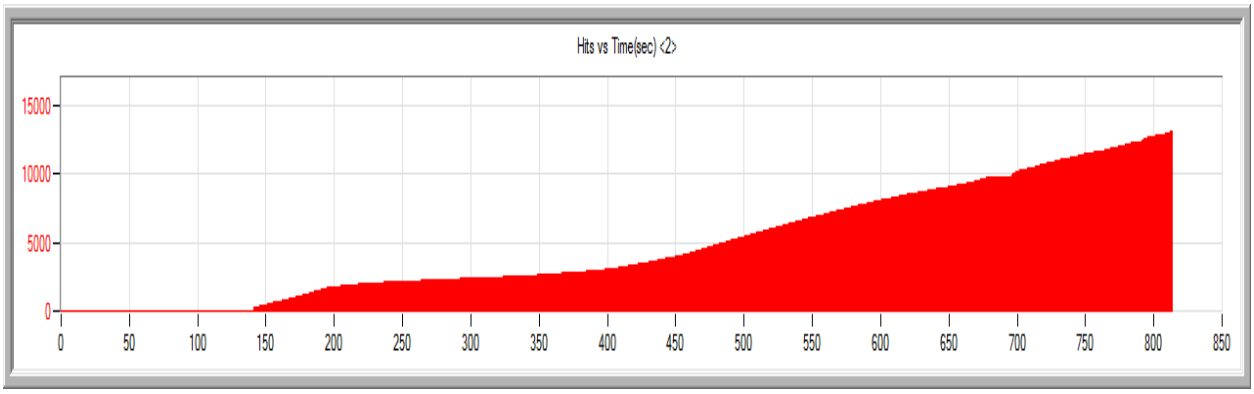
Legend – Page 19: Statistics and Isometric Views

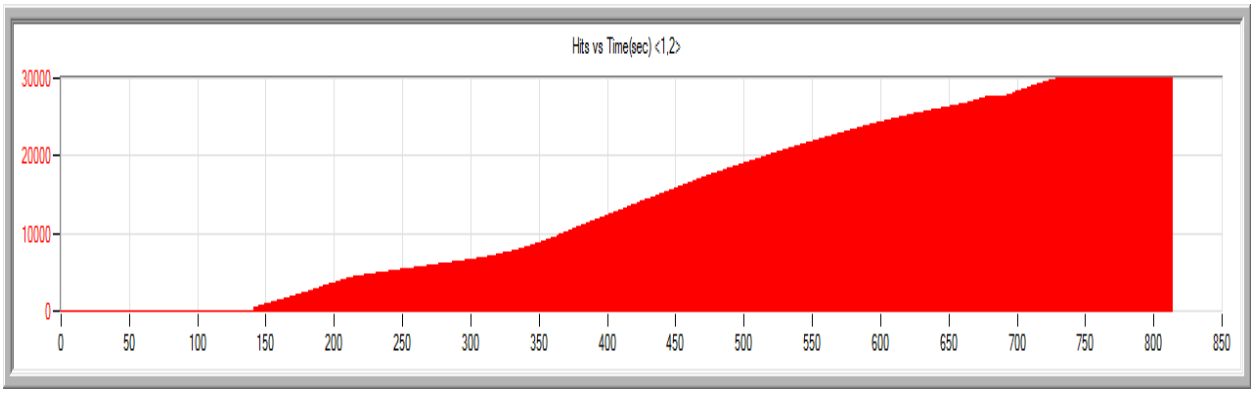
- Statistics of Test BH01-UC005-567.77-U (Top of page)
- Isometric View: (1) Hits vs Time (sec) vs Load (Parametric, in kN) (Bottom of page, left)
- Isometric View: (2) Amplitude (dB) vs Duration (µsec) vs Time (sec) (Bottom of page, right)

Legend – Page 20: Hits Count vs Time (sec) – Per Time Period

- Hits vs Time (sec) – Channel 1 (Top of page)
- Hits vs Time (sec) – Channel 2 (Middle of page)
- Hits vs Time (sec) – Channels 1 and 2, combined (Bottom of page)

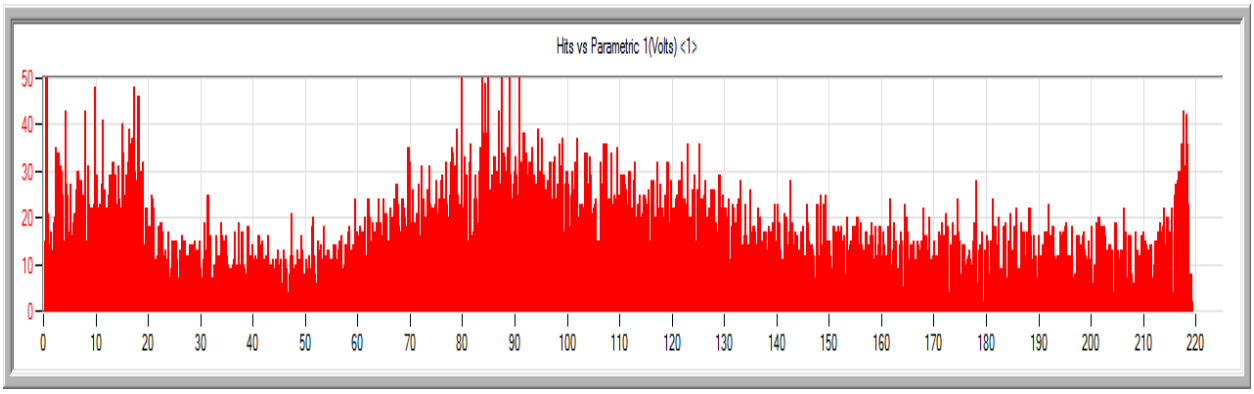


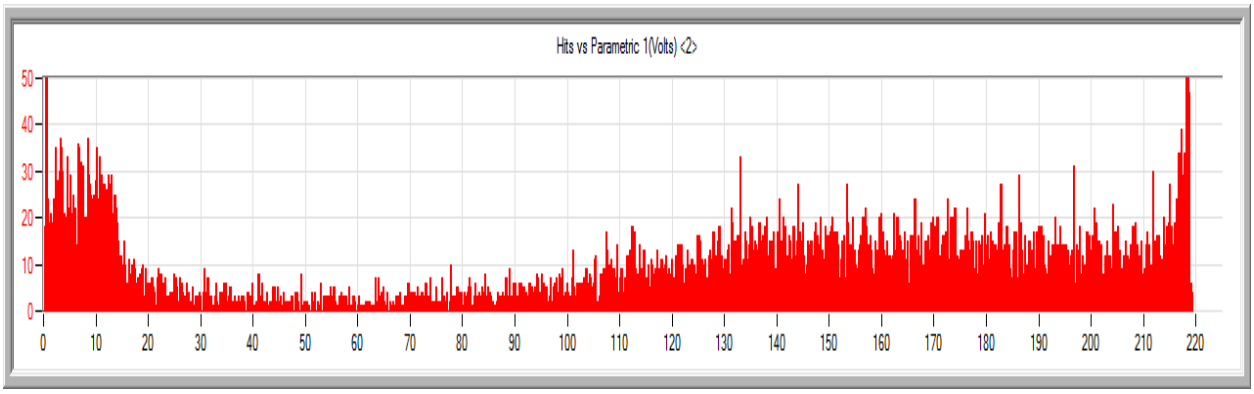


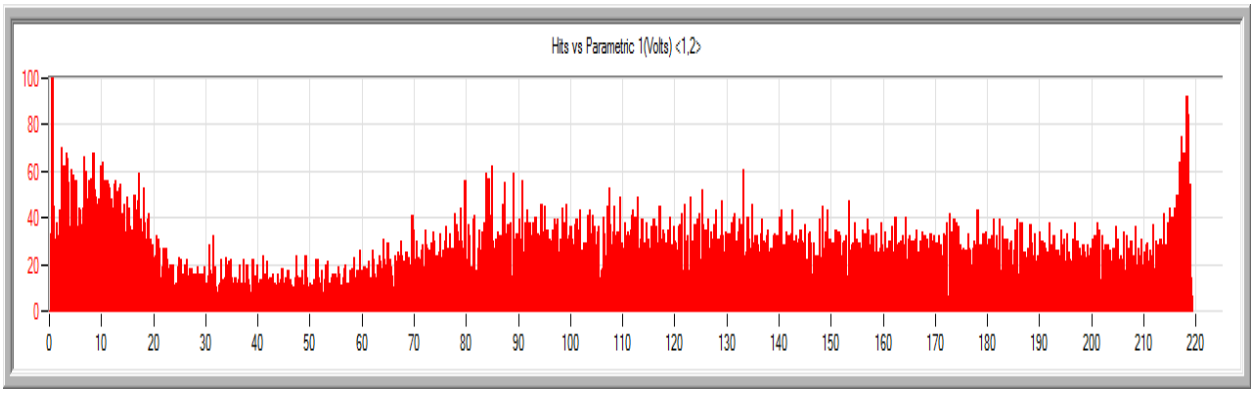


Legend – Page 21: Hits Count vs Time (sec) – Cumulative

- Hits vs Time (sec) – Channel 1 (Top of page)
- Hits vs Time (sec) – Channel 2 (Middle of page)
- Hits vs Time (sec) – Channels 1 and 2, combined (Bottom of page)

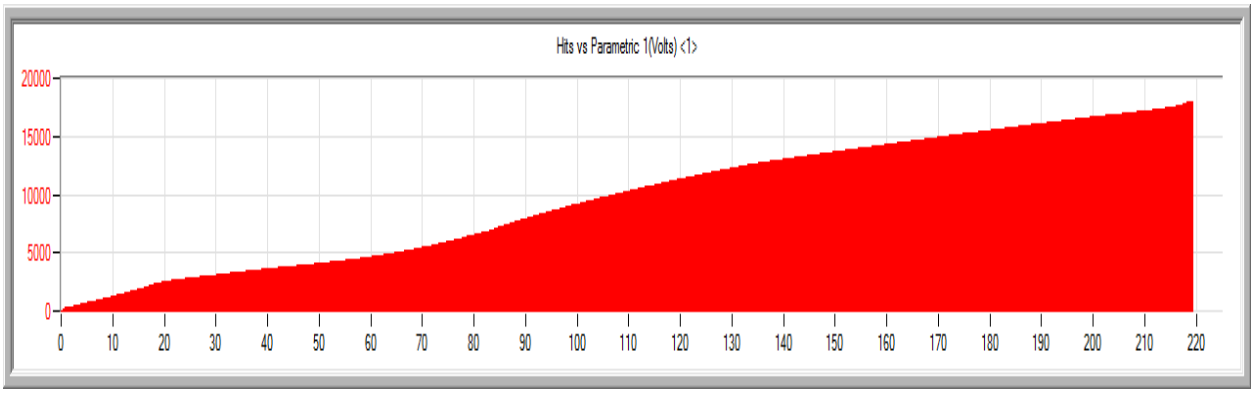


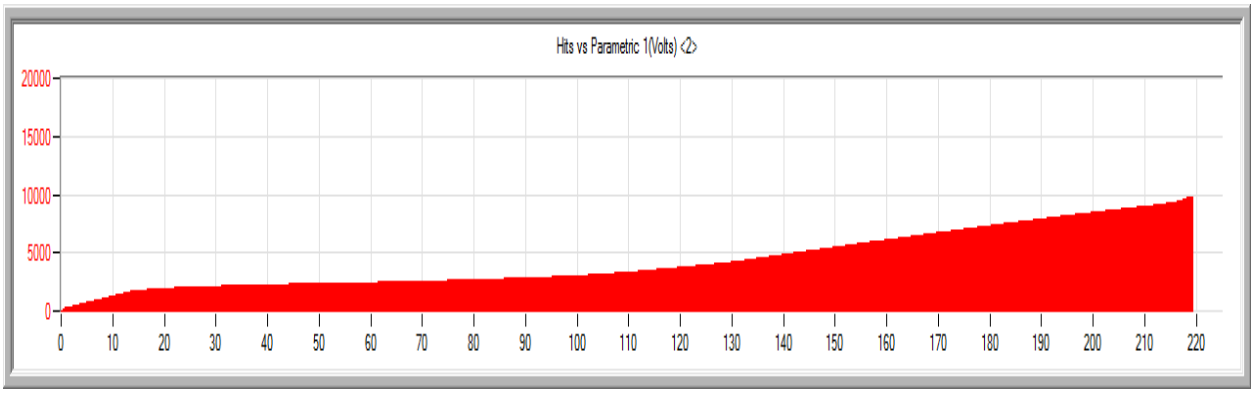


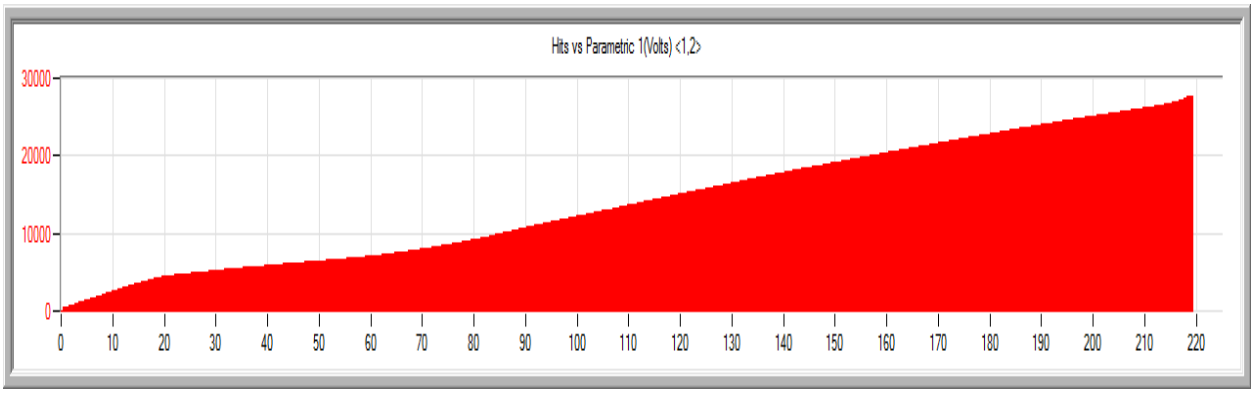


Legend – Page 22: Hits Count vs Stress (MPa) – Per Time Period

- Hits vs Stress (MPa) – Channel 1 (Top of page)
- Hits vs Stress (MPa) – Channel 2 (Middle of page)
- Hits vs Stress (MPa) – Channels 1 and 2, combined (Bottom of page)

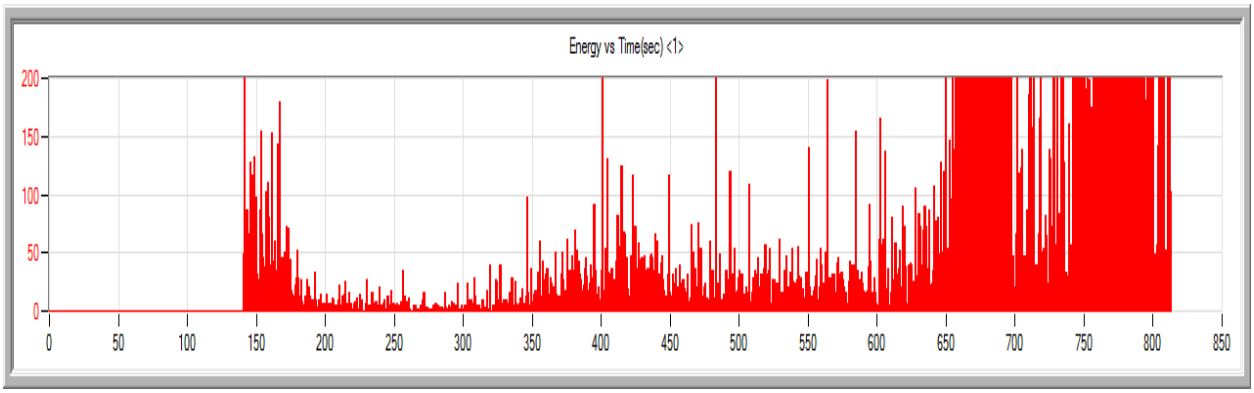


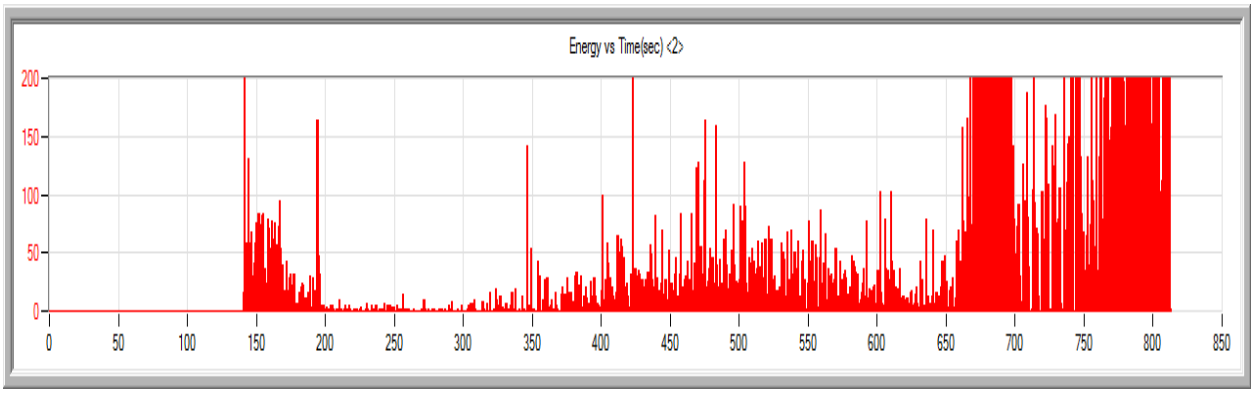


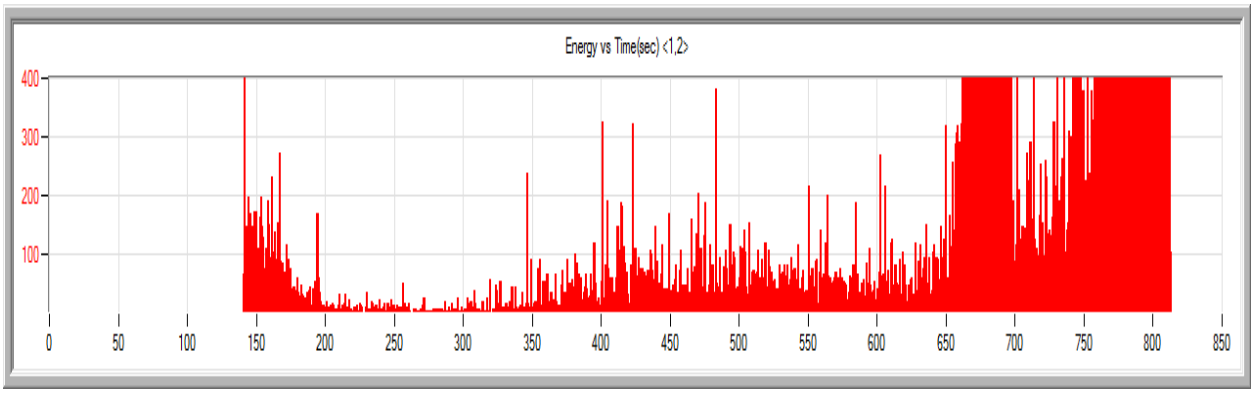


Legend – Page 23: Hits Count vs Stress (MPa) – Cumulative

- Hits vs Stress (MPa) – Channel 1 (Top of page)
- Hits vs Stress (MPa) – Channel 2 (Middle of page)
- Hits vs Stress (MPa) – Channels 1 and 2, combined (Bottom of page)

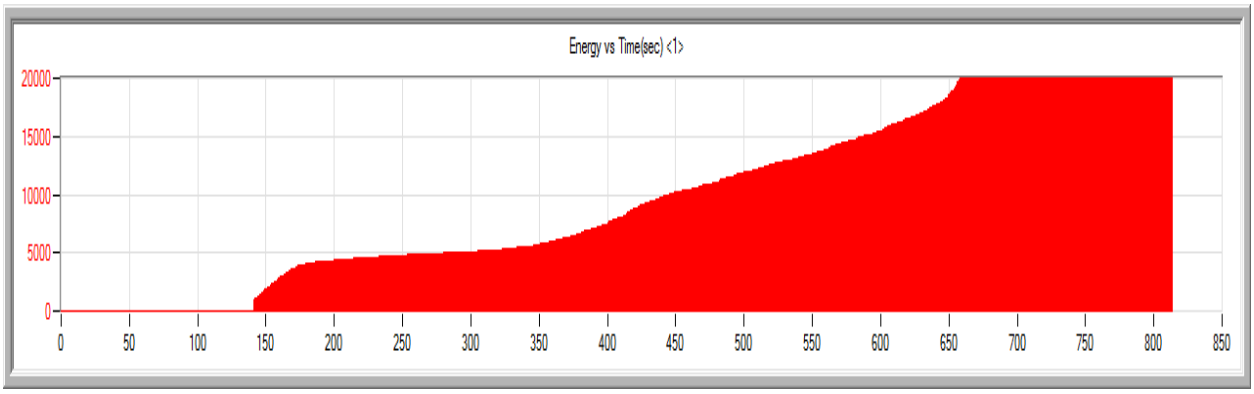


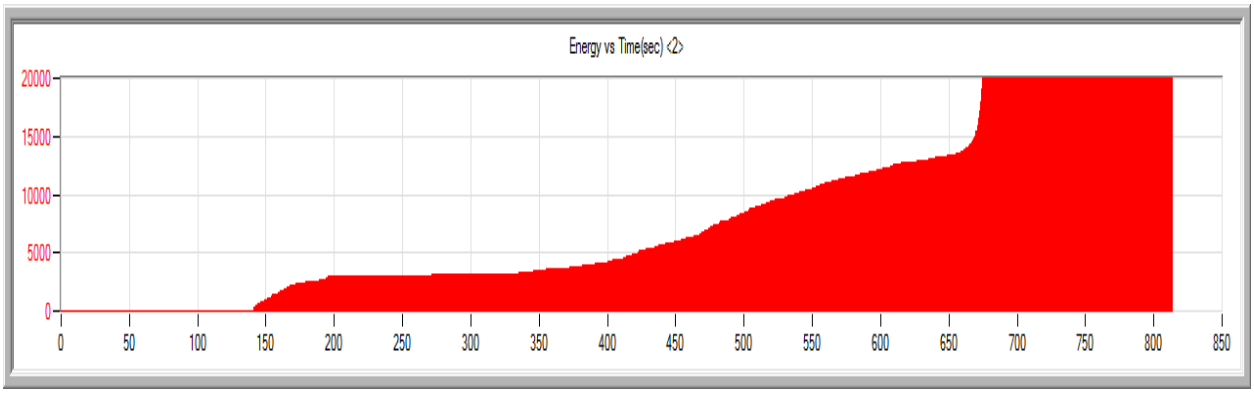


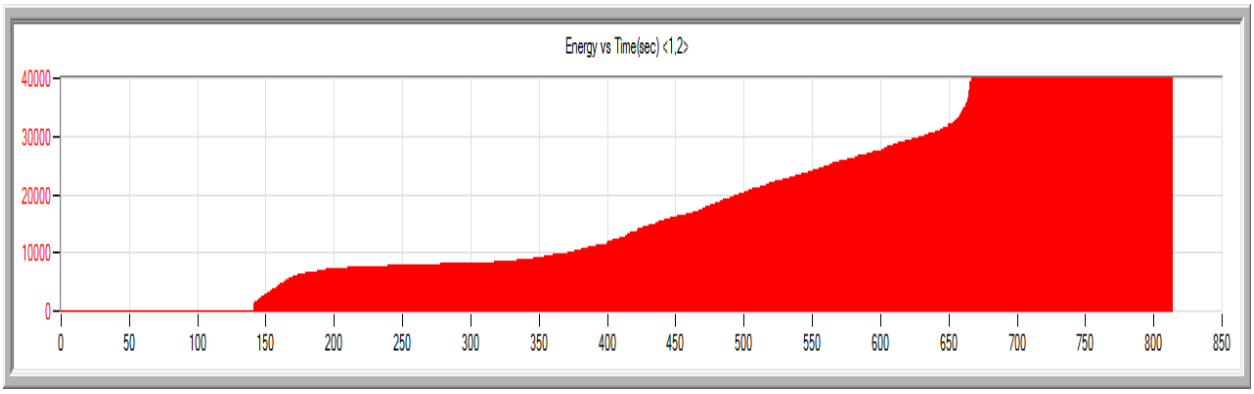


Legend – Page 24: Energy vs Time (sec) – Per Time Period

- Energy vs Time (sec) – Channel 1 (Top of page)
- Energy vs Time (sec) – Channel 2 (Middle of page)
- Energy vs Time (sec) – Channels 1 and 2, combined (Bottom of page)

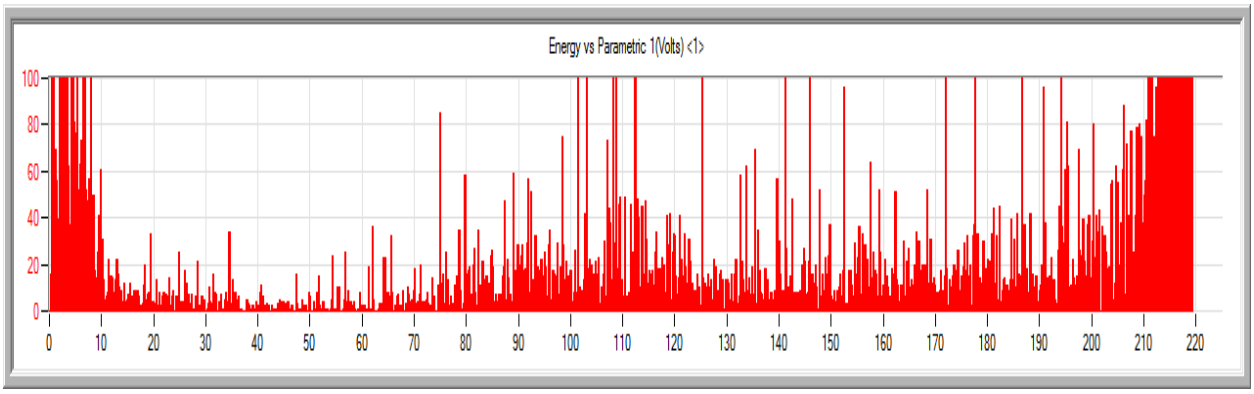


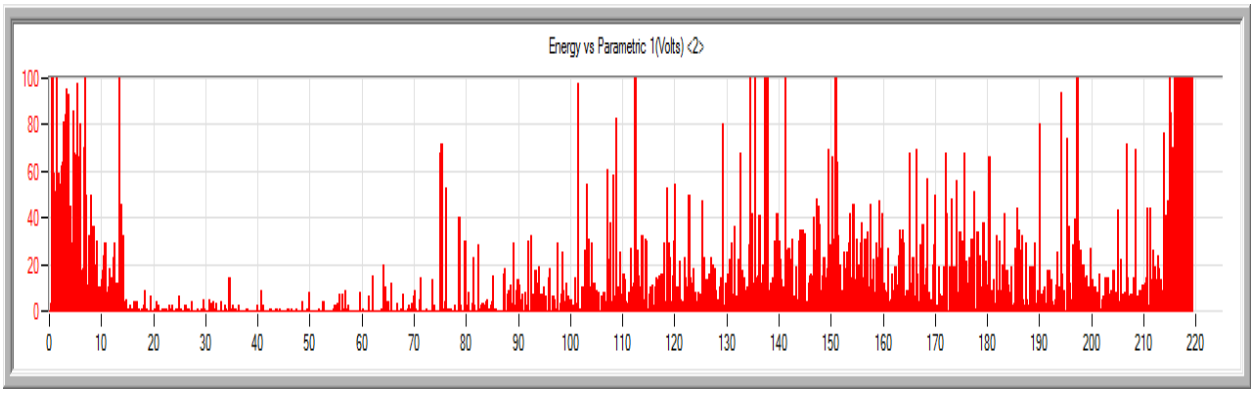


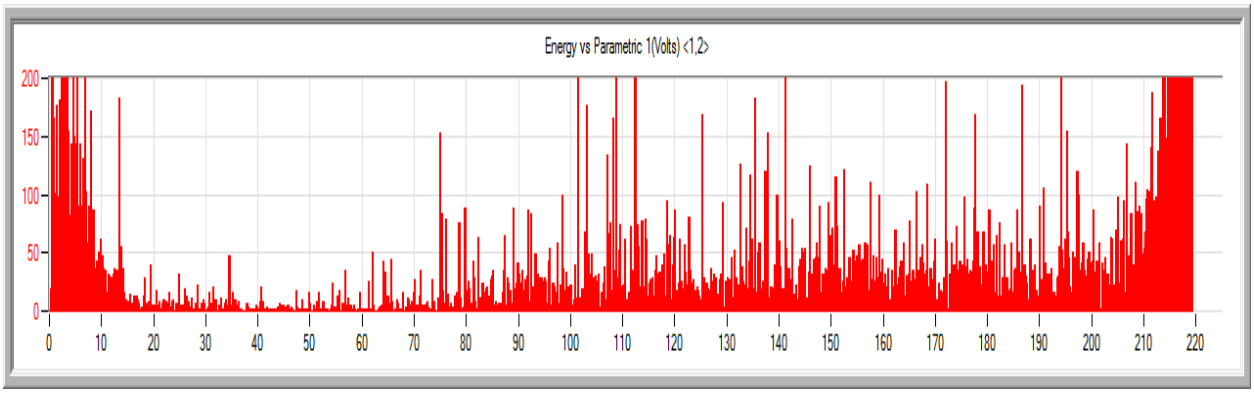


Legend – Page 25: Energy vs Time (sec) - Cumulative

- Energy vs Time (sec) – Channel 1 (Top of page)
- Energy vs Time (sec) – Channel 2 (Middle of page)
- Energy vs Time (sec) – Channels 1 and 2, combined (Bottom of page)

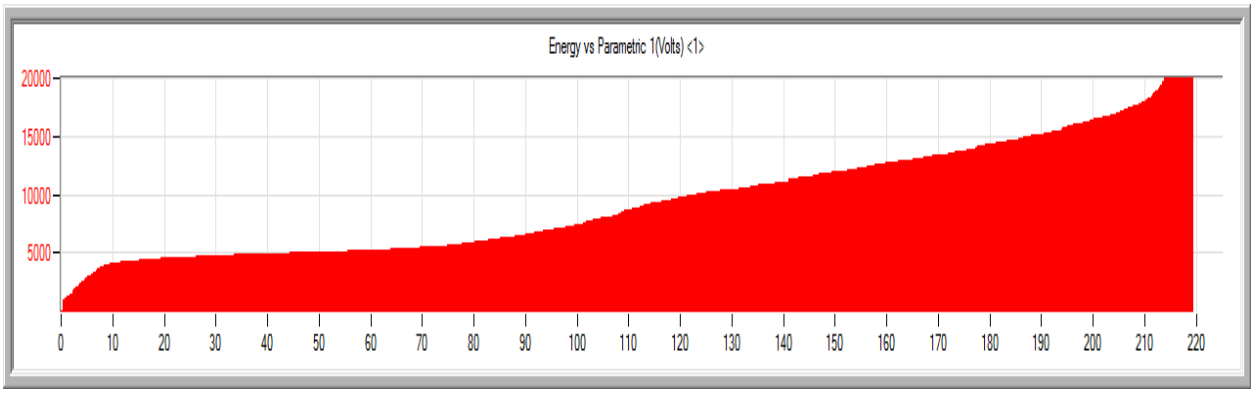


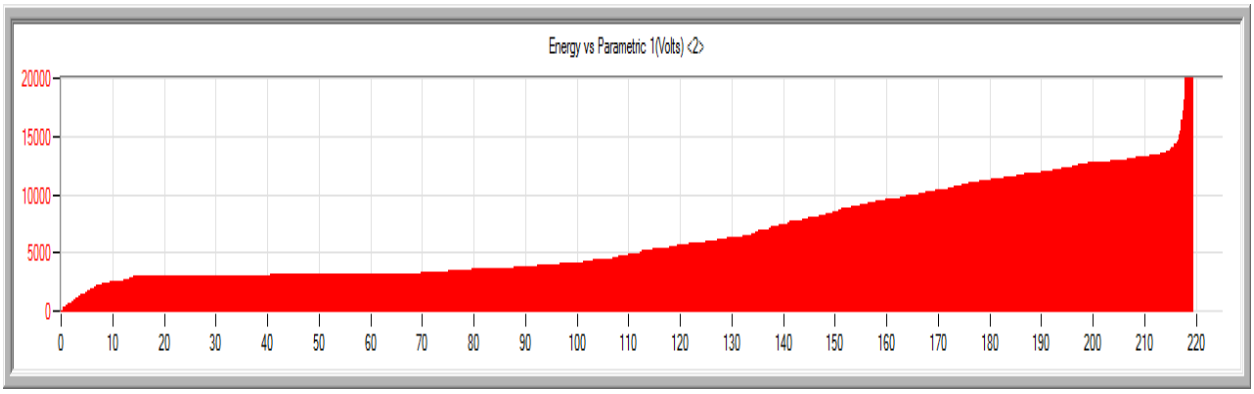


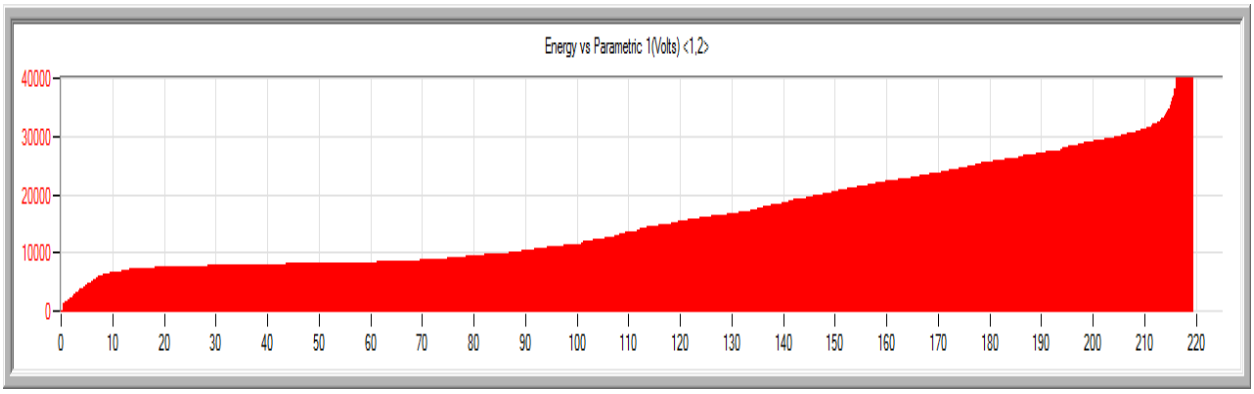


Legend – Page 26: Energy vs Stress (MPa) – Per Time Period

- Energy vs Stress (MPa) – Channel 1 (Top of page)
- Energy vs Stress (MPa) – Channel 2 (Middle of page)
- Energy vs Stress (MPa) – Channels 1 and 2, combined (Bottom of page)







Legend – Page 27: Energy vs Stress (MPa) - Cumulative

- Energy vs Stress (MPa) – Channel 1 (Top of page)
- Energy vs Stress (MPa) – Channel 2 (Middle of page)
- Energy vs Stress (MPa) – Channels 1 and 2, combined (Bottom of page)

References:

1. MISTRAS Group, 2010. *Pocket AE-2: Portable 2-Channel Acoustic Emission System*, Product Bulletin, MISTRAS Group Inc, Princeton Junction (NJ), USA: 2 p. (*www.mistrasgroup.com*)
2. Durrheim, R.J. and Labrie, D., 2007. *Data-driven simulation of the rock mass response to mining, Part I: Laboratory experiments using Nepean sandstone models,* Challenges in Deep and High Stress Mining, Editors: Y. Potvin, J. Hadjigeorgiou and Dick Stacey, Australian Centre for Geomechanics (ACG), Perth (WA), Australia, Chapter 34: 25 p. (acg.uwa.edu.au)

Acoustic Emission Data Analysis: Specimen IG-BH01-UC002

Test Summary

P:\lab data\S Gaines\P-002797.002_Golder_NWMO\Data\AE\IG-UC-002\IG-UC002.dta

Total AEHits :	27556
Total TDDs :	67
Total Waveforms:	27556
Total Resumes :	1
Total Pauses :	1
Total TimeMarks:	0

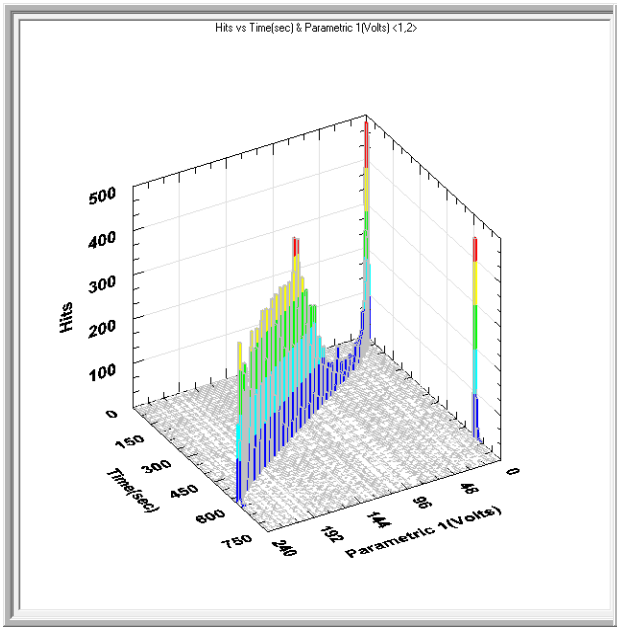
Channel	AEHits
1	13269
2	14287

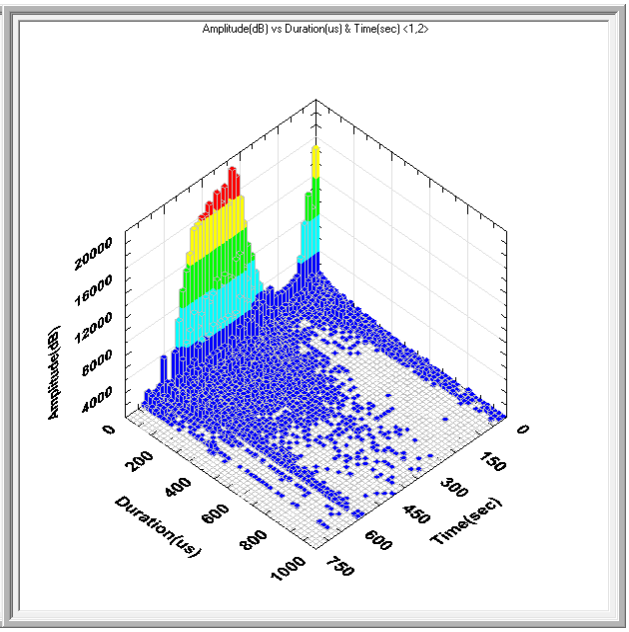
HIT DRIVEN DATA:

Feature	Chan	Minimum	Maximum	Average	Std Dev
Risetime	1	0.0000	12845.0000	131.5186	785.5584
Counts	1	1.0000	32375.0000	65.5942	864.5902
Energy	1	0.0000	65535.0000	84.9641	1953.6910
Duration	1	0.0000	1000000.0000	2051.9629	37636.6685
Amplitude	1	40.0000	100.0000	47.2799	7.8760
Threshold	1	40.0000	40.0000	40.0000	0.0073
SigStrength	1	0.0000	12746679296.0000	1664567.5000	112742692.5903
AbsEnergy	1	0.0000	89380937728.0000	7428239.0000	776440173.0948
Parametric1	1	-0.1422	238.9802	136.8525	71.2121
Risetime	2	0.0000	12975.0000	137.7023	800.7371
Counts	2	1.0000	32472.0000	59.5791	790.8634
Energy	2	0.0000	65535.0000	71.5303	1800.0014
Duration	2	0.0000	1000000.0000	1921.5918	35854.7064
Amplitude	2	40.0000	100.0000	46.9544	7.5605
Threshold	2	40.0000	40.0000	40.0000	0.0062
SigStrength	2	0.0000	8970976256.0000	1257225.1250	78140633.4289
AbsEnergy	2	0.0000	36278386688.0000	2975435.7500	304550248.7029
Parametric1	2	-0.1707	238.9517	124.0337	79.9234

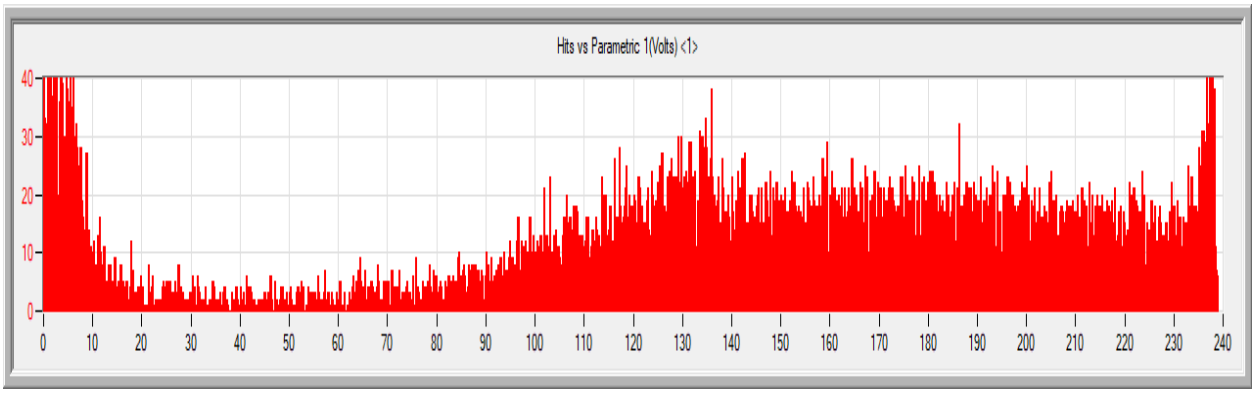
TIME DRIVEN DATA:

Feature	Chan	Minimum	Maximum	Average	Std Dev
asl	1	15.0000	60.0000	29.5970	9.9086
asl	2	21.0000	60.0000	30.0746	8.7457
asl	104	0.0000	0.0000	0.0000	0.0000
Parametric1		-0.1138	238.6958	107.8615	81.6910

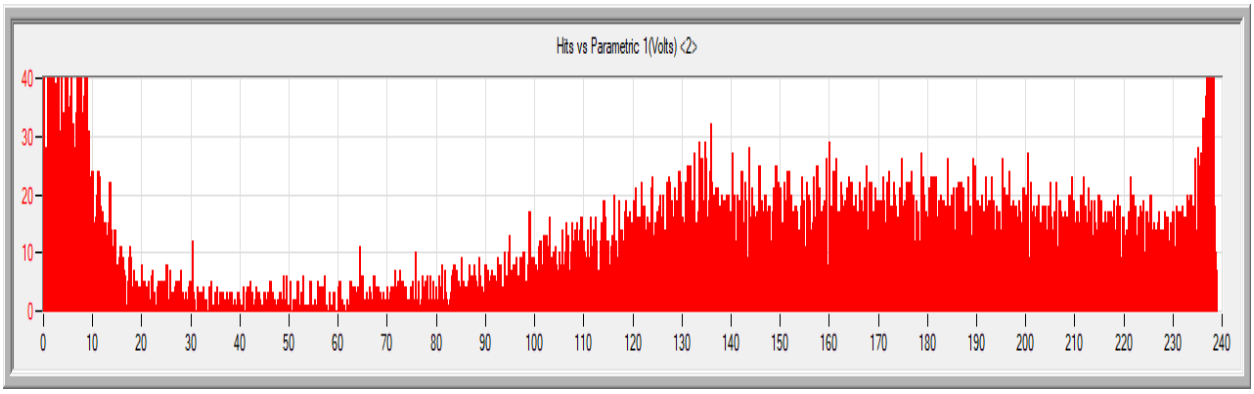




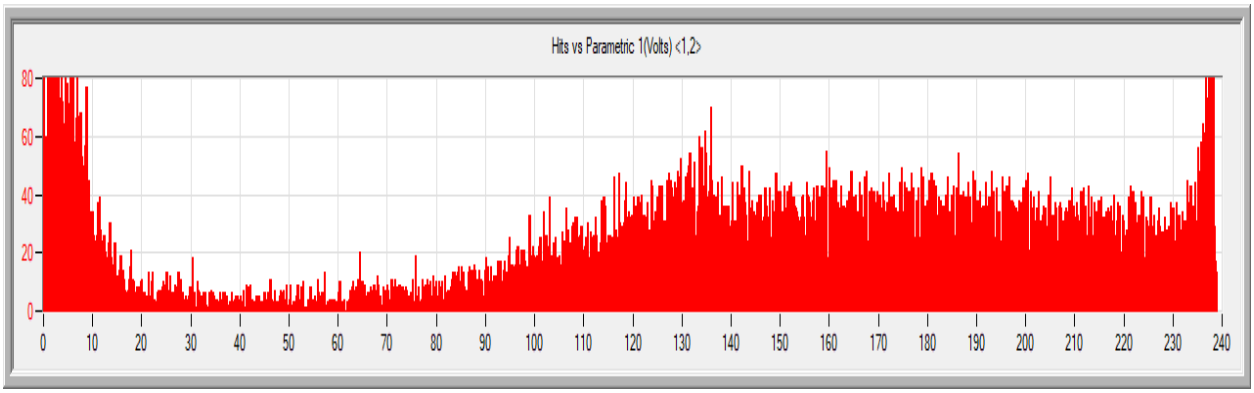
Number of Hits vs. Axial Stress (MPa): Channel 1



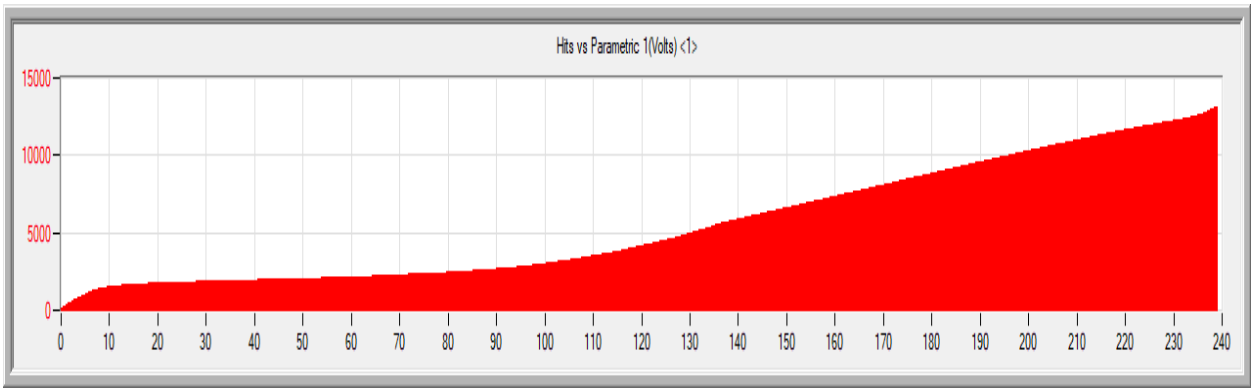
Number of Hits vs. Axial Stress (MPa): Channel 2



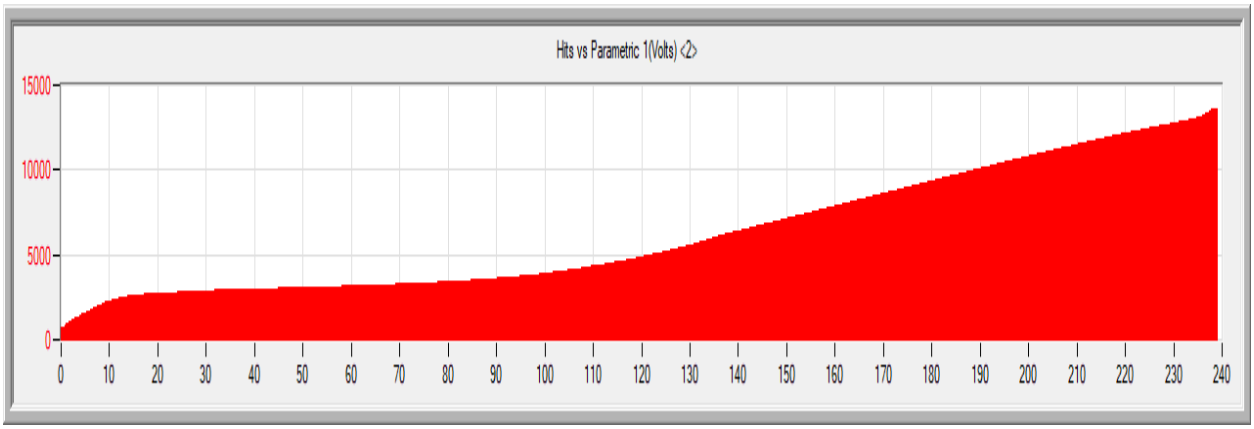
Number of Hits vs. Axial Stress (MPa): Channels 1+2



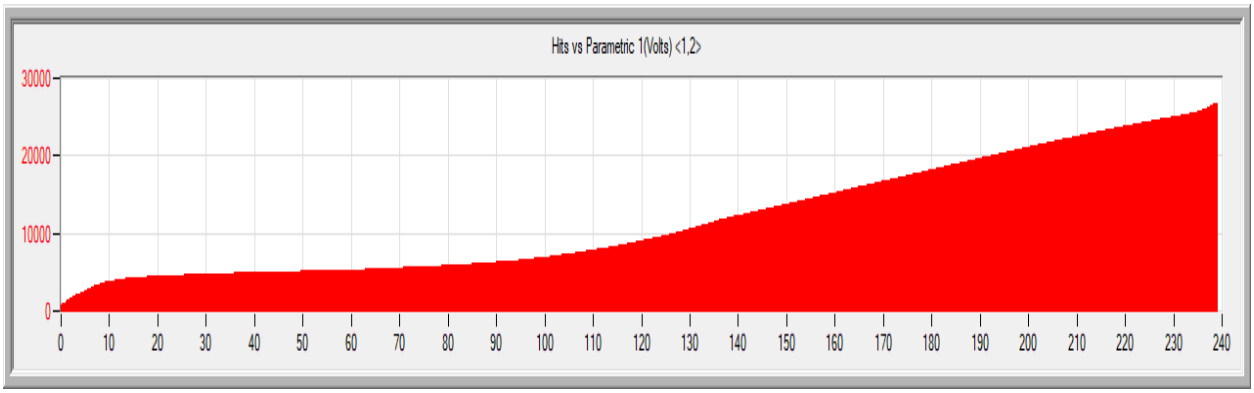
Cumulative Number of Hits vs. Axial Stress (MPa): Channel 1



Cumulative Number of Hits vs. Axial Stress (MPa): Channel 2



Cumulative Number of Hits vs. Axial Stress (MPa): Channels 1+2



Acoustic Emission Data Analysis: Specimen IG-BH01-UC004

Test Summary

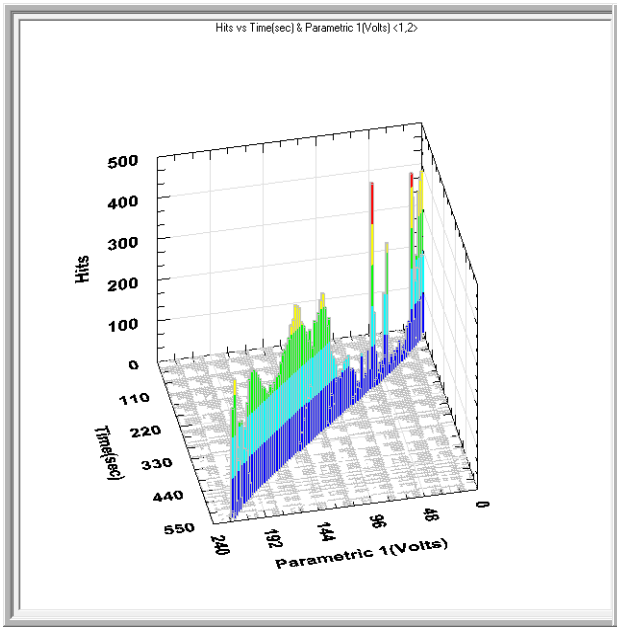
P:\lab data\S Gaines\P-002797.002_Golder_NWMO\Data\AE\IG-UC-004\IG-UC004.dta

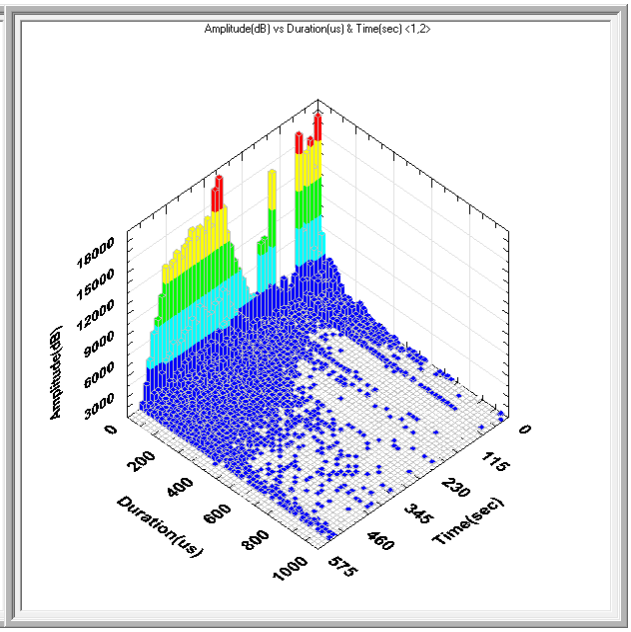
```
Total AEHits    :        26059
Total TDDs      :           56
Total Waveforms:        26059
Total Resumes   :            1
Total Pauses    :            1
Total TimeMarks:             0

Channel          AEHits
      1           13331
      2           12728

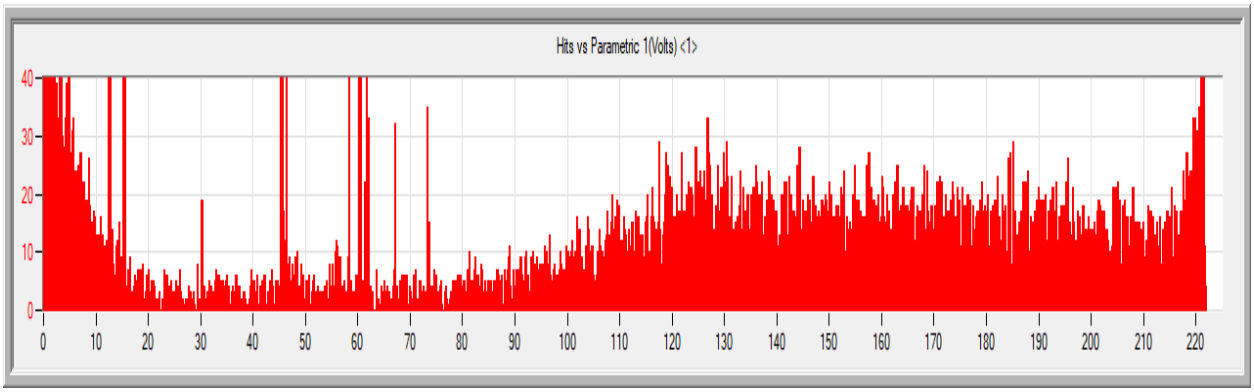

HIT DRIVEN DATA:
          Feature Chan          Minimum          Maximum          Average          Std Dev
         Risetime    1           0.0000       12912.0000         126.4843         780.7738
           Counts    1           1.0000       28081.0000          60.9357         809.0187
           Energy    1           0.0000       65535.0000          94.1355        2326.7101
         Duration    1           0.0000     1000000.0000        1858.5563       36205.4585
        Amplitude    1          40.0000         100.0000          46.4350           7.3898
        Threshold    1          40.0000          40.0000          40.0000          -1.#IND
      SigStrength    1           0.0000  4938477568.0000     1936264.5000    69495074.8805
        AbsEnergy    1           0.0000 11506904064.0000     2860887.7500   142179885.7331
      Parametric1    1          -0.2844         221.9711         118.0348          70.2229
         Risetime    2           0.0000       12965.0000         119.7740         780.4454
           Counts    2           1.0000       32651.0000          49.2128         806.7238
           Energy    2           0.0000       65535.0000         100.4091        2415.9632
         Duration    2           0.0000     1000000.0000        1992.5125       38468.7237
        Amplitude    2          40.0000         100.0000          46.0902           7.1615
        Threshold    2          40.0000          40.0000          40.0000           0.0050
      SigStrength    2           0.0000  8343750656.0000     4147775.7500   139878925.9954
        AbsEnergy    2           0.0000 75300233216.0000    15041093.0000   772523975.4776
      Parametric1    2          -0.2560         221.9427         121.1092          69.5085

TIME DRIVEN DATA:
          Feature Chan          Minimum          Maximum          Average          Std Dev
              asl    1          24.0000          69.0000          32.8393           8.9697
              asl    2          25.0000          79.0000          33.6250           9.8463
              asl  104           0.0000           0.0000           0.0000           0.0000
      Parametric1                 0.9386         221.4591         113.3078          71.1041
```

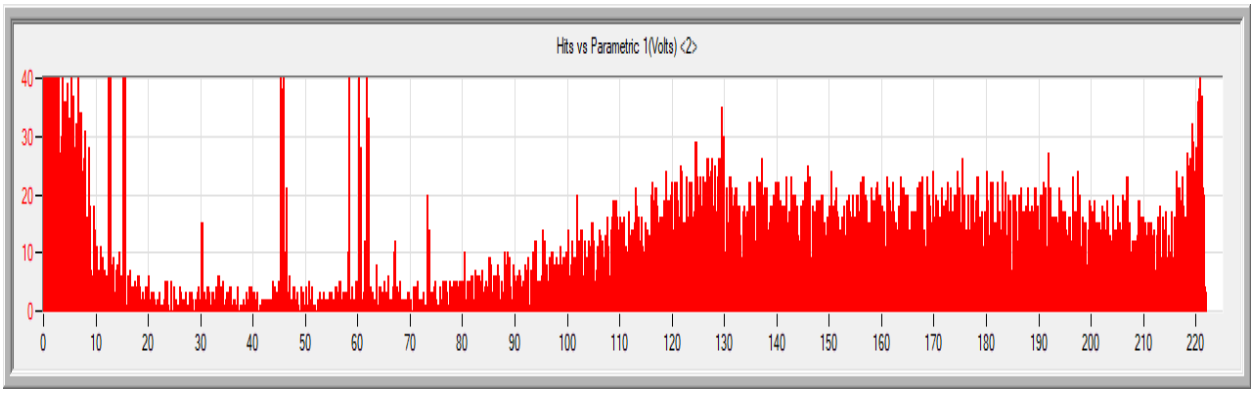




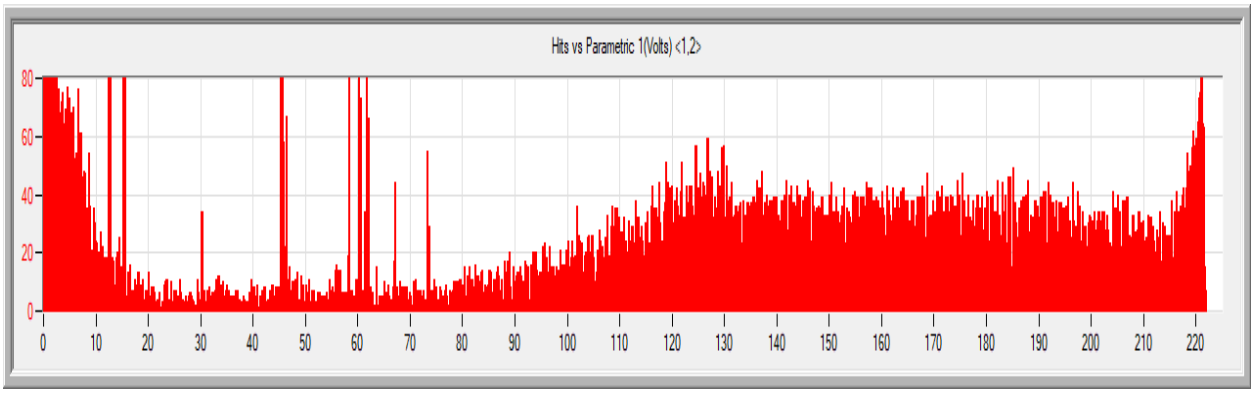
Number of Hits vs. Axial Stress (MPa): Channel 1



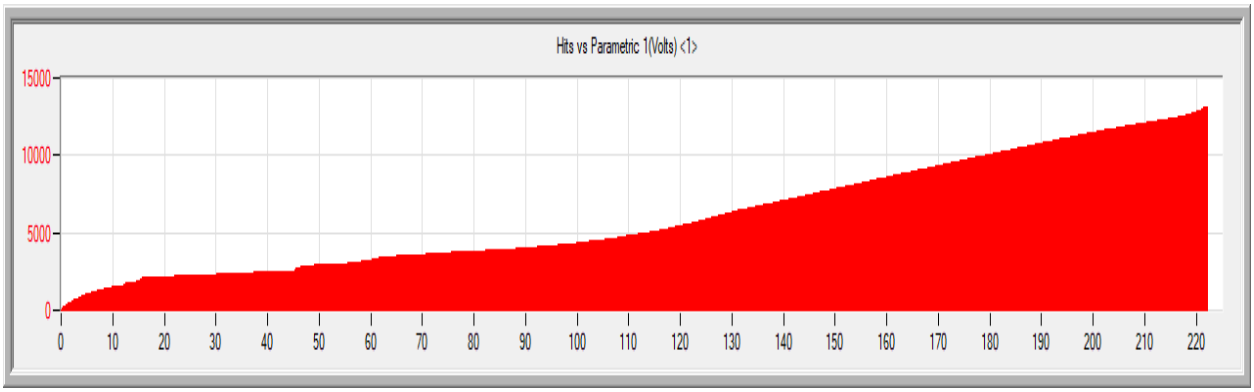
Number of Hits vs. Axial Stress (MPa): Channel 2



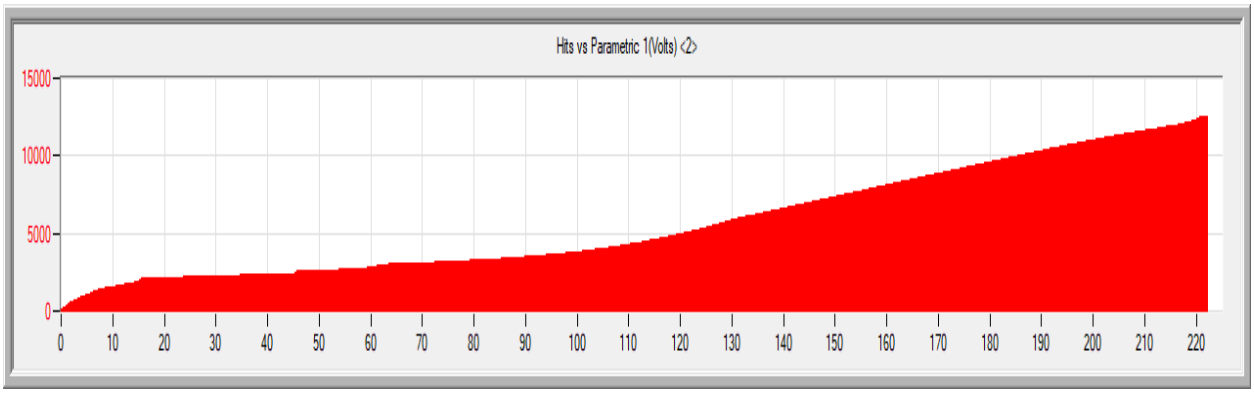
Number of Hits vs. Axial Stress (MPa): Channels 1+2



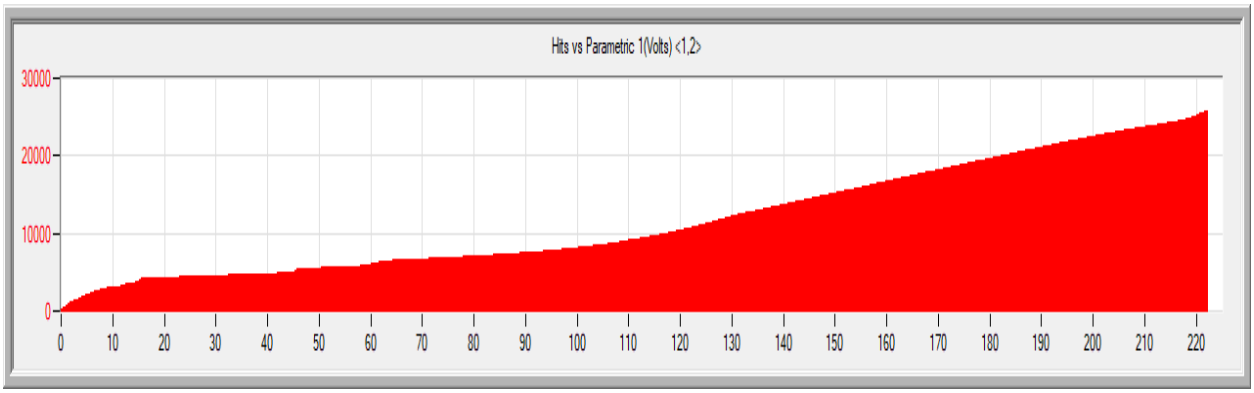
Cumulative Number of Hits vs. Axial Stress (MPa): Channel 1



Cumulative Number of Hits vs. Axial Stress (MPa): Channel 2



Cumulative Number of Hits vs. Axial Stress (MPa): Channels 1+2



Acoustic Emission Data Analysis: Specimen IG-BH01-UC006

Test Summary

P:\lab data\S Gaines\P-002797.002_Golder_NWMO\Data\AE\IG-UC-006\IG-UC006.dta

Total AEHits :	24199
Total TDDs :	58
Total Waveforms:	24199
Total Resumes :	1
Total Pauses :	1
Total TimeMarks:	0

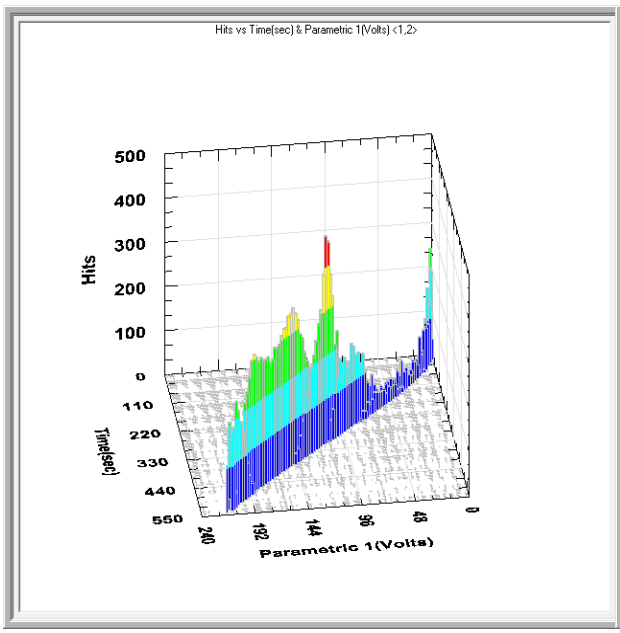
Channel	AEHits
1	11926
2	12273

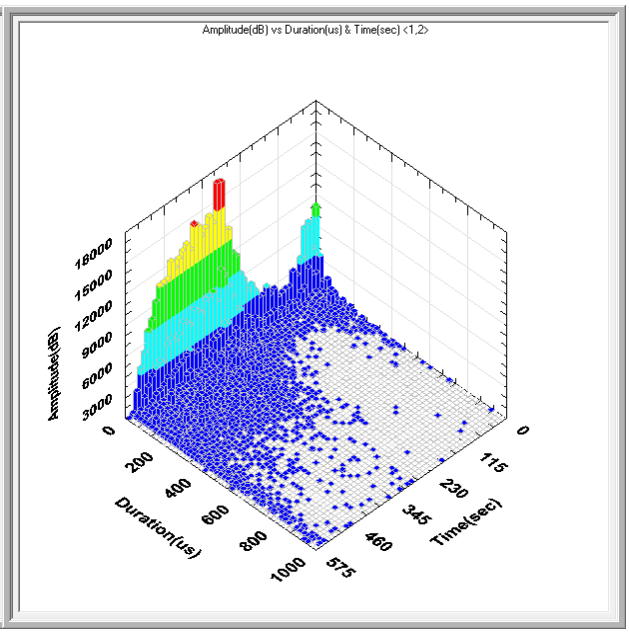
HIT DRIVEN DATA:

Feature	Chan	Minimum	Maximum	Average	Std Dev
Risetime	1	0.0000	13070.0000	116.0280	769.8447
Counts	1	1.0000	30999.0000	61.1628	780.6249
Energy	1	0.0000	65535.0000	71.7791	1863.8252
Duration	1	0.0000	1000000.0000	1819.0897	35045.8662
Amplitude	1	40.0000	100.0000	46.8326	7.3763
Threshold	1	40.0000	40.0000	40.0000	0.0055
SigStrength	1	0.0000	5246152192.0000	1729983.7500	74607052.1073
AbsEnergy	1	0.0000	91639439360.0000	14735119.0000	1029654722.4863
Parametric1	1	-0.1707	220.6627	132.8884	59.0208
Risetime	2	0.0000	12890.0000	119.7816	802.9348
Counts	2	1.0000	29510.0000	61.8068	794.6442
Energy	2	0.0000	65535.0000	65.9034	1765.2991
Duration	2	0.0000	1000000.0000	1700.7637	32804.7740
Amplitude	2	40.0000	100.0000	46.8185	7.4143
Threshold	2	40.0000	40.0000	40.0000	-1.#IND
SigStrength	2	0.0000	11685744640.0000	2197903.7500	123984747.7046
AbsEnergy	2	0.0000	50691317760.0000	6430420.5000	483748397.5546
Parametric1	2	-0.1707	220.6627	130.2055	61.5020

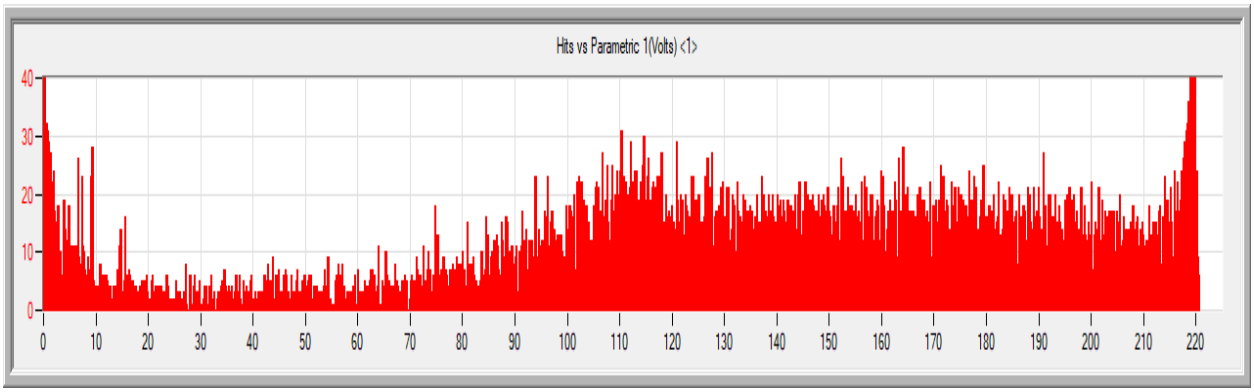
TIME DRIVEN DATA:

Feature	Chan	Minimum	Maximum	Average	Std Dev
asl	1	24.0000	73.0000	30.9828	8.7425
asl	2	21.0000	72.0000	30.2414	8.7322
asl	30	92647055355262140000000000000000.0000		92647055355262140000000000	
asl	41	0.0000	0.0000	0.0000	0.0000
asl	96	0.0000	0.0000	0.0000	0.0000
asl	104	0.0000	0.0000	0.0000	0.0000
Parametric1		1.1093	220.3783	109.8925	71.4735

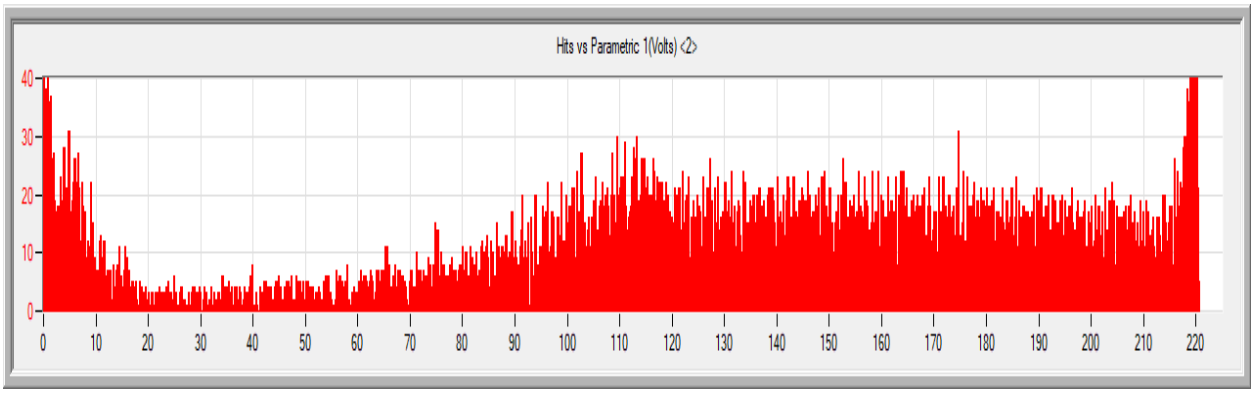




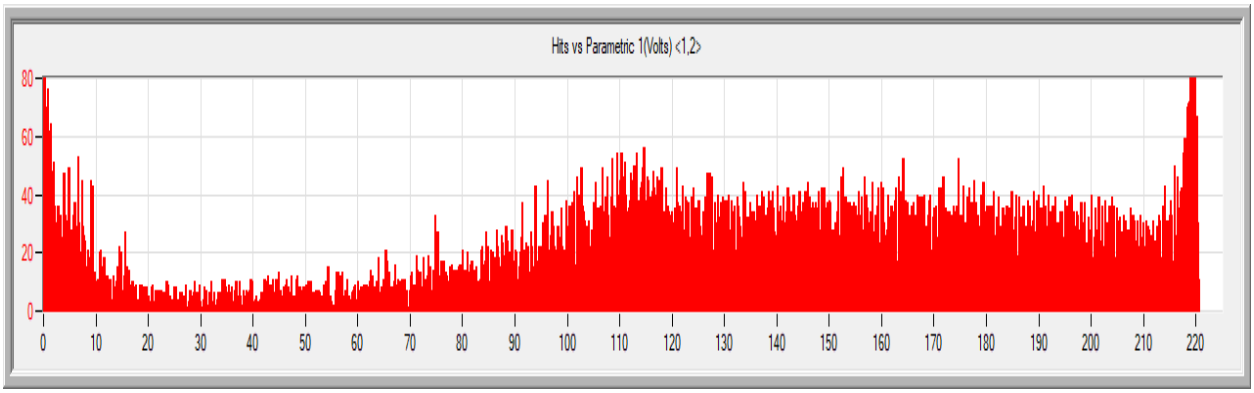
Number of Hits vs. Axial Stress (MPa): Channel 1



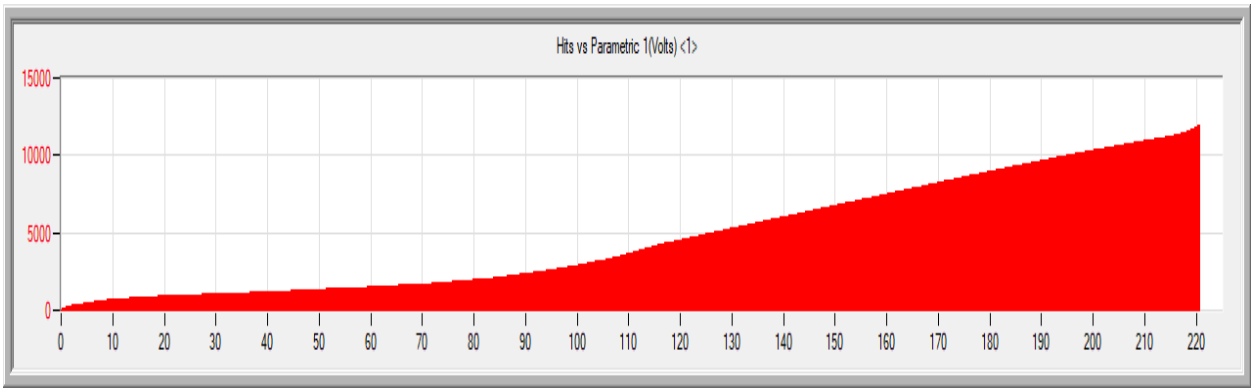
Number of Hits vs. Axial Stress (MPa): Channel 2



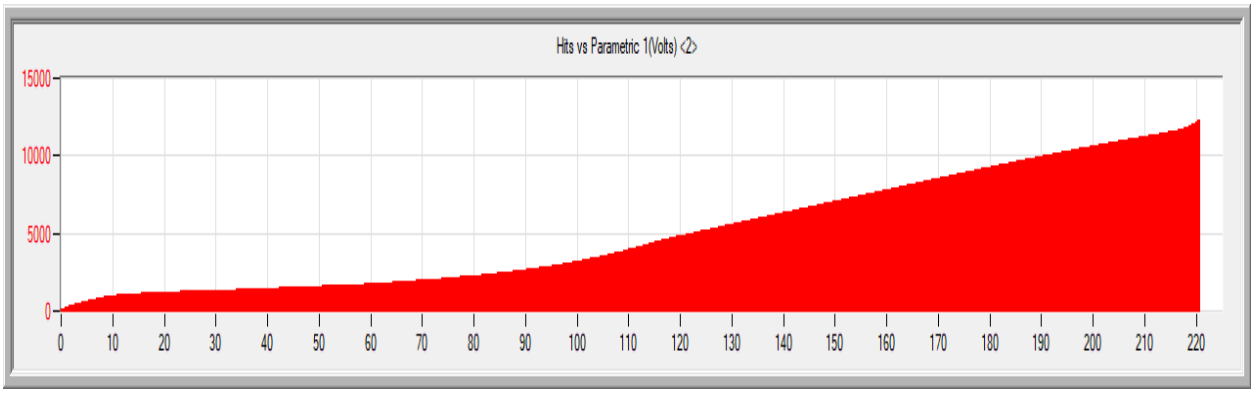
Number of Hits vs. Axial Stress (MPa): Channels 1+2



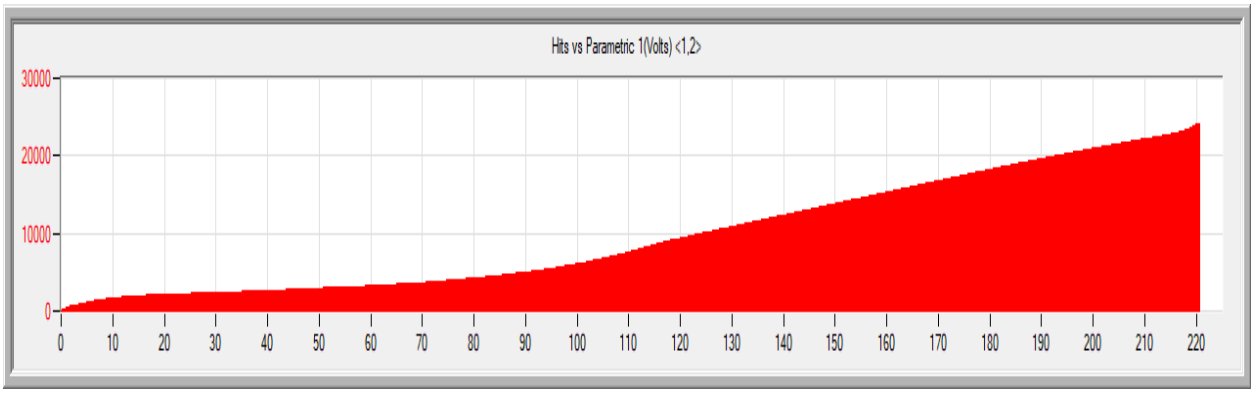
Cumulative Number of Hits vs. Axial Stress (MPa): Channel 1



Cumulative Number of Hits vs. Axial Stress (MPa): Channel 2



Cumulative Number of Hits vs. Axial Stress (MPa): Channels 1+2



Acoustic Emission Data Analysis: Specimen IG-BH01-UC007

Test Summary

P:\lab data\S Gaines\P-002797.002_Golder_NWMO\Data\AE\IG-UC-007\IG-UC007.dta

Total AEHits : 25905
Total TDDs : 61
Total Waveforms: 25905
Total Resumes : 1
Total Pauses : 1
Total TimeMarks: 0

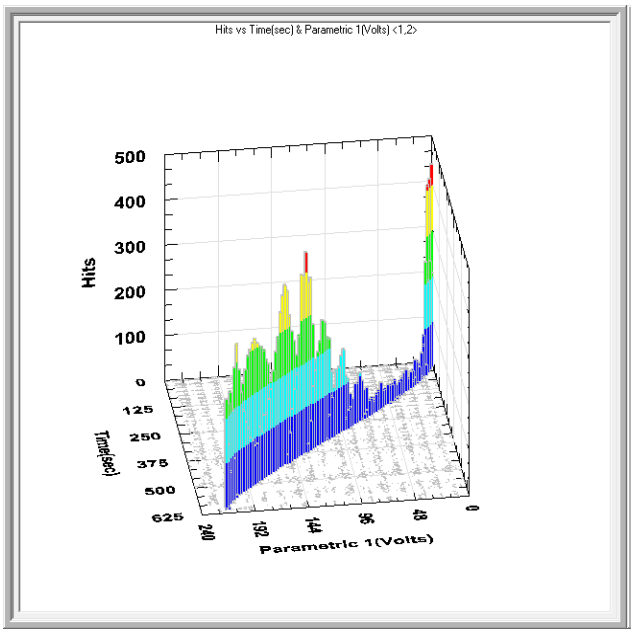
Channel	AEHits
1	12729
2	13176

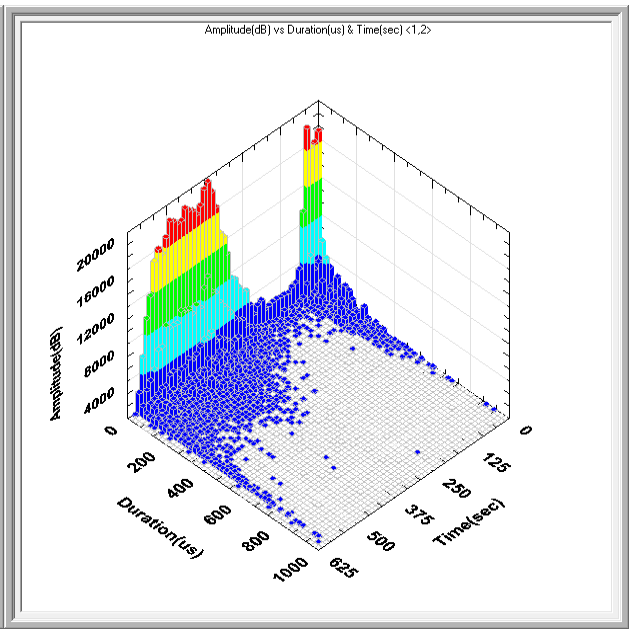
HIT DRIVEN DATA:

Feature	Chan	Minimum	Maximum	Average	Std Dev
Risetime	1	0.0000	12672.0000	46.5952	471.3130
Counts	1	1.0000	32686.0000	25.3258	619.1433
Energy	1	0.0000	65535.0000	34.7268	1426.0946
Duration	1	0.0000	1000000.0000	695.6659	22159.8021
Amplitude	1	40.0000	100.0000	45.3971	5.8778
Threshold	1	40.0000	40.0000	40.0000	0.0054
SigStrength	1	0.0000	9830507520.0000	1327373.0000	93825909.7220
AbsEnergy	1	0.0000	71291494400.0000	8418392.0000	696302687.3717
Parametric1	1	-0.3129	216.6238	129.8582	66.5812
Risetime	2	0.0000	12618.0000	51.4368	467.2740
Counts	2	1.0000	25336.0000	20.6911	380.9666
Energy	2	0.0000	65535.0000	35.0723	1418.8831
Duration	2	0.0000	1000000.0000	740.8906	23154.4632
Amplitude	2	40.0000	100.0000	45.7507	6.2026
Threshold	2	40.0000	40.0000	40.0000	0.0049
SigStrength	2	0.0000	5225734144.0000	969462.0000	58099551.4457
AbsEnergy	2	0.0000	11957812224.0000	1577525.1250	118130973.8362
Parametric1	2	-0.3413	216.5954	124.9741	68.8636

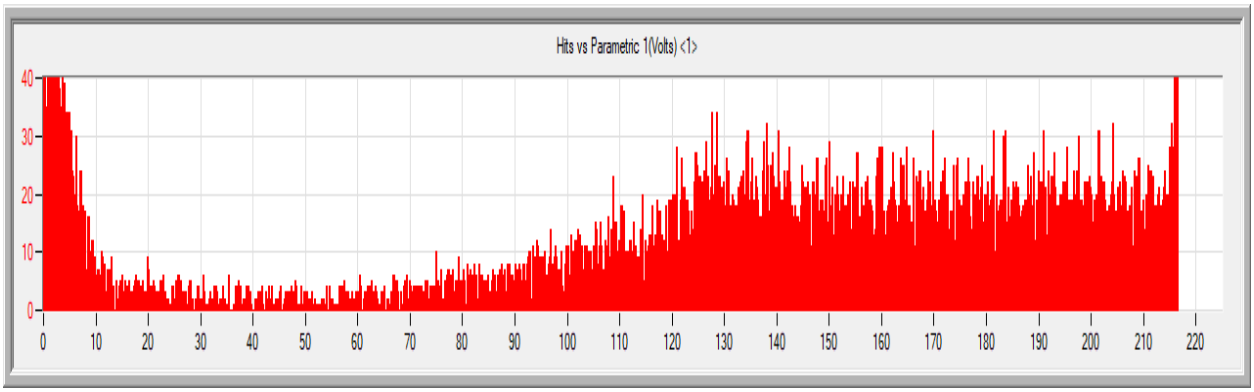
TIME DRIVEN DATA:

Feature	Chan	Minimum	Maximum	Average	Std Dev
asl	1	22.0000	86.0000	30.5738	8.2828
asl	2	24.0000	83.0000	29.3443	8.5198
Parametric1		0.8817	216.3678	106.9951	70.1707

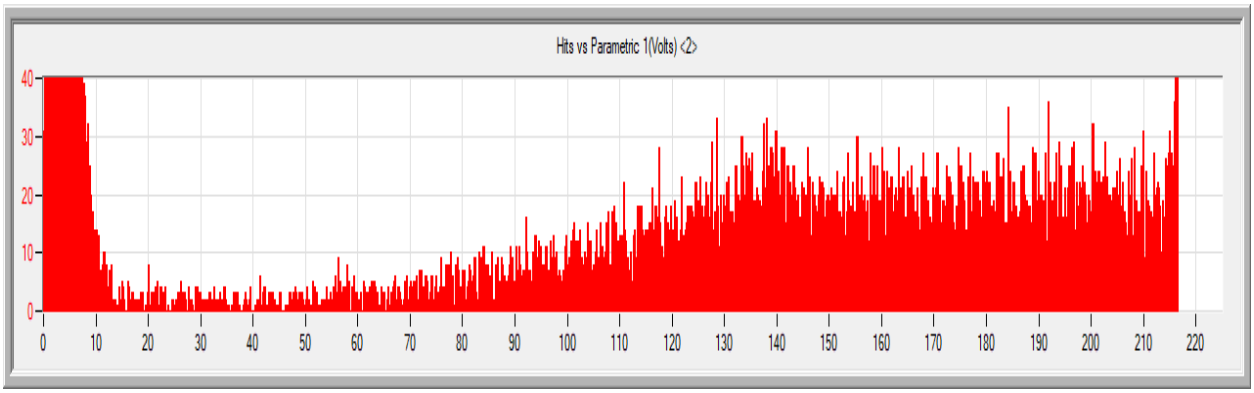




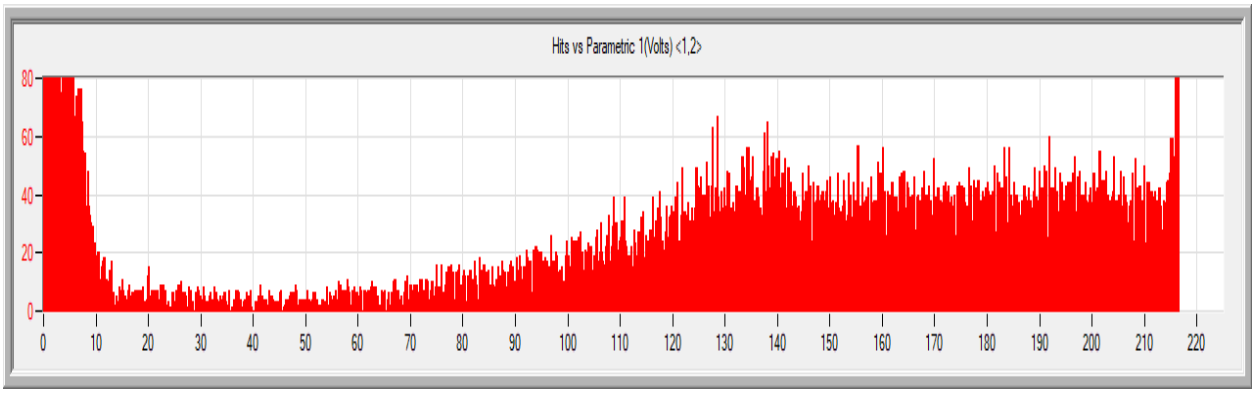
Number of Hits vs. Axial Stress (MPa): Channel 1



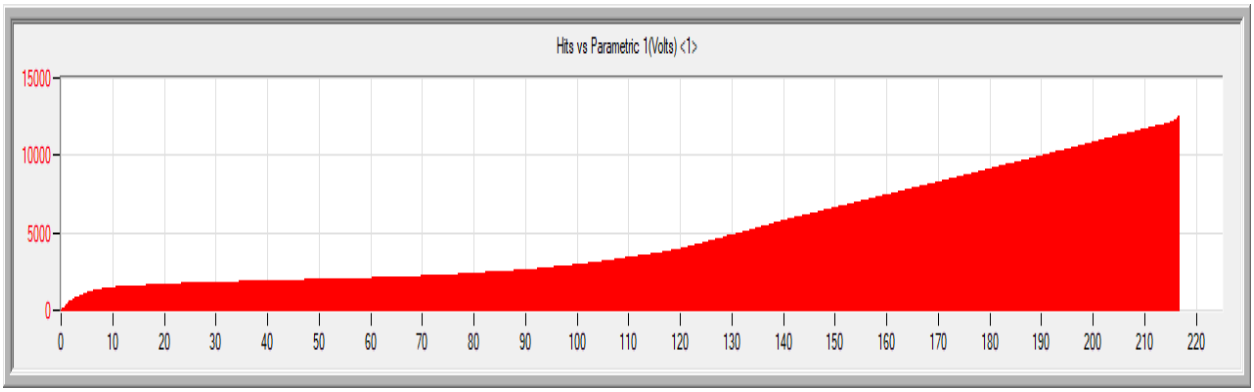
Number of Hits vs. Axial Stress (MPa): Channel 2



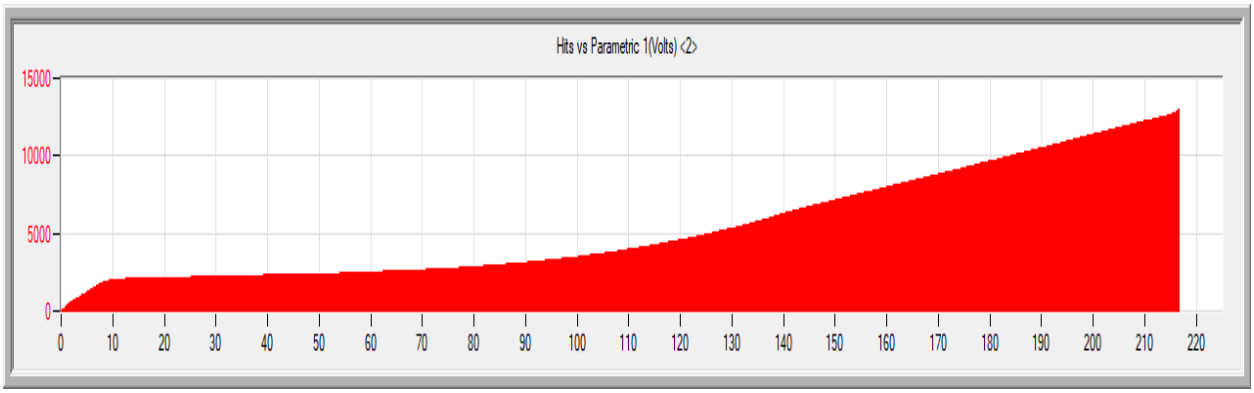
Number of Hits vs. Axial Stress (MPa): Channels 1+2



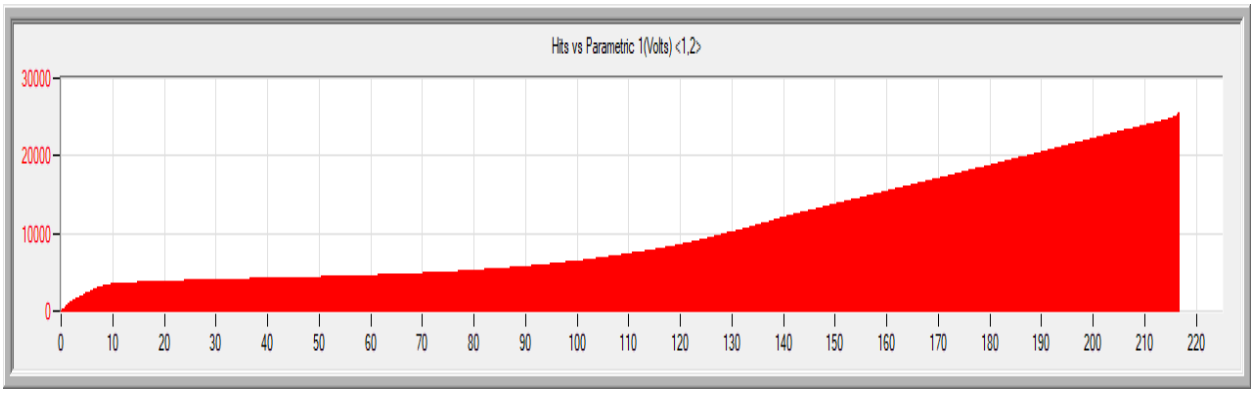
Cumulative Number of Hits vs. Axial Stress (MPa): Channel 1



Cumulative Number of Hits vs. Axial Stress (MPa): Channel 2



Cumulative Number of Hits vs. Axial Stress (MPa): Channels 1+2



Acoustic Emission Data Analysis: Specimen IG-BH01-UC008

Test Summary

P:\lab data\S Gaines\P-002797.002_Golder_NWMO\Data\AE\IG-UC-008\IG-UC008.dta

Total AEHits :	12392
Total TDDs :	76
Total Waveforms:	12392
Total Resumes :	1
Total Pauses :	1
Total TimeMarks:	0

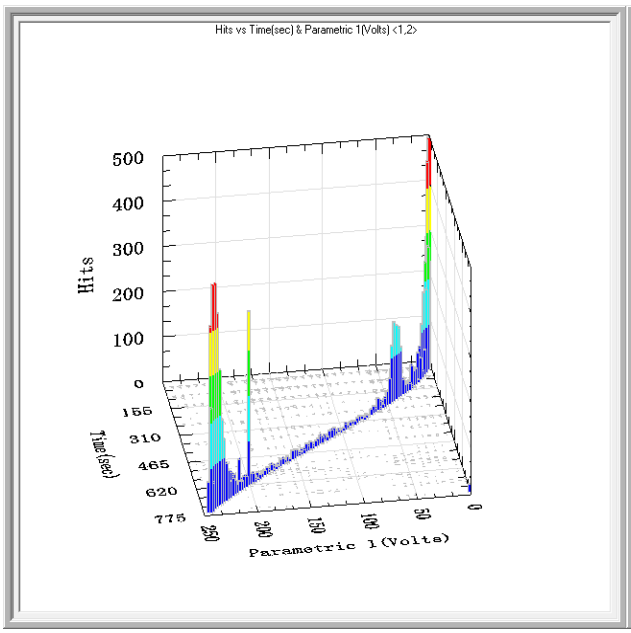
Channel	AEHits
1	4512
2	7880

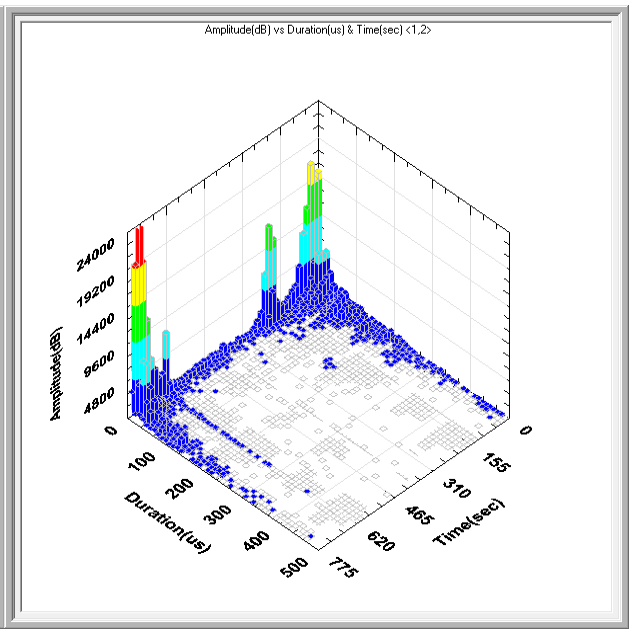
HIT DRIVEN DATA:

Feature	Chan	Minimum	Maximum	Average	Std Dev
Risetime	1	0.0000	13018.0000	47.0421	483.3408
Counts	1	1.0000	28126.0000	16.6631	439.3469
Energy	1	0.0000	65535.0000	34.7376	1391.1139
Duration	1	0.0000	693557.0000	520.2345	14526.5037
Amplitude	1	40.0000	100.0000	44.4218	5.0236
Threshold	1	40.0000	40.0000	40.0000	0.0000
SigStrength	1	0.0000	2644726016.0000	800593.3750	41143281.5600
AbsEnergy	1	0.0000	17815078912.0000	4618686.0000	268621416.4706
Parametric1	1	-0.2275	245.3515	158.3412	104.1543
Risetime	2	0.0000	13023.0000	20.8311	314.7480
Counts	2	1.0000	9632.0000	5.6876	114.7757
Energy	2	0.0000	9918.0000	2.3194	113.1512
Duration	2	0.0000	85429.0000	98.7061	1586.6332
Amplitude	2	40.0000	100.0000	44.2487	5.1026
Threshold	2	40.0000	40.0000	40.0000	0.0081
SigStrength	2	0.0000	61957620.0000	15871.9141	706850.9483
AbsEnergy	2	0.0000	179184832.0000	23099.1680	2018443.0282
Parametric1	2	-0.2275	245.3230	88.4803	99.6858

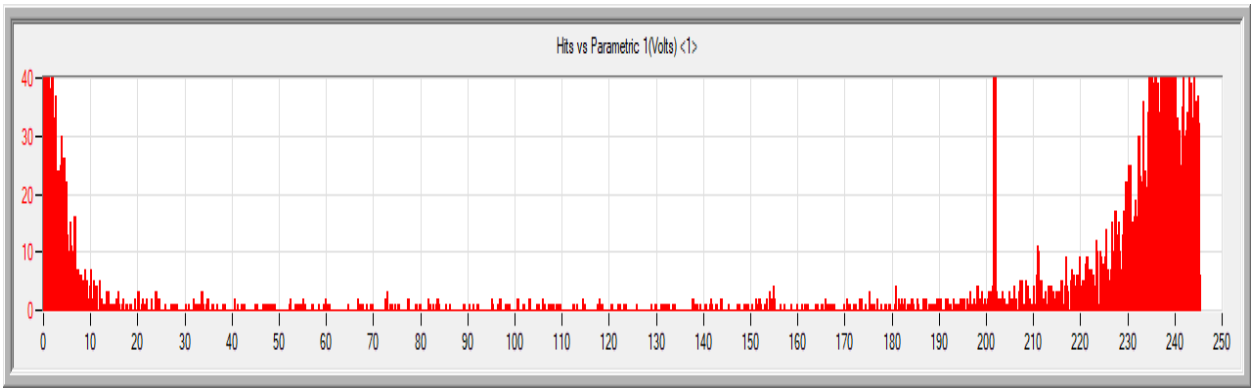
TIME DRIVEN DATA:

Feature	Chan	Minimum	Maximum	Average	Std Dev
asl	1	24.0000	44.0000	25.4605	2.2445
asl	2	26.0000	51.0000	29.6974	2.9692
Parametric1		0.4266	244.2138	112.7794	78.0254

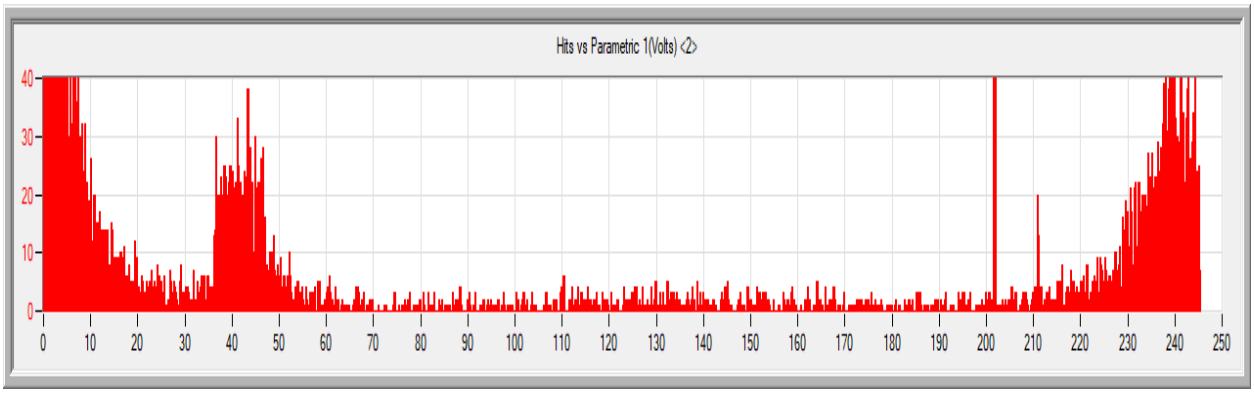




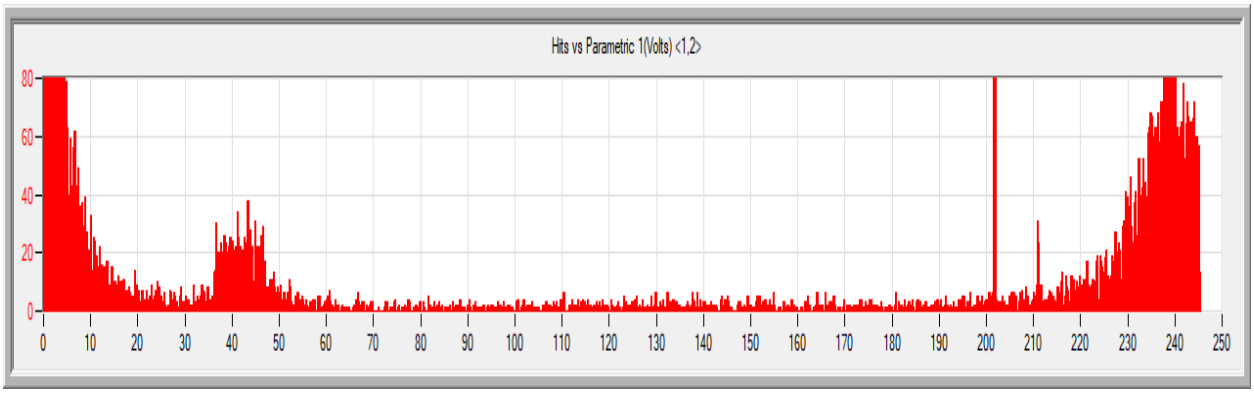
Number of Hits vs. Axial Stress (MPa): Channel 1



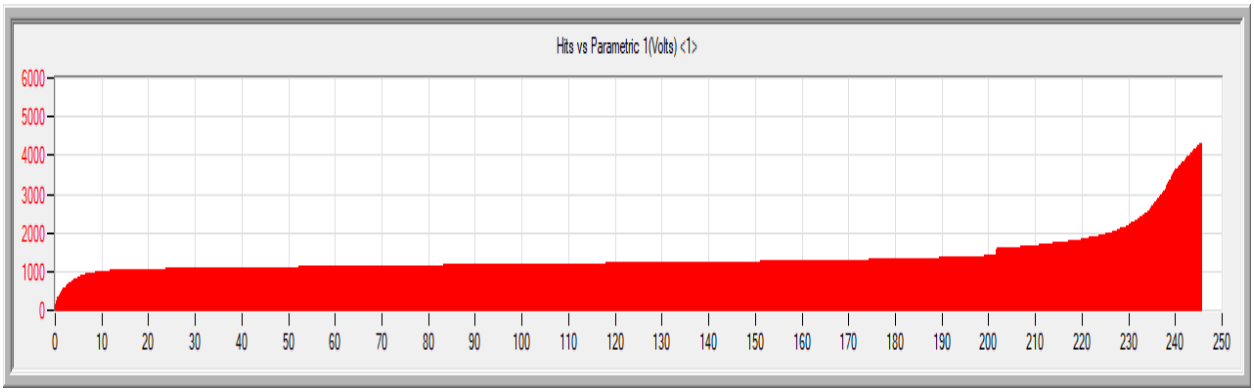
Number of Hits vs. Axial Stress (MPa): Channel 2



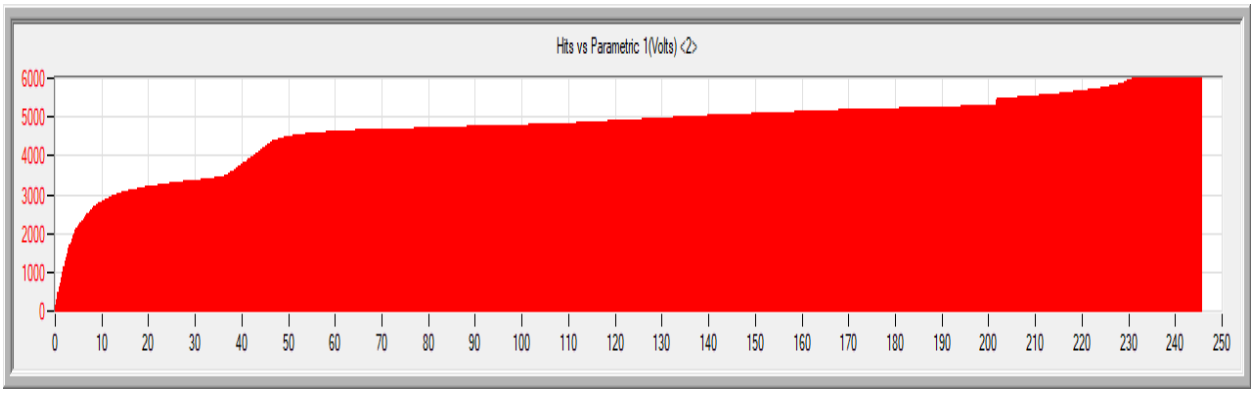
Number of Hits vs. Axial Stress (MPa): Channels 1+2



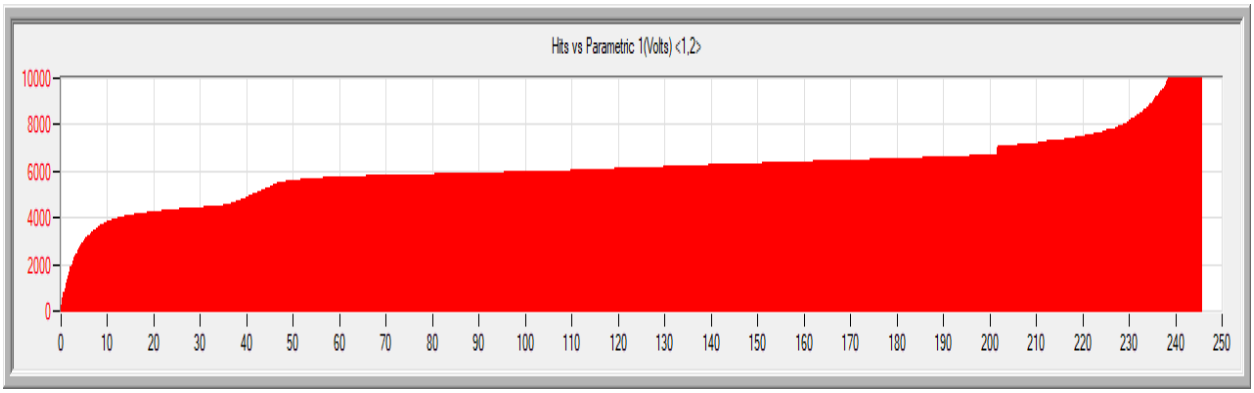
Cumulative Number of Hits vs. Axial Stress (MPa): Channel 1



Cumulative Number of Hits vs. Axial Stress (MPa): Channel 2



Cumulative Number of Hits vs. Axial Stress (MPa): Channels 1+2



Acoustic Emission Data Analysis: Specimen IG-BH01-UC009

Test Summary

P:\lab data\S Gaines\P-002797.002_Golder_NWMO\Data\AE\IG-UC-009\IG-UC009.dta

Total AEHits :	25337
Total TDDs :	38
Total Waveforms:	25337
Total Resumes :	1
Total Pauses :	1
Total TimeMarks:	0

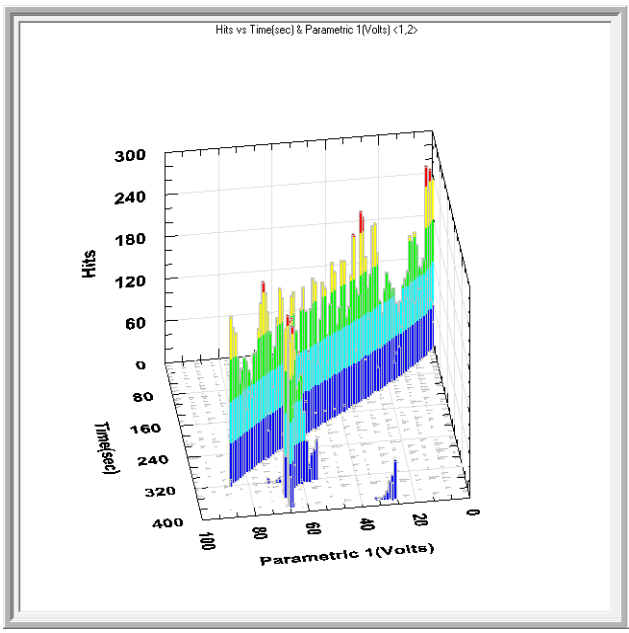
Channel	AEHits
1	12920
2	12417

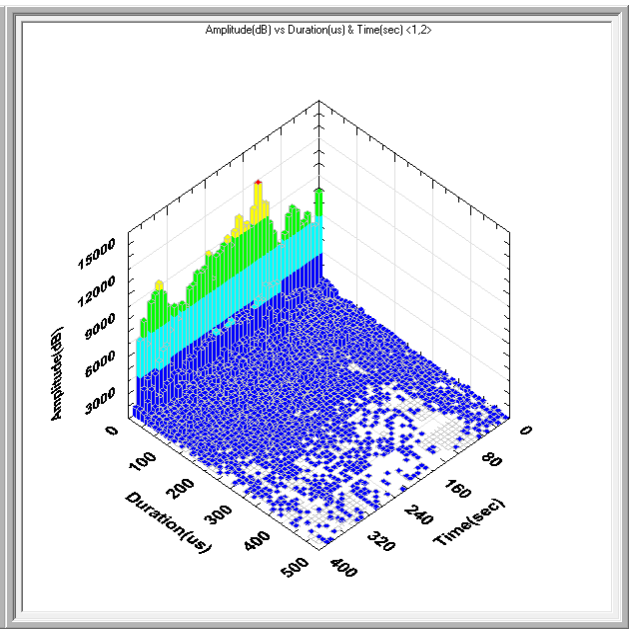
HIT DRIVEN DATA:

Feature	Chan	Minimum	Maximum	Average	Std Dev
Risetime	1	0.0000	5157.0000	19.7591	104.5496
Counts	1	1.0000	391.0000	4.6512	11.6633
Energy	1	0.0000	628.0000	0.9841	8.8940
Duration	1	0.0000	16505.0000	90.0133	339.7370
Amplitude	1	40.0000	87.0000	44.3593	4.8529
Threshold	1	40.0000	40.0000	40.0000	0.0050
SigStrength	1	0.0000	3926502.7500	7891.7344	55738.4485
AbsEnergy	1	0.0000	2250790.7500	471.2711	20753.6892
Parametric1	1	-0.2844	86.7804	45.0470	26.0420
Risetime	2	0.0000	12214.0000	34.1322	260.5984
Counts	2	1.0000	8402.0000	5.9563	78.3607
Energy	2	0.0000	3024.0000	2.1548	39.5598
Duration	2	0.0000	170556.0000	155.0510	1782.1786
Amplitude	2	40.0000	92.0000	44.4978	4.8898
Threshold	2	40.0000	40.0000	40.0000	0.0032
SigStrength	2	0.0000	18895124.0000	15355.0352	247177.3101
AbsEnergy	2	0.0000	3565496.7500	1219.0062	48552.7502
Parametric1	2	-0.2275	86.7519	45.2873	26.3689

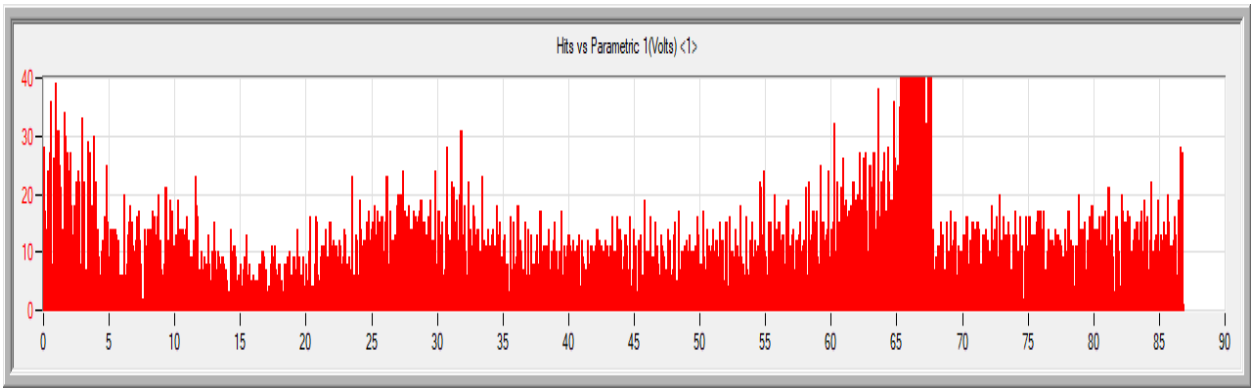
TIME DRIVEN DATA:

Feature	Chan	Minimum	Maximum	Average	Std Dev
asl	1	28.0000	41.0000	30.4737	2.5520
asl	2	27.0000	41.0000	31.4474	2.7115
asl	91	-0.0000	-0.0000	-0.0000	0.0000
asl	104	0.0000	0.0000	0.0000	0.0000
Parametric1		0.7395	86.7519	46.1207	26.6232

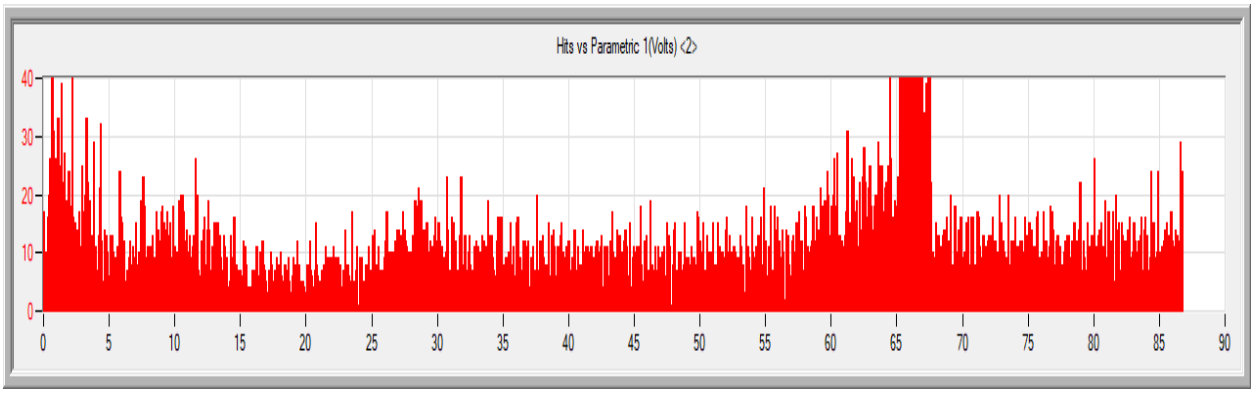




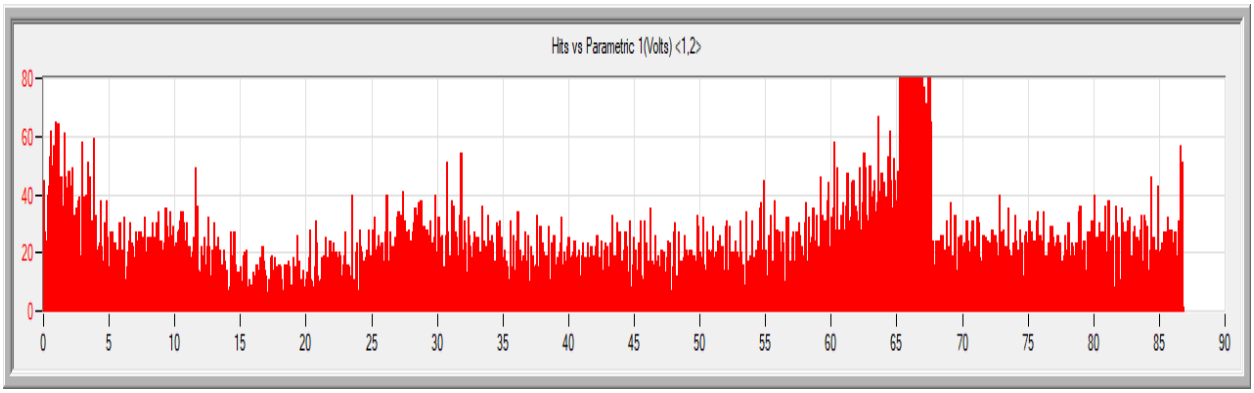
Number of Hits vs. Axial Stress (MPa): Channel 1



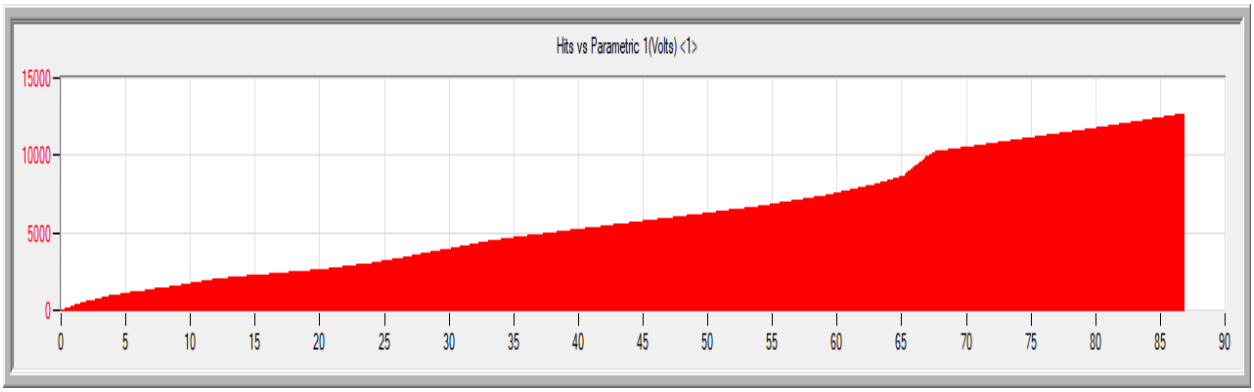
Number of Hits vs. Axial Stress (MPa): Channel 2



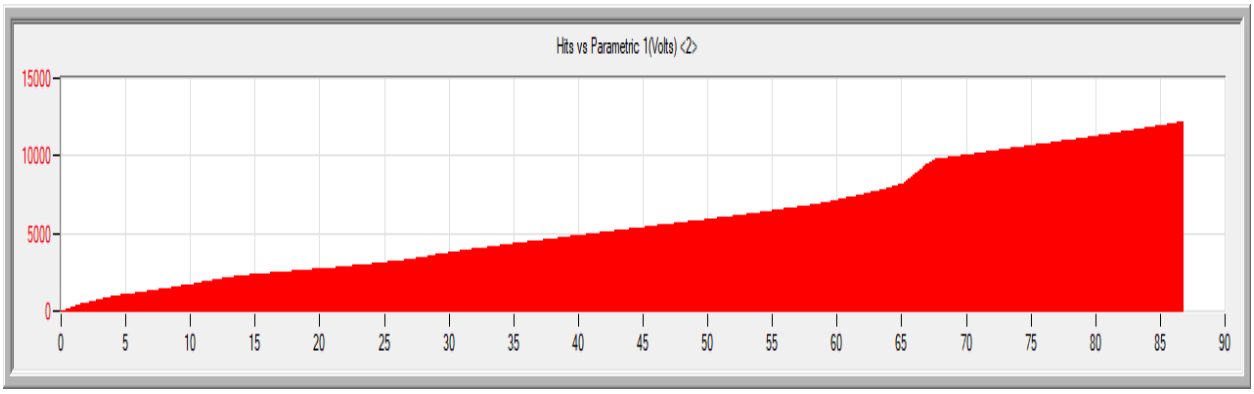
Number of Hits vs. Axial Stress (MPa): Channels 1+2



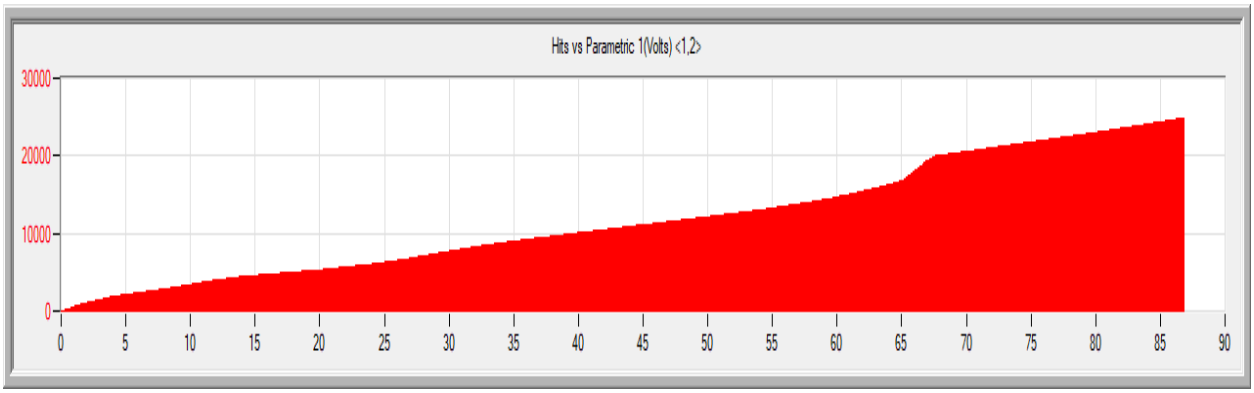
Cumulative Number of Hits vs. Axial Stress (MPa): Channel 1



Cumulative Number of Hits vs. Axial Stress (MPa): Channel 2



Cumulative Number of Hits vs. Axial Stress (MPa): Channels 1+2



Acoustic Emission Data Analysis: Specimen IG-BH01-UC010

Test Summary

P:\lab data\S Gaines\P-002797.002_Golder_NWMO\Data\AE\IG-UC-010\IG-UC010.dta

Total AEHits :	19403
Total TDDs :	51
Total Waveforms:	19403
Total Resumes :	1
Total Pauses :	1
Total TimeMarks:	0

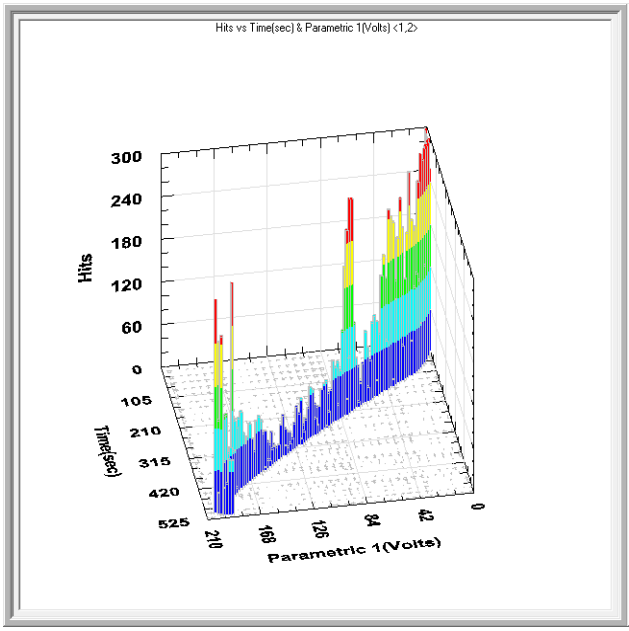
Channel	AEHits
1	10957
2	8446

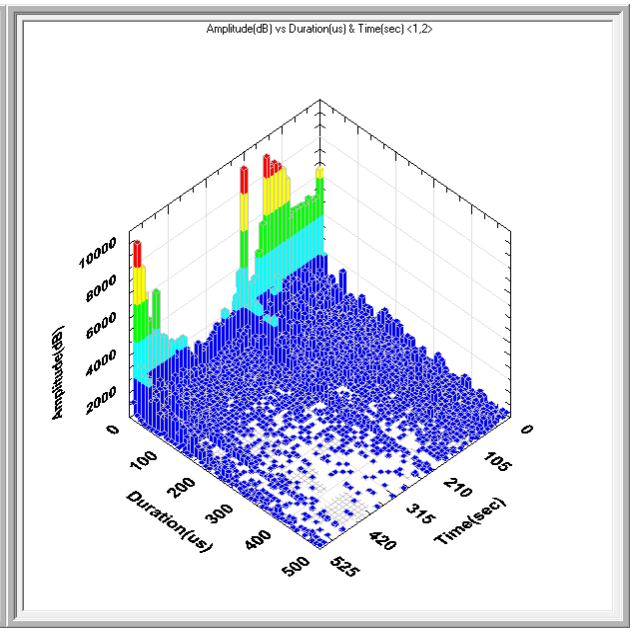
HIT DRIVEN DATA:

Feature	Chan	Minimum	Maximum	Average	Std Dev
Risetime	1	0.0000	13038.0000	42.4340	402.7202
Counts	1	1.0000	31202.0000	18.1861	408.4721
Energy	1	0.0000	63291.0000	12.8725	702.0560
Duration	1	0.0000	999995.0000	324.3711	10046.8426
Amplitude	1	40.0000	100.0000	45.6003	6.2872
Threshold	1	40.0000	40.0000	40.0000	0.0007
SigStrength	1	0.0000	395346720.0000	82417.1094	4385366.4383
AbsEnergy	1	0.0000	720981248.0000	108009.9063	7513567.2148
Parametric1	1	-0.1707	202.4022	73.4287	71.1831
Risetime	2	0.0000	12640.0000	52.7660	323.5843
Counts	2	1.0000	27646.0000	20.2990	324.1399
Energy	2	0.0000	28548.0000	9.3868	378.1382
Duration	2	0.0000	723191.0000	386.2654	9495.6724
Amplitude	2	40.0000	97.0000	46.4860	6.5640
Threshold	2	40.0000	40.0000	40.0000	-1.#IND
SigStrength	2	0.0000	178324048.0000	61056.0703	2361993.5740
AbsEnergy	2	0.0000	65007444.0000	12783.8506	741435.9529
Parametric1	2	-0.1707	202.4022	65.7183	71.5488

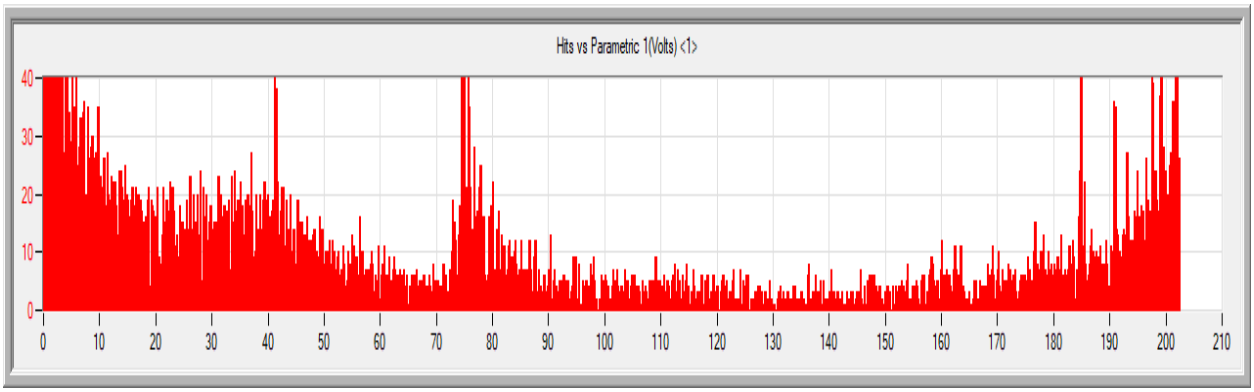
TIME DRIVEN DATA:

Feature	Chan	Minimum	Maximum	Average	Std Dev
asl	1	29.0000	57.0000	31.5686	4.9597
asl	2	24.0000	57.0000	28.5490	6.3688
asl	104	0.0000	0.0000	0.0000	0.0000
Parametric1		0.0853	200.4111	97.5230	66.9841

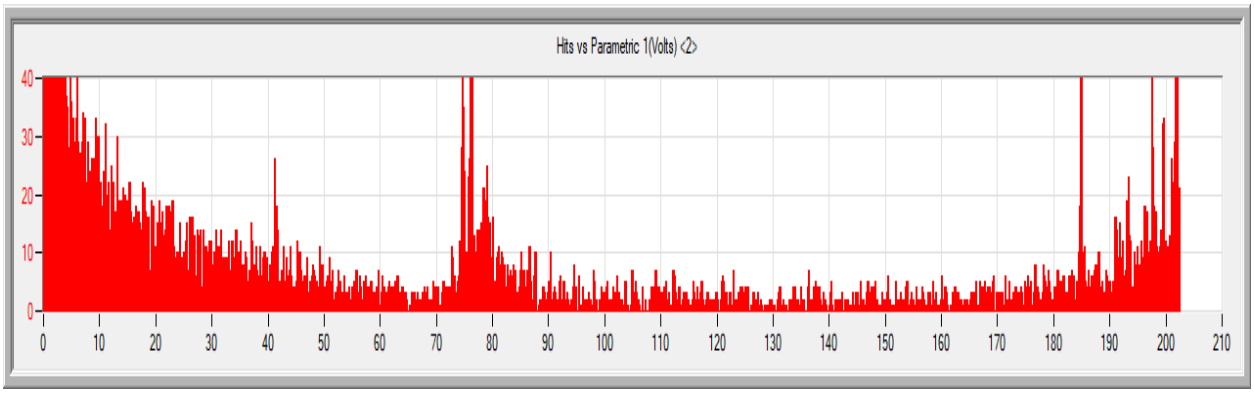




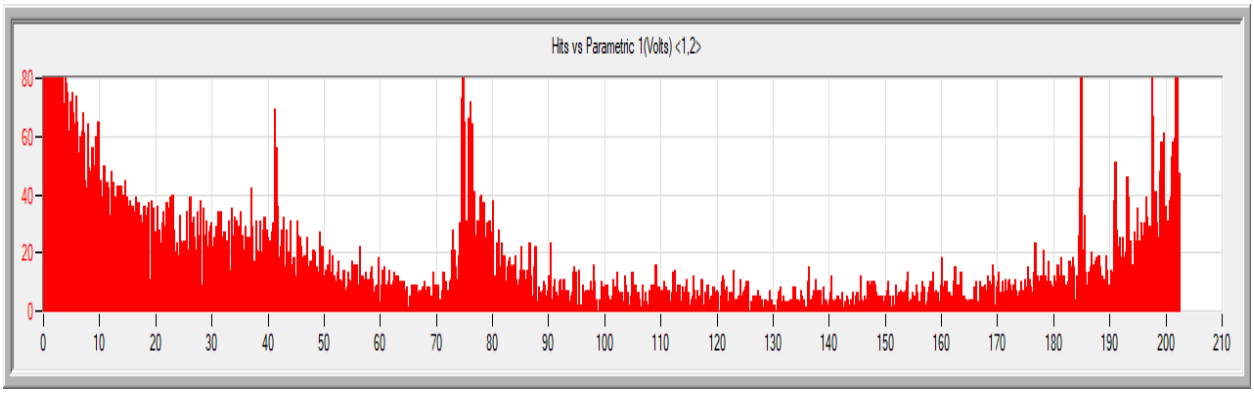
Number of Hits vs. Axial Stress (MPa): Channel 1



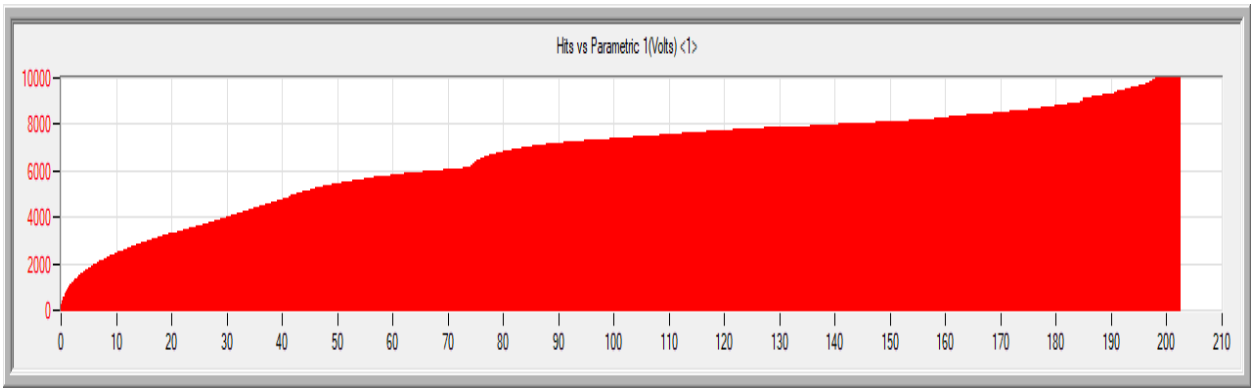
Number of Hits vs. Axial Stress (MPa): Channel 2



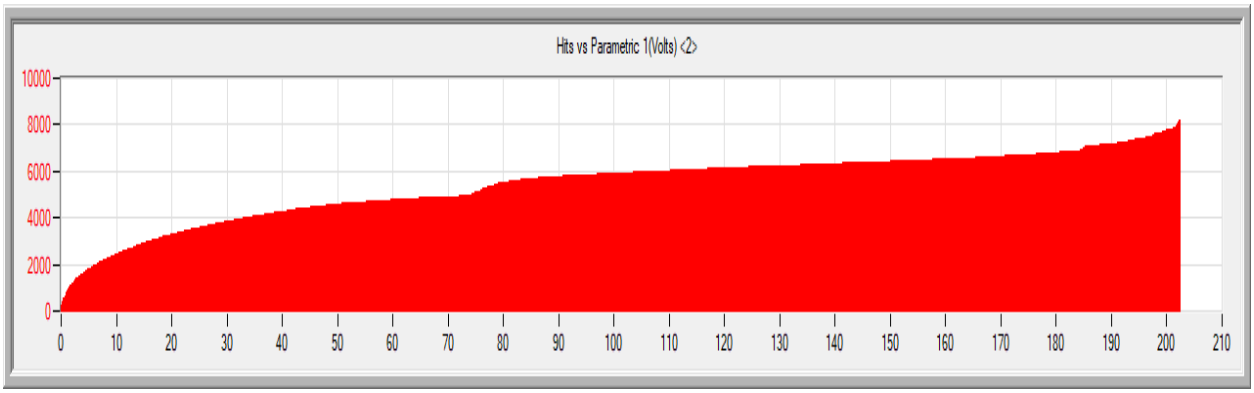
Number of Hits vs. Axial Stress (MPa): Channels 1+2



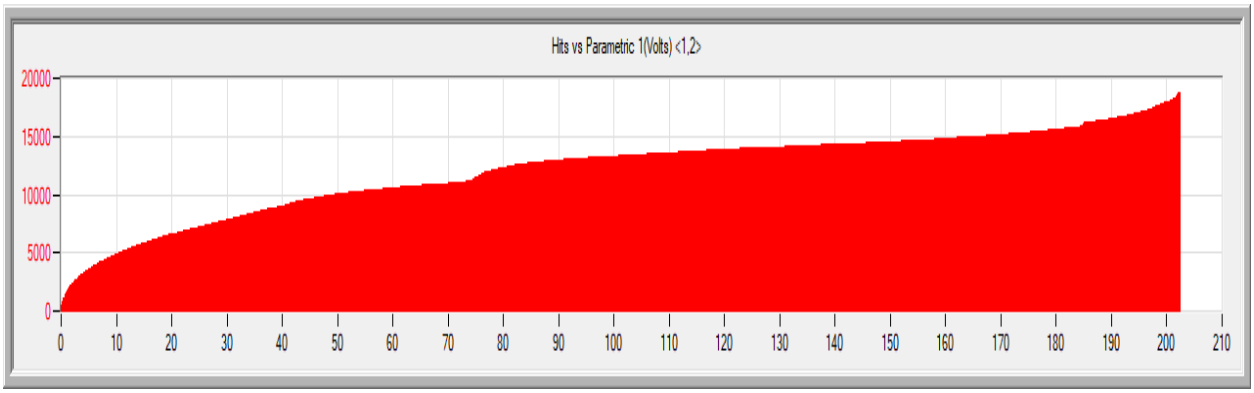
Cumulative Number of Hits vs. Axial Stress (MPa): Channel 1



Cumulative Number of Hits vs. Axial Stress (MPa): Channel 2



Cumulative Number of Hits vs. Axial Stress (MPa): Channels 1+2



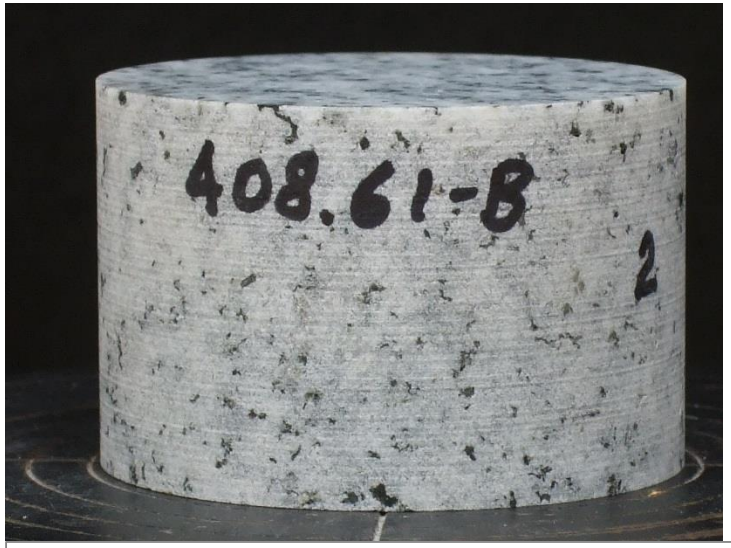
APPENDIX C

Indirect Tensile (Brazilian) Strength Tests: Load-Time and Stress-Displacement Graphs and Photographs of Intact and Broken Test Specimens

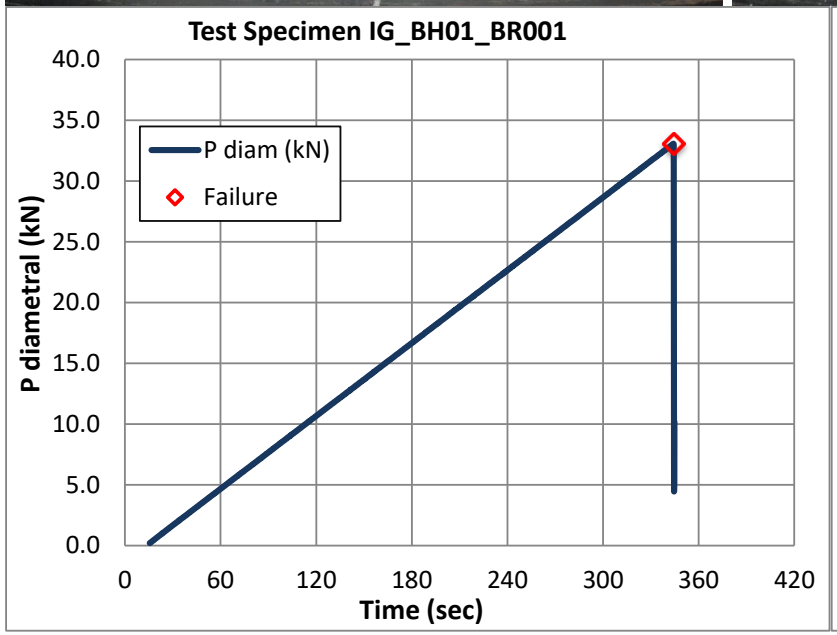
Table C-1: List of indirect tensile (Brazilian) test specimens

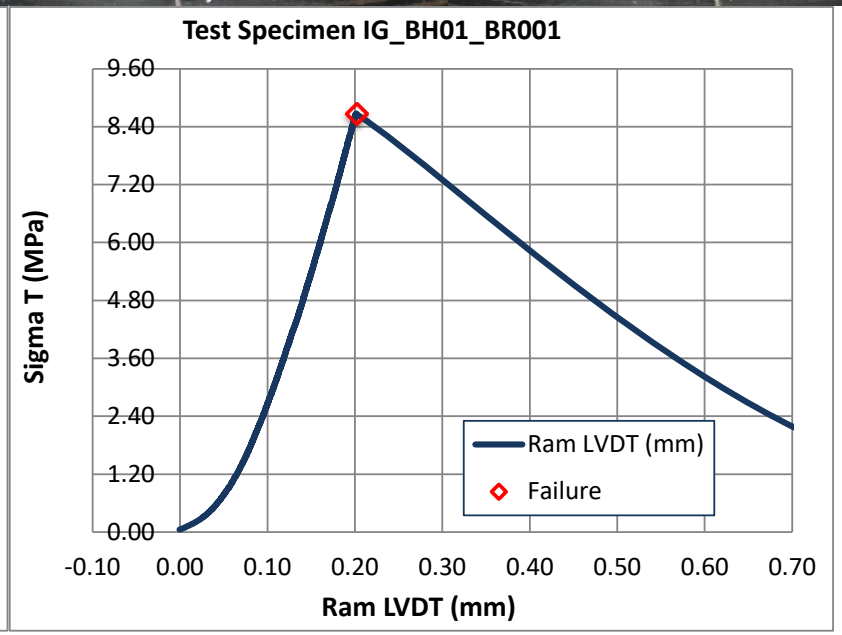
Specimen No.	Depth (m)[1]	Rock Type	Page
IG_BH01_BR001	408.61	Biotite Granodiorite-Tonalite	C-2
IG_BH01_BR002	442.26	Biotite Granodiorite-Tonalite	C-3
IG_BH01_BR003	468.23	Biotite Granodiorite-Tonalite	C-4
IG_BH01_BR004	522.90	Biotite Granodiorite-Tonalite	C-5
IG_BH01_BR005	568.04	Biotite Granodiorite-Tonalite	C-6
IG_BH01_BR006	601.00	Biotite Granodiorite-Tonalite	C-7
IG_BH01_BR007	451.06	Biotite Tonalite	C-8
IG_BH01_BR008	560.11	Feldspar-phyric Tonalite Dyke	C-9
IG_BH01_BR009	655.46	Amphibolite	C-10
IG_BH01_BR010	658.55	Amphibolite	C-11

[1]Top depth of prepared sub-sample

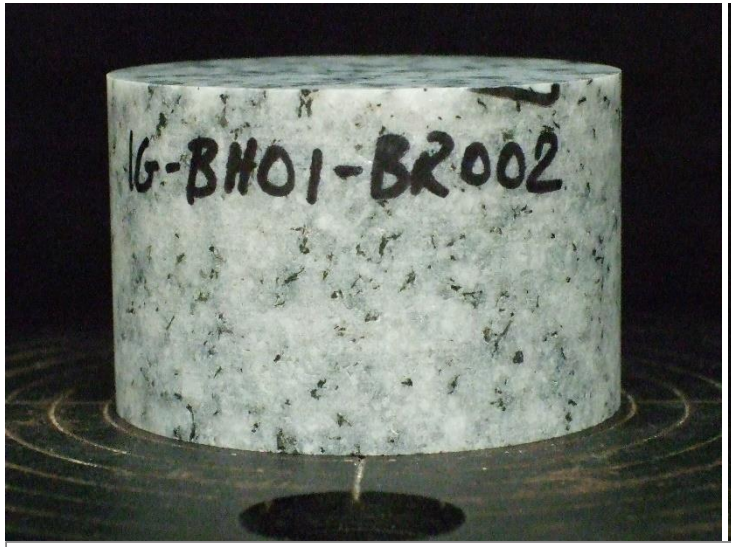


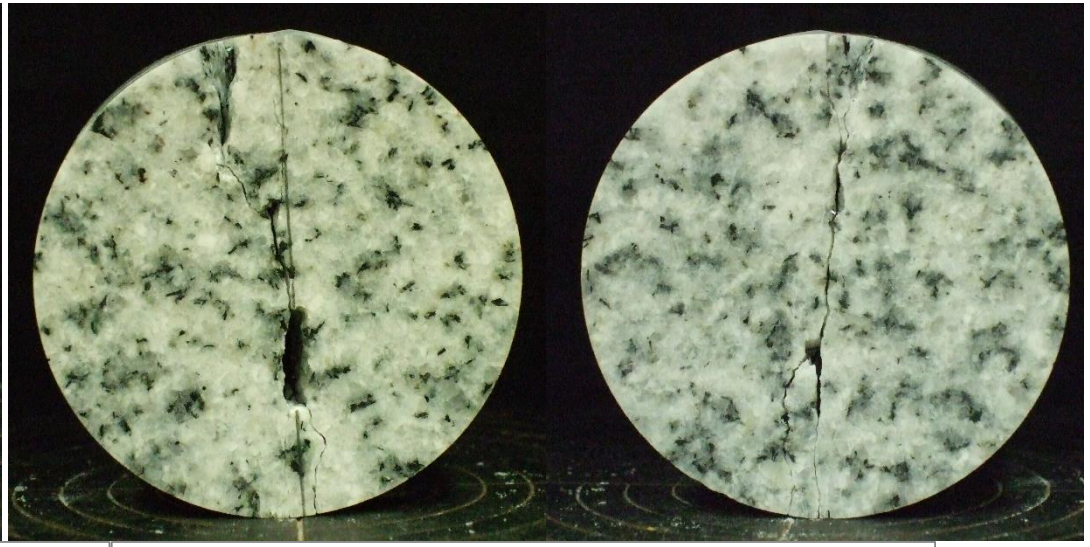


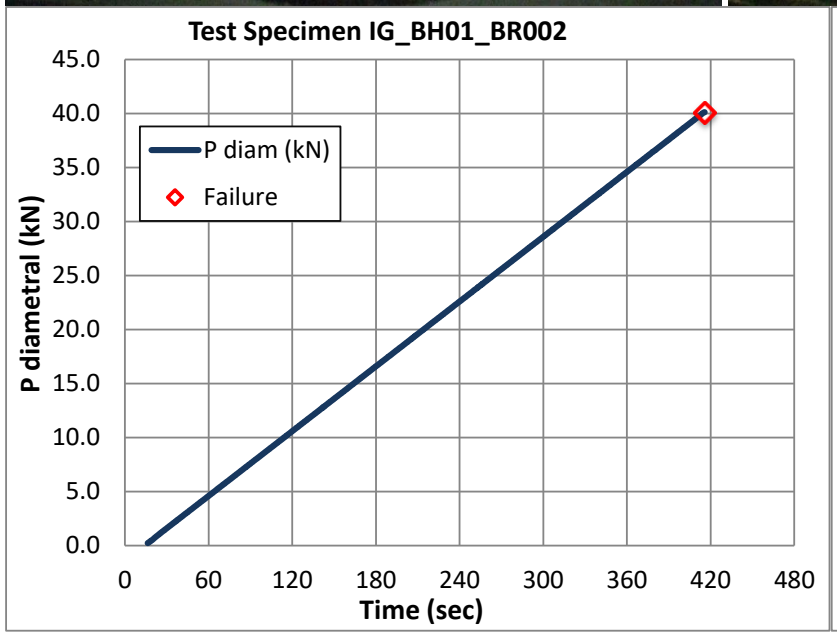


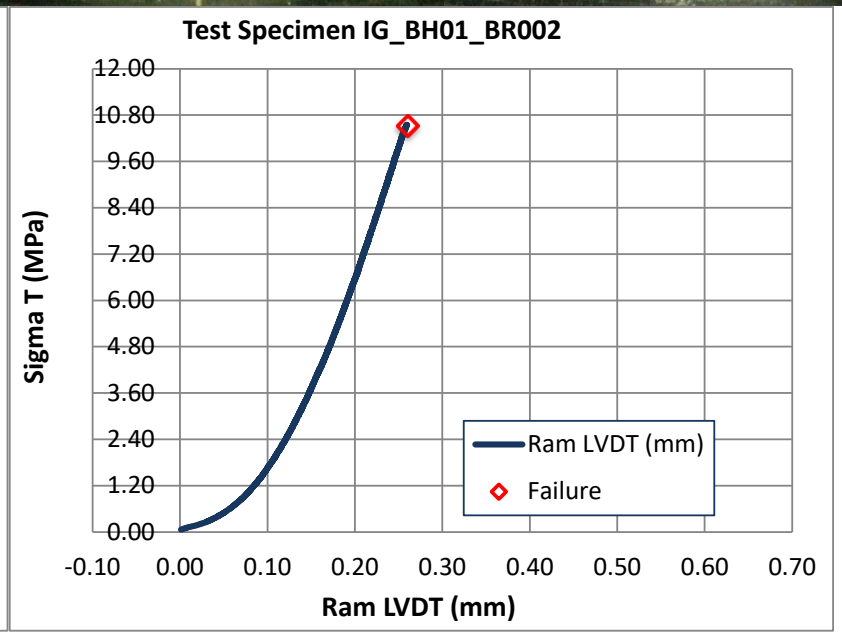


Test Specimen IG_BH01_BR001 – Depth = 408.61 m: Intact and broken specimen photographs; load-time and stress-displacement curves



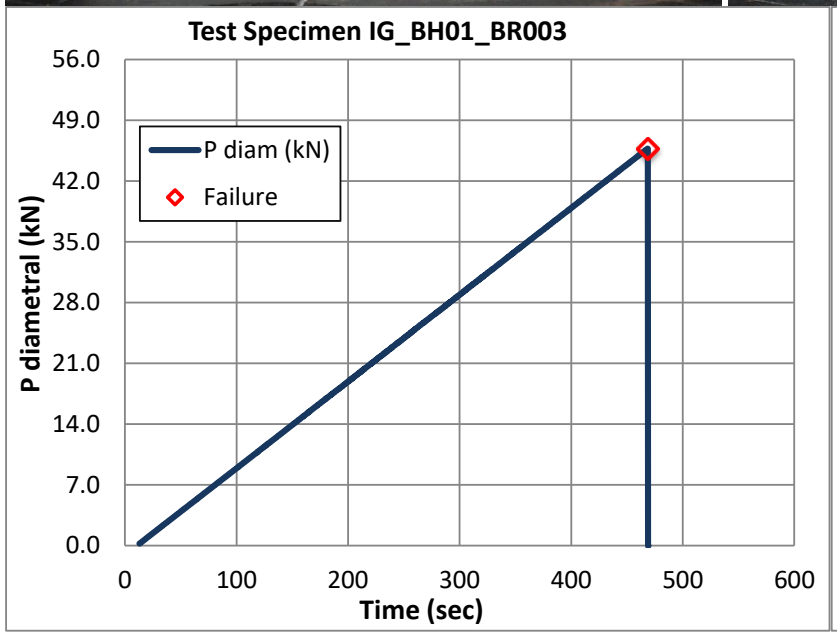


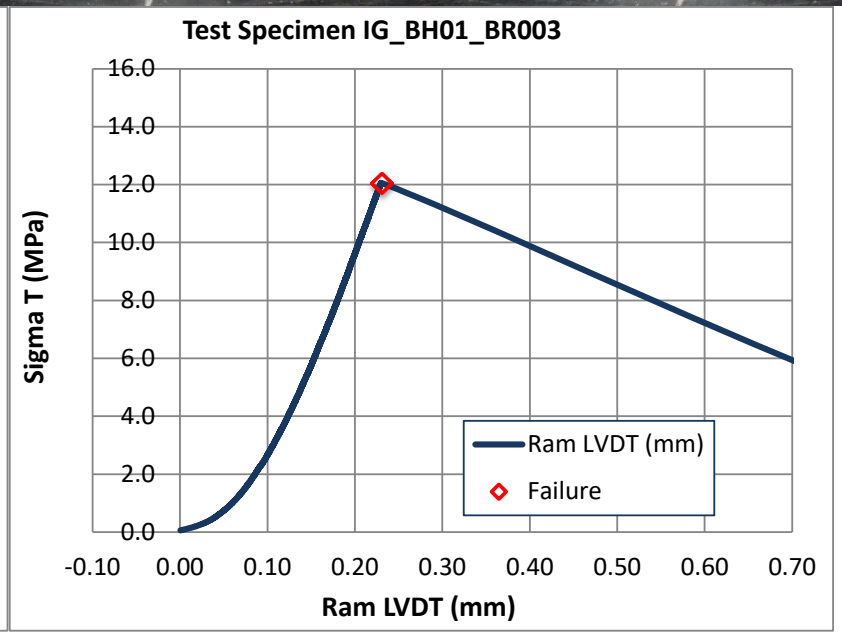




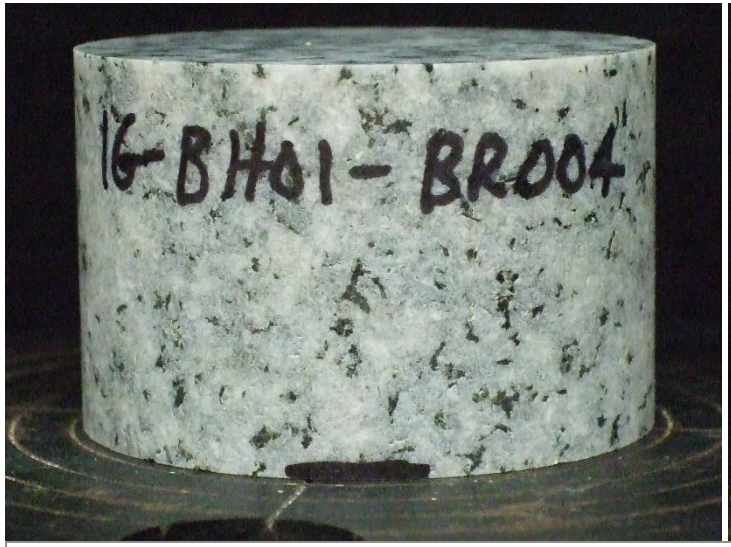
Test Specimen IG_BH01_BR002 – Depth = 442.26 m: Intact and broken specimen photographs; load-time and stress-displacement curves

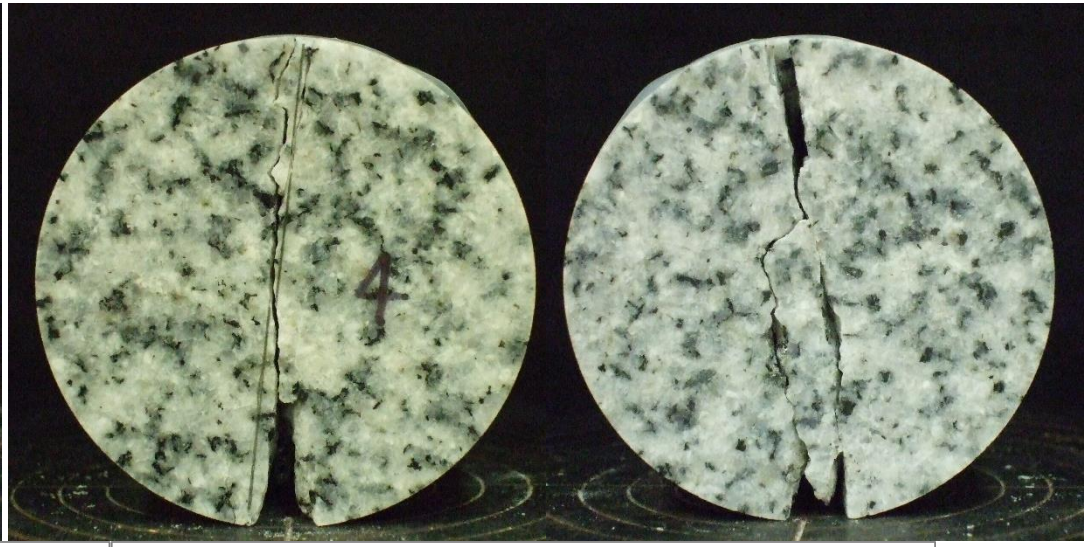


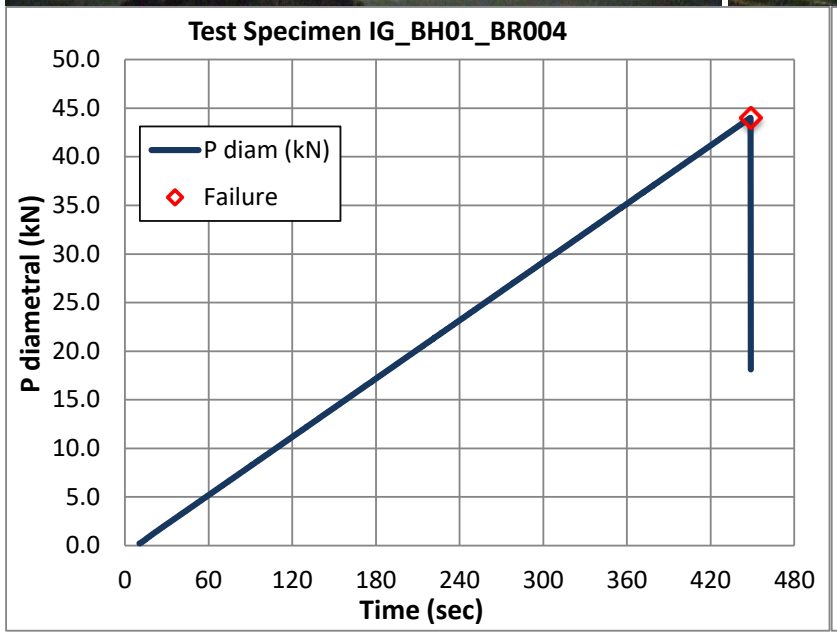


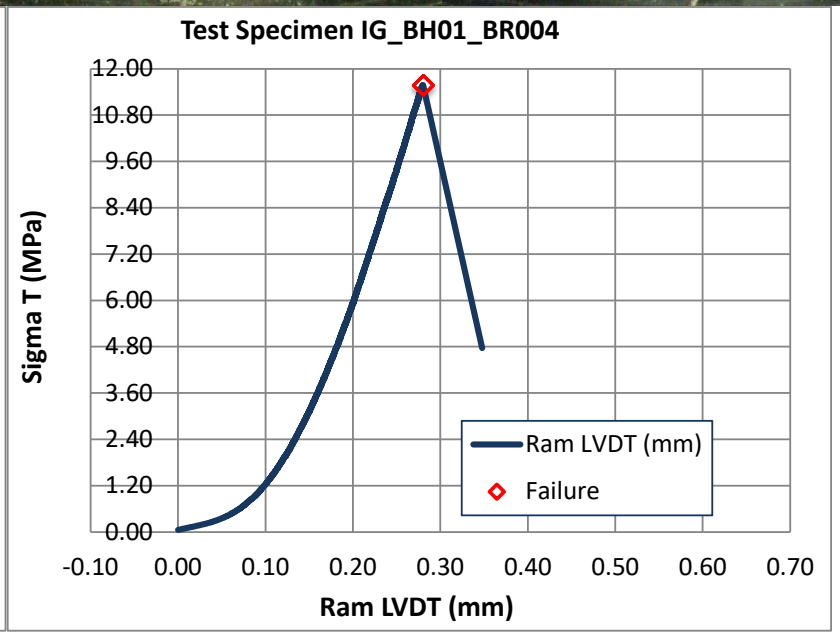


Test Specimen IG_BH01_BR003 – Depth = 468.23 m: Intact and broken specimen photographs; load-time and stress-displacement curves

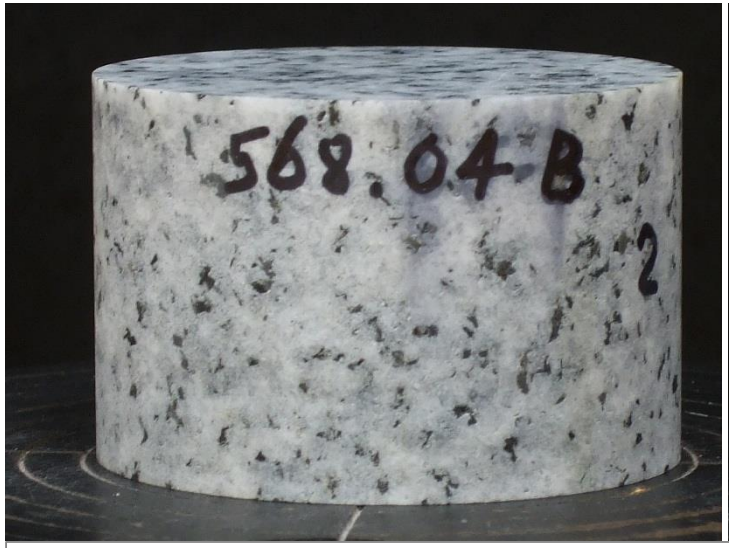




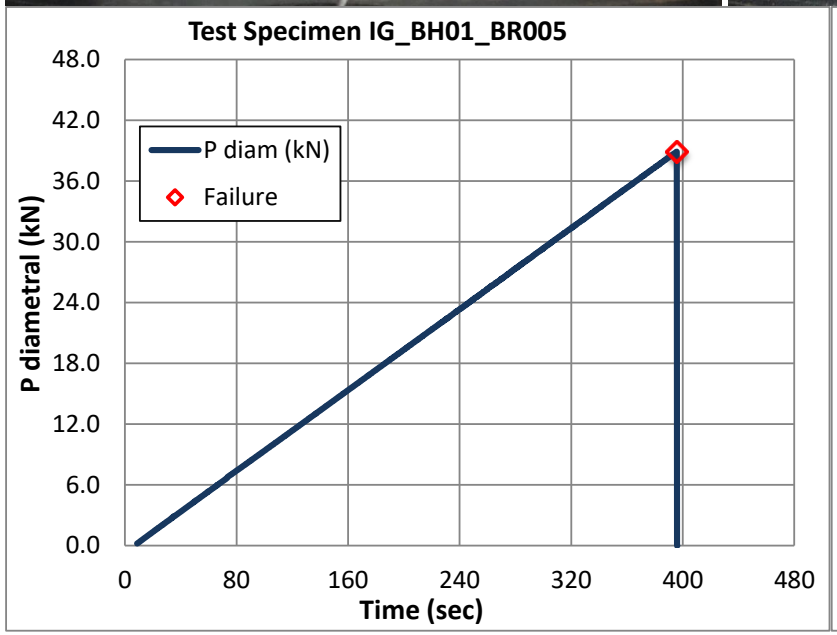


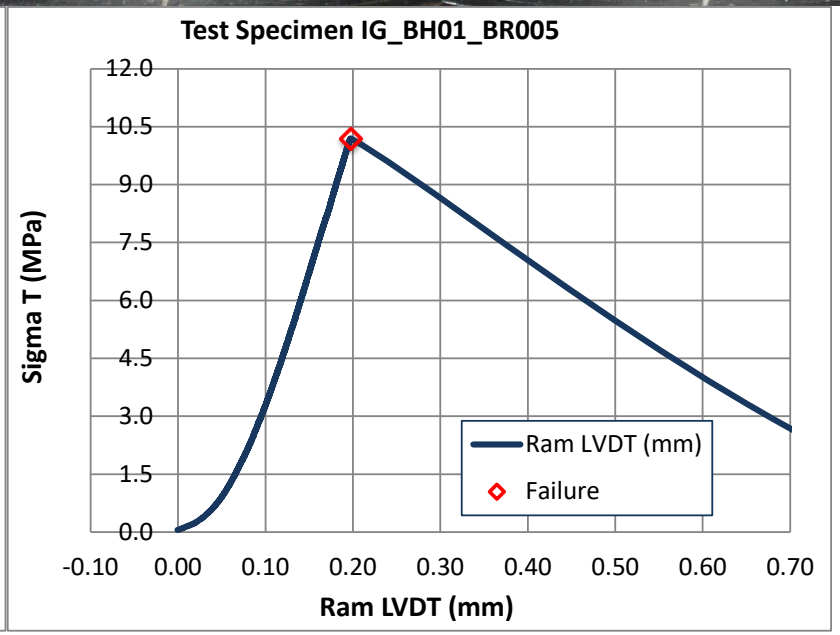


Test Specimen IG_BH01_BR004 – Depth = 522.90 m: Intact and broken specimen photographs; load-time and stress-displacement curves

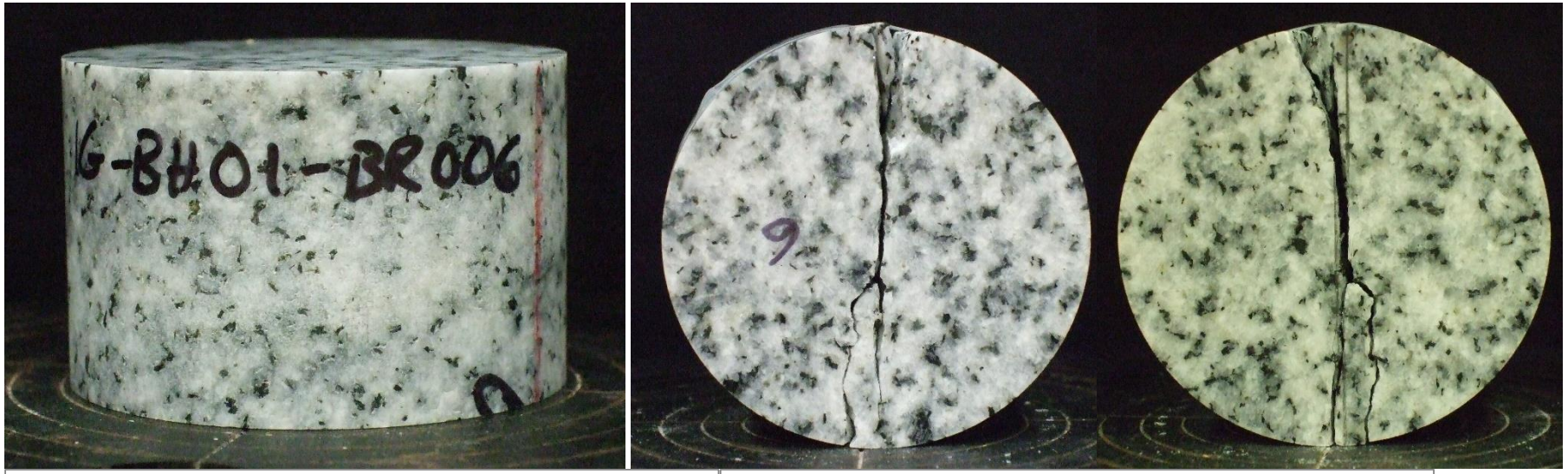


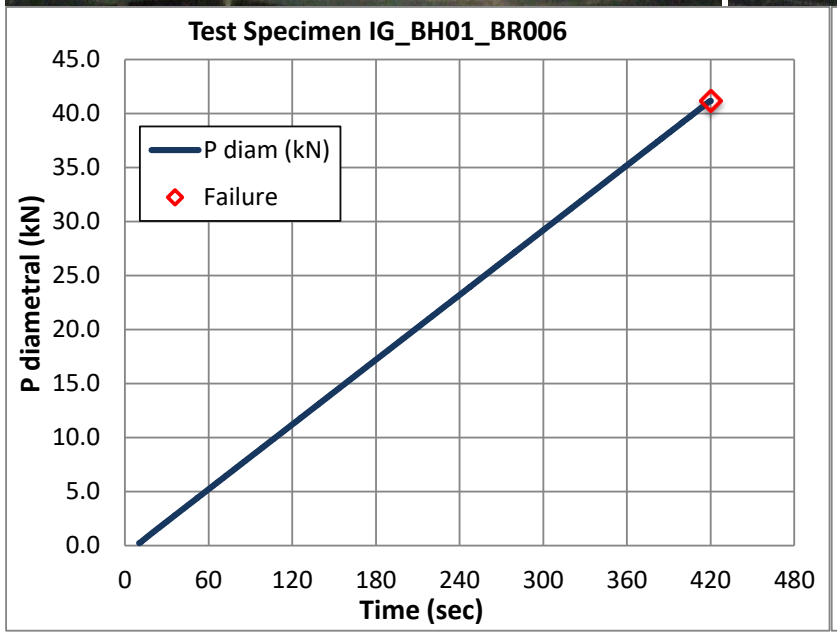


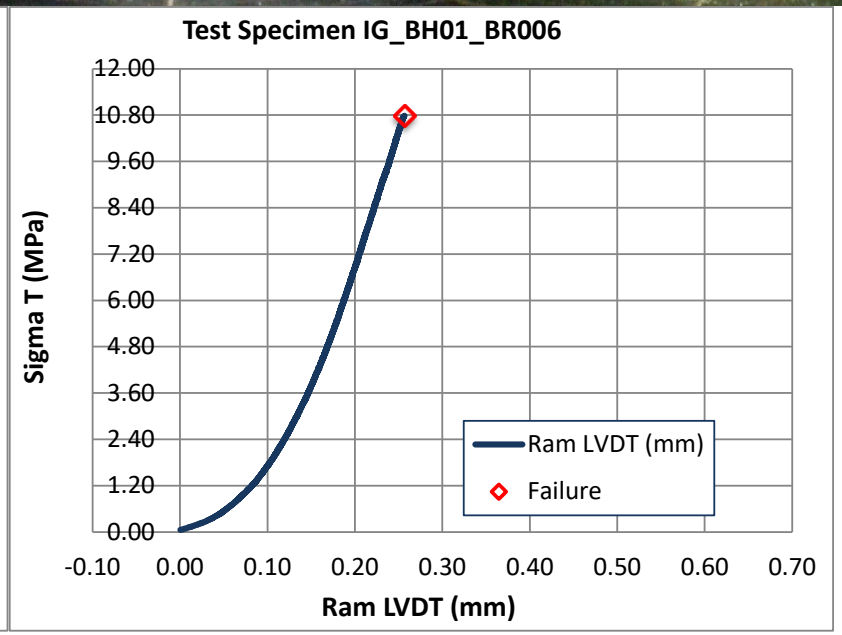




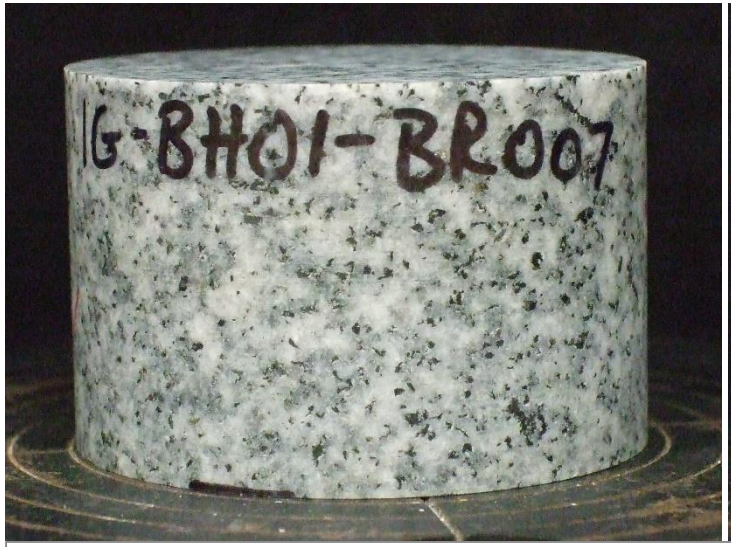
Test Specimen IG_BH01_BR005 – Depth = 568.04 m: Intact and broken specimen photographs; load-time and stress-displacement curves



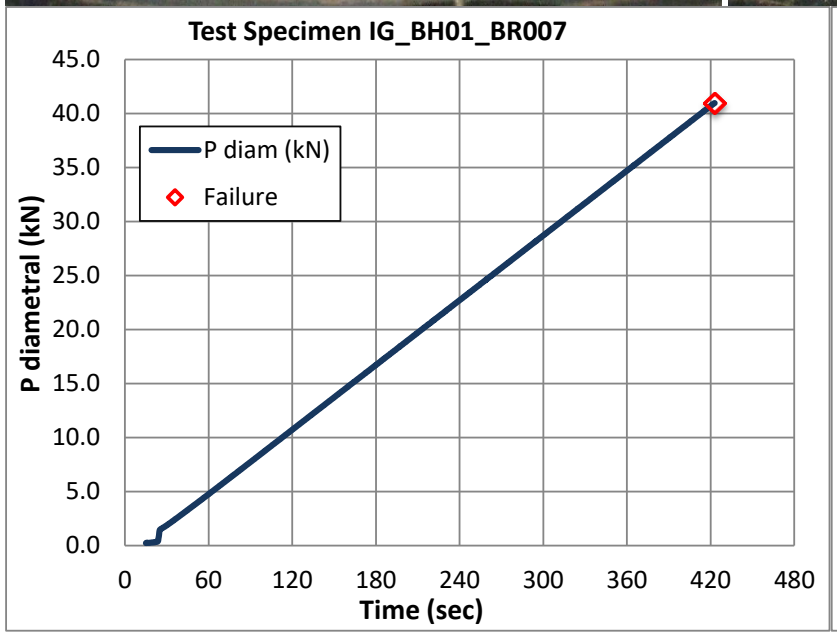


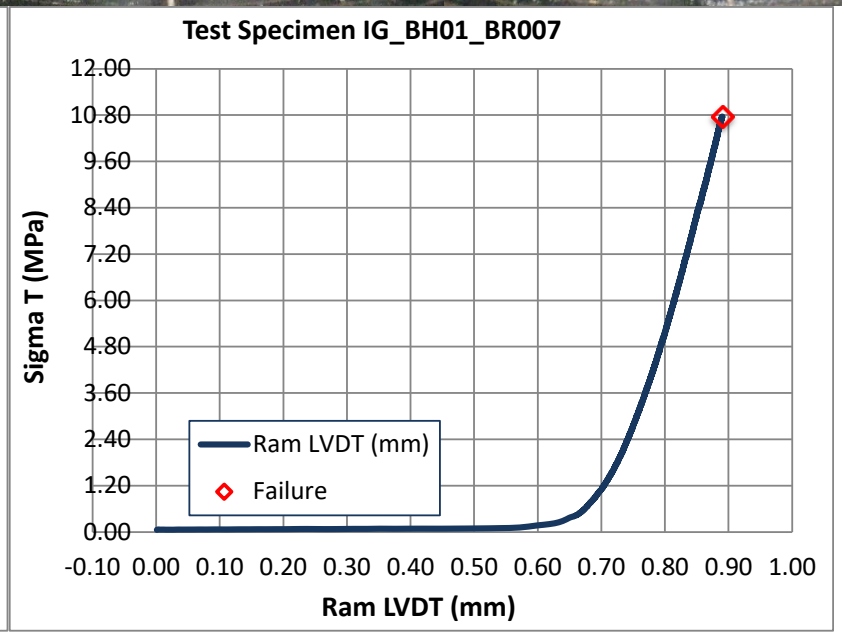


Test Specimen IG_BH01_BR006 – Depth = 601.00 m: Intact and broken specimen photographs; load-time and stress-displacement curves

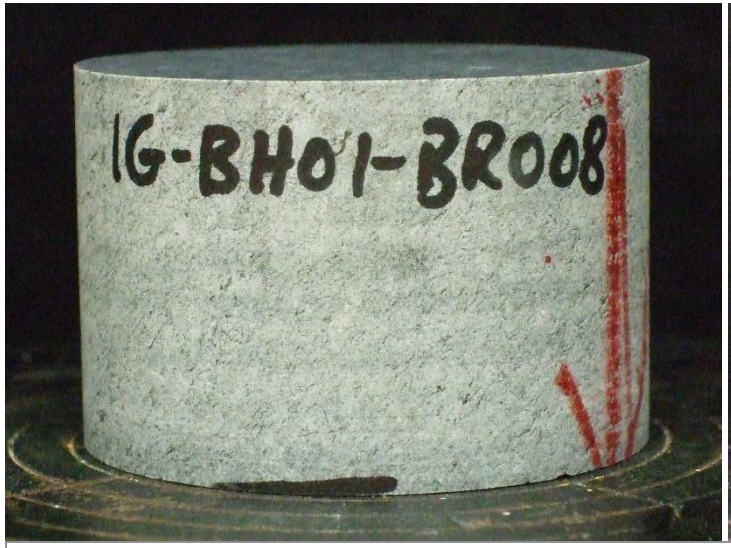


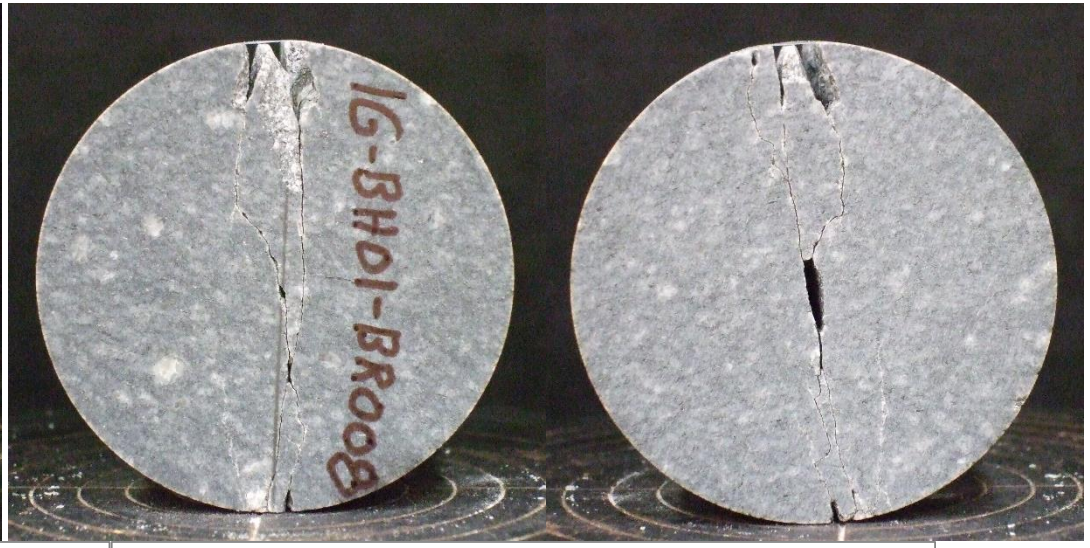


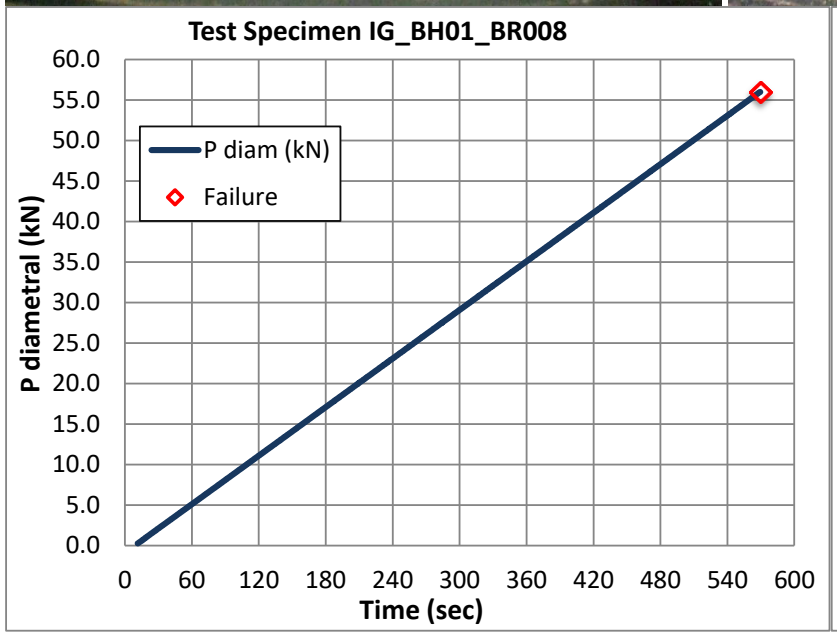


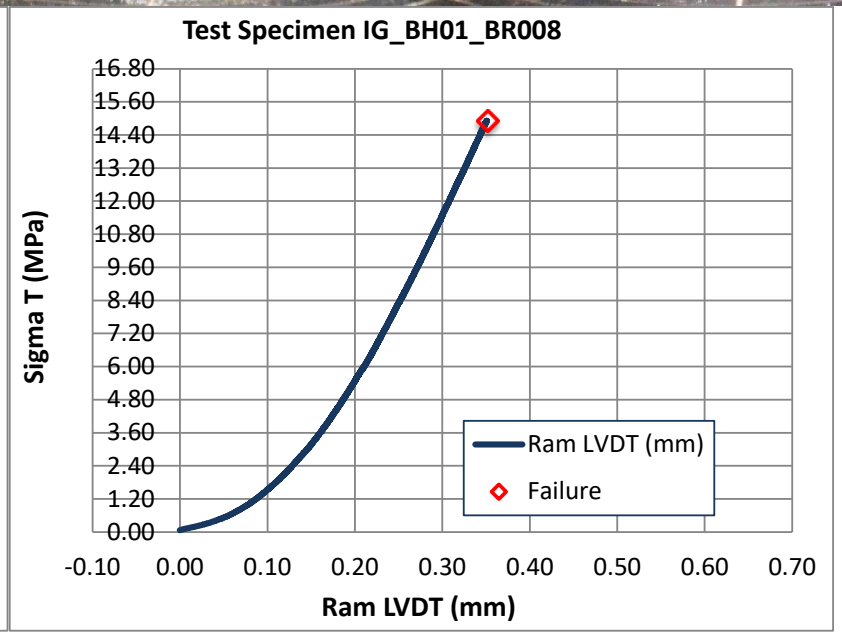


Test Specimen IG_BH01_BR007 – Depth = 451.06 m: Intact and broken specimen photographs; load-time and stress-displacement curves

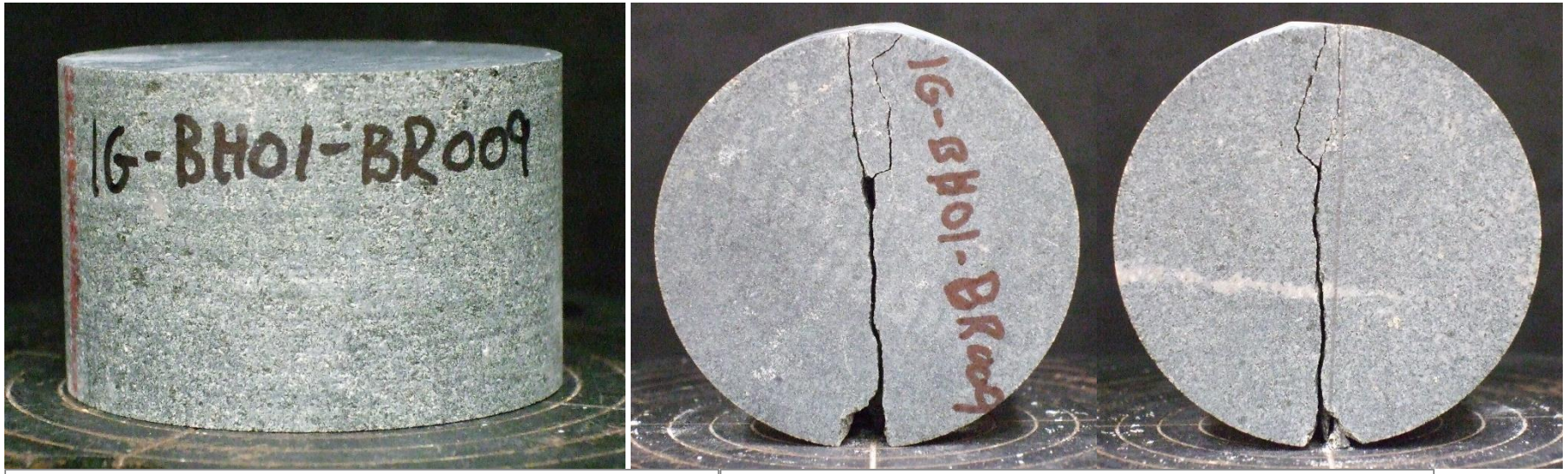


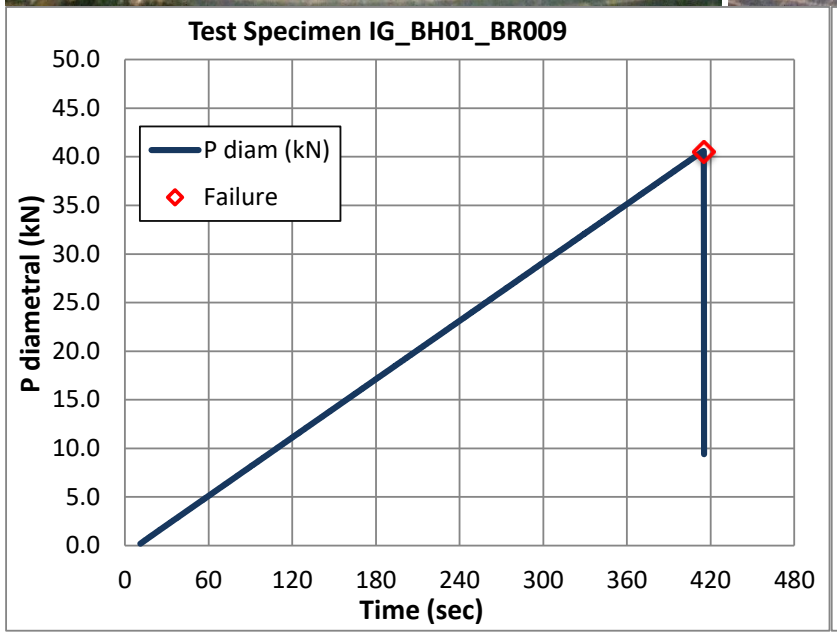


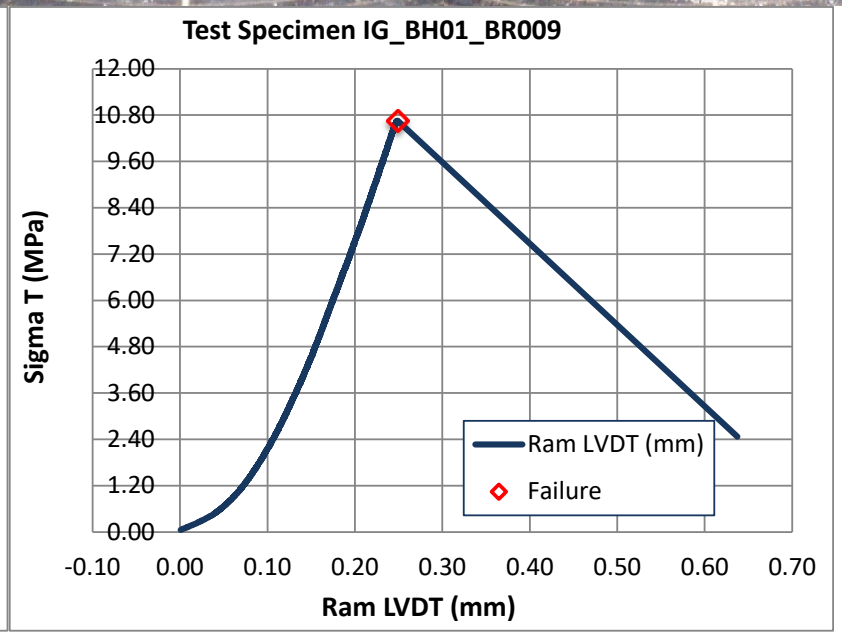




Test Specimen IG_BH01_BR008 – Depth = 560.11 m: Intact and broken specimen photographs; load-time and stress-displacement curves

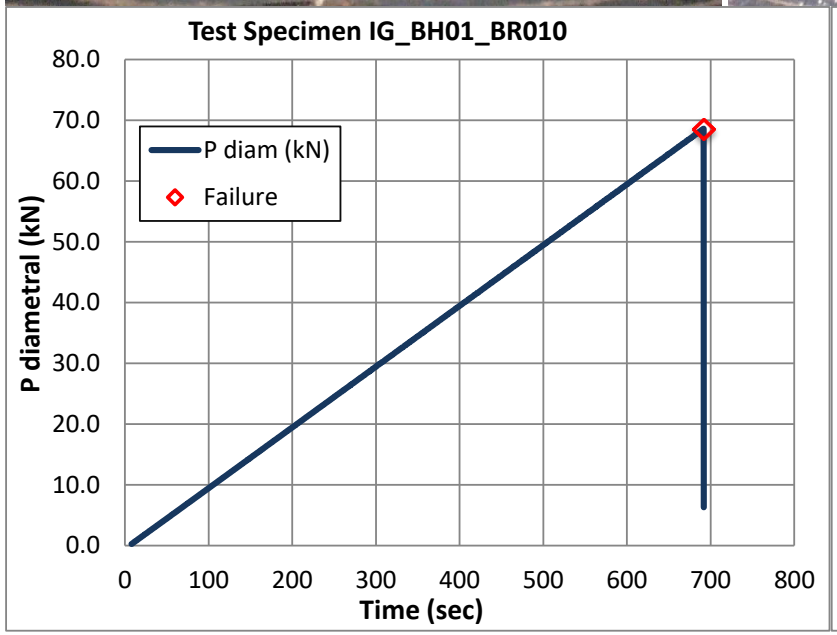


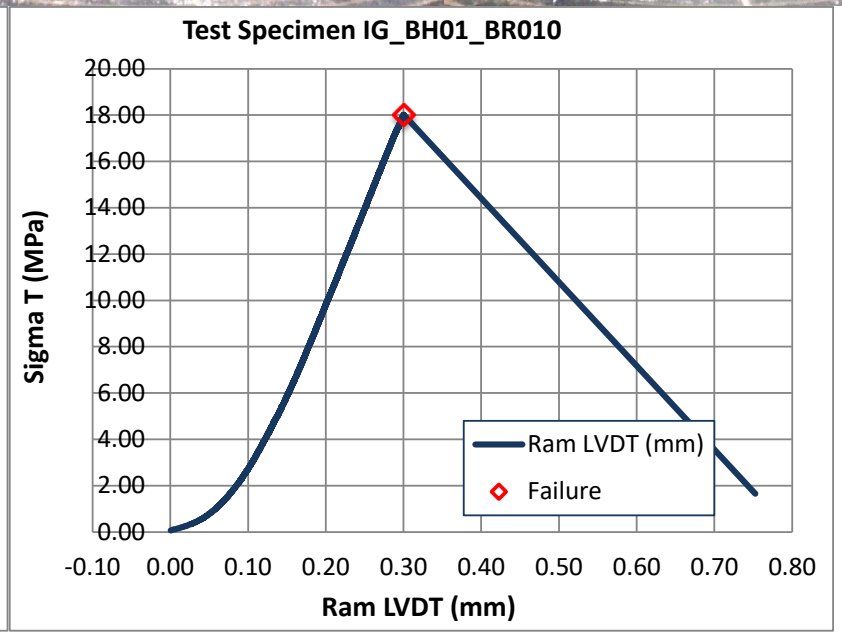




Test Specimen IG_BH01_BR009 – Depth = 655.46 m: Intact and broken specimen photographs; load-time and stress-displacement curves







Test Specimen IG_BH01_BR010 – Depth = 658.55 m: Intact and broken specimen photographs; load-time and stress-displacement curves

APPENDIX D

Thermal Conductivity, Volumetric Heat Capacity and Thermal Diffusion Tests: Test Data and Graphs

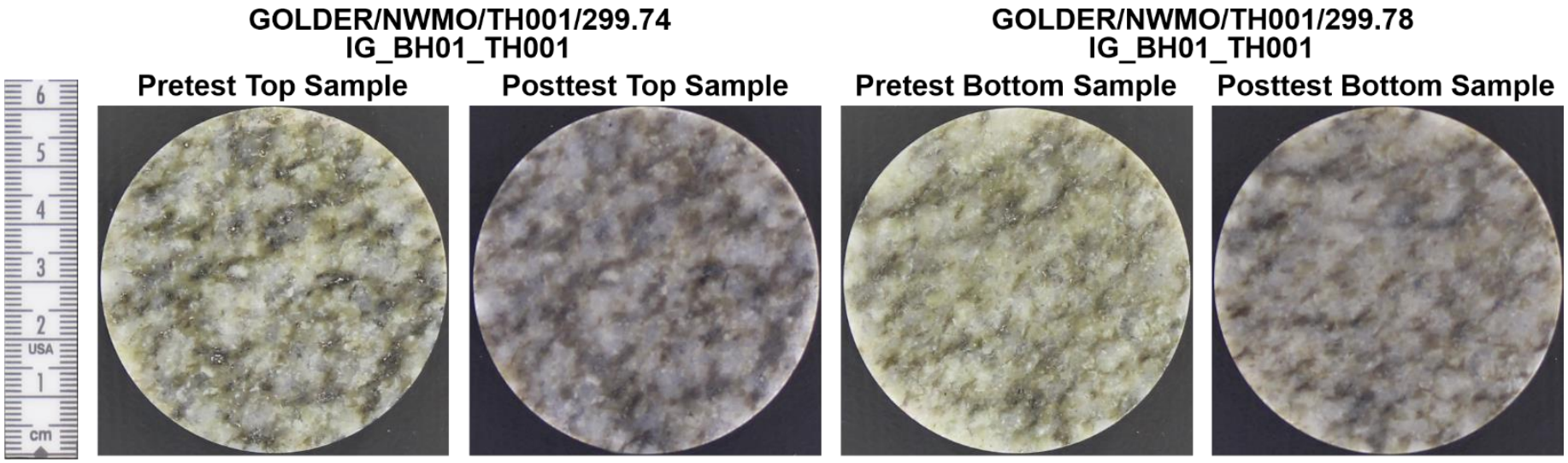
Table D-1: List of hot disk (volumetric heat capacity, thermal conductivity and thermal diffusivity) test specimens

Specimen No.	Depth (m)[1]	Rock Type	Page
IG_BH01_TH001[2]	299.74	Biotite Granodiorite-Tonalite	D-2
IG_BH01_TH002[2]	-	Biotite Granodiorite-Tonalite	Broken in transit
IG_BH01_TH003[2]	352.98	Biotite Granodiorite-Tonalite	D-4
IG_BH01_TH004[2]	401.71	Aplite Dyke	D-6
IG_BH01_TH005[2]	421.80	Biotite Granodiorite-Tonalite	D-8
IG_BH01_TH006[2]	448.64	Biotite Tonalite	D-10
IG_BH01_TH007[2]	450.50	Biotite Tonalite	D-12
IG_BH01_TH008[2]	456.86	Biotite Granodiorite-Tonalite	D-14
IG_BH01_TH009[2]	501.76	Biotite Granodiorite-Tonalite	D-16
IG_BH01_TH010[2]	530.30	Biotite Granodiorite-Tonalite	D-18
IG_BH01_TH011[2]	555.97	Biotite Granodiorite-Tonalite	D-20
IG_BH01_TH012[2]	560.36	Feldspar-phyric Tonalite Dyke	D-22
IG_BH01_TH013[2]	603.56	Biotite Granodiorite-Tonalite	D-24
IG_BH01_TH014[2]	657.97	Amphibolite	D-26
IG_BH01_TH017[3]	402.05	Aplite Dyke	D-28
IG_BH01_TH020[3]	451.68	Biotite Tonalite	D-31
IG_BH01_TH021[3]	457.17	Biotite Granodiorite-Tonalite	D-34
IG_BH01_TH024[3]	556.28	Biotite Granodiorite-Tonalite	D-37
IG_BH01_TH025[3]	561.31	Feldspar-phyric Tonalite Dyke	D-40
IG_BH01_TH026[3]	603.95	Biotite Granodiorite-Tonalite	D-43
IG_BH01_TH027[3]	657.67	Amphibolite	D-46

[1] Top depth of prepared sub-sample.

[2] Sample was saturated before testing. Sample was tested to temperatures beyond those specified in the Test Plan.

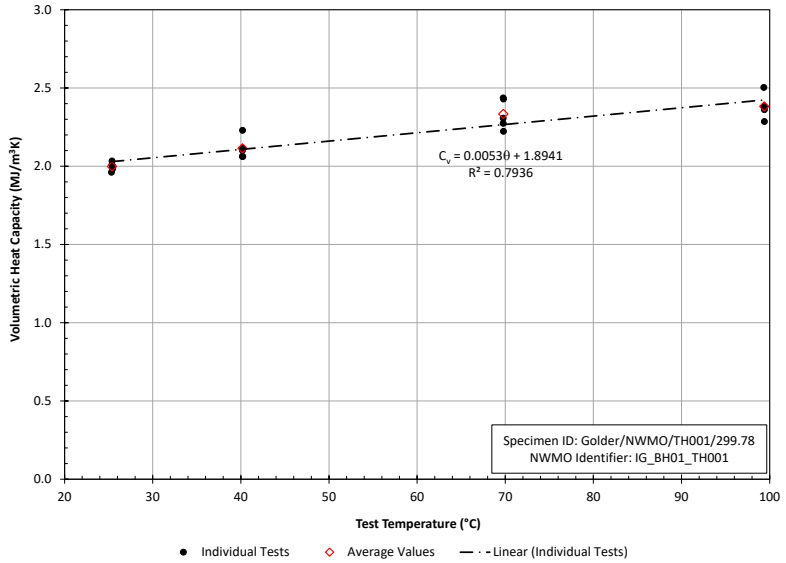
[3] Sample was dried at 80°C before testing.

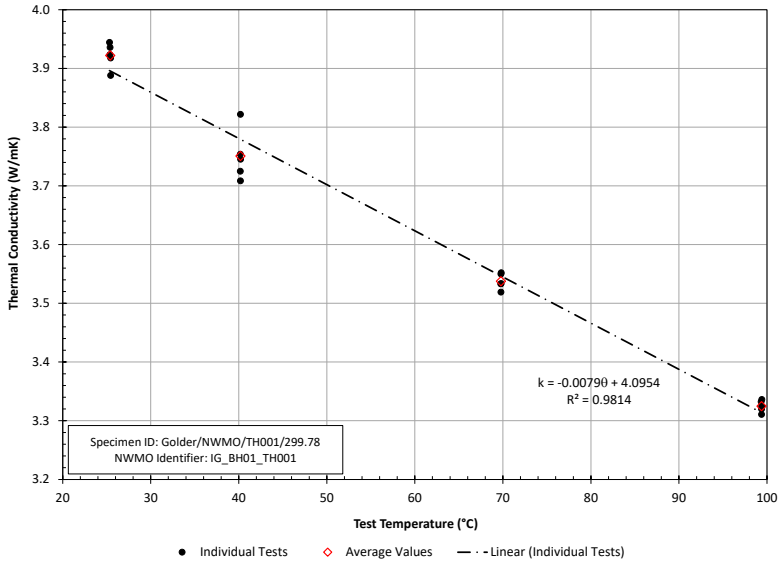


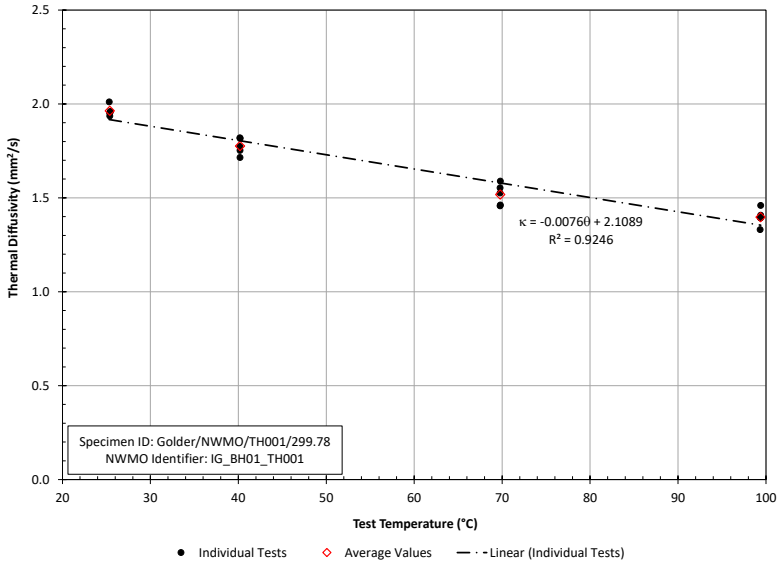
Test Specimen IG_BH01_TH001 – Depth = 299.74 m: specimen photographs

Table D-2: Hot Disk Results – Test Specimen IG_BH01_TH001 – Depth = 299.74 m

Average Temperature (°C)	Average Volumetric Heat Capacity ($MJ/m^3°K$)	Average Thermal Conductivity (W/m°K)	Average Thermal Diffusivity (mm^2/s)
25.39	2.00	3.92	1.96
40.19	2.11	3.75	1.78
69.78	2.33	3.54	1.52
99.38	2.38	3.32	1.40
128.98	2.54	3.15	1.25
158.55	2.64	2.97	1.13
188.16	2.72	2.83	1.04
217.75	2.78	2.71	0.98
247.36	2.88	2.58	0.90
276.9	2.95	2.45	0.83
294.68	2.89	2.39	0.83

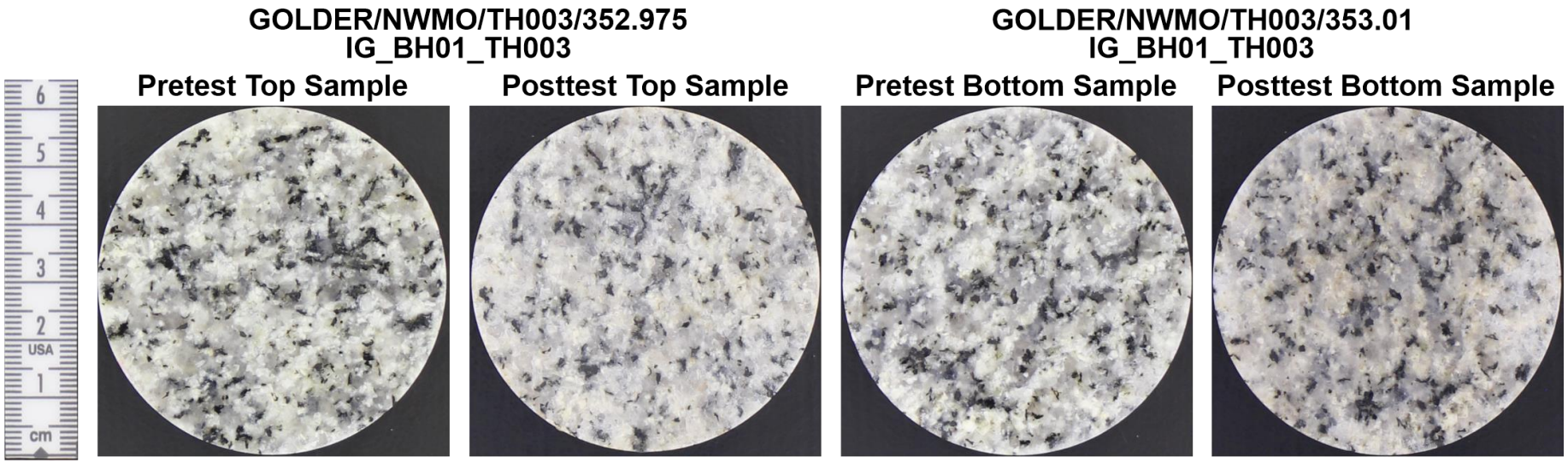






NOTE: Sample depths in the graph legends refer to the depth of the original sample as collected (part of the id), not the depth of the sub-samples

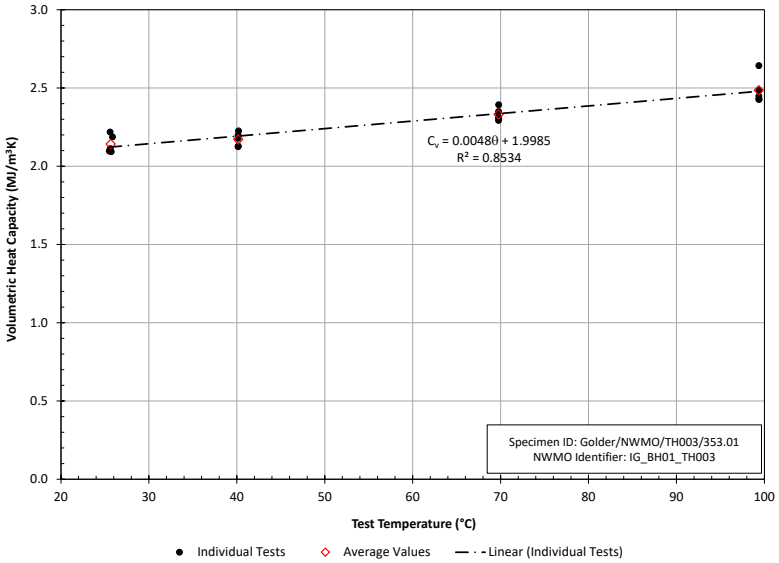
Test Specimen IG_BH01_TH001 – Depth = 299.74 m: Volumetric Heat Capacity, Thermal Conductivity and Thermal Diffusivity

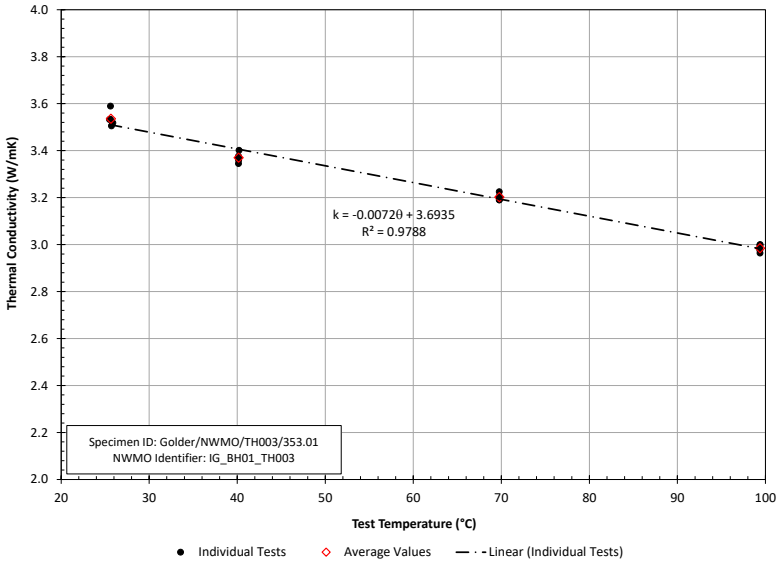


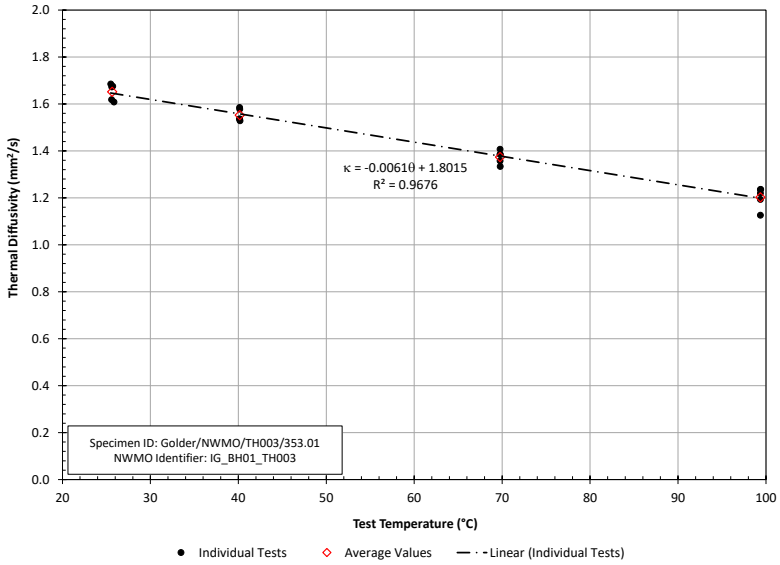
Test Specimen IG_BH01_TH003 – Depth = 352.98 m: specimen photographs

Table D-3: Hot Disk Results – Test Specimen IG_BH01_TH003 – Depth = 352.98 m

Average Temperature (°C)	Average Volumetric Specific Heat (MJ/m^3°K)	Average Thermal Conductivity (W/m°K)	Average Thermal Diffusivity (mm^2/s)
25.66	2.14	3.54	1.65
40.16	2.17	3.37	1.55
69.77	2.33	3.20	1.37
99.37	2.49	2.98	1.20
128.98	2.57	2.86	1.11
158.56	2.73	2.75	1.01
188.16	2.87	2.63	0.92
217.76	2.85	2.57	0.90
247.36	2.88	2.50	0.87
276.91	2.97	2.39	0.80
294.69	2.93	2.35	0.80

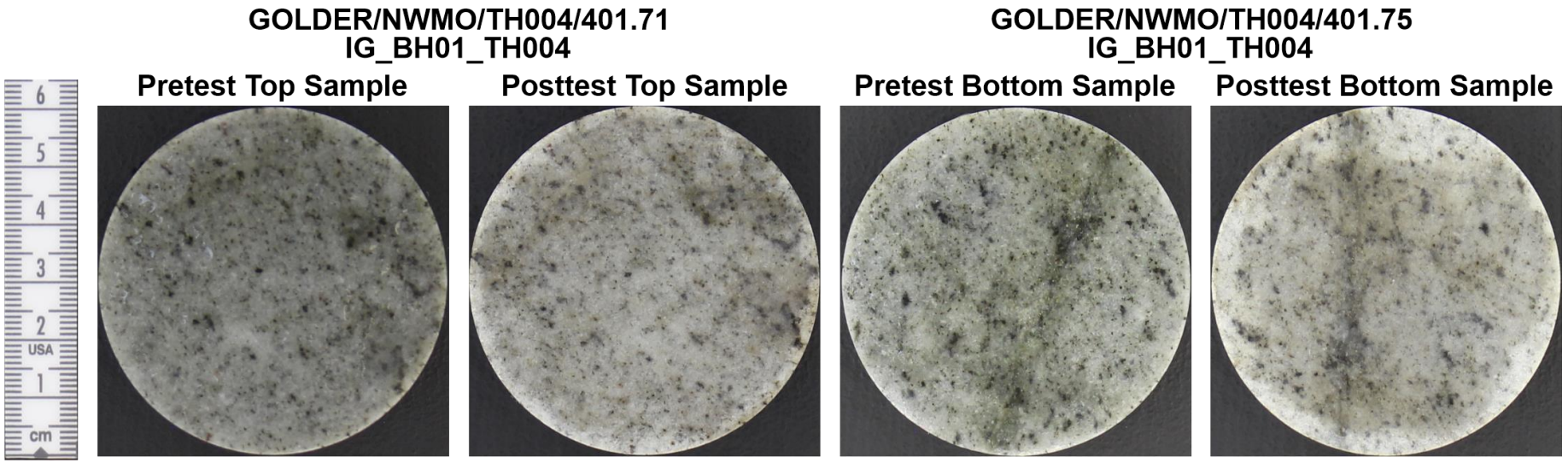






NOTE: Sample depths in the graph legends refer to the depth of the original sample as collected (part of the id), not the depth of the sub-samples

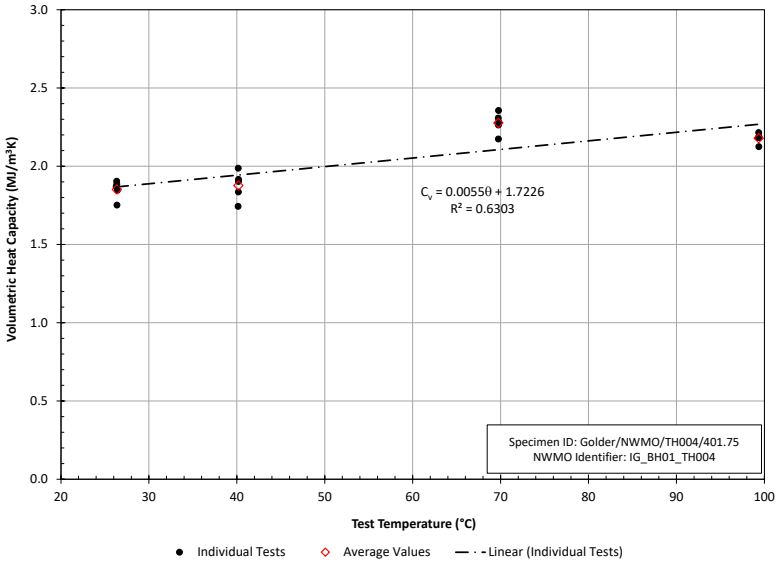
Test Specimen IG_BH01_TH003 – Depth = 352.98 m: Volumetric Heat Capacity, Thermal Conductivity and Thermal Diffusivity

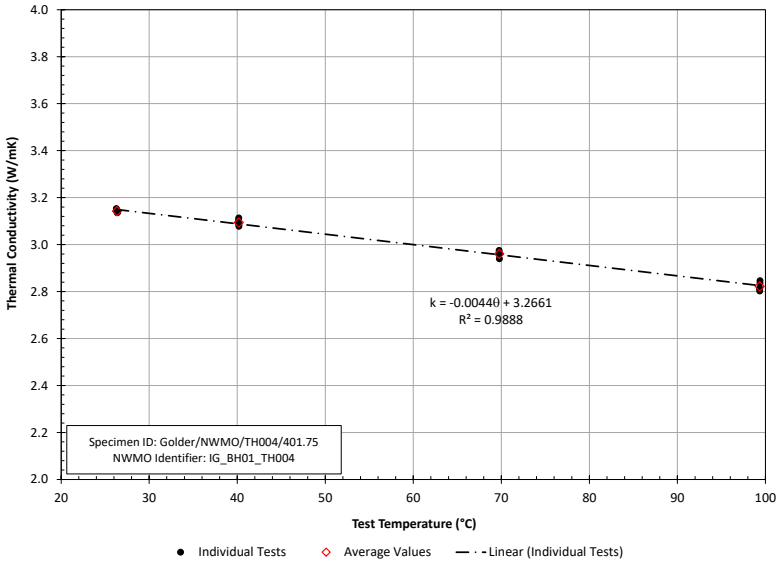


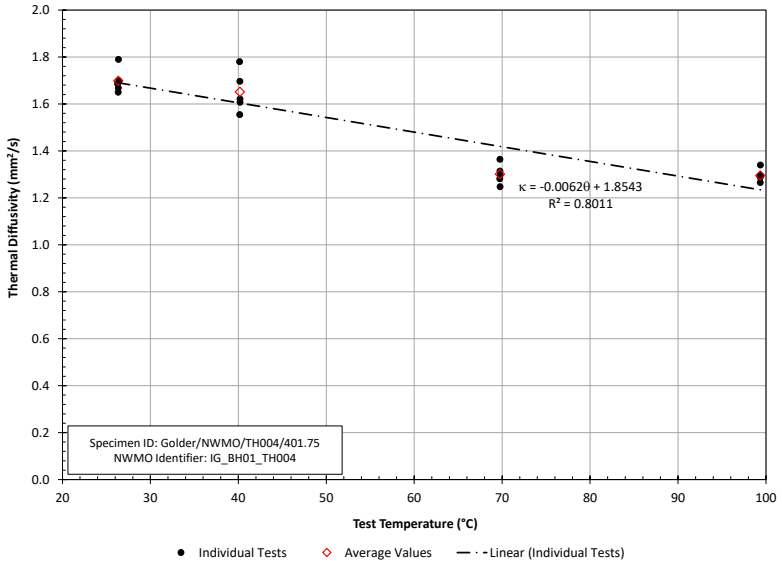
Test Specimen IG_BH01_TH004 – Depth = 401.71 m: specimen photographs

Table D-4: Hot Disk Results – Test Specimen IG_BH01_TH004 – Depth = 401.71 m

Average Temperature (°C)	Average Volumetric Specific Heat (MJ/m^3°K)	Average Thermal Conductivity (W/m°K)	Average Thermal Diffusivity (mm^2/s)
26.35	1.85	3.14	1.70
40.17	1.88	3.09	1.65
69.76	2.28	2.96	1.30
99.36	2.18	2.82	1.30
128.95	2.29	2.71	1.18
158.57	2.39	2.57	1.08
188.16	2.47	2.44	0.99
217.76	2.64	2.31	0.87
247.36	2.65	2.21	0.83
276.97	2.67	2.12	0.79
294.71	2.69	2.02	0.75

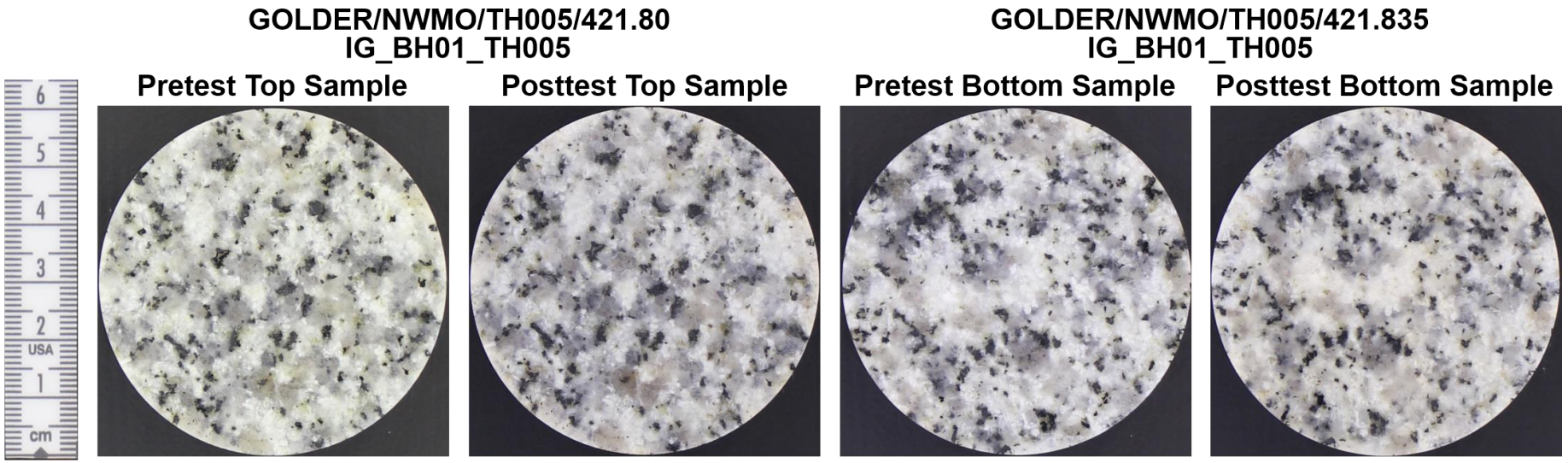






NOTE: Sample depths in the graph legends refer to the depth of the original sample as collected (part of the id), not the depth of the sub-samples

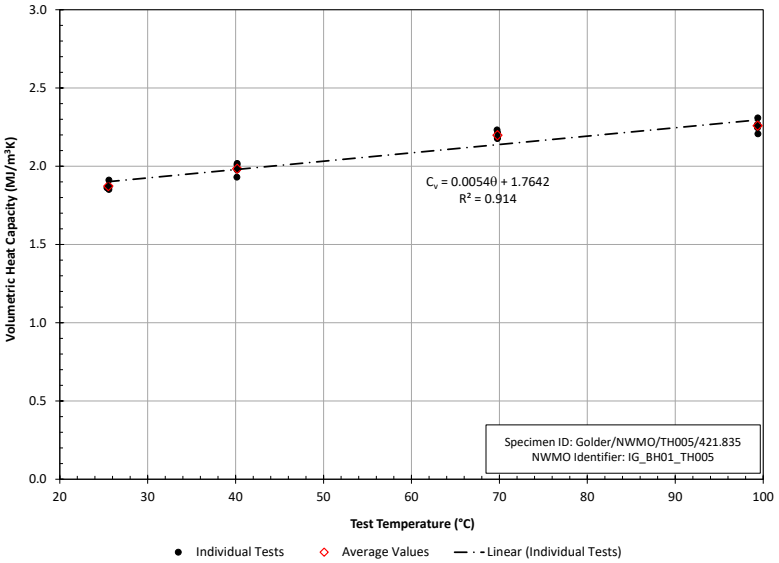
Test Specimen IG_BH01_TH004 – Depth = 401.71 m: Volumetric Heat Capacity, Thermal Conductivity and Thermal Diffusivity

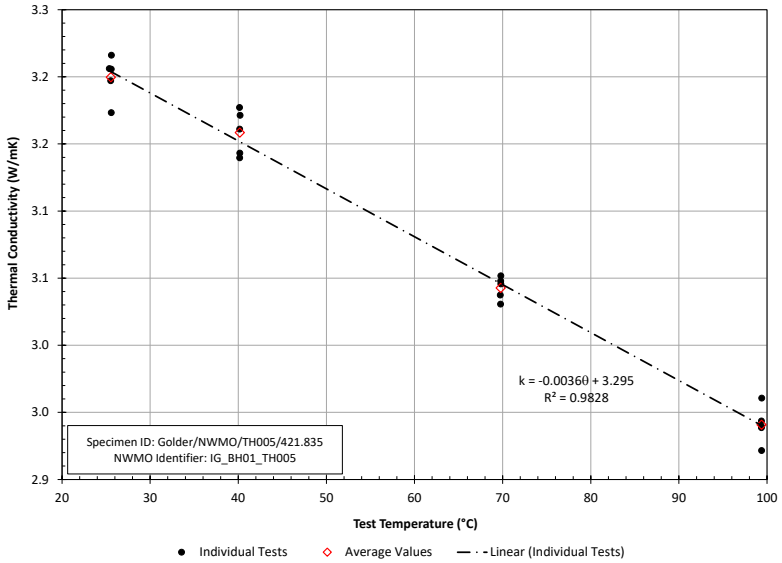


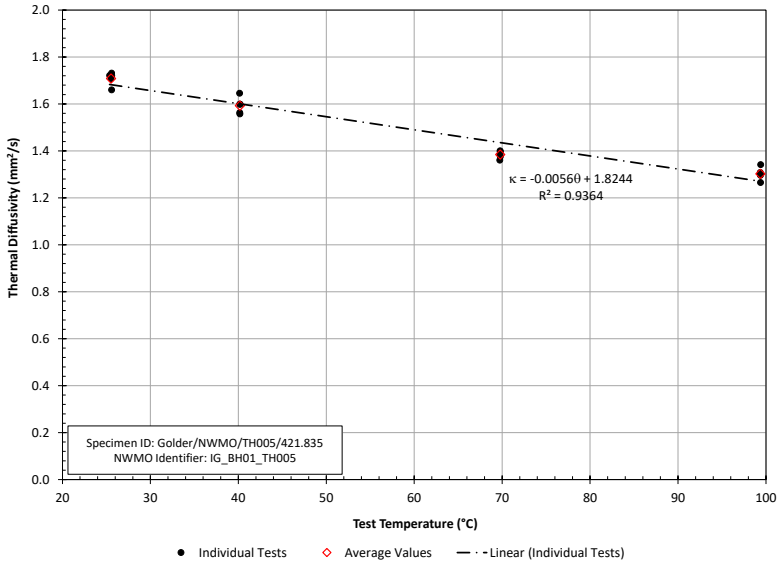
Test Specimen IG_BH01_TH005 – Depth = 421.80 m: specimen photographs

Table D-5: Hot Disk Results – Test Specimen IG_BH01_TH005 – Depth = 421.80 m

Average Temperature (°C)	Average Volumetric Specific Heat (MJ/m^3°K)	Average Thermal Conductivity (W/m°K)	Average Thermal Diffusivity (mm^2/s)
25.53	1.87	3.20	1.71
40.17	1.98	3.16	1.59
69.77	2.20	3.04	1.38
99.37	2.26	2.94	1.30
128.96	2.38	2.85	1.20
158.56	2.53	2.74	1.08
188.17	2.59	2.61	1.01
217.76	2.68	2.51	0.94
247.36	2.74	2.41	0.88
276.94	2.79	2.31	0.83
294.71	2.87	2.22	0.78

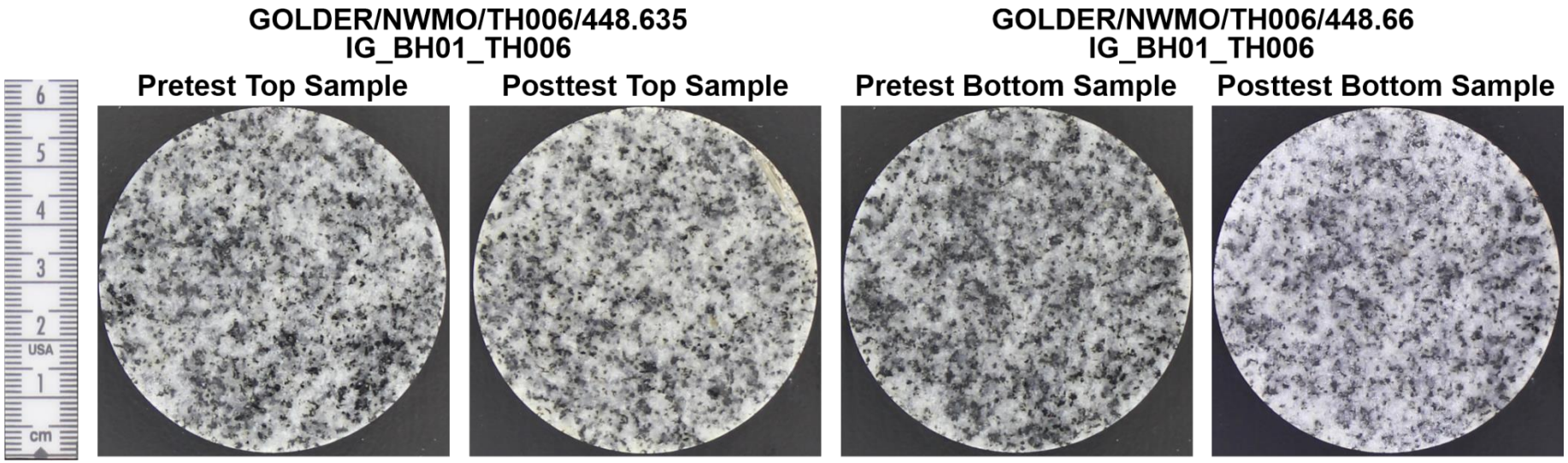






NOTE: Sample depths in the graph legends refer to the depth of the original sample as collected (part of the id), not the depth of the sub-samples

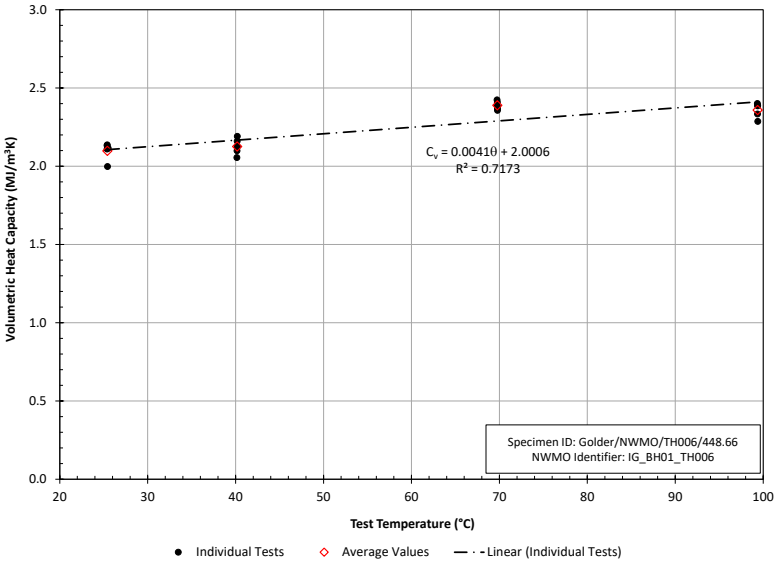
Test Specimen IG_BH01_TH005 – Depth = 421.80 m: Volumetric Heat Capacity, Thermal Conductivity and Thermal Diffusivity

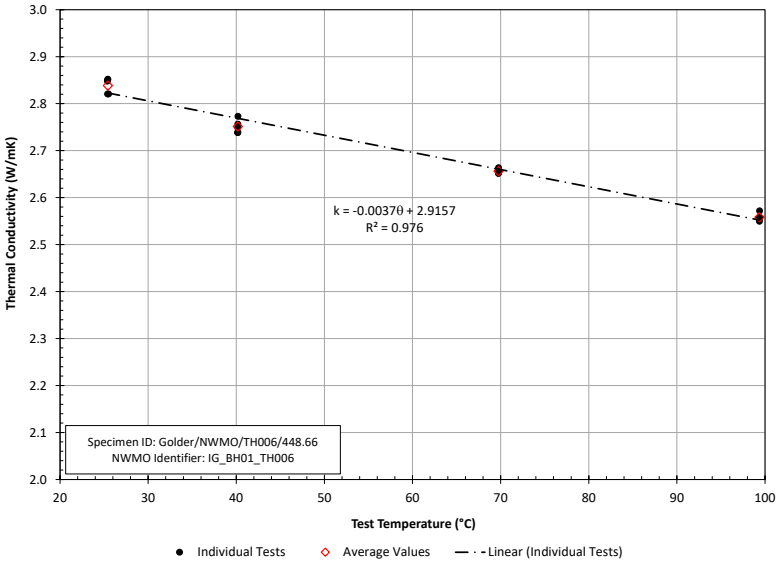


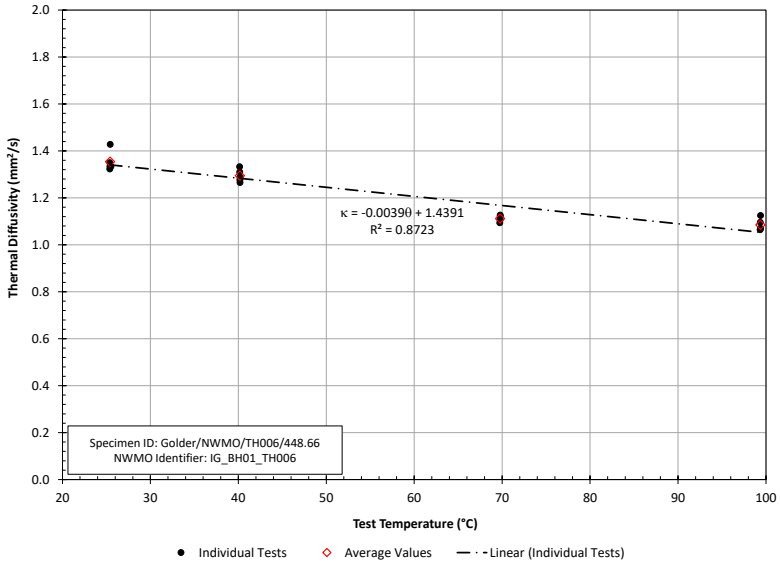
Test Specimen IG_BH01_TH006 – Depth = 448.64 m: specimen photographs

Table D-6: Hot Disk Results – Test Specimen IG_BH01_TH006 – Depth = 448.64 m

Average Temperature (°C)	Average Volumetric Specific Heat (MJ/m^3°K)	Average Thermal Conductivity (W/m°K)	Average Thermal Diffusivity (mm^2/s)
25.42	2.10	2.84	1.35
40.17	2.13	2.75	1.29
69.76	2.39	2.66	1.11
99.36	2.36	2.56	1.08
128.95	2.48	2.49	1.00
158.57	2.59	2.41	0.93
188.17	2.65	2.34	0.88
217.76	2.75	2.27	0.82
247.35	2.84	2.19	0.77
276.96	2.86	2.12	0.74
294.72	2.86	2.07	0.72

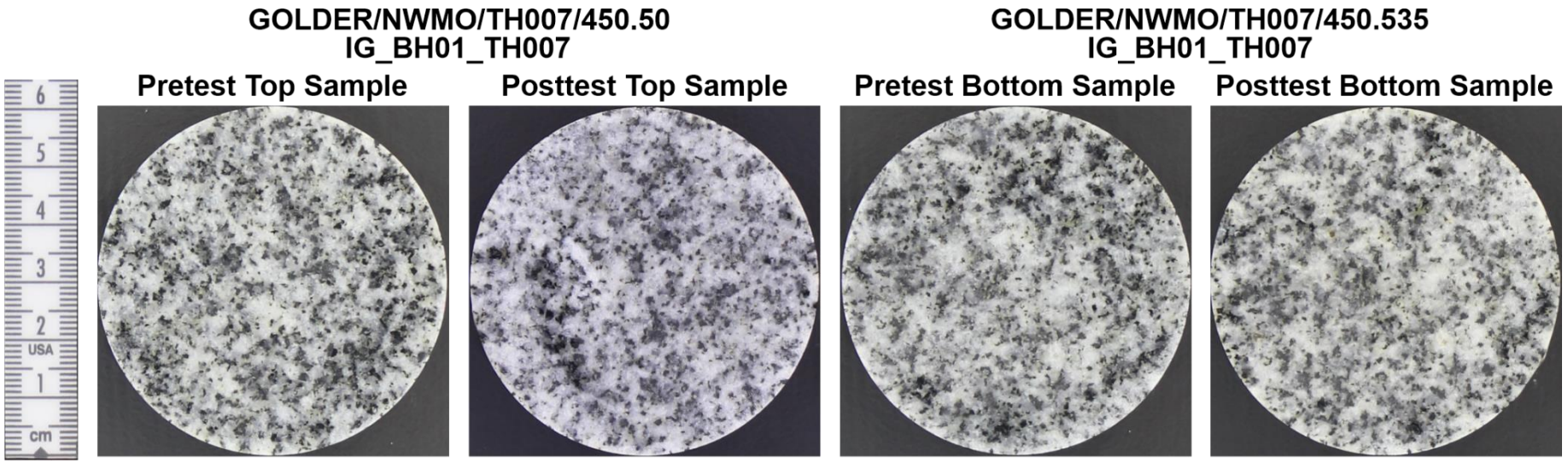






NOTE: Sample depths in the graph legends refer to the depth of the original sample as collected (part of the id), not the depth of the sub-samples

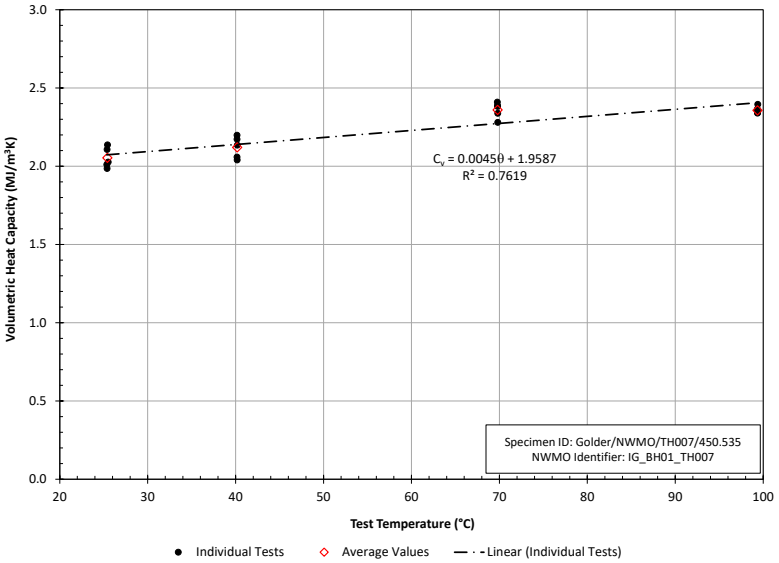
Test Specimen IG_BH01_TH006 – Depth = 448.64 m: Volumetric Heat Capacity, Thermal Conductivity and Thermal Diffusivity

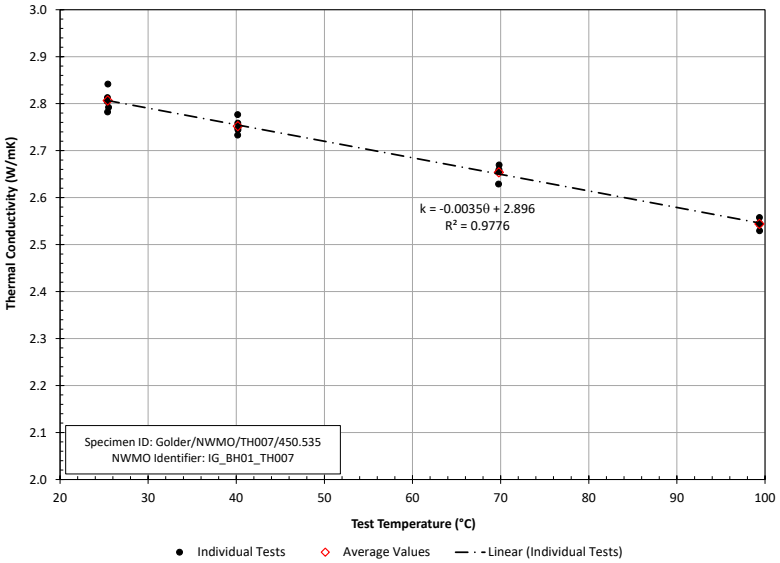


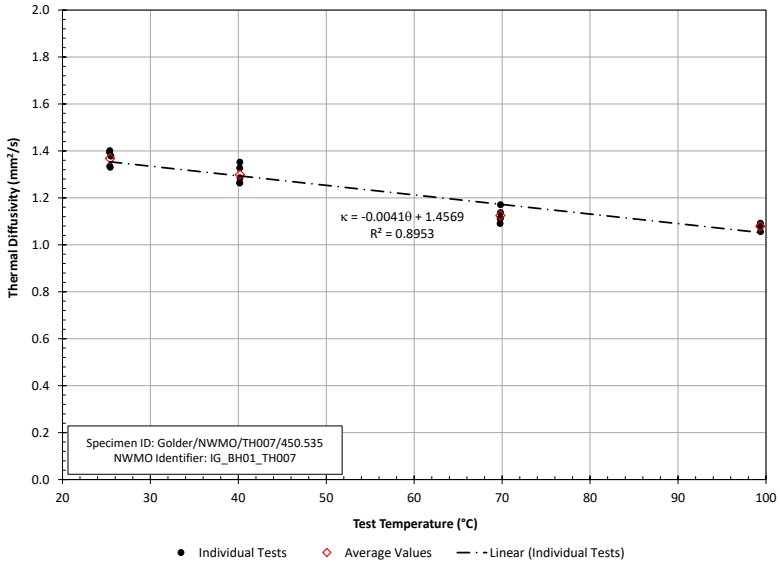
Test Specimen IG_BH01_TH007 – Depth = 450.50 m: specimen photographs

Table D-7: Hot Disk Results – Test Specimen IG_BH01_TH007 – Depth = 450.50 m

Average Temperature (°C)	Average Volumetric Specific Heat (MJ/m^3°K)	Average Thermal Conductivity (W/m°K)	Average Thermal Diffusivity (mm^2/s)
25.41	2.05	2.81	1.37
40.17	2.12	2.75	1.30
69.79	2.36	2.65	1.13
99.36	2.36	2.54	1.08
128.98	2.56	2.47	0.97
158.56	2.62	2.40	0.92
188.16	2.72	2.32	0.85
217.75	2.79	2.26	0.81
247.38	2.77	2.20	0.80
276.99	2.88	2.10	0.73
294.70	2.87	2.06	0.72

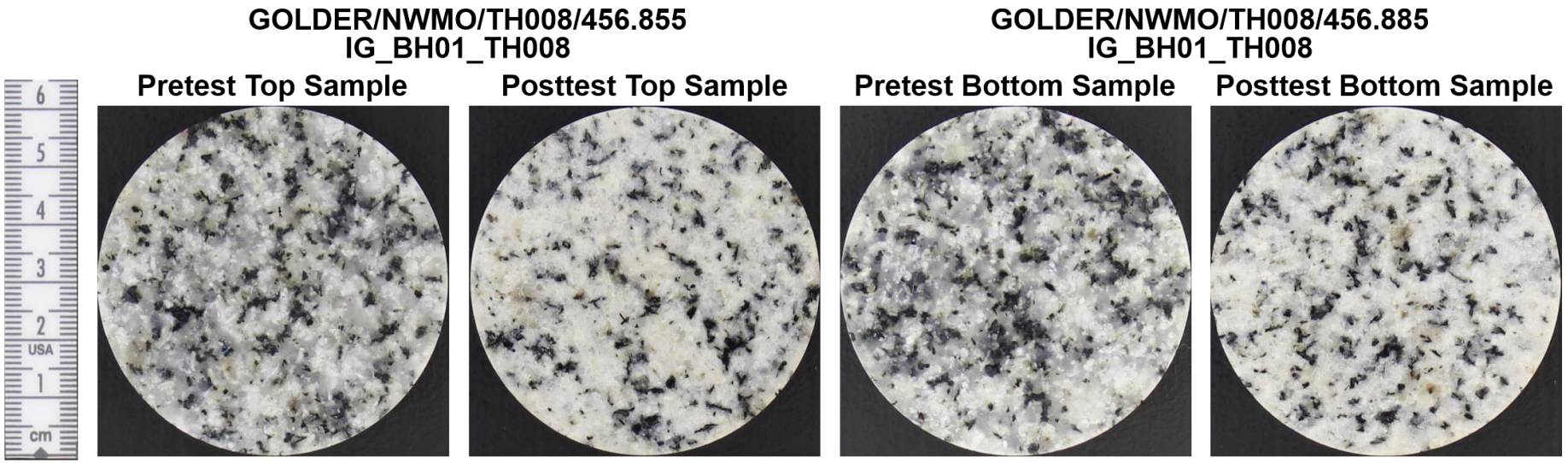






NOTE: Sample depths in the graph legends refer to the depth of the original sample as collected (part of the id), not the depth of the sub-samples

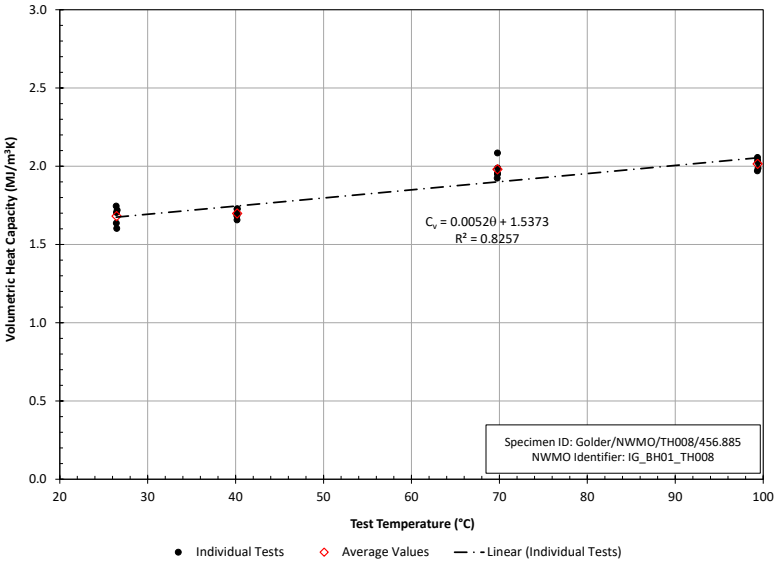
Test Specimen IG_BH01_TH007 – Depth = 450.50 m: Volumetric Heat Capacity, Thermal Conductivity and Thermal Diffusivity

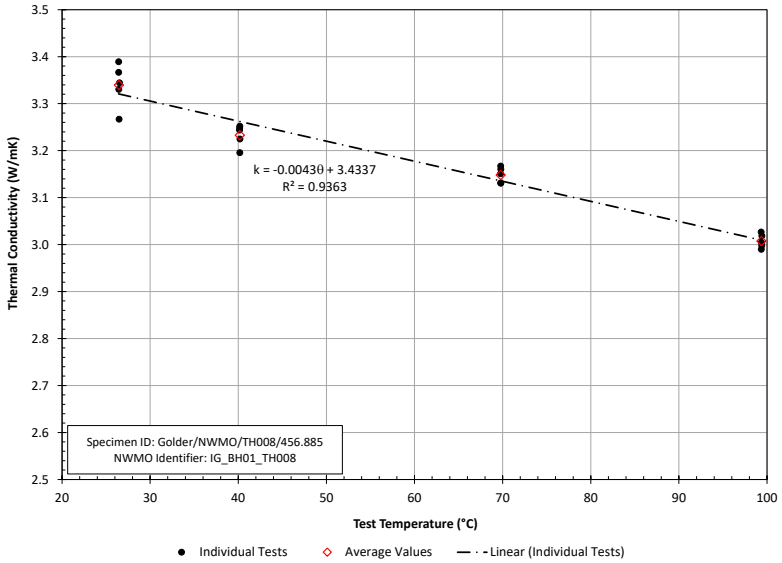


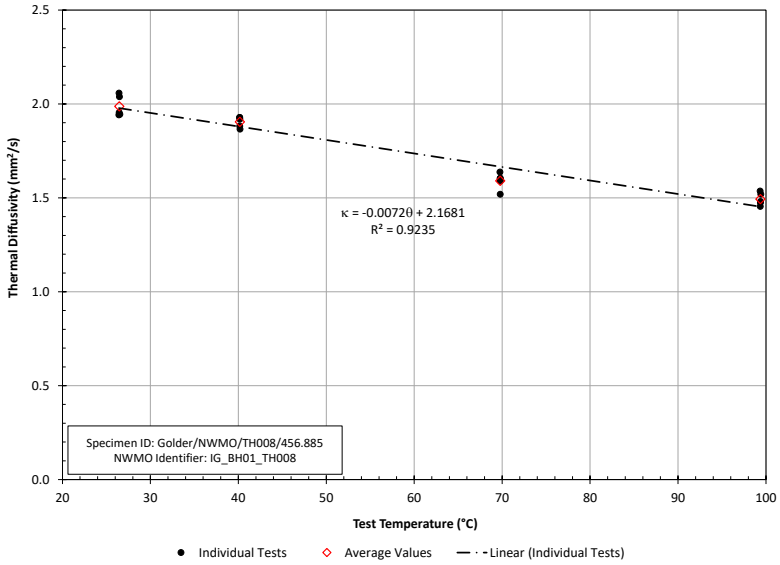
Test Specimen IG_BH01_TH008 – Depth = 456.86 m: specimen photographs

Table D-8: Hot Disk Results – Test Specimen IG_BH01_TH008 – Depth = 456.86 m

Average Temperature (°C)	Average Volumetric Specific Heat (MJ/m^3°K)	Average Thermal Conductivity (W/m°K)	Average Thermal Diffusivity (mm^2/s)
26.46	1.68	3.34	1.99
40.17	1.70	3.23	1.90
69.78	1.98	3.15	1.59
99.37	2.02	3.01	1.49
128.96	2.14	2.88	1.34
158.55	2.26	2.75	1.22
188.18	2.33	2.62	1.13
217.77	2.44	2.53	1.04
247.37	2.49	2.43	0.98
276.97	2.53	2.33	0.92
294.70	2.53	2.24	0.89

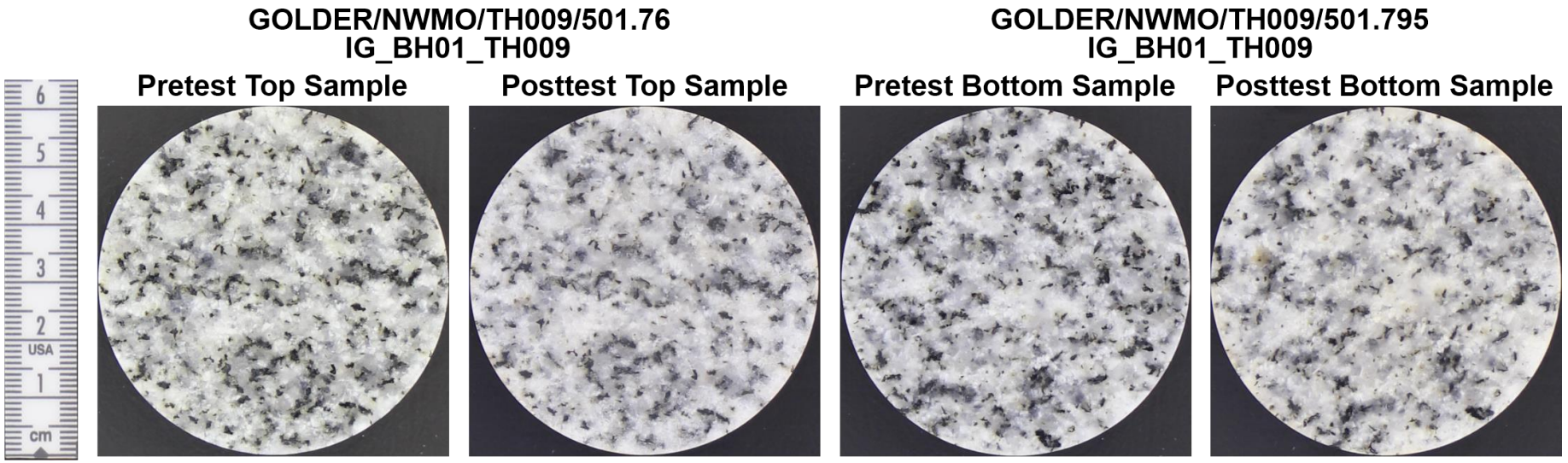






NOTE: Sample depths in the graph legends refer to the depth of the original sample as collected (part of the id), not the depth of the sub-samples

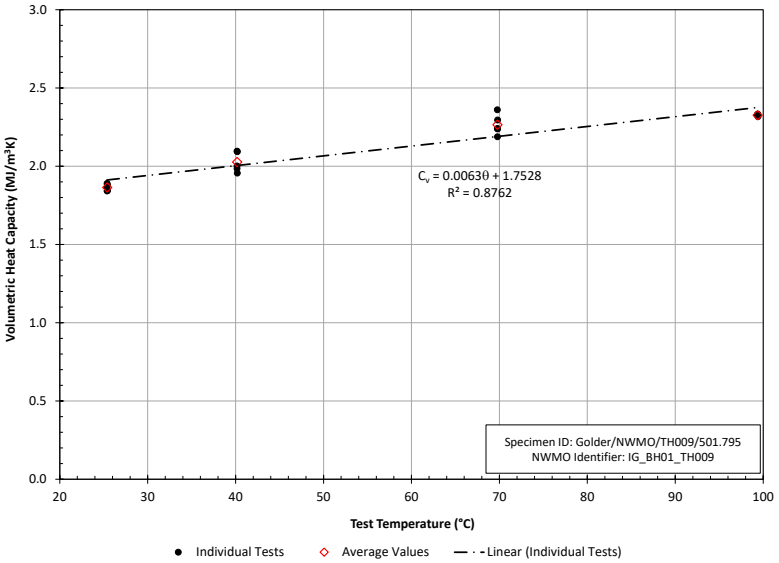
Test Specimen IG_BH01_TH008 – Depth = 456.86 m: Volumetric Heat Capacity, Thermal Conductivity and Thermal Diffusivity

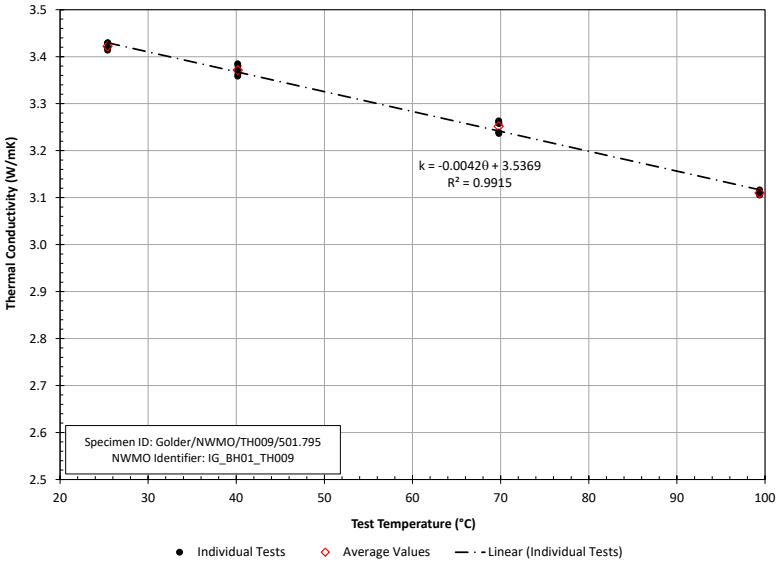


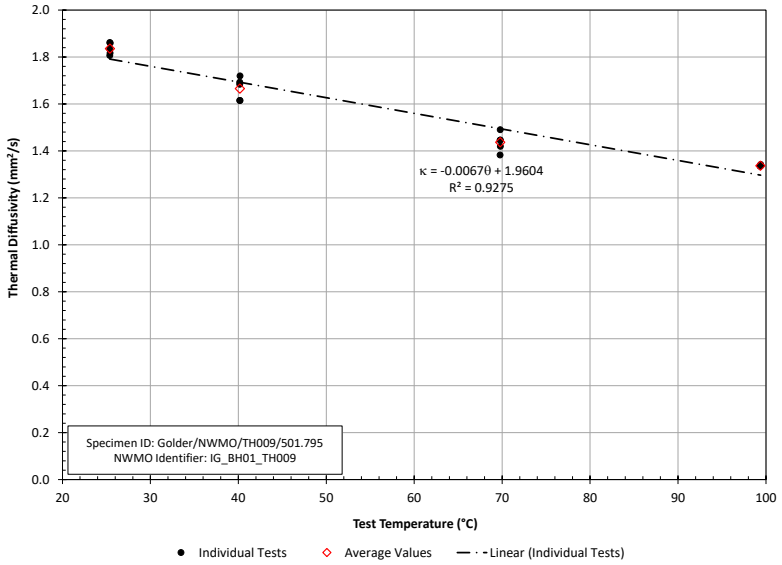
Test Specimen IG_BH01_TH009 – Depth = 501.76 m: specimen photographs

Table D-9: Hot Disk Results – Test Specimen IG_BH01_TH009 – Depth = 501.76 m

Average Temperature (°C)	Average Volumetric Specific Heat (MJ/m^3°K)	Average Thermal Conductivity (W/m°K)	Average Thermal Diffusivity (mm^2/s)
25.40	1.86	3.42	1.84
40.17	2.03	3.37	1.67
69.78	2.26	3.25	1.44
99.37	2.33	3.11	1.34
128.96	2.43	3.00	1.23
158.55	2.56	2.86	1.12
188.17	2.63	2.73	1.04
217.77	2.74	2.62	0.96
247.34	2.81	2.50	0.89
276.97	2.87	2.37	0.83
294.72	2.83	2.32	0.82

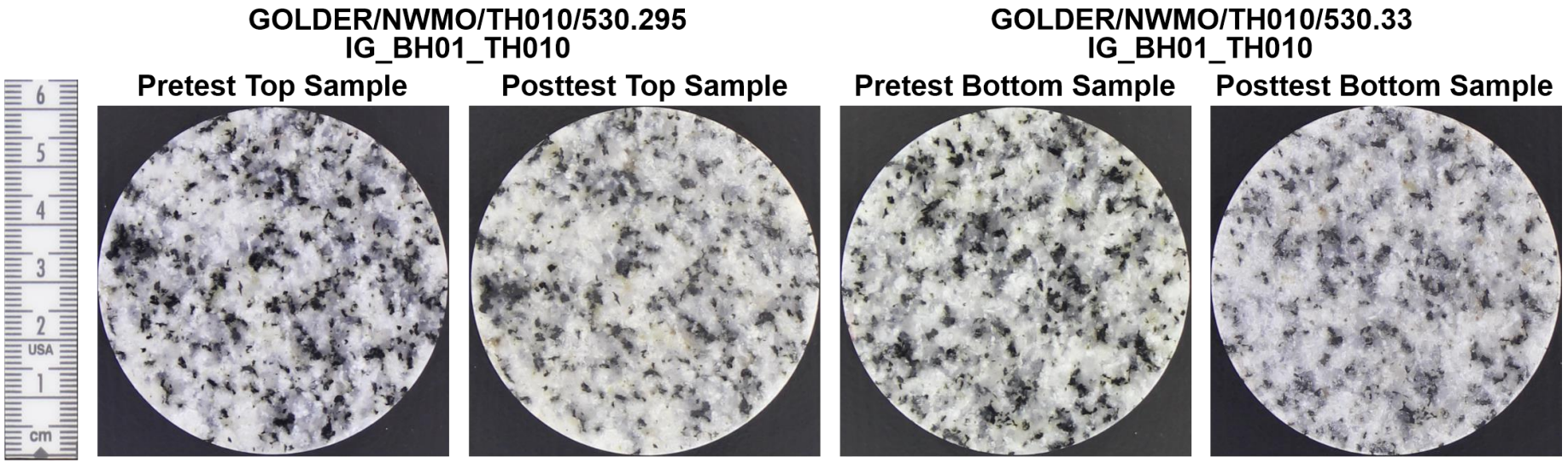






NOTE: Sample depths in the graph legends refer to the depth of the original sample as collected (part of the id), not the depth of the sub-samples

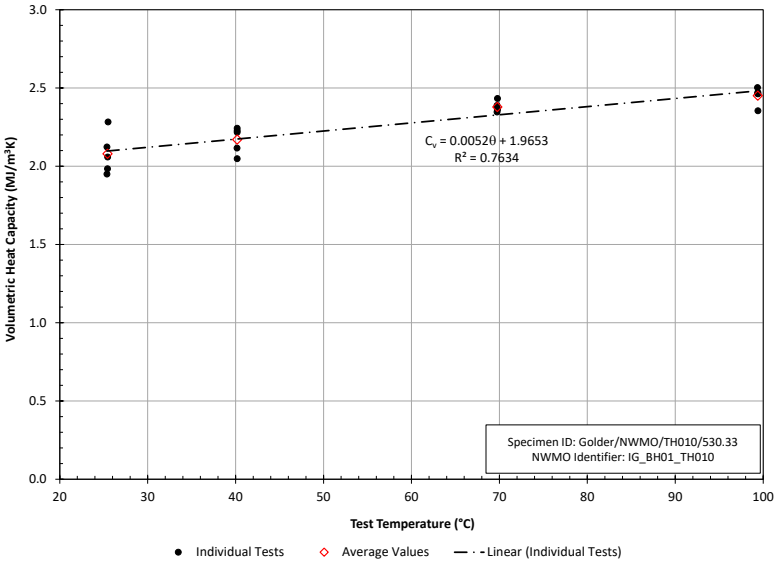
Test Specimen IG_BH01_TH009 – Depth = 501.76 m: Volumetric Heat Capacity, Thermal Conductivity and Thermal Diffusivity

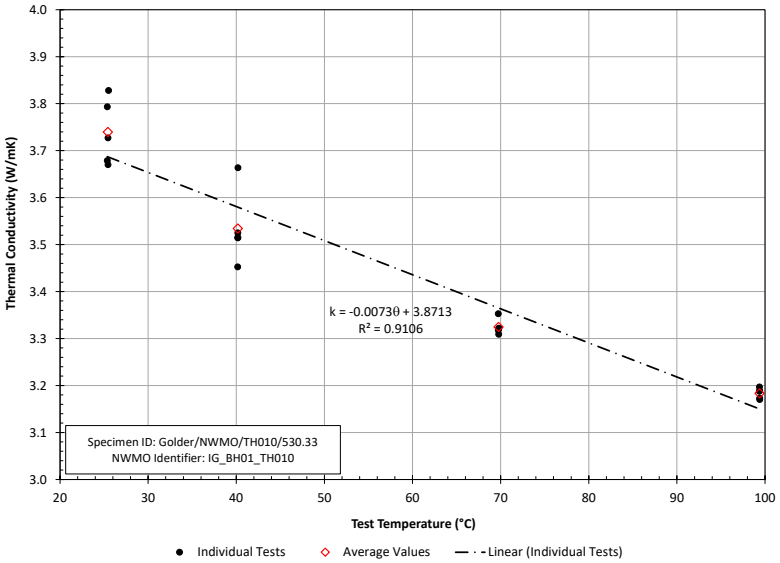


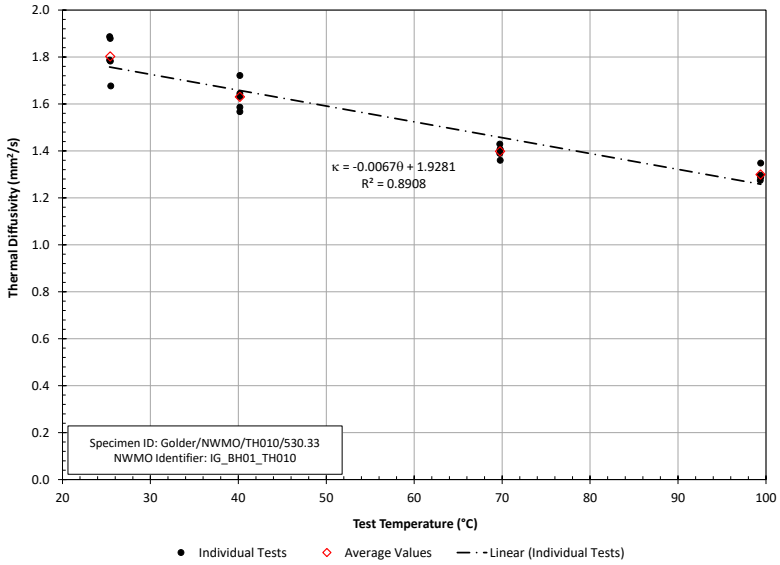
Test Specimen IG_BH01_TH010 – Depth = 530.30 m: specimen photographs

Table D-10: Hot Disk Results – Test Specimen IG_BH01_TH010 – Depth = 530.30 m

Average Temperature (°C)	Average Volumetric Specific Heat (MJ/m^3°K)	Average Thermal Conductivity (W/m°K)	Average Thermal Diffusivity (mm^2/s)
25.42	2.08	3.74	1.80
40.18	2.17	3.53	1.63
69.76	2.38	3.32	1.40
99.38	2.45	3.18	1.30
128.95	2.56	3.06	1.20
158.57	2.66	2.91	1.09
188.17	2.78	2.77	1.00
217.75	2.84	2.66	0.94
247.36	2.79	2.57	0.92
276.96	2.86	2.43	0.85
294.69	2.96	2.36	0.80

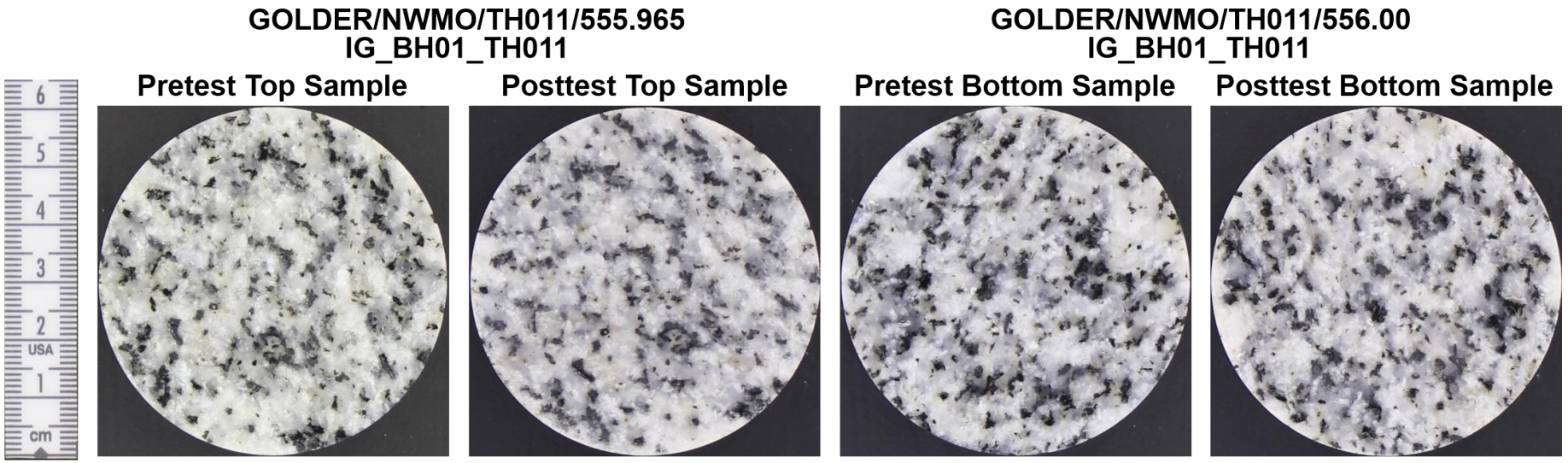






NOTE: Sample depths in the graph legends refer to the depth of the original sample as collected (part of the id), not the depth of the sub-samples

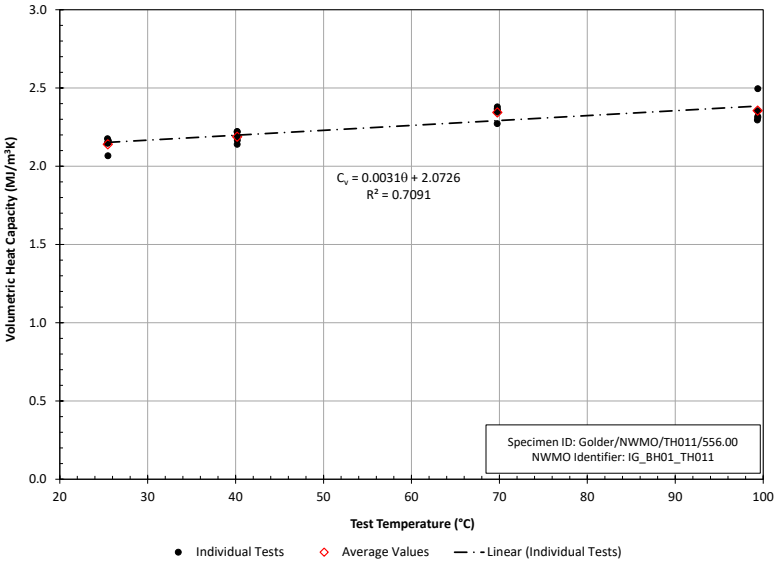
Test Specimen IG_BH01_TH010 – Depth = 530.30 m: Volumetric Heat Capacity, Thermal Conductivity and Thermal Diffusivity

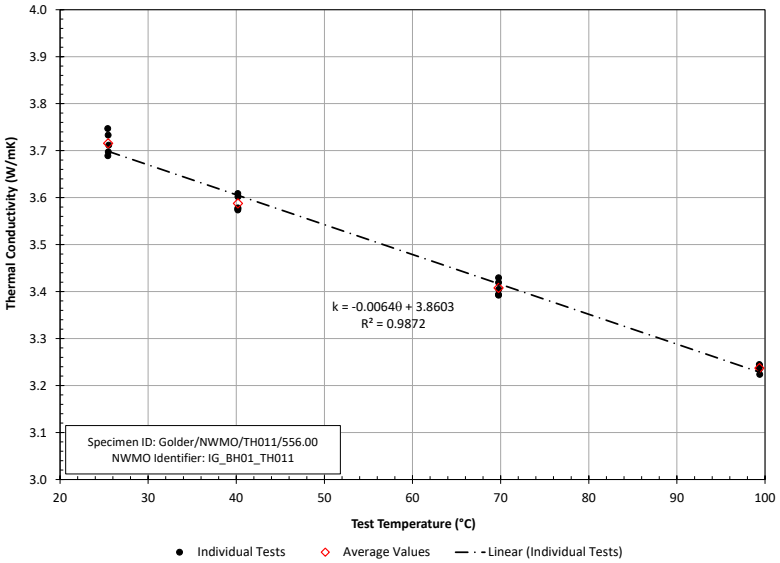


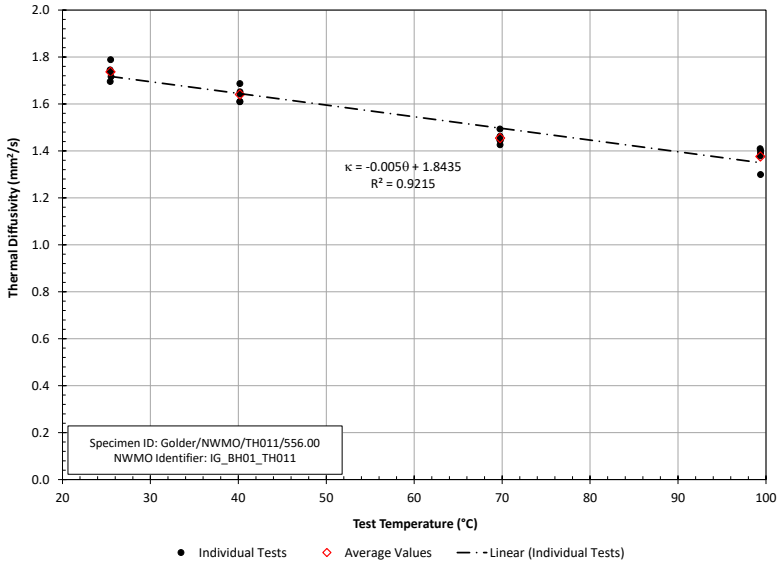
Test Specimen IG_BH01_TH011 – Depth = 555.97 m: specimen photographs

Table D-11: Hot Disk Results – Test Specimen IG_BH01_TH011 – Depth = 555.97 m

Average Temperature (°C)	Average Volumetric Specific Heat (MJ/m^3°K)	Average Thermal Conductivity (W/m°K)	Average Thermal Diffusivity (mm^2/s)
25.46	2.14	3.72	1.74
40.18	2.19	3.59	1.64
69.76	2.34	3.41	1.45
99.37	2.35	3.24	1.38
128.96	2.55	3.12	1.23
158.56	2.61	2.97	1.14
188.16	2.72	2.83	1.04
217.77	2.76	2.72	0.99
247.37	2.83	2.59	0.92
276.97	2.86	2.47	0.86
294.70	2.90	2.41	0.83

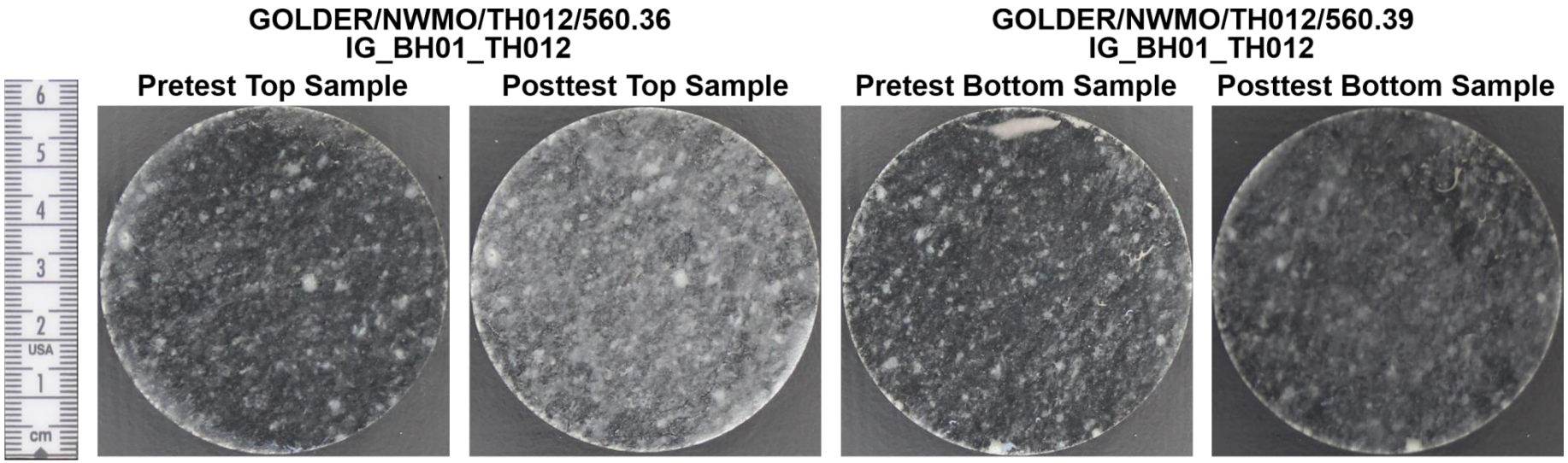






NOTE: Sample depths in the graph legends refer to the depth of the original sample as collected (part of the id), not the depth of the sub-samples

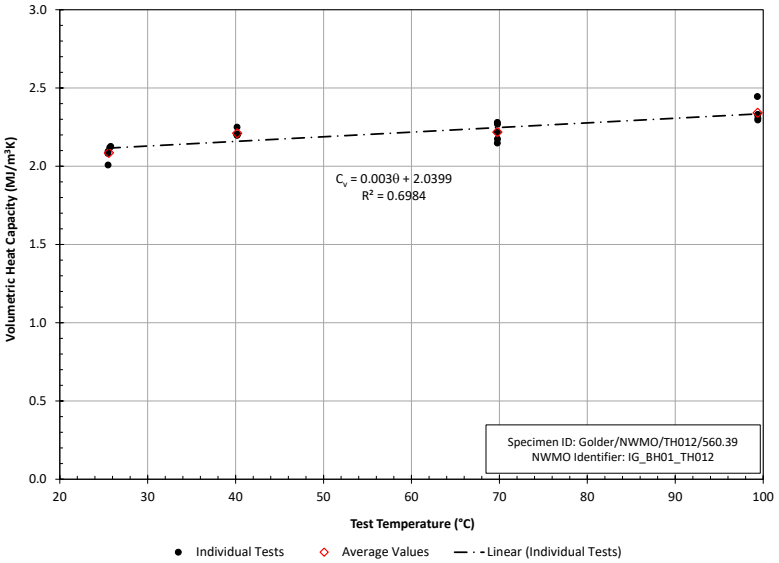
Test Specimen IG_BH01_TH011 – Depth = 555.97 m: Volumetric Heat Capacity, Thermal Conductivity and Thermal Diffusivity

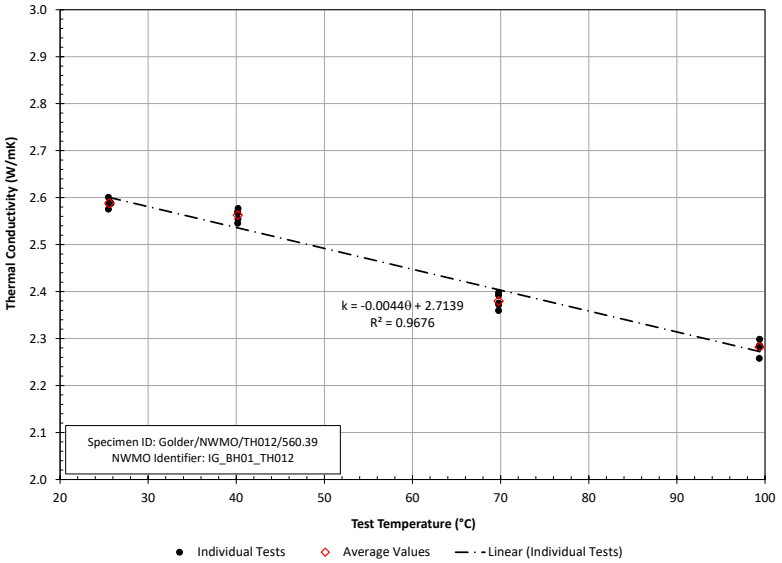


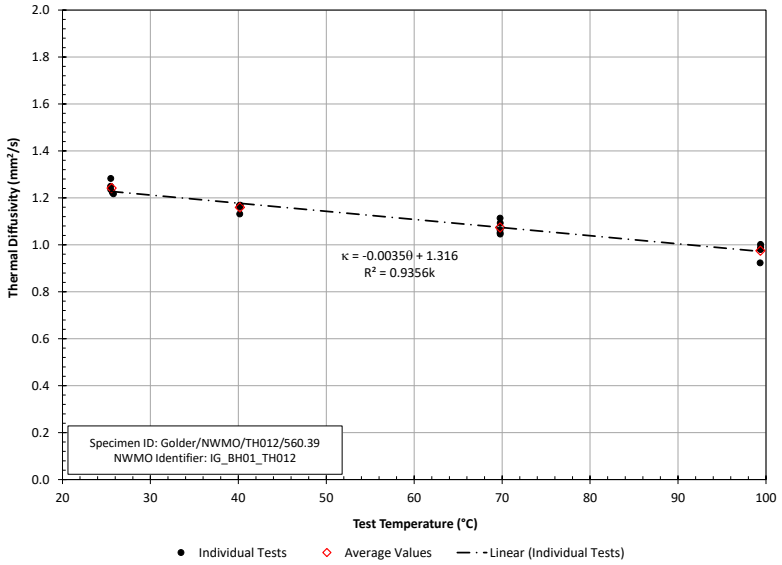
Test Specimen IG_BH01_TH012 – Depth = 560.36 m: specimen photographs

Table D-12: Hot Disk Results – Test Specimen IG_BH01_TH012 – Depth = 560.36 m

Average Temperature (°C)	Average Volumetric Specific Heat (MJ/m^3°K)	Average Thermal Conductivity (W/m°K)	Average Thermal Diffusivity (mm^2/s)
25.59	2.09	2.59	1.24
40.17	2.21	2.56	1.16
69.77	2.22	2.38	1.07
99.37	2.34	2.28	0.98
128.95	2.54	2.18	0.86
158.56	2.63	2.16	0.82
188.13	2.67	2.14	0.80
217.78	2.78	2.11	0.76
247.35	2.81	2.07	0.74
276.94	2.87	1.98	0.69
294.70	2.88	1.95	0.68

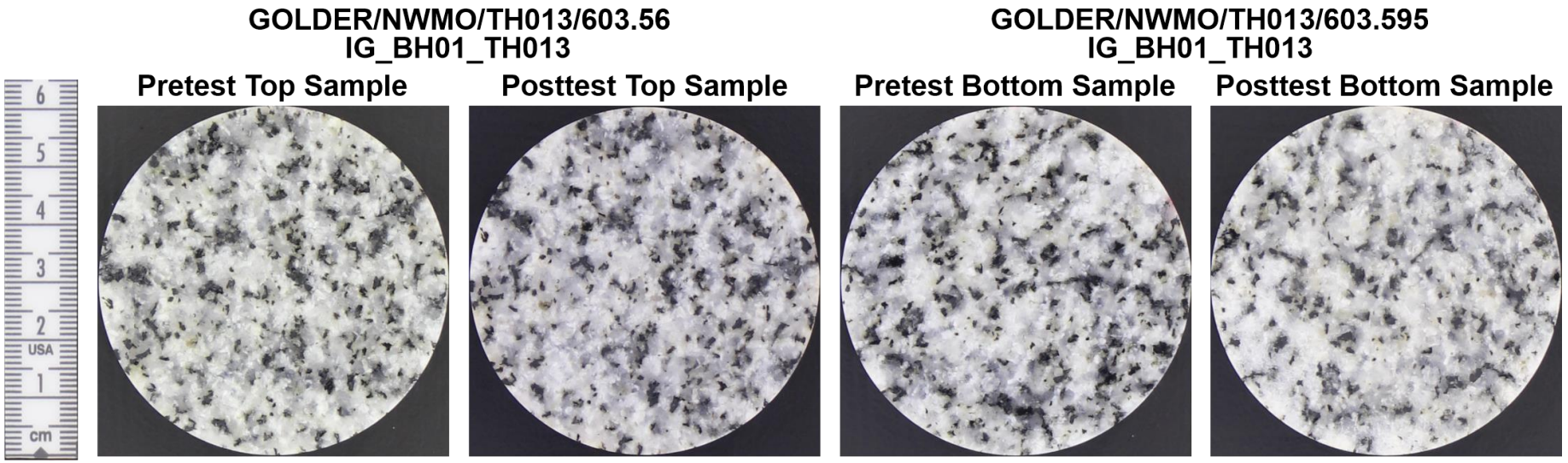






NOTE: Sample depths in the graph legends refer to the depth of the original sample as collected (part of the id), not the depth of the sub-samples

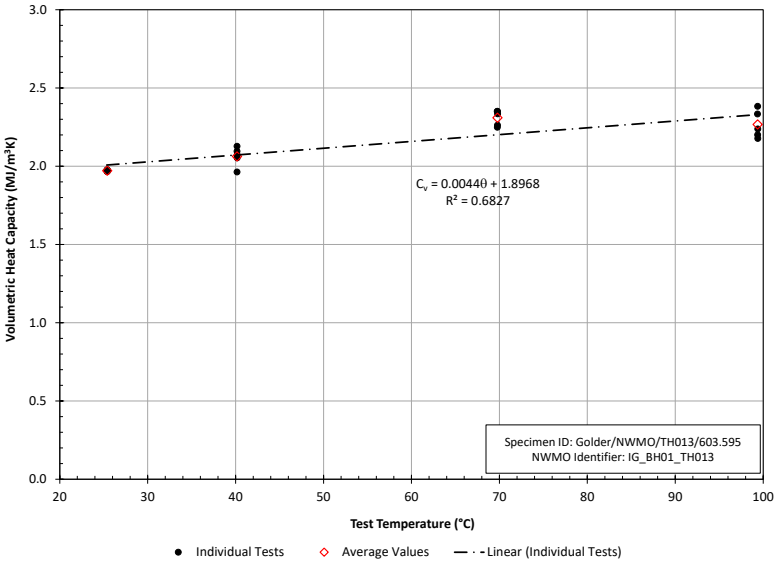
Test Specimen IG_BH01_TH012 – Depth = 560.36 m: Volumetric Heat Capacity, Thermal Conductivity and Thermal Diffusivity

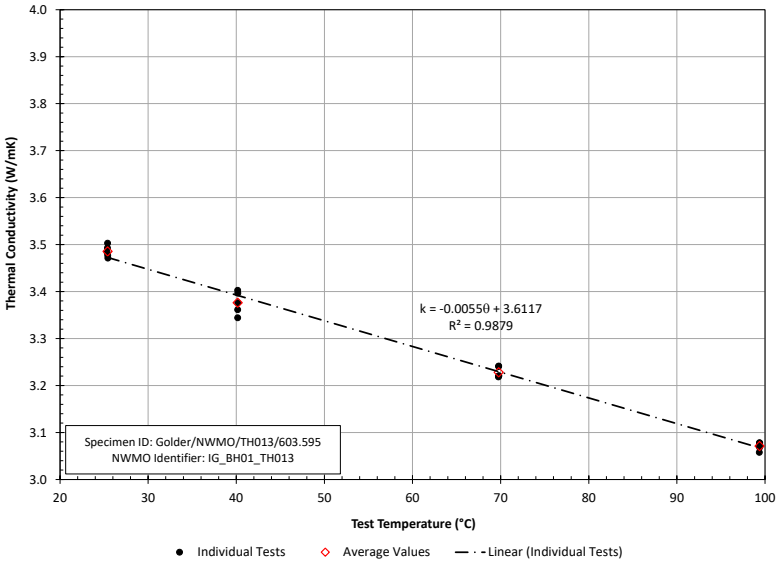


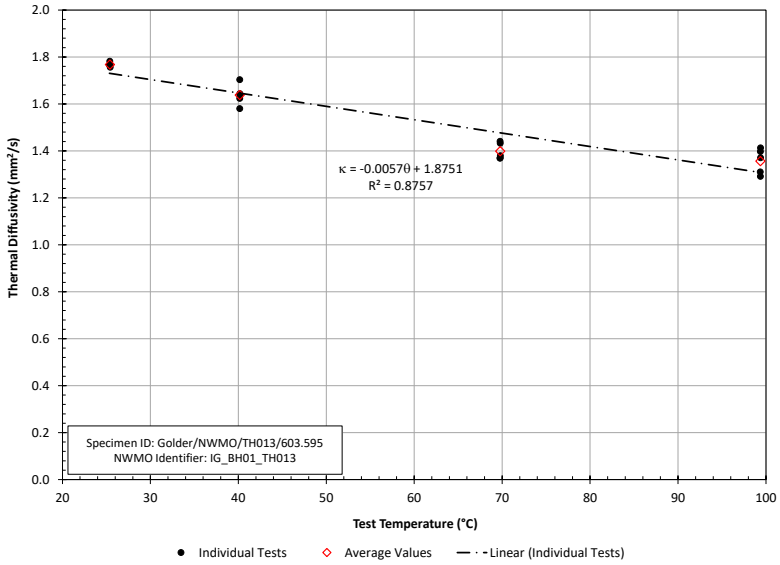
Test Specimen IG_BH01_TH013 – Depth = 603.56 m: specimen photographs

Table D-13: Hot Disk Results – Test Specimen IG_BH01_TH013 – Depth = 603.56 m

Average Temperature (°C)	Average Volumetric Specific Heat (MJ/m^3°K)	Average Thermal Conductivity (W/m°K)	Average Thermal Diffusivity (mm^2/s)
25.39	1.97	3.49	1.77
40.17	2.06	3.38	1.64
69.77	2.31	3.23	1.40
99.37	2.27	3.07	1.36
128.94	2.35	2.95	1.26
158.56	2.43	2.83	1.17
188.16	2.52	2.71	1.07
217.78	2.58	2.60	1.01
247.36	2.65	2.50	0.94
276.96	2.71	2.38	0.88
294.71	2.74	2.30	0.84

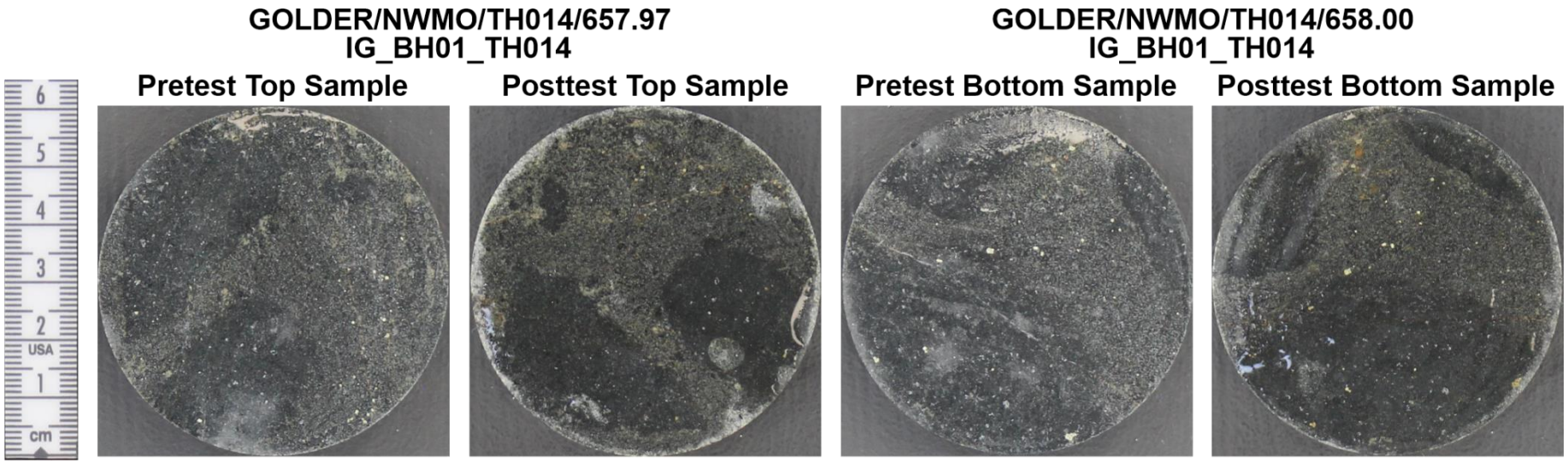






NOTE: Sample depths in the graph legends refer to the depth of the original sample as collected (part of the id), not the depth of the sub-samples

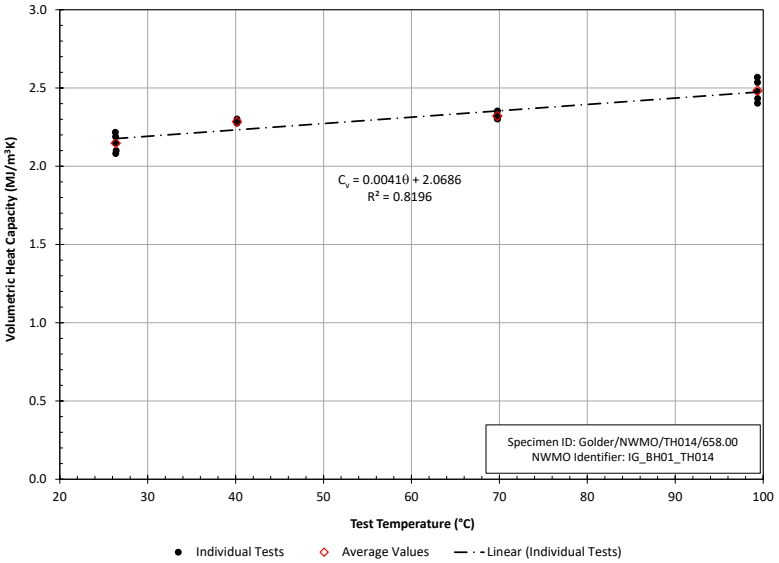
Test Specimen IG_BH01_TH013 – Depth = 603.56 m: Volumetric Heat Capacity, Thermal Conductivity and Thermal Diffusivity

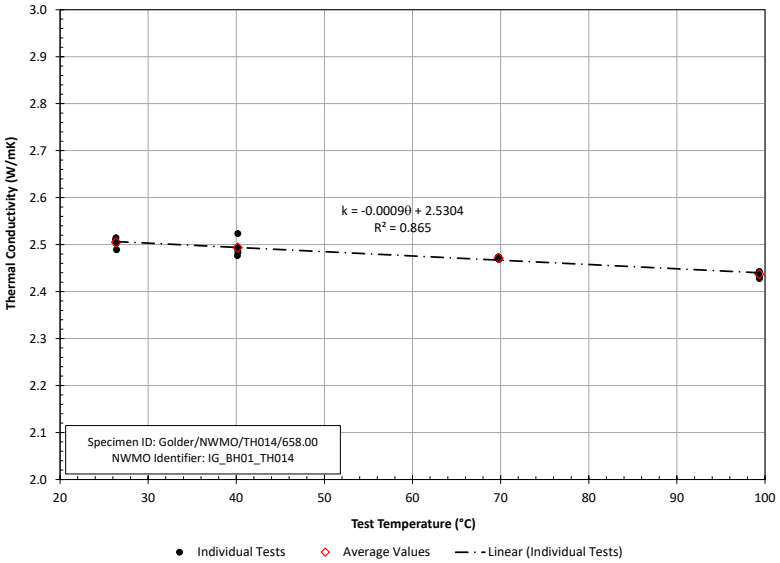


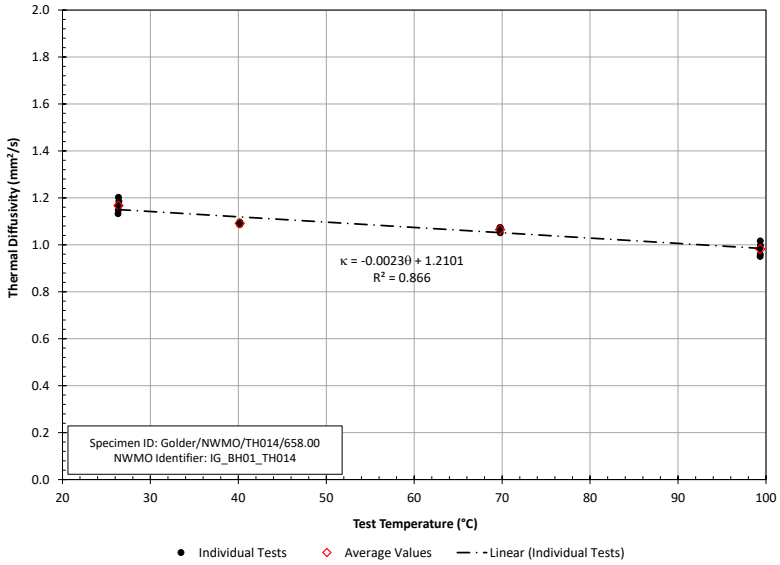
Test Specimen IG_BH01_TH014 – Depth = 657.97 m: specimen photographs

Table D-14: Hot Disk Results – Test Specimen IG_BH01_TH014 – Depth = 657.97 m

Average Temperature (°C)	Average Volumetric Specific Heat (MJ/m^3°K)	Average Thermal Conductivity (W/m°K)	Average Thermal Diffusivity (mm^2/s)
26.36	2.15	2.50	1.17
40.16	2.28	2.49	1.09
69.76	2.32	2.47	1.07
99.35	2.48	2.44	0.98
128.98	2.59	2.38	0.92
158.56	2.68	2.36	0.88
188.15	2.77	2.30	0.83
217.76	2.89	2.28	0.79
247.36	2.88	2.25	0.78
276.97	2.95	2.17	0.73
294.69	2.88	2.13	0.74

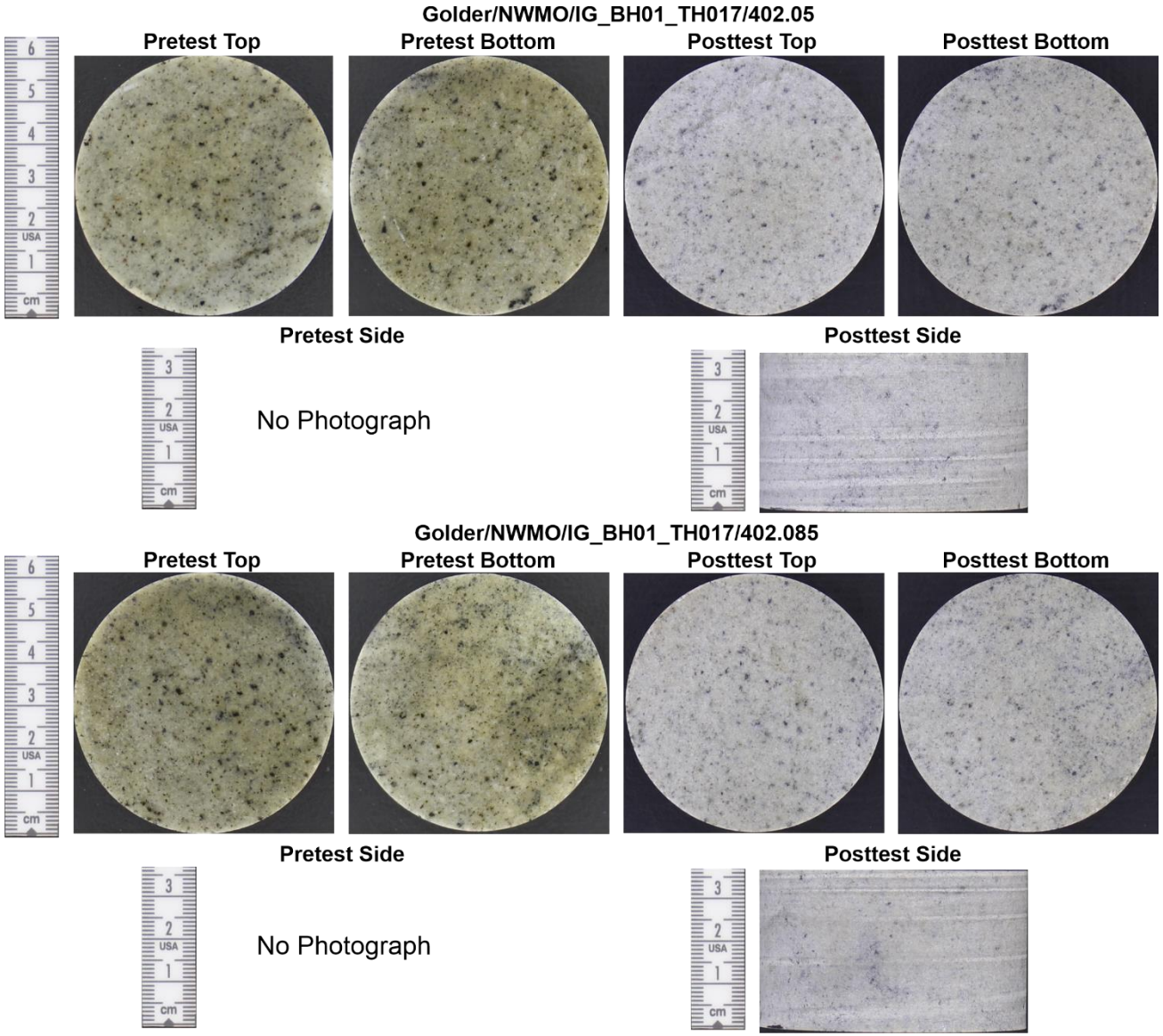






NOTE: Sample depths in the graph legends refer to the depth of the original sample as collected (part of the id), not the depth of the sub-samples

Test Specimen IG_BH01_TH014 – Depth = 657.97 m: Volumetric Heat Capacity, Thermal Conductivity and Thermal Diffusivity

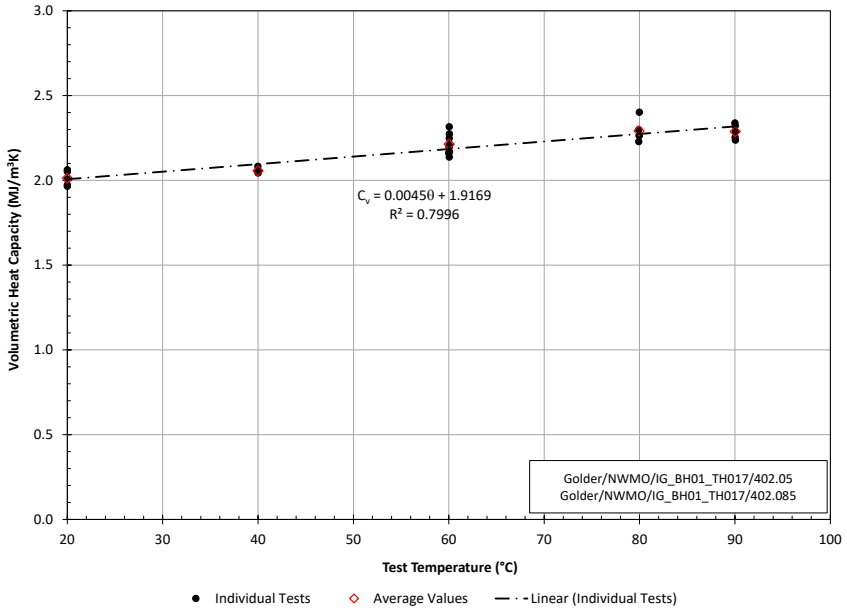


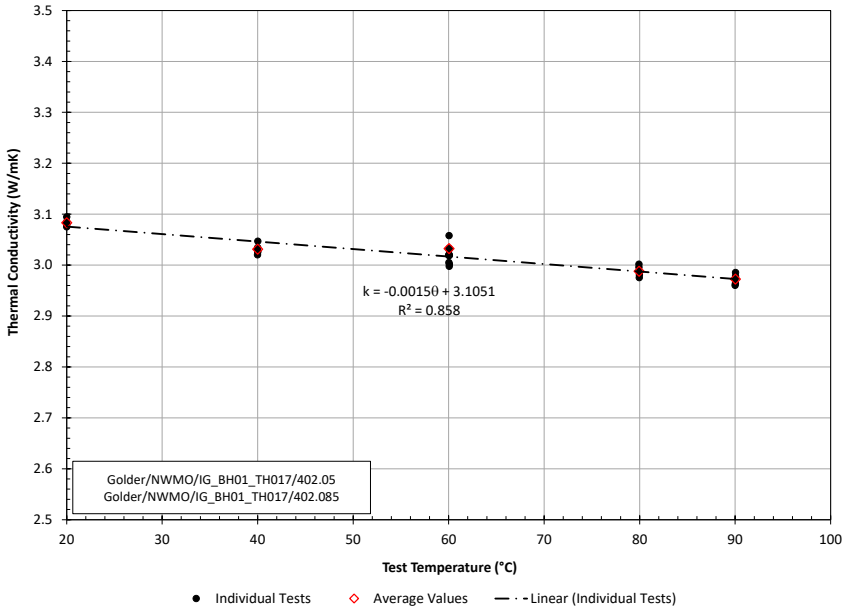
Test Specimen IG_BH01_TH017 – Depth = 402.05 m: specimen photographs

Table D-15: Hot Disk Results – Test Specimen IG_BH01_TH017 – Depth = 402.05 m

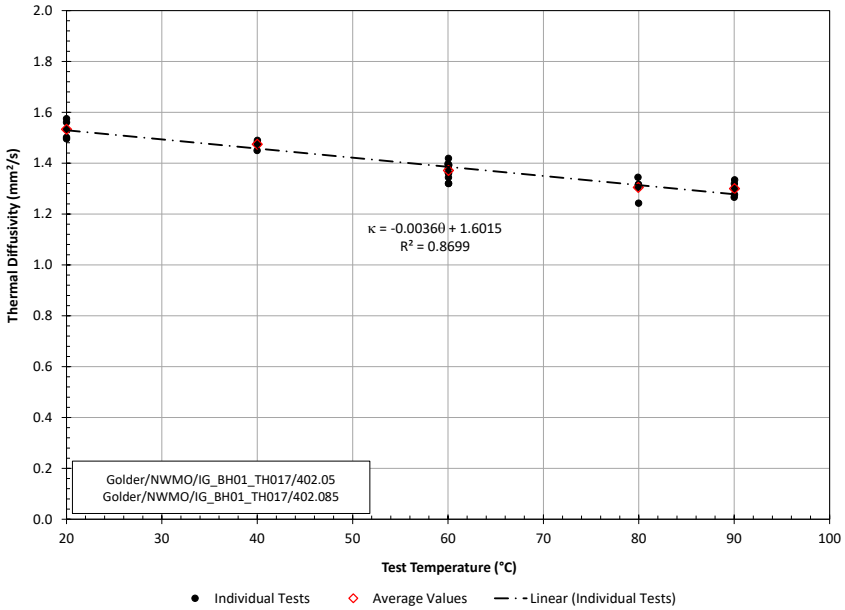
Average Temperature (°C)	Average Volumetric Specific Heat (MJ/m³°K)	Average Thermal Conductivity (W/m°K)	Average Thermal Diffusivity (mm²/s)
20.01	2.01	3.08	1.53
40.01	2.06	3.03	1.47
60.04	2.21	3.03	1.37
79.95	2.29	2.99	1.30
90.02	2.29	2.97	1.30
60.05	2.20	3.01	1.37

NOTE: Sample depths in the graph legends refer to the depth of the original sample as collected (part of the id), not the depth of the sub-samples

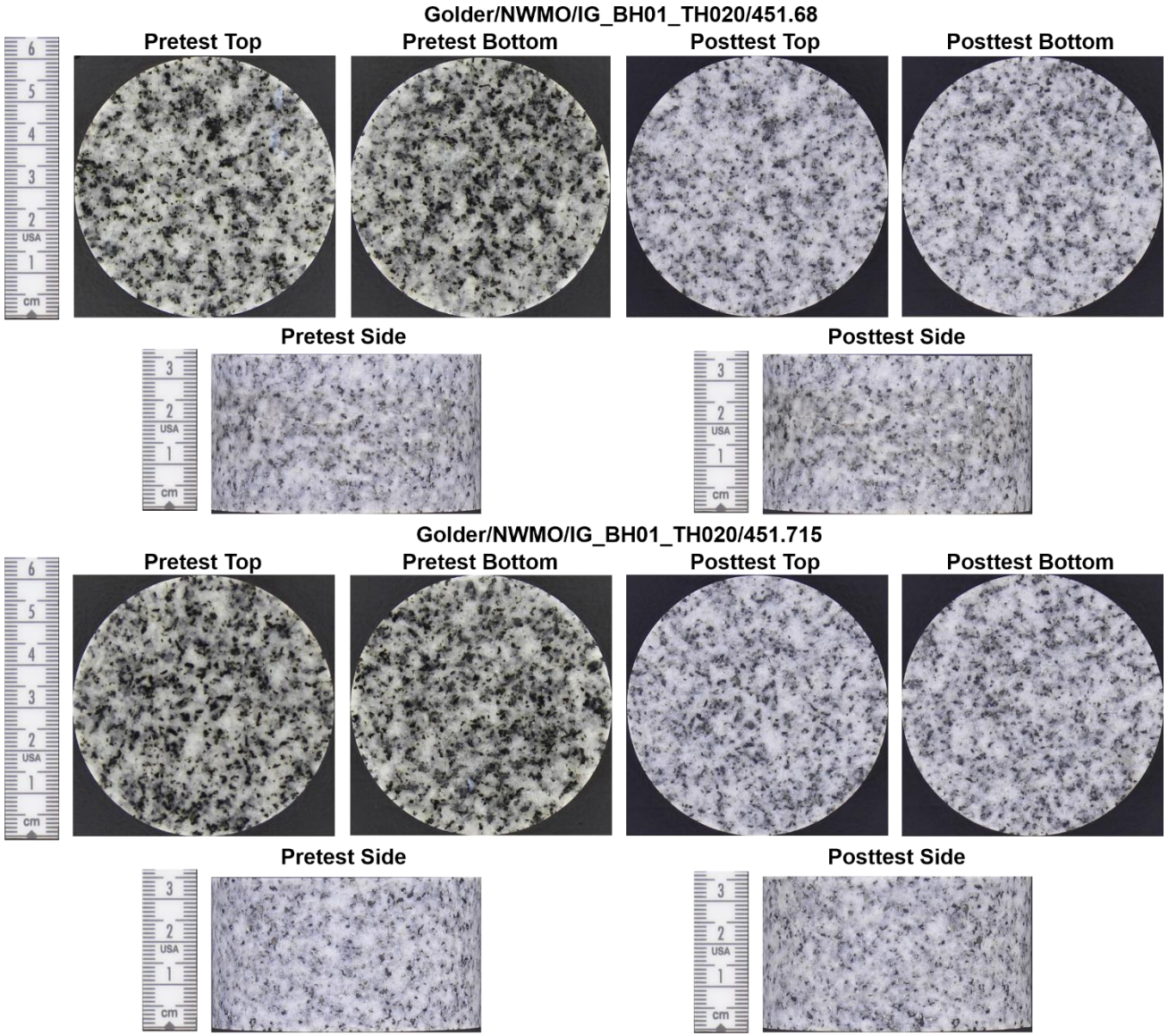




Test Specimen IG_BH01_TH017 – Depth = 402.05 m: Volumetric Heat Capacity and Thermal Conductivity



Test Specimen IG_BH01_TH017 – Depth = 402.05 m: Thermal Diffusivity

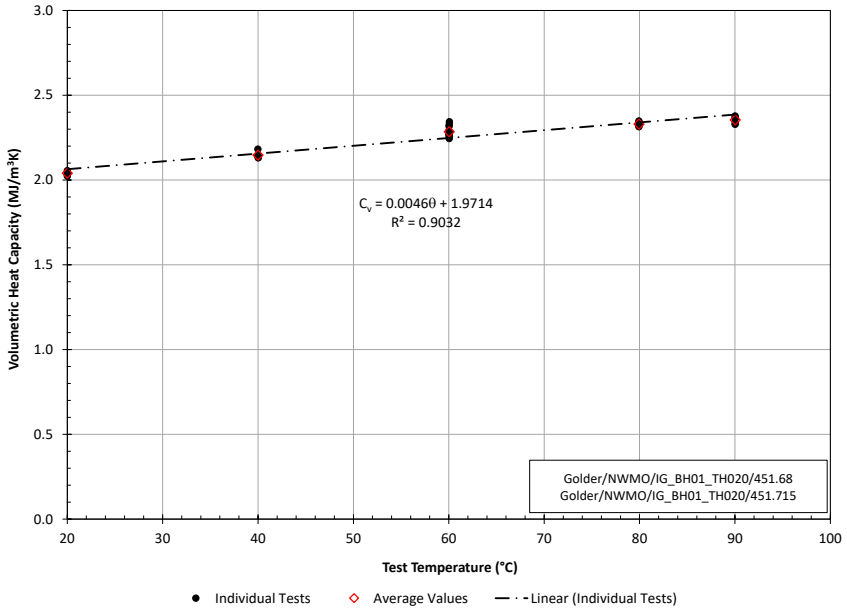


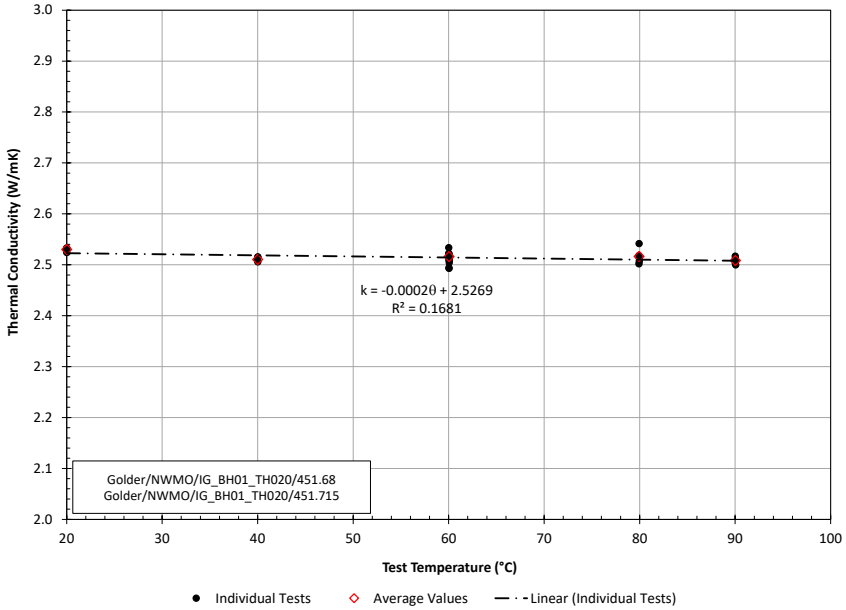
Test Specimen IG_BH01_TH020 – Depth = 451.68 m: specimen photographs

Table D-16: Hot Disk Results – Test Specimen IG_BH01_TH020 – Depth = 451.68 m

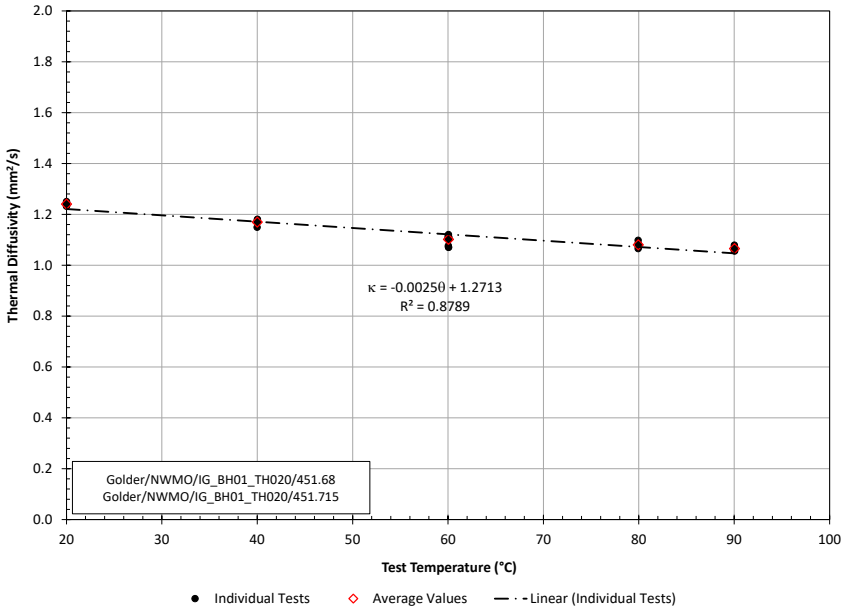
Average Temperature (°C)	Average Volumetric Specific Heat (MJ/m^3°K)	Average Thermal Conductivity (W/m°K)	Average Thermal Diffusivity (mm^2/s)
20.01	2.04	2.53	1.24
40.01	2.15	2.51	1.17
60.05	2.28	2.52	1.10
79.94	2.33	2.52	1.08
90.02	2.35	2.51	1.07
60.03	2.29	2.51	1.10

NOTE: Sample depths in the graph legends refer to the depth of the original sample as collected (part of the id), not the depth of the sub-samples

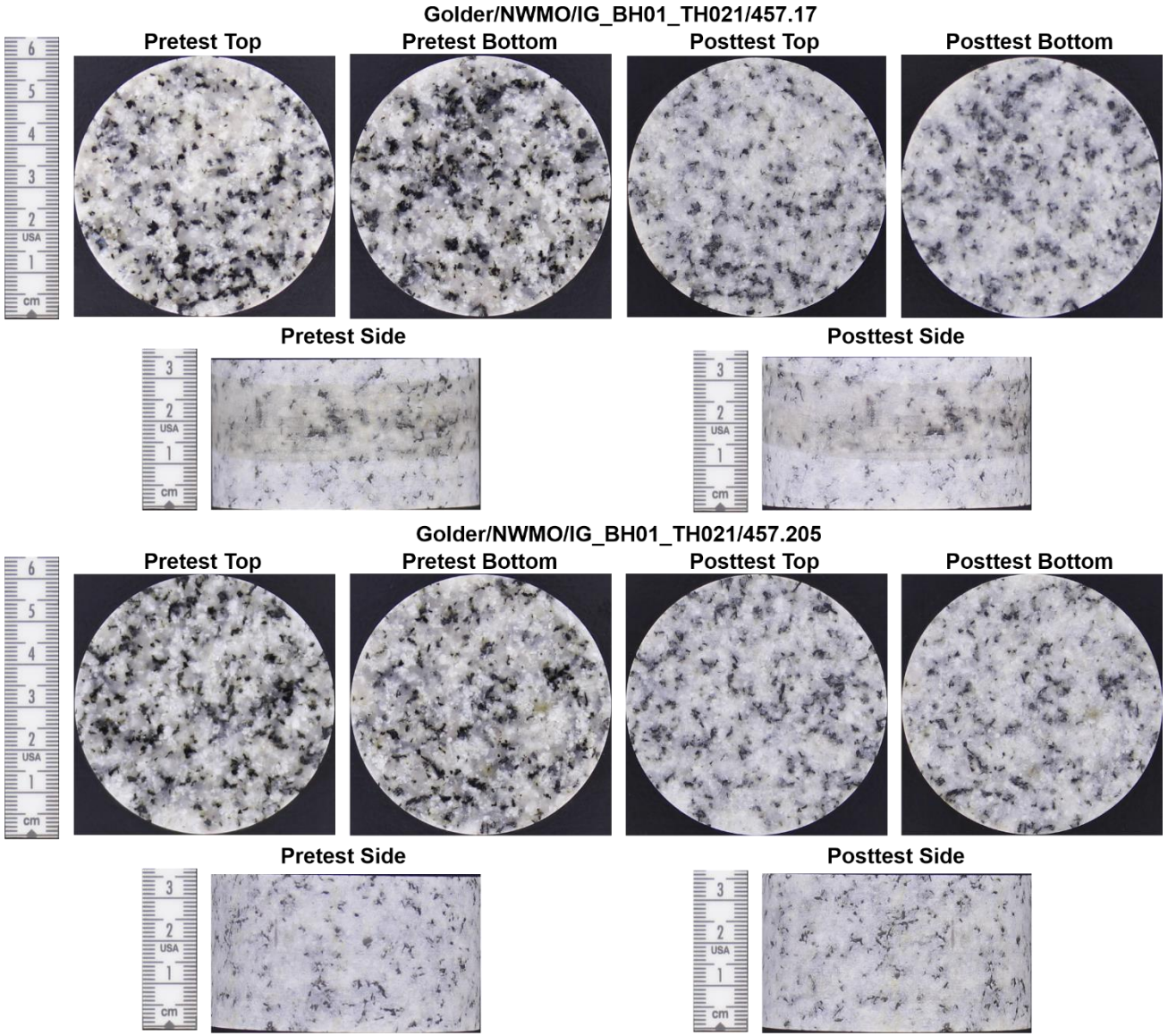




Test Specimen IG_BH01_TH020 – Depth = 451.68 m: Volumetric Heat Capacity and Thermal Conductivity



Test Specimen IG_BH01_TH020 – Depth = 451.68 m: Thermal Diffusivity

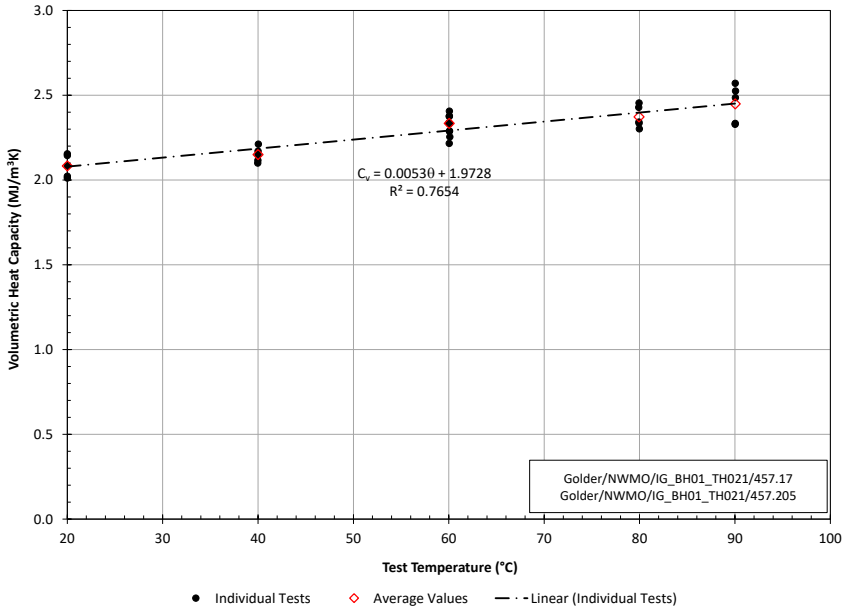


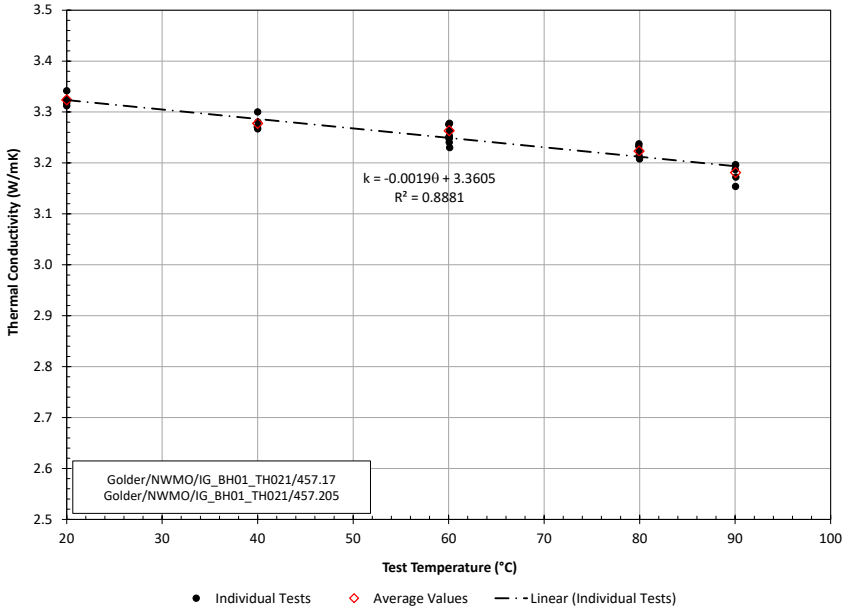
Test Specimen IG_BH01_TH021 – Depth = 457.17 m: specimen photographs

Table D-17: Hot Disk Results – Test Specimen IG_BH01_TH021 – Depth = 457.17 m

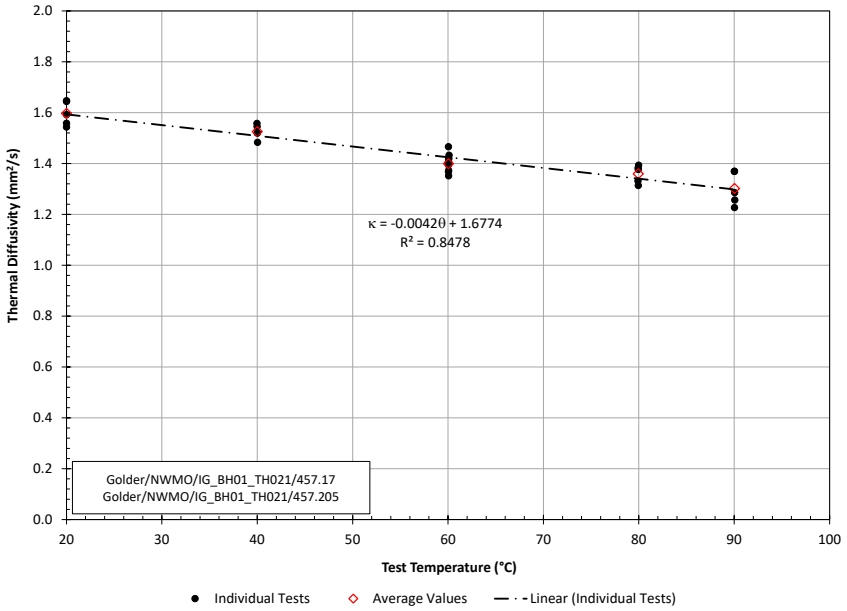
Average Temperature (°C)	Average Volumetric Specific Heat (MJ/m^3°K)	Average Thermal Conductivity (W/m°K)	Average Thermal Diffusivity (mm^2/s)
20.01	2.08	3.32	1.60
40.00	2.15	3.28	1.53
60.05	2.33	3.26	1.40
79.94	2.37	3.22	1.36
90.04	2.45	3.18	1.30
60.07	2.31	3.24	1.41

NOTE: Sample depths in the graph legends refer to the depth of the original sample as collected (part of the id), not the depth of the sub-samples

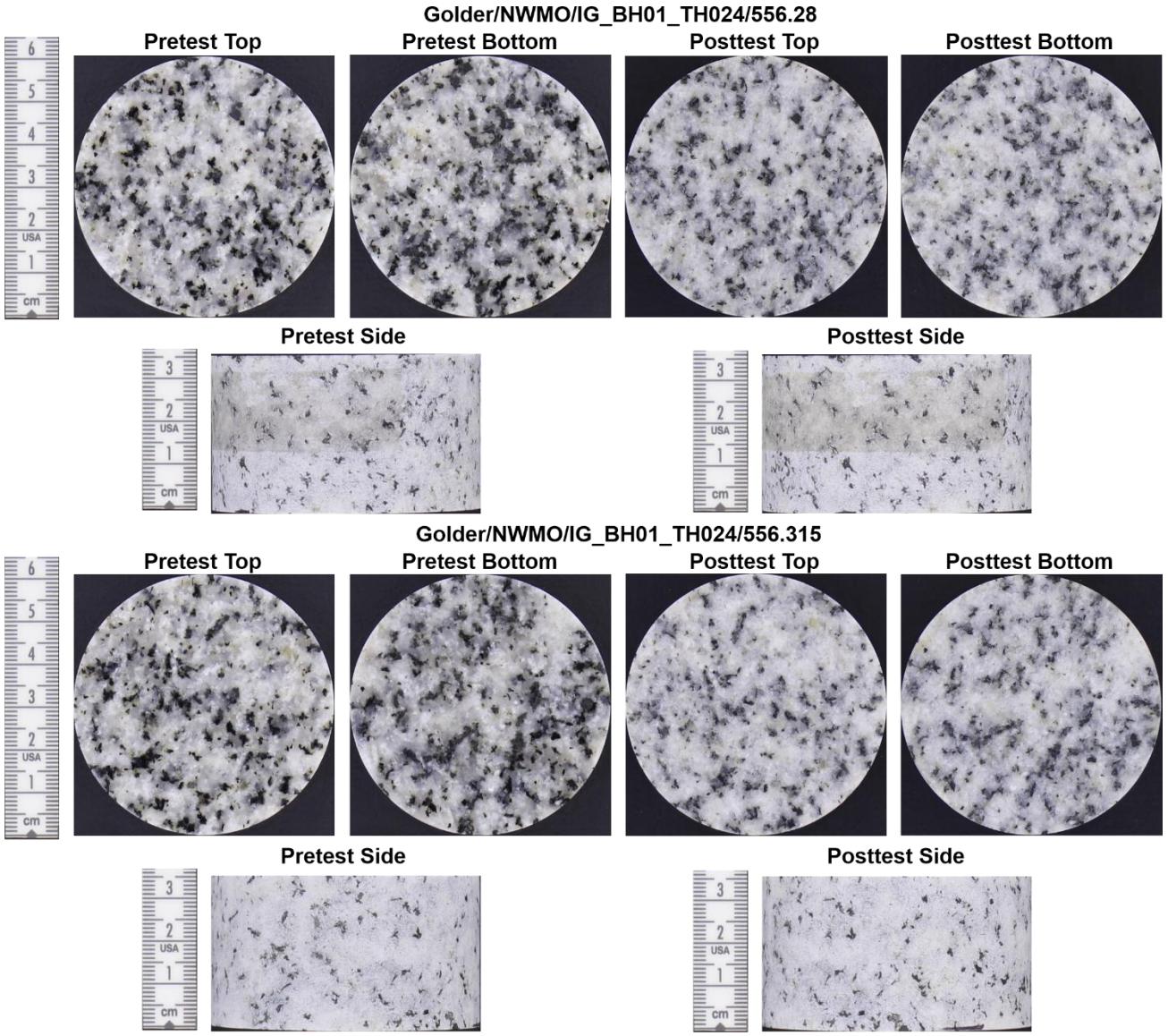




Test Specimen IG_BH01_TH021 – Depth = 457.17 m: Volumetric Heat Capacity and Thermal Conductivity



Test Specimen IG_BH01_TH021 – Depth = 457.17 m: Thermal Diffusivity

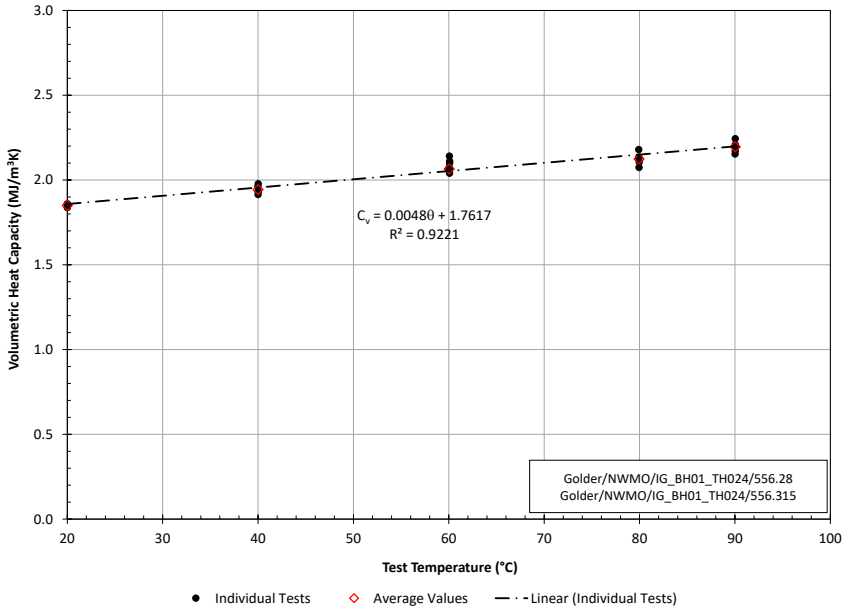


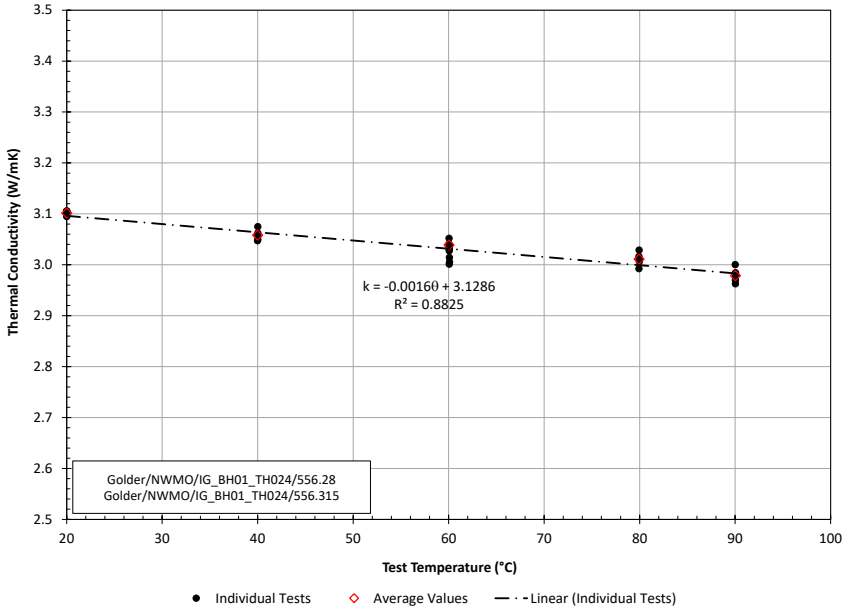
Test Specimen IG_BH01_TH024 – Depth = 556.28 m: specimen photographs

Table D-18: Hot Disk Results – Test Specimen IG_BH01_TH024 – Depth = 556.28 m

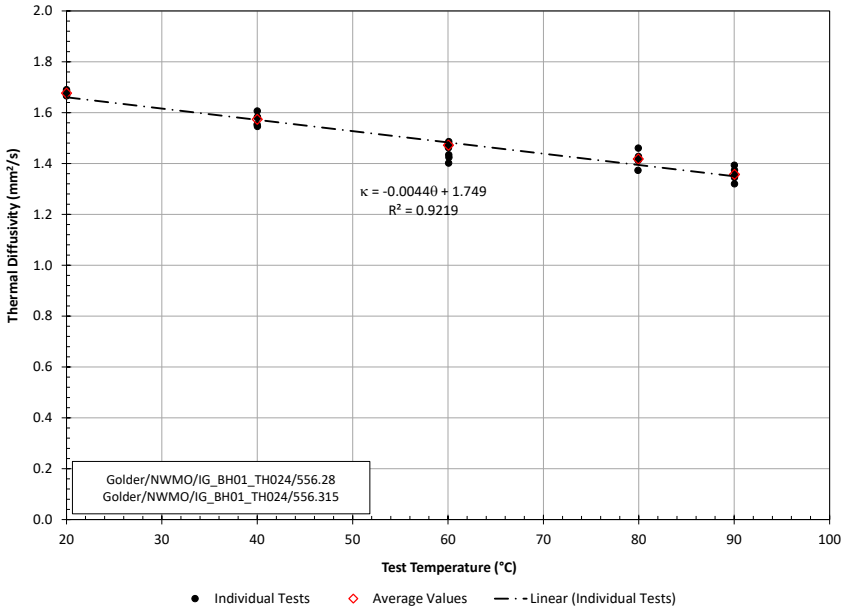
Average Temperature (°C)	Average Volumetric Specific Heat (MJ/m³°K)	Average Thermal Conductivity (W/m°K)	Average Thermal Diffusivity (mm²/s)
20.01	1.85	3.10	1.68
40.01	1.94	3.06	1.57
60.05	2.06	3.04	1.47
79.94	2.12	3.01	1.42
90.03	2.20	2.98	1.36
60.07	2.09	3.02	1.44

NOTE: Sample depths in the graph legends refer to the depth of the original sample as collected (part of the id), not the depth of the sub-samples

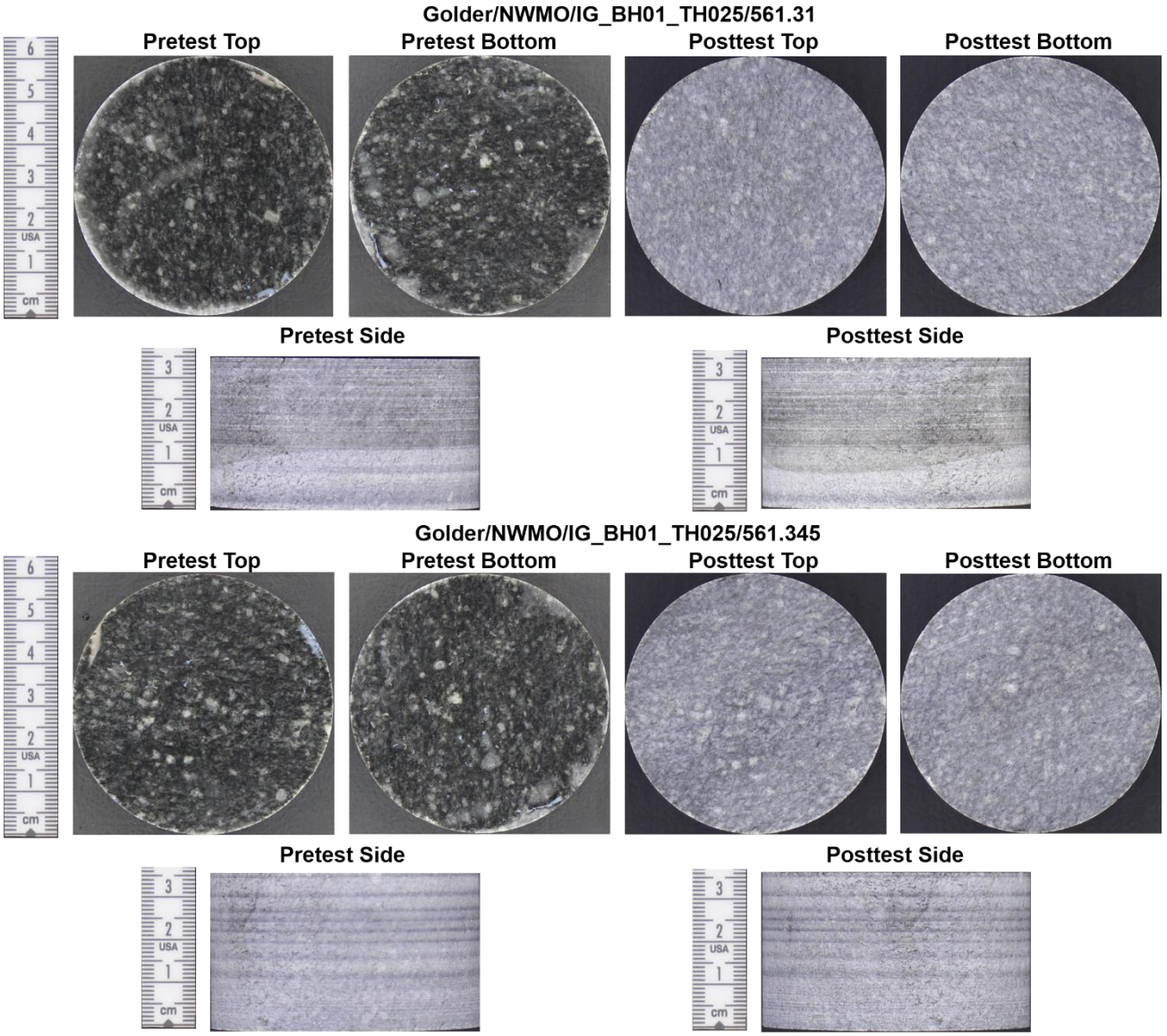




Test Specimen IG_BH01_TH024 – Depth = 556.28 m: Volumetric Heat Capacity and Thermal Conductivity



Test Specimen IG_BH01_TH024 – Depth = 556.28 m: Thermal Diffusivity

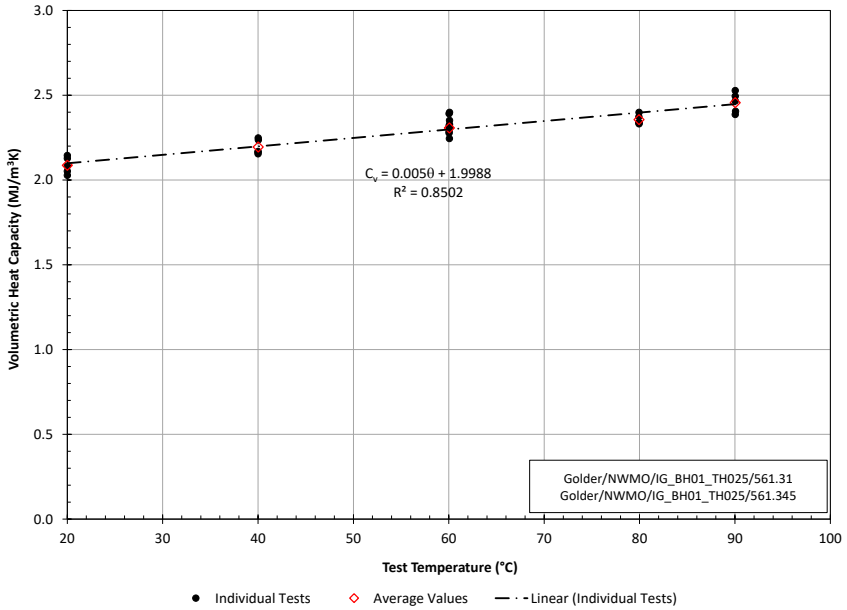


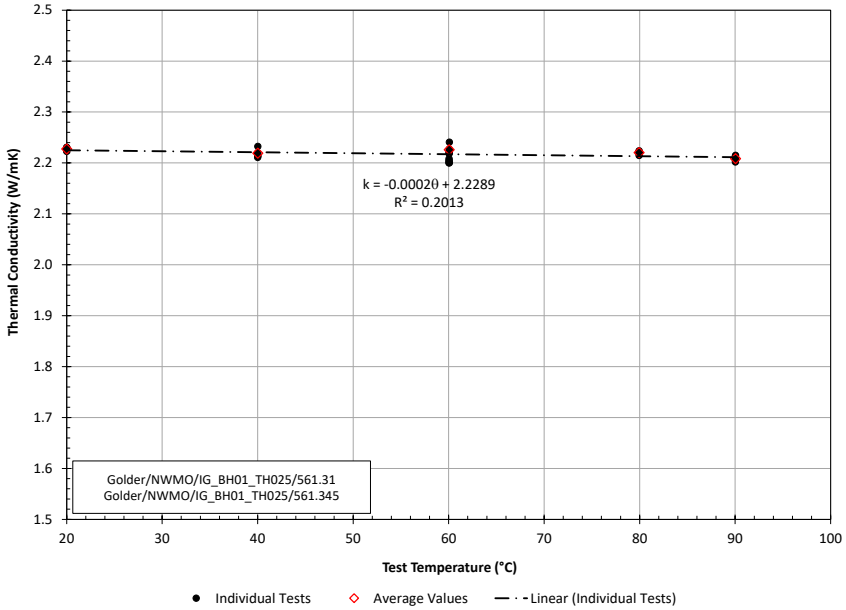
Test Specimen IG_BH01_TH025 – Depth = 561.31 m: specimen photographs

Table D-19: Hot Disk Results – Test Specimen IG_BH01_TH025 – Depth = 561.31 m

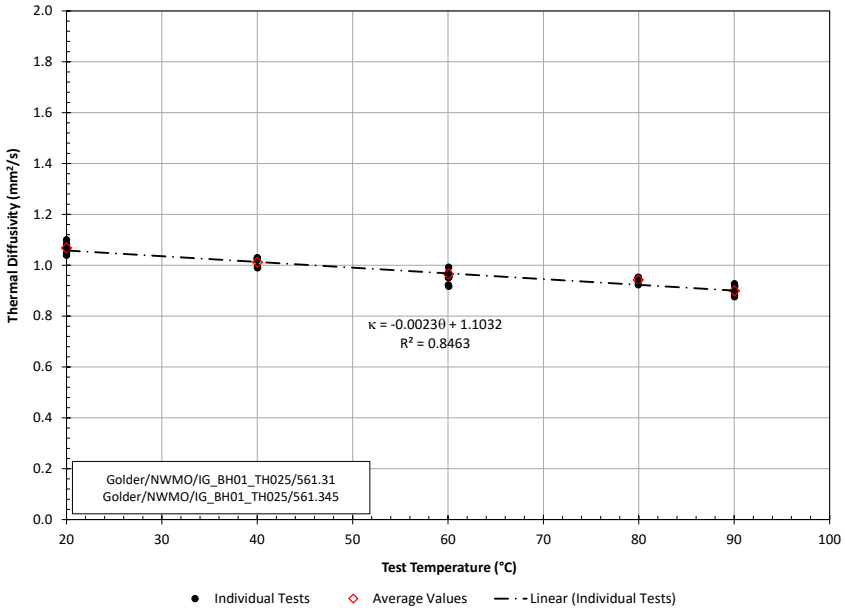
Average Temperature (°C)	Average Volumetric Specific Heat (MJ/m^3°K)	Average Thermal Conductivity (W/m°K)	Average Thermal Diffusivity (mm^2/s)
20.01	2.09	2.23	1.07
40.01	2.19	2.22	1.01
60.06	2.31	2.23	0.97
79.94	2.36	2.22	0.94
90.04	2.46	2.21	0.90
60.04	2.34	2.20	0.94

NOTE: Sample depths in the graph legends refer to the depth of the original sample as collected (part of the id), not the depth of the sub-samples

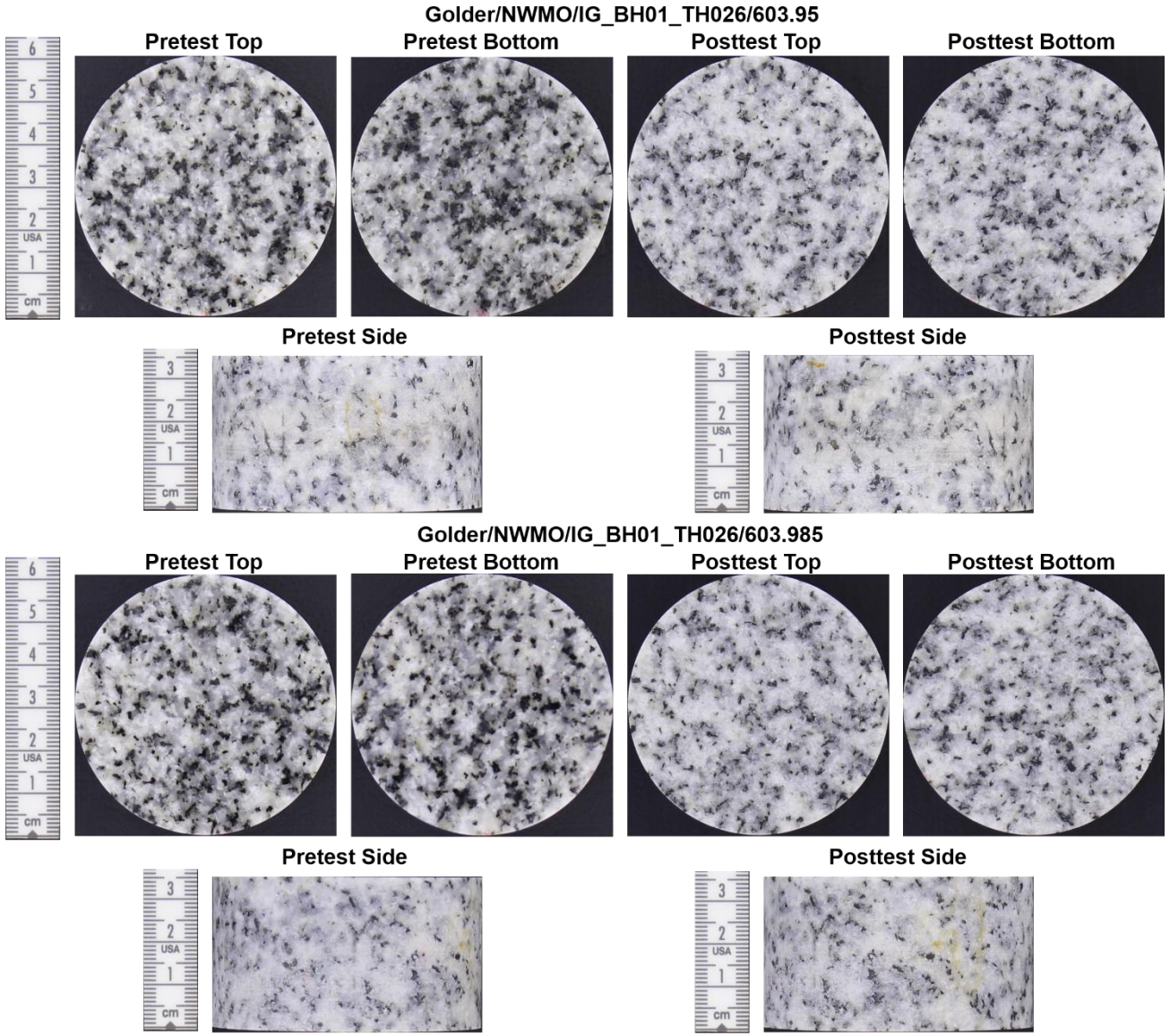




Test Specimen IG_BH01_TH025 – Depth = 561.31 m: Volumetric Heat Capacity and Thermal Conductivity



Test Specimen IG_BH01_TH025 – Depth = 561.31 m: Thermal Diffusivity

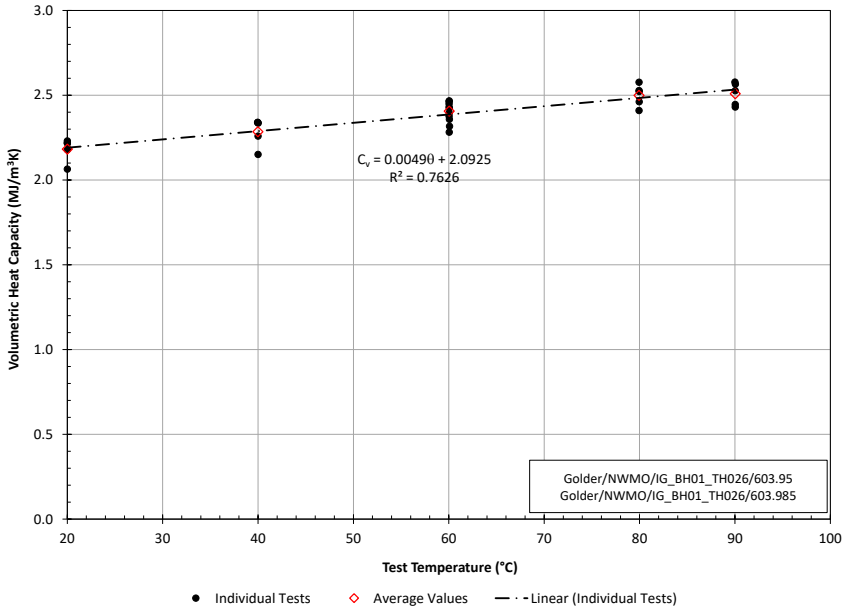


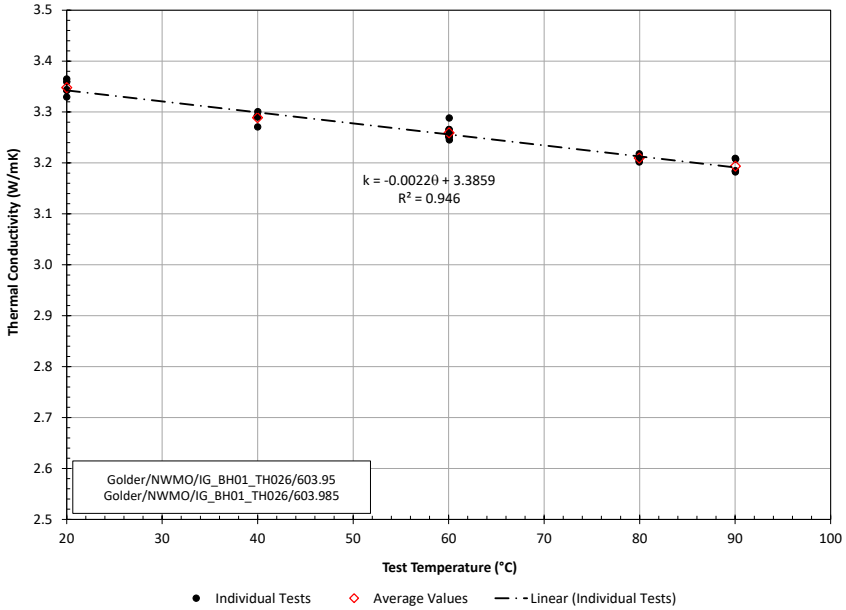
Test Specimen IG_BH01_TH026 – Depth = 603.95 m: specimen photographs

Table D-20: Hot Disk Results – Test Specimen IG_BH01_TH026 – Depth = 603.95 m

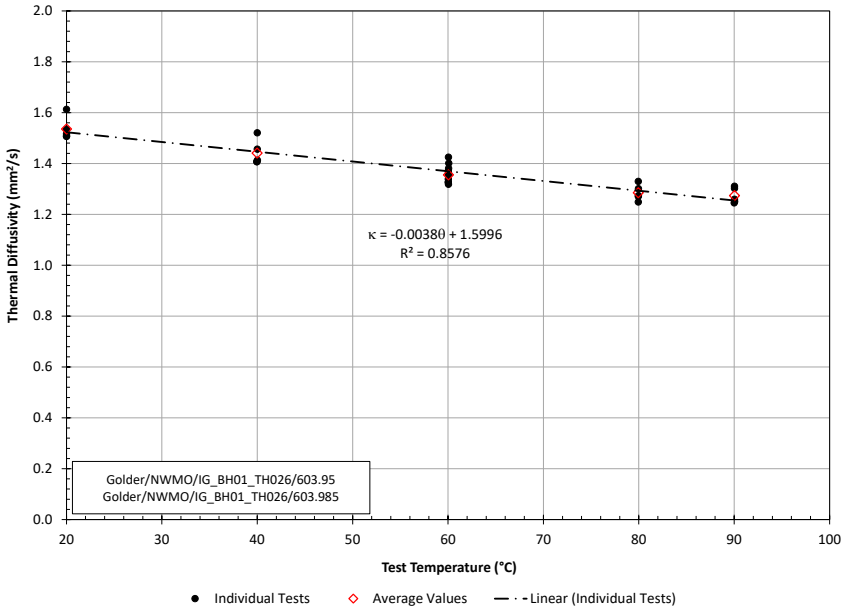
Average Temperature (°C)	Average Volumetric Specific Heat (MJ/m^3°K)	Average Thermal Conductivity (W/m°K)	Average Thermal Diffusivity (mm^2/s)
20.01	2.18	3.35	1.54
39.99	2.28	3.29	1.44
60.05	2.41	3.26	1.36
79.95	2.50	3.21	1.28
90.03	2.51	3.19	1.27
60.05	2.39	3.26	1.37

NOTE: Sample depths in the graph legends refer to the depth of the original sample as collected (part of the id), not the depth of the sub-samples

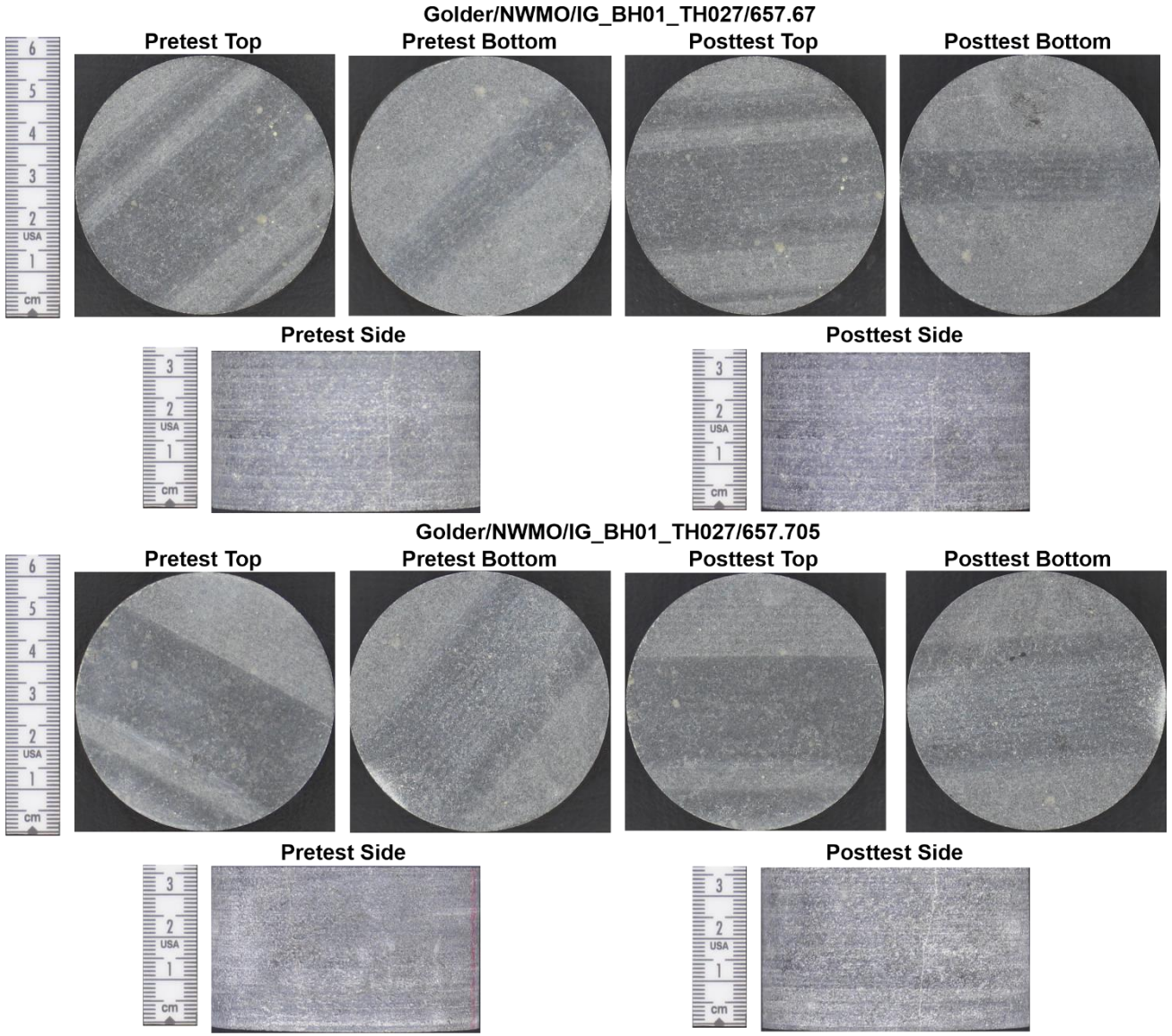




Test Specimen IG_BH01_TH026 – Depth = 603.95 m: Volumetric Heat Capacity and Thermal Conductivity



Test Specimen IG_BH01_TH026 – Depth = 603.95 m: Thermal Diffusivity

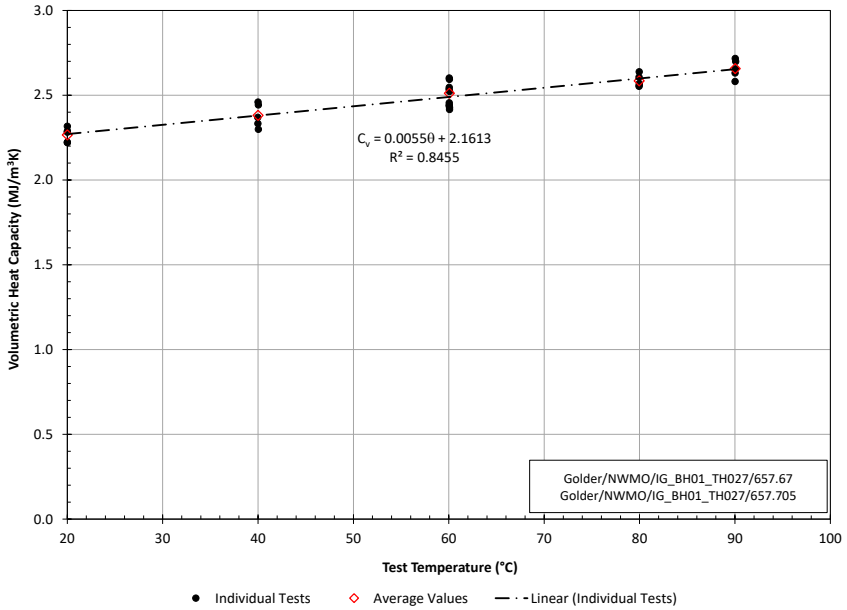


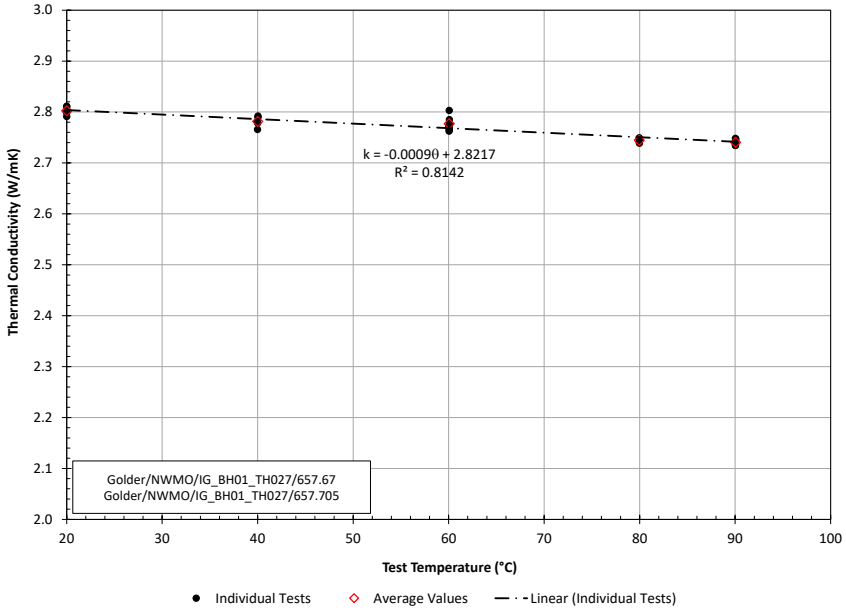
Test Specimen IG_BH01_TH027 – Depth = 657.67 m: specimen photographs

Table D-21: Hot Disk Results – Test Specimen IG_BH01_TH027 – Depth = 657.67 m

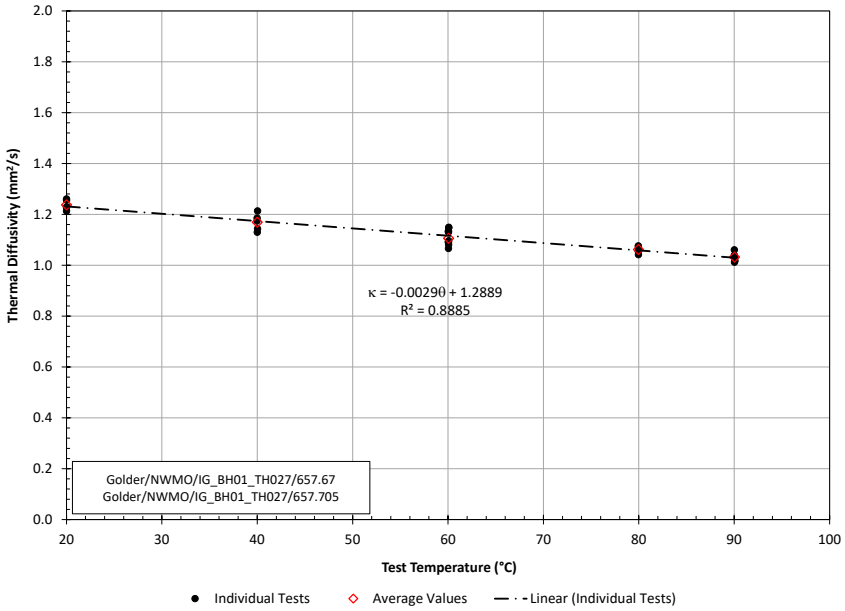
Average Temperature (°C)	Average Volumetric Specific Heat (MJ/m³°K)	Average Thermal Conductivity (W/m°K)	Average Thermal Diffusivity (mm²/s)
20.01	2.27	2.80	1.24
40.01	2.38	2.78	1.17
60.05	2.51	2.78	1.11
79.96	2.58	2.74	1.06
90.04	2.66	2.74	1.03
60.05	2.48	2.77	1.12

NOTE: Sample depths in the graph legends refer to the depth of the original sample as collected (part of the id), not the depth of the sub-samples





Test Specimen IG_BH01_TH027 – Depth = 657.67 m: Volumetric Heat Capacity and Thermal Conductivity



Test Specimen IG_BH01_TH027 – Depth = 657.67 m: Thermal Diffusivity

APPENDIX E

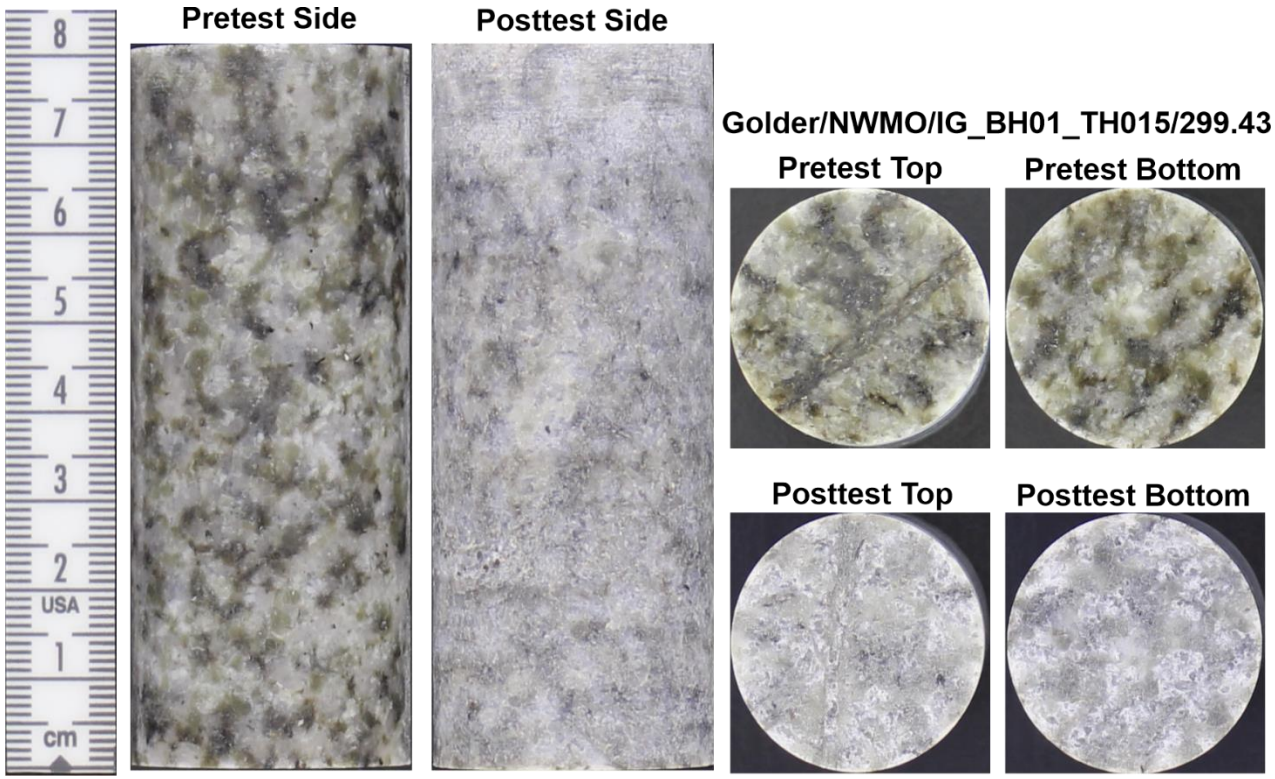
Thermal Expansion Tests: Test Data and Graphs

Table E-1: List of thermal expansion test specimens

Specimen No.	Depth (m)[1]	Rock Type	Page
IG_BH01_TH015[2]	299.43	Biotite Granodiorite-Tonalite	E-2
IG_BH01_TH016[2]	353.54	Biotite Granodiorite-Tonalite	E-4
IG_BH01_TH017[2]	401.95	Aplite Dyke	E-6
IG_BH01_TH018[2]	422.33	Biotite Granodiorite-Tonalite	E-8
IG_BH01_TH019[2]	448.22	Biotite Tonalite	E-10
IG_BH01_TH020[2]	451.57	Biotite Tonalite	E-12
IG_BH01_TH021[2]	457.06	Biotite Granodiorite-Tonalite	E-14
IG_BH01_TH022[2]	501.98	Biotite Granodiorite-Tonalite	E-16
IG_BH01_TH023[2]	529.63	Biotite Granodiorite-Tonalite	E-18
IG_BH01_TH024[2]	556.17	Biotite Granodiorite-Tonalite	E-20
IG_BH01_TH025[2]	561.20	Feldspar-phyric Tonalite Dyke	E-22
IG_BH01_TH026[2]	603.84	Biotite Granodiorite-Tonalite	E-24
IG_BH01_TH027[2]	657.79	Amphibolite	E-26

[1] Top depth of prepared sub-sample.

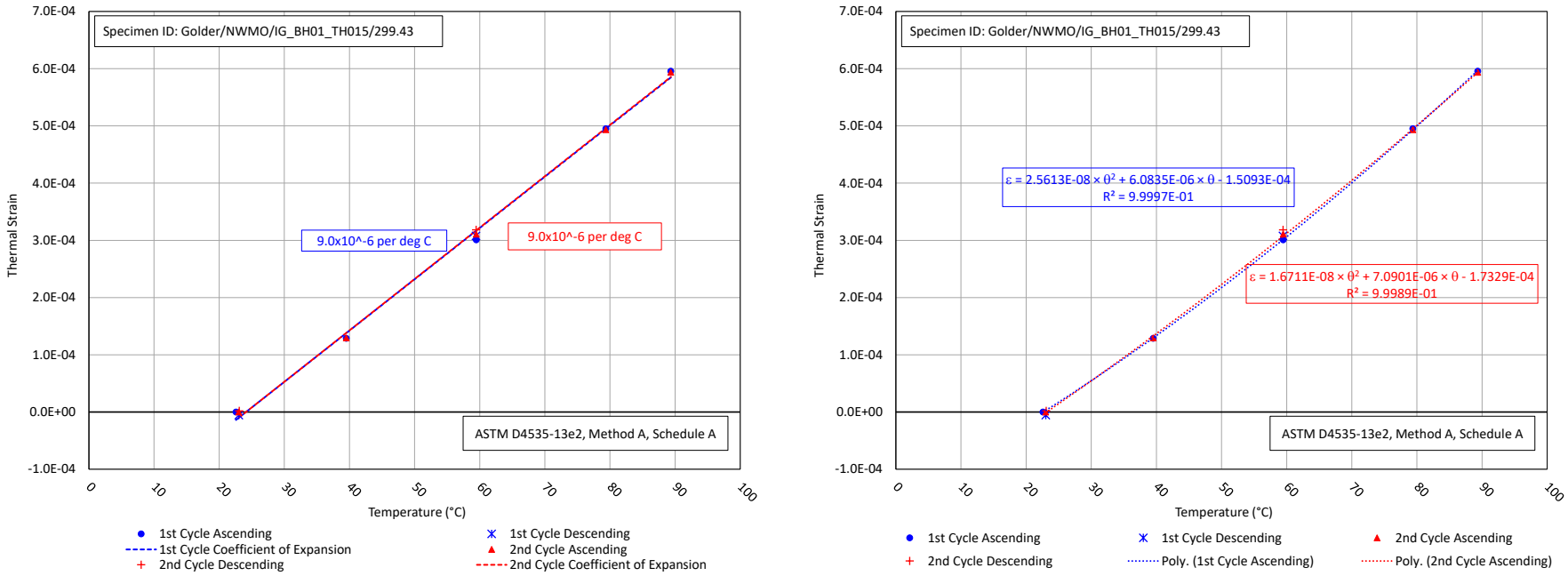
[2] Sample was saturated before testing.



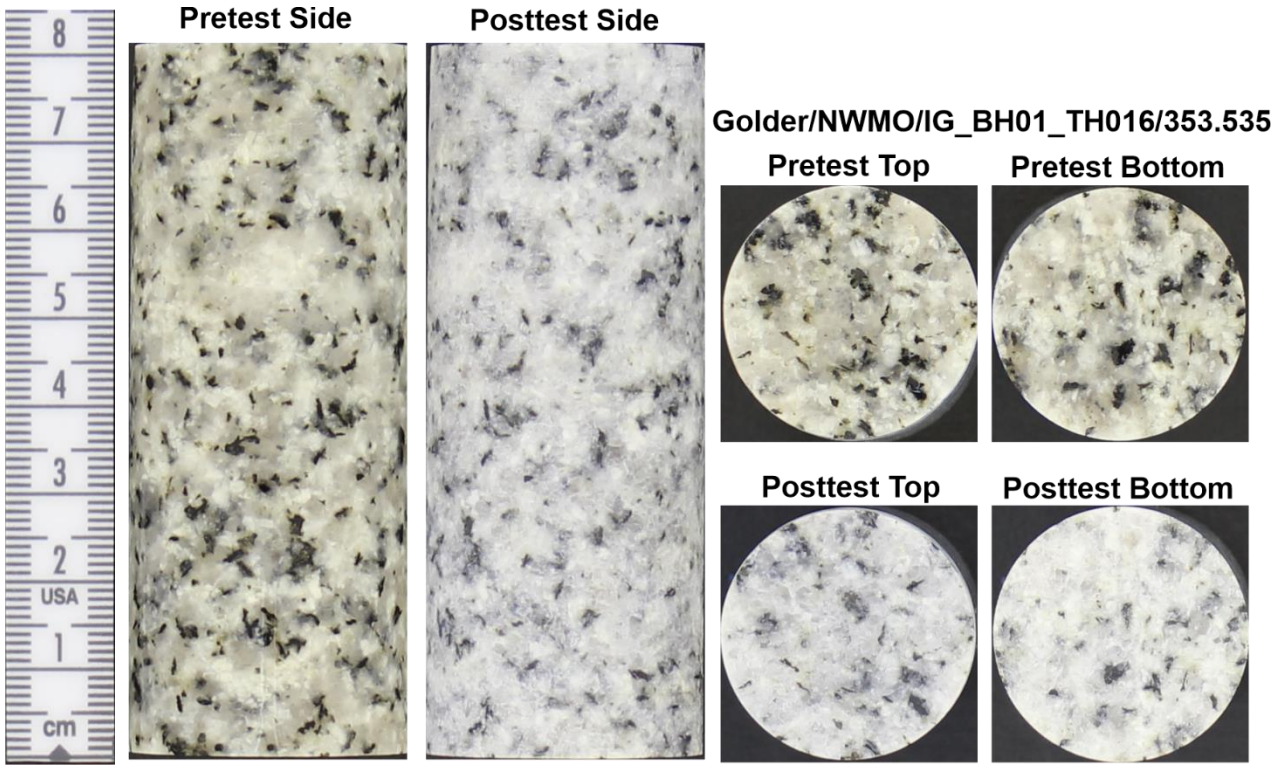
Test Specimen IG_BH01_TH015 – Depth = 299.43 m: specimen photographs

Table E-2: Thermal Expansion Results – Test Specimen IG_BH01_TH015 – Depth = 299.43 m

Average Temperature (°C)	Average Coeff. Linear Thermal Expansion – Linear (1/°K)	Coeff. Linear Thermal Expansion – Quadratic (1/°K)	Average Coeff. Linear Thermal Expansion – Linear (1/°K)	Coeff. Linear Thermal Expansion – Quadratic (1/°K)
	1st Temperature Cycle		2nd Temperature Cycle	
20	8.97E-06	7.11E-06	8.98E-06	7.76E-06
40		8.13E-06		8.43E-06
60		9.16E-06		9.10E-06
80		1.02E-05		9.76E-06
90		1.07E-05		1.01E-05



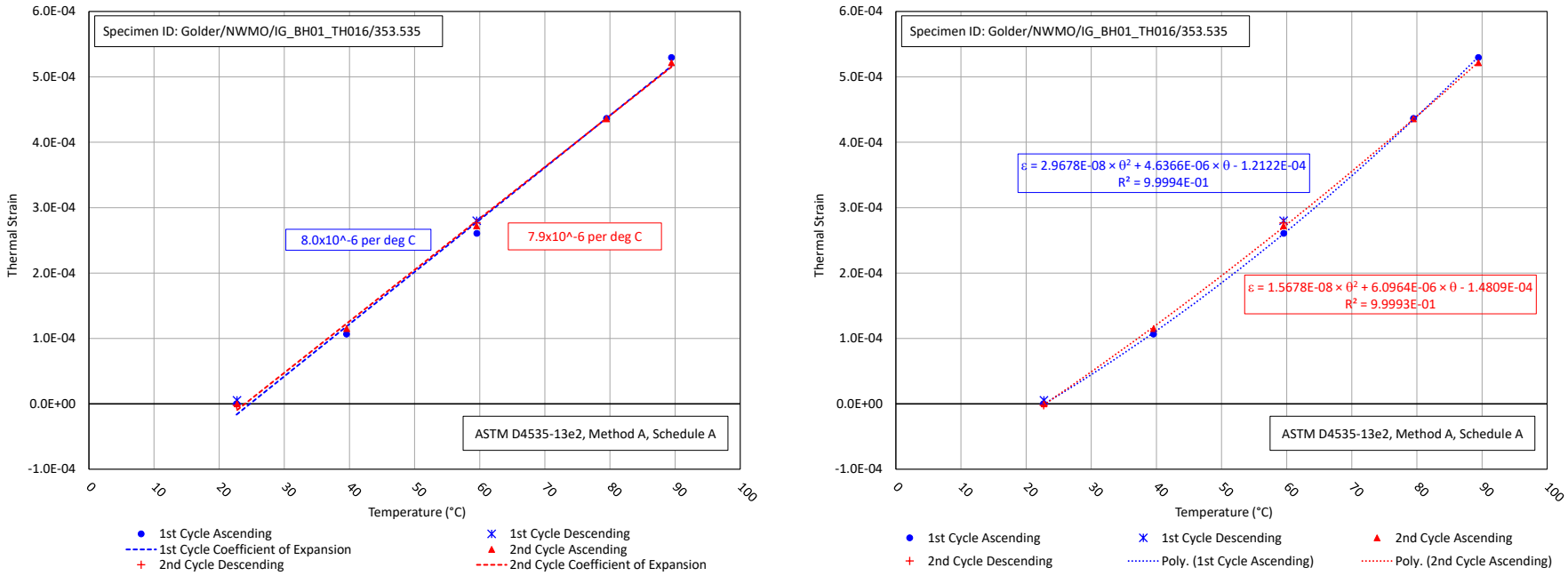
Test Specimen IG_BH01_TH015 – Depth = 299.43 m: Linear fit and quadratic fit for the thermal expansion data



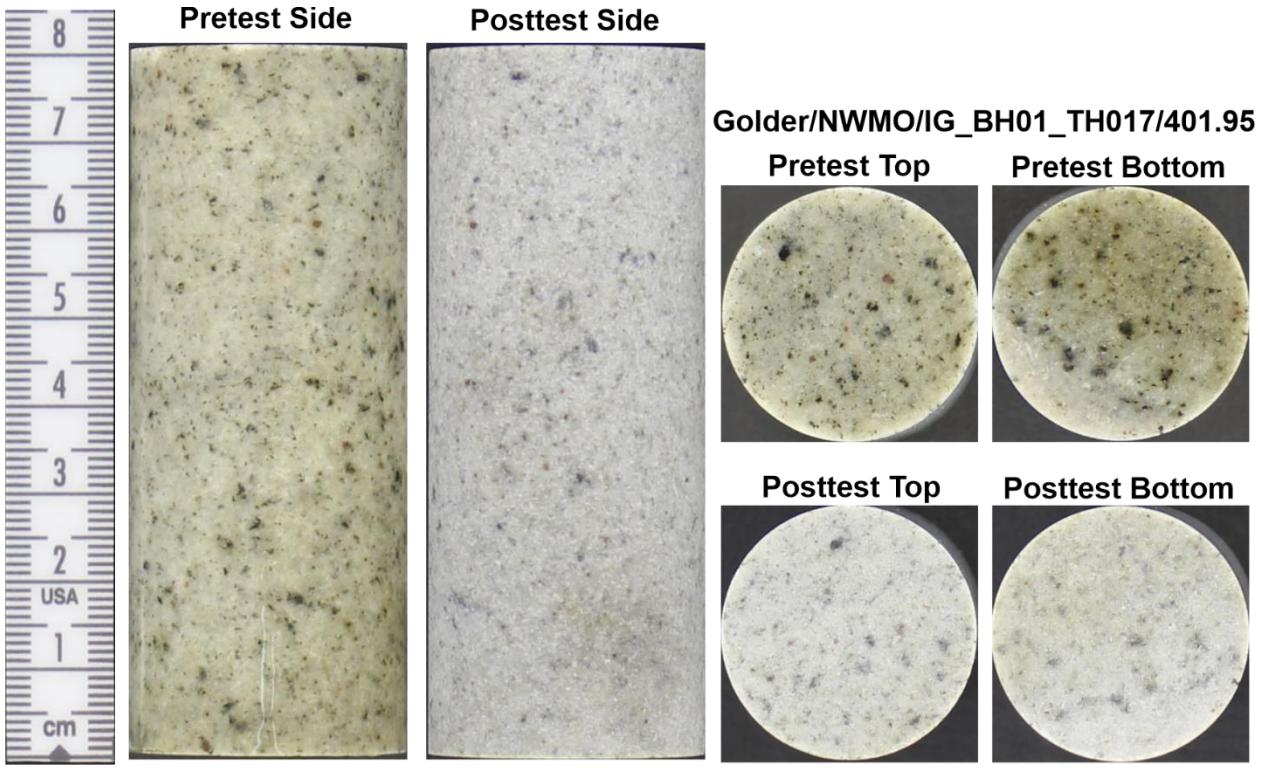
Test Specimen IG_BH01_TH016 – Depth = 353.535 m: specimen photographs

Table E-3: Thermal Expansion Results – Test Specimen IG_BH01_TH016 – Depth = 353.535 m

Average Temperature (°C)	Average Coeff. Linear Thermal Expansion – Linear (1/°K)	Coeff. Linear Thermal Expansion – Quadratic (1/°K)	Average Coeff. Linear Thermal Expansion – Linear (1/°K)	Coeff. Linear Thermal Expansion – Quadratic (1/°K)
	1st Temperature Cycle		2nd Temperature Cycle	
20	7.98E-06	5.82E-06	7.87E-06	6.72E-06
40		7.01E-06		7.35E-06
60		8.20E-06		7.98E-06
80		9.39E-06		8.60E-06
90		9.98E-06		8.92E-06



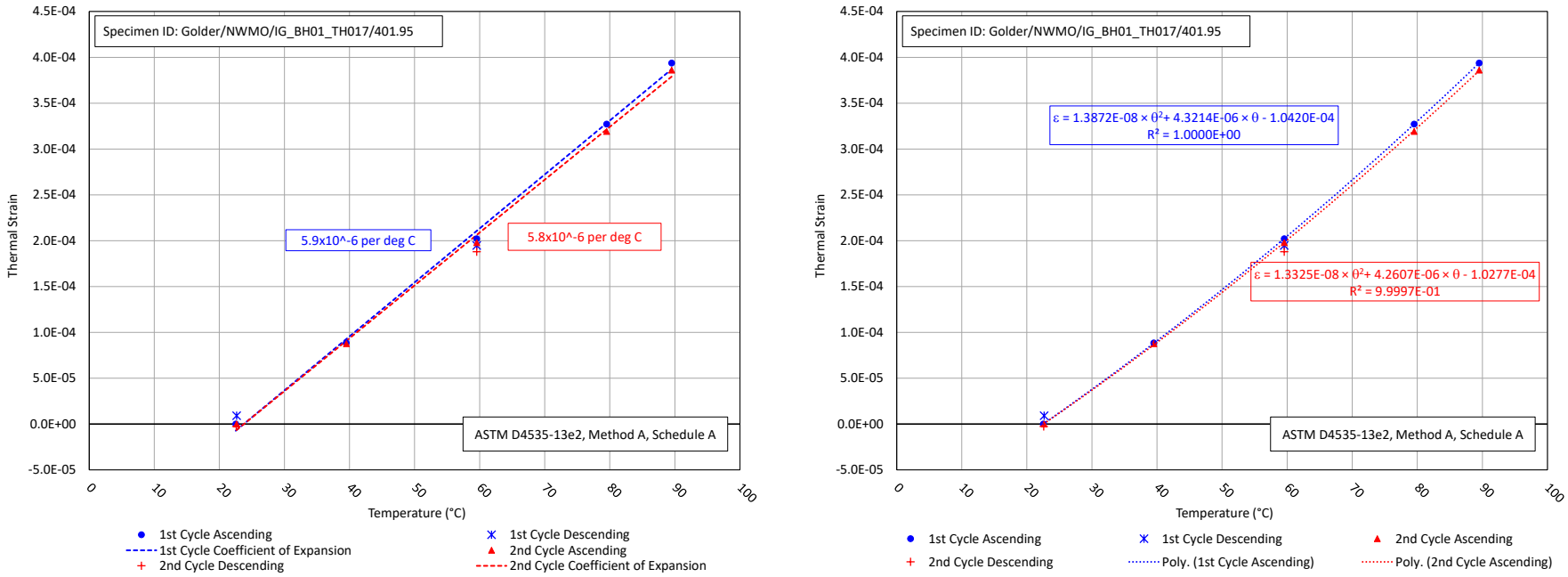
Test Specimen IG_BH01_TH016 – Depth = 353.535 m: Linear fit and quadratic fit for the thermal expansion data



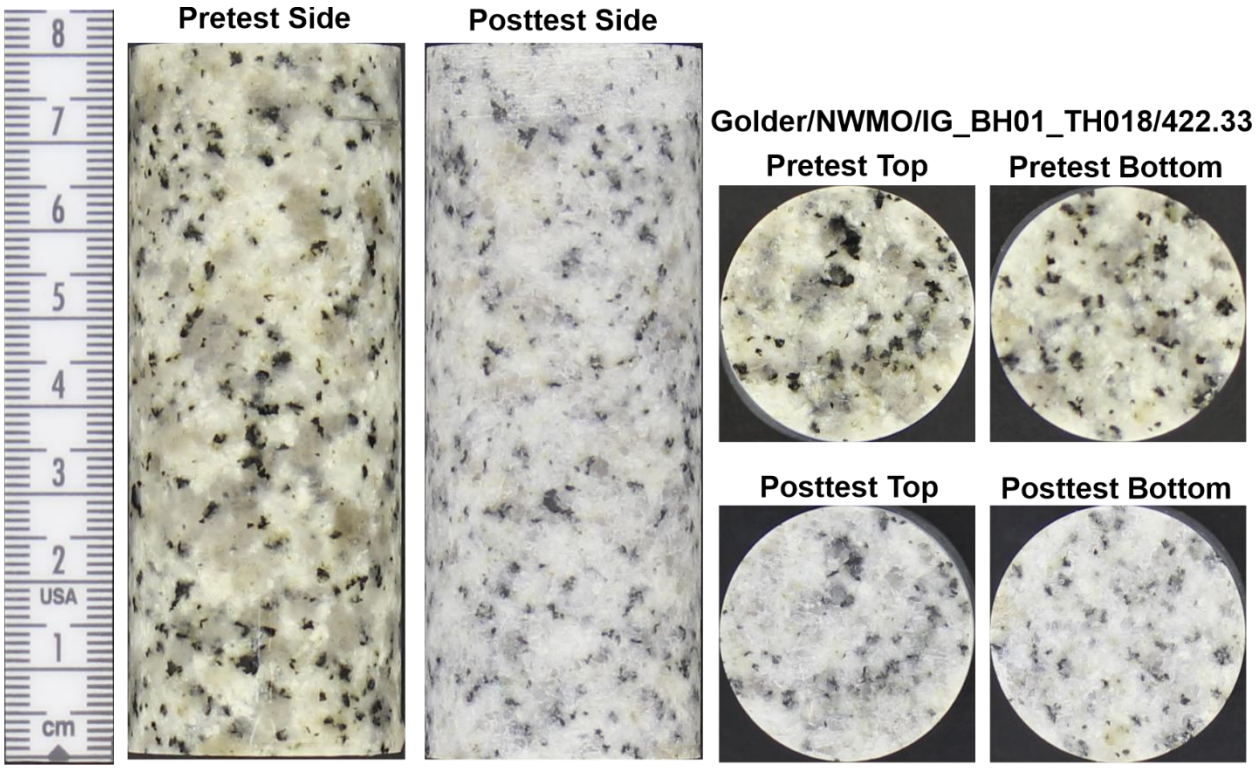
Test Specimen IG_BH01_TH017 – Depth = 401.95 m: specimen photographs

Table E-4: Thermal Expansion Results – Test Specimen IG_BH01_TH017 – Depth = 401.95 m

Average Temperature (°C)	Average Coeff. Linear Thermal Expansion – Linear (1/°K)	Coeff. Linear Thermal Expansion – Quadratic (1/°K)	Average Coeff. Linear Thermal Expansion – Linear (1/°K)	Coeff. Linear Thermal Expansion – Quadratic (1/°K)
	1st Temperature Cycle		2nd Temperature Cycle	
20	5.88E-06	4.88E-06	5.76E-06	4.79E-06
40		5.43E-06		5.33E-06
60		5.99E-06		5.86E-06
80		6.54E-06		6.39E-06
90		6.82E-06		6.66E-06



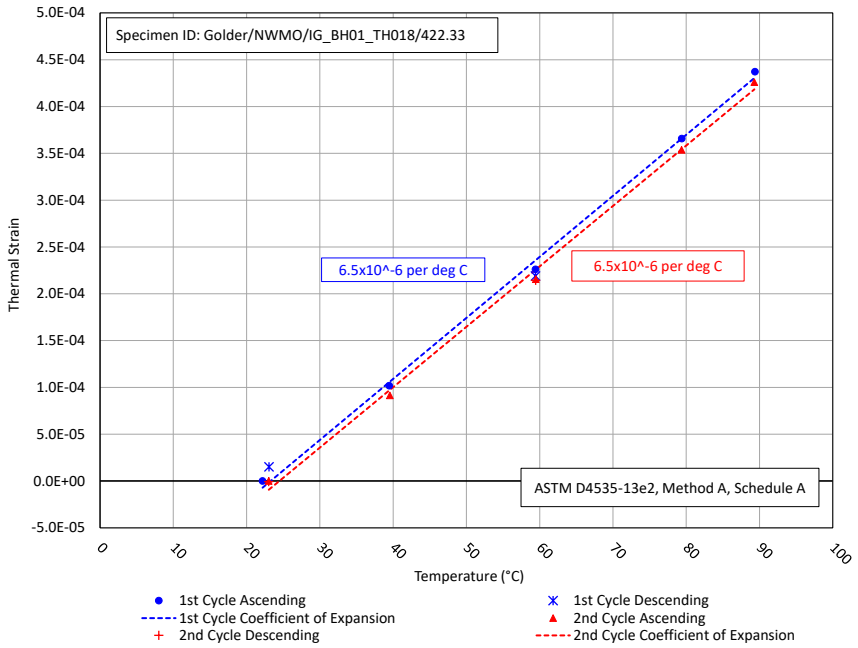
Test Specimen IG_BH01_TH017 – Depth = 401.95 m: Linear fit and quadratic fit for the thermal expansion data

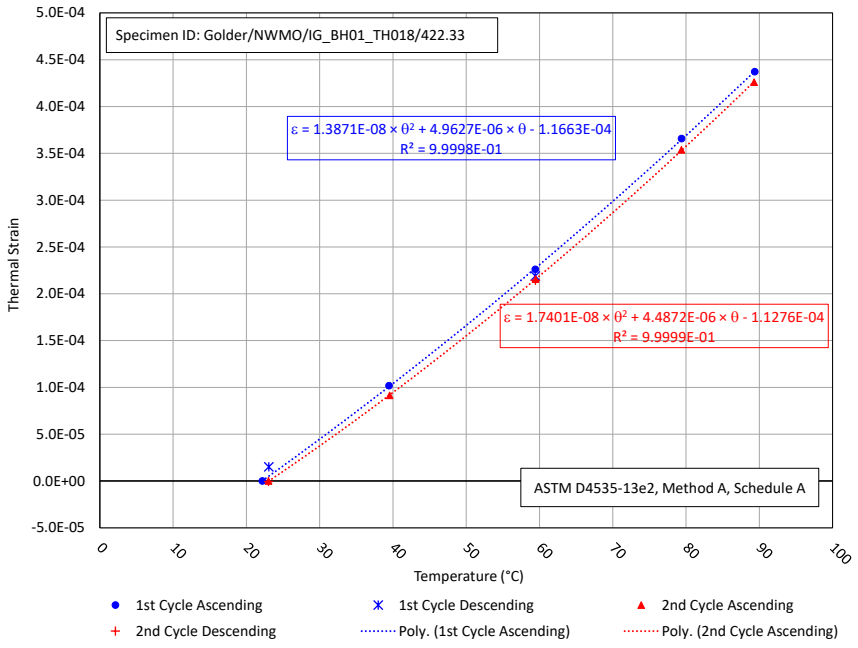


Test Specimen IG_BH01_TH018 – Depth = 422.33 m: specimen photographs

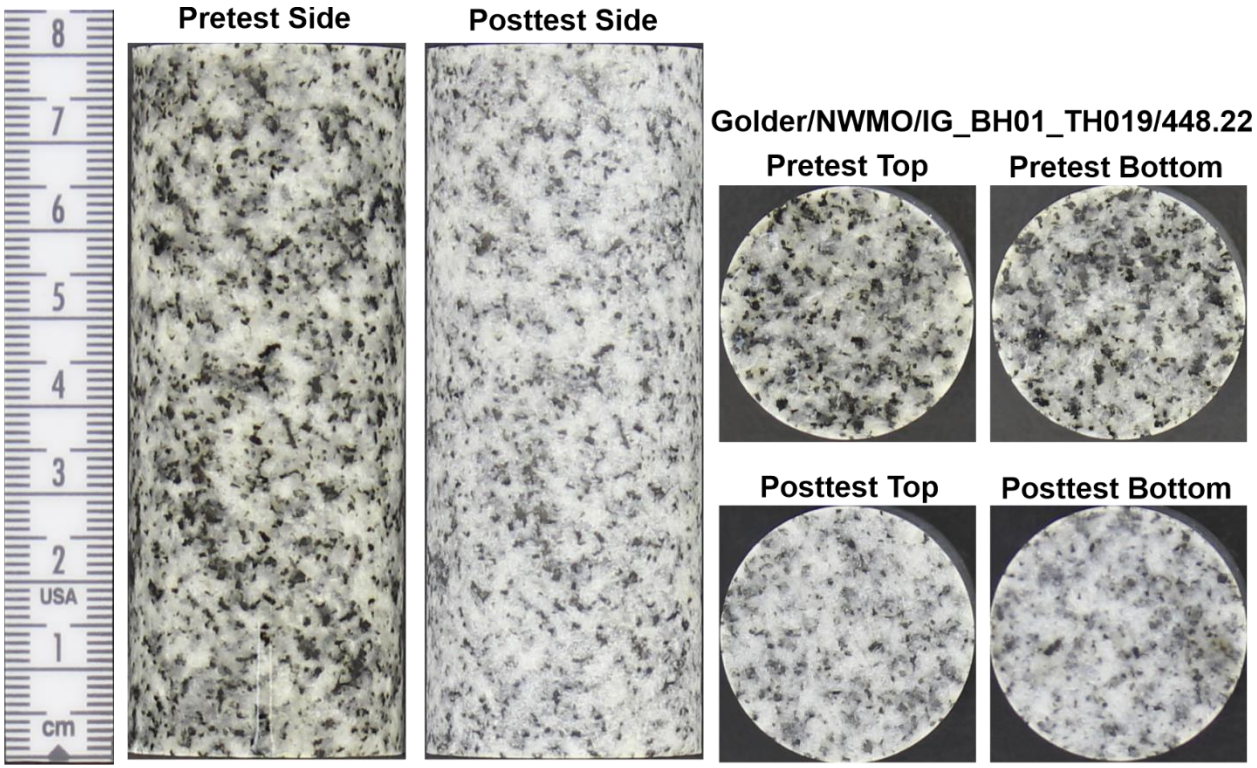
Table E-5: Thermal Expansion Results – Test Specimen IG_BH01_TH018 – Depth = 422.33 m

Average Temperature (°C)	Average Coeff. Linear Thermal Expansion – Linear (1/°K)	Coeff. Linear Thermal Expansion – Quadratic (1/°K)	Average Coeff. Linear Thermal Expansion – Linear (1/°K)	Coeff. Linear Thermal Expansion – Quadratic (1/°K)
	1st Temperature Cycle		2nd Temperature Cycle	
20	6.52E-06	5.52E-06	6.45E-06	5.18E-06
40		6.07E-06		5.88E-06
60		6.63E-06		6.58E-06
80		7.18E-06		7.27E-06
90		7.46E-06		7.62E-06





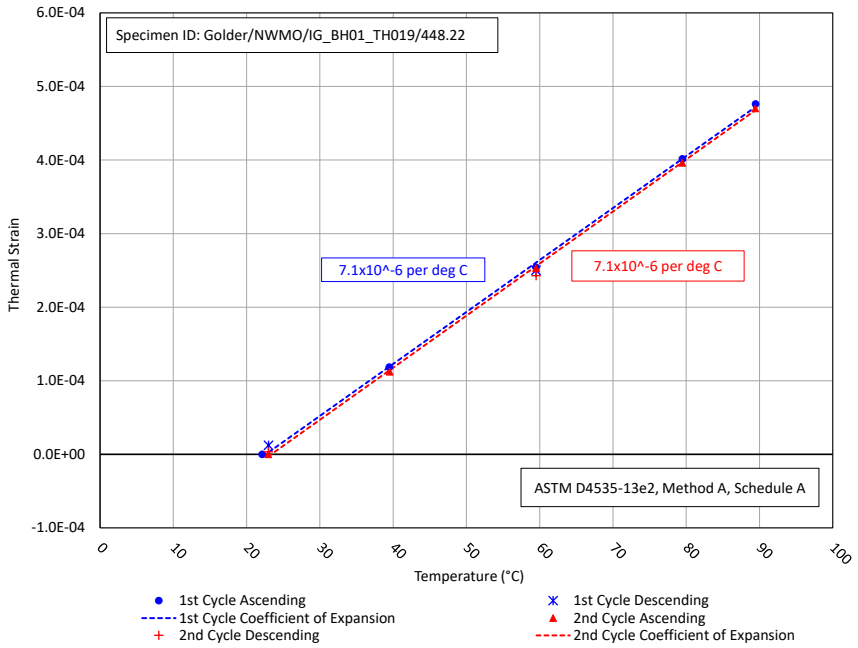
Test Specimen IG_BH01_TH018 – Depth = 422.33 m: Linear fit and quadratic fit for the thermal expansion data

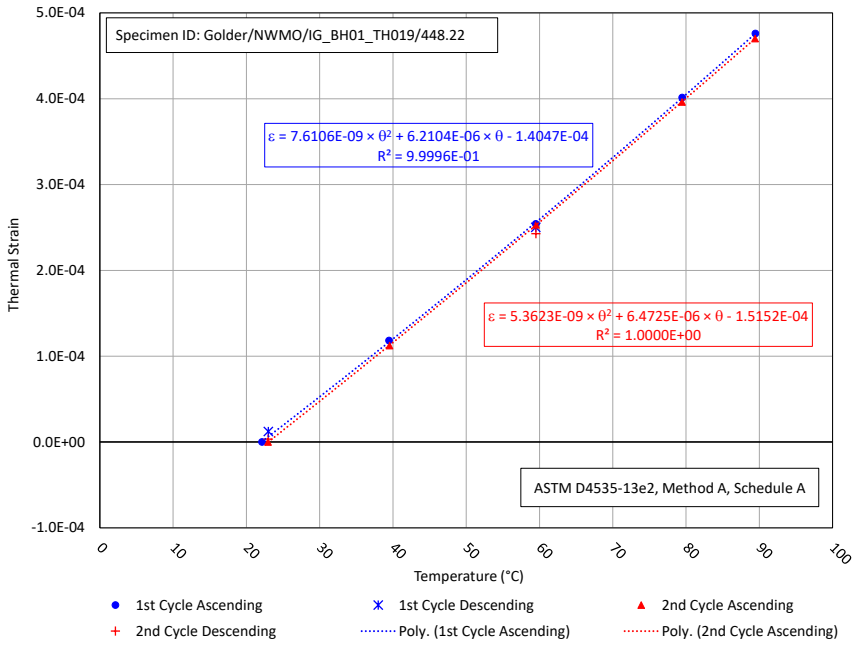


Test Specimen IG_BH01_TH019 – Depth = 448.22 m: specimen photographs

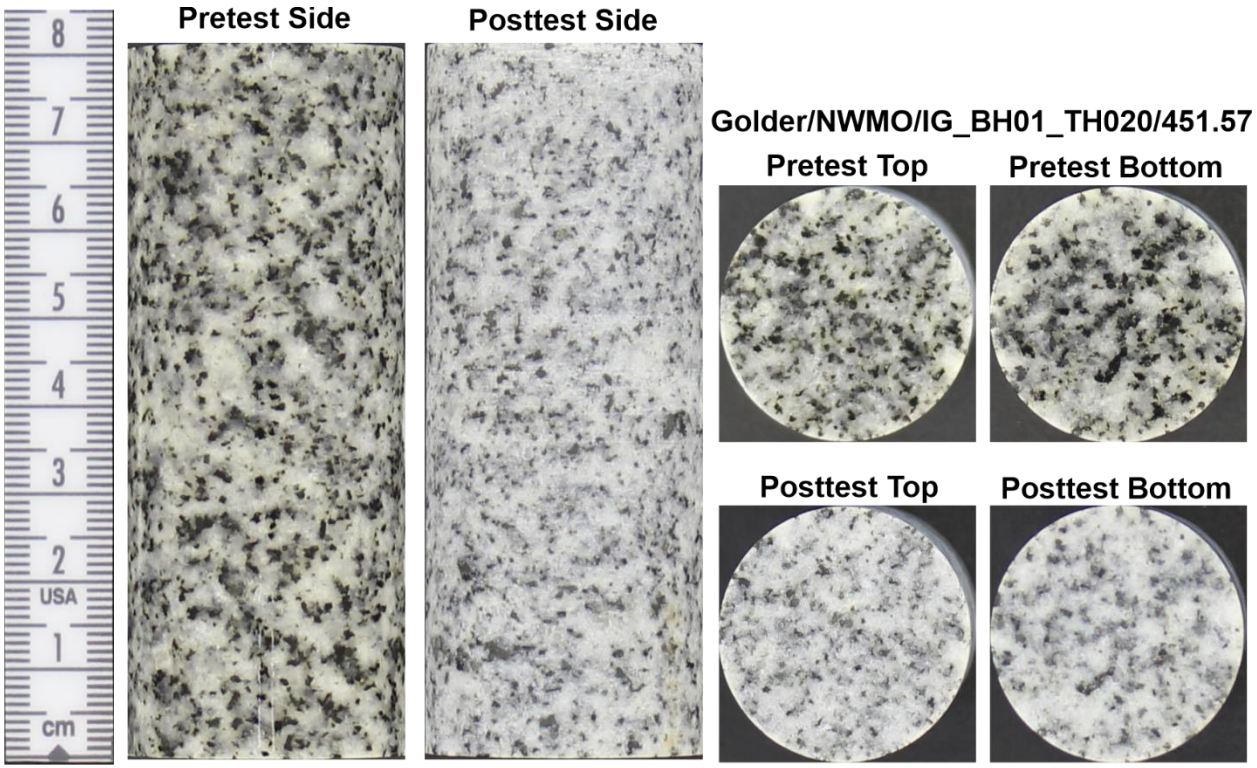
Table E-6: Thermal Expansion Results – Test Specimen IG_BH01_TH019 – Depth = 448.22 m

Average Temperature (°C)	Average Coeff. Linear Thermal Expansion – Linear (1/°K)	Coeff. Linear Thermal Expansion – Quadratic (1/°K)	Average Coeff. Linear Thermal Expansion – Linear (1/°K)	Coeff. Linear Thermal Expansion – Quadratic (1/°K)
	1st Temperature Cycle		2nd Temperature Cycle	
20	7.06E-06	6.51E-06	7.08E-06	6.69E-06
40		6.82E-06		6.90E-06
60		7.12E-06		7.12E-06
80		7.43E-06		7.33E-06
90		7.58E-06		7.44E-06





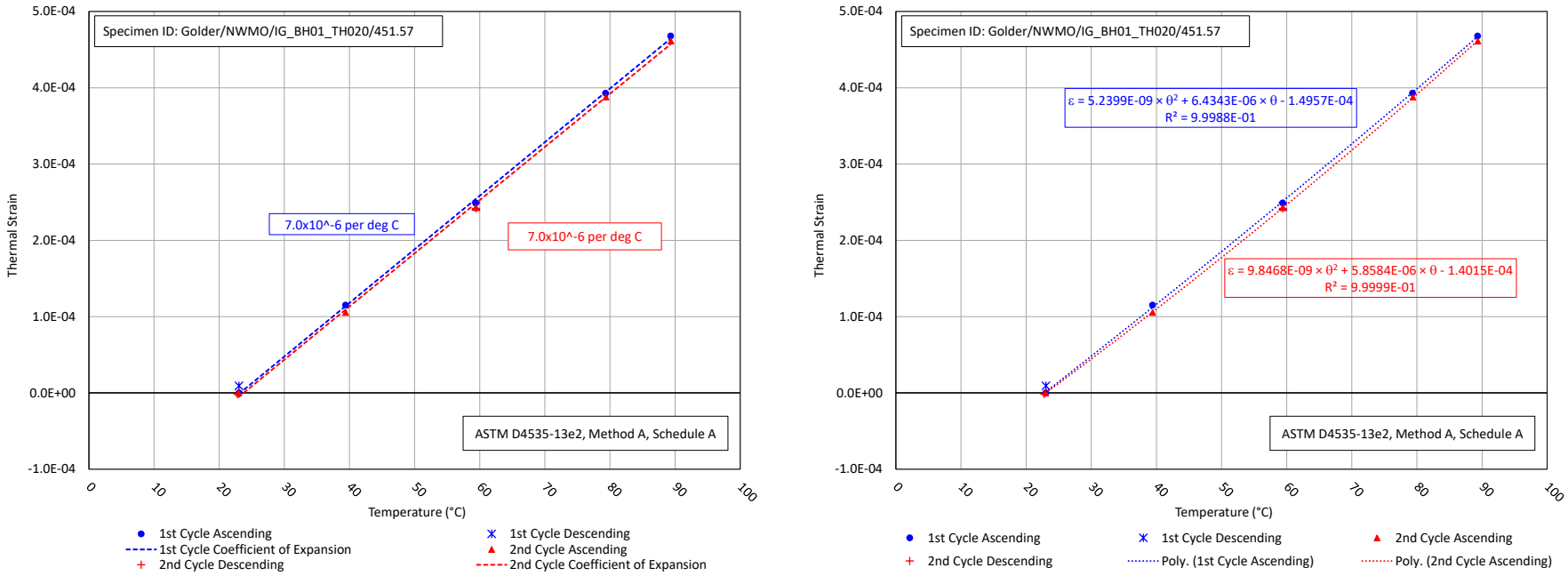
Test Specimen IG_BH01_TH019 – Depth = 448.22 m: Linear fit and quadratic fit for the thermal expansion data



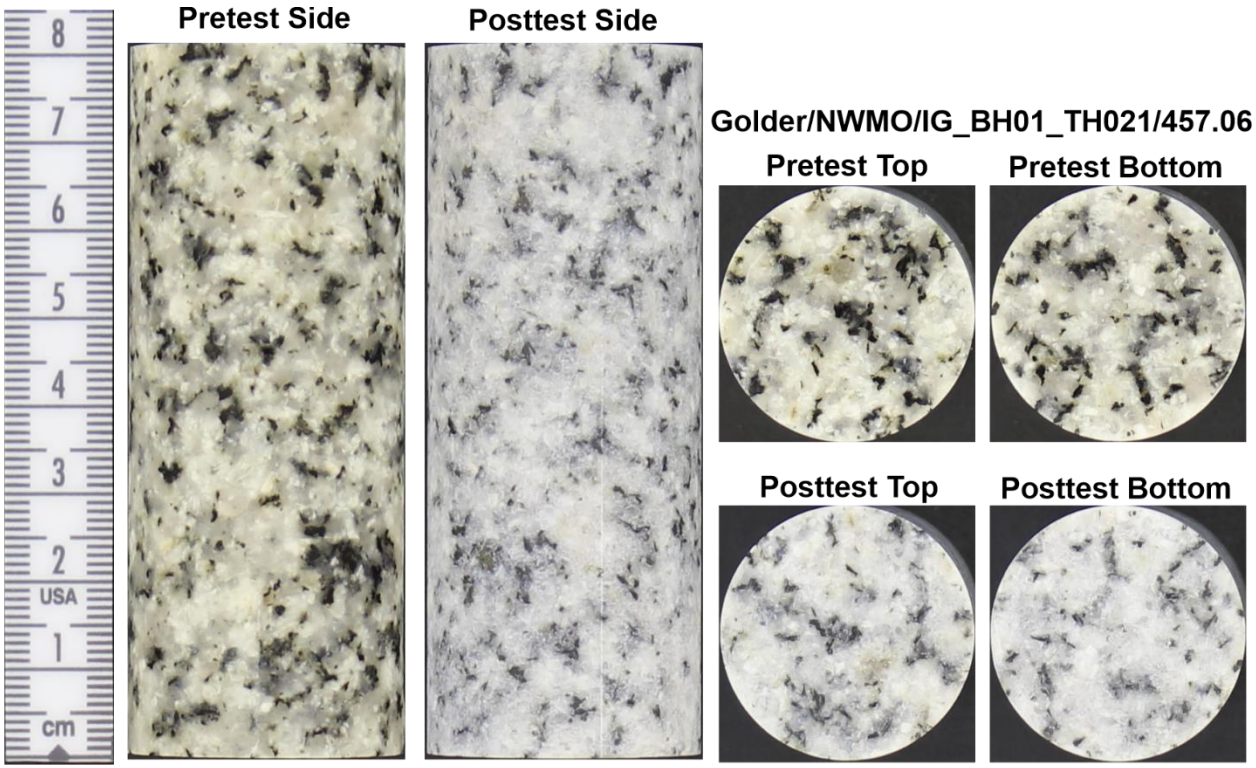
Test Specimen IG_BH01_TH020 – Depth = 451.57 m: specimen photographs

Table E-7: Thermal Expansion Results – Test Specimen IG_BH01_TH020 – Depth = 451.57 m

Average Temperature (°C)	Average Coeff. Linear Thermal Expansion – Linear (1/°K)	Coeff. Linear Thermal – Quadratic Expansion (1/°K)	Average Coeff. Linear Thermal Expansion – Linear (1/°K)	Coeff. Linear Thermal – Quadratic Expansion (1/°K)
	1st Temperature Cycle		2nd Temperature Cycle	
20	7.03E-06	6.64E-06	6.97E-06	6.25E-06
40		6.85E-06		6.65E-06
60		7.06E-06		7.04E-06
80		7.27E-06		7.43E-06
90		7.38E-06		7.63E-06



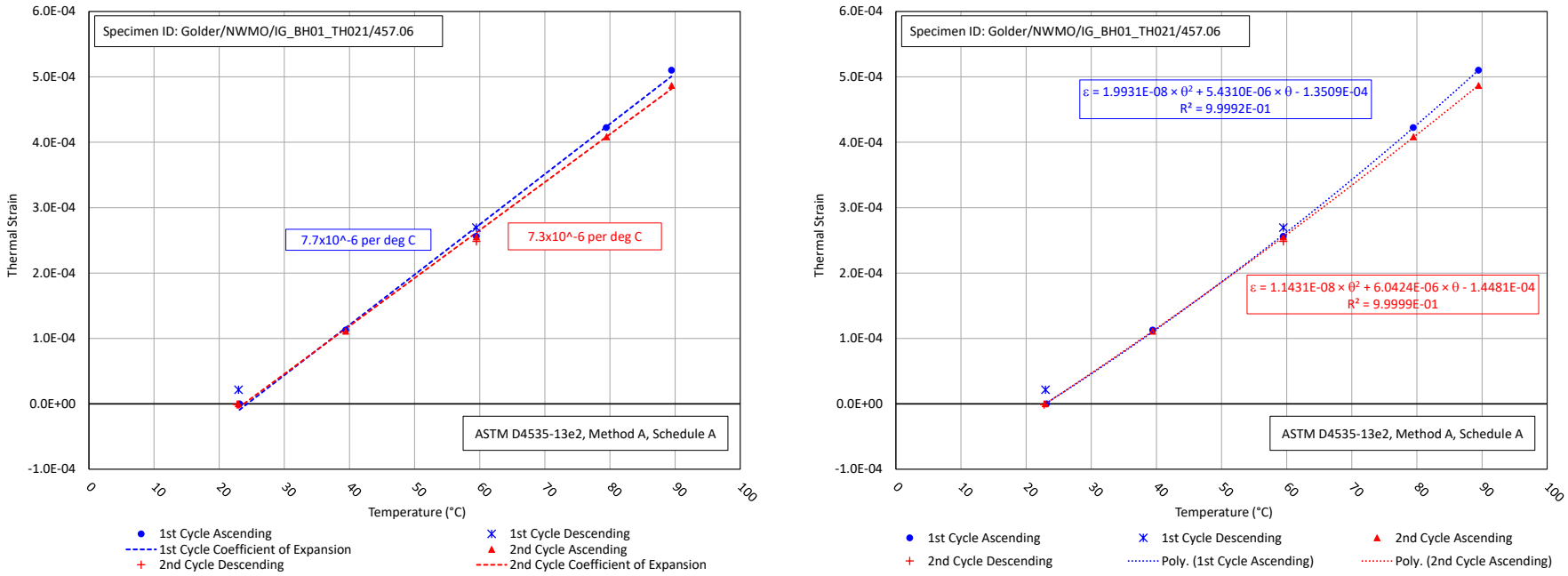
Test Specimen IG_BH01_TH020 – Depth = 451.57 m: Linear fit and quadratic fit for the thermal expansion data



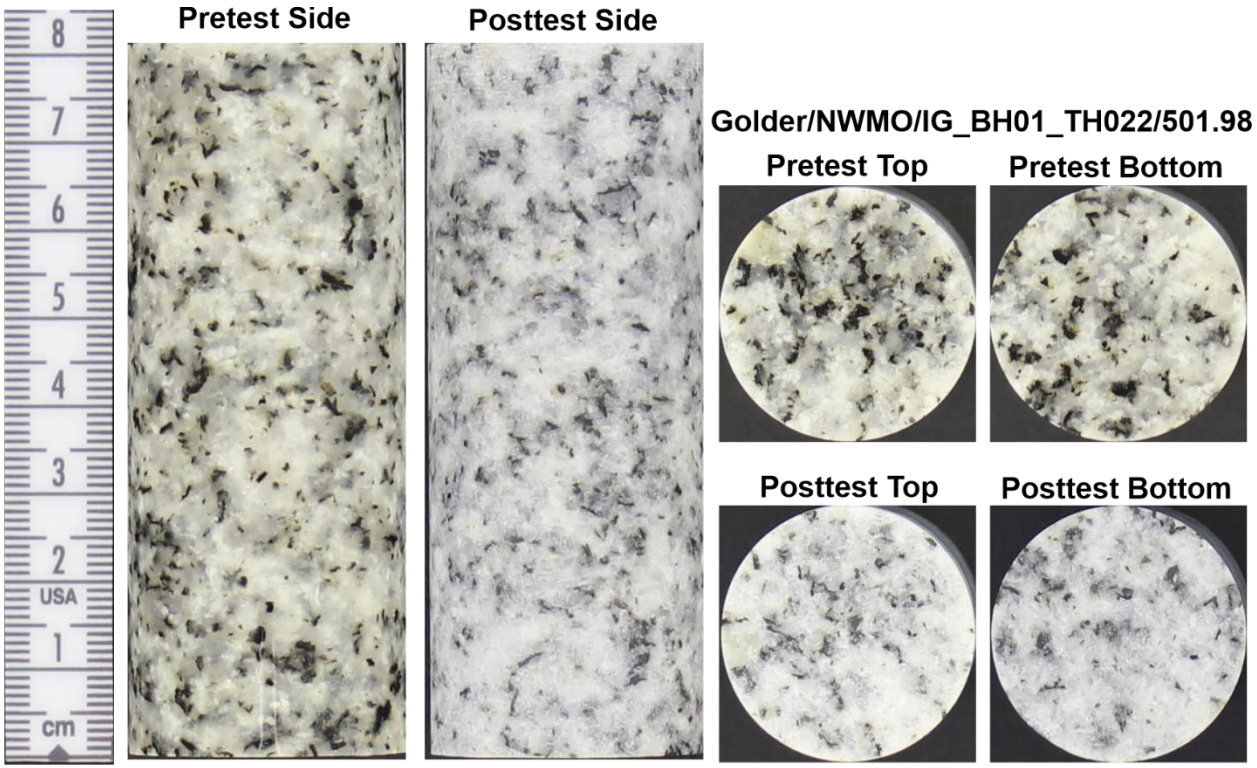
Test Specimen IG_BH01_TH021 – Depth = 457.06 m: specimen photographs

Table E-8: Thermal Expansion Results – Test Specimen IG_BH01_TH021 – Depth = 457.06 m

Average Temperature (°C)	Average Coeff. Linear Thermal Expansion – Linear (1/°K)	Coeff. Linear Thermal Expansion – Quadratic (1/°K)	Average Coeff. Linear Thermal Expansion – Linear (1/°K)	Coeff. Linear Thermal Expansion – Quadratic (1/°K)
	1st Temperature Cycle		2nd Temperature Cycle	
20	7.69E-06	6.23E-06	7.33E-06	6.50E-06
40		7.03E-06		6.96E-06
60		7.82E-06		7.41E-06
80		8.62E-06		7.87E-06
90		9.02E-06		8.10E-06



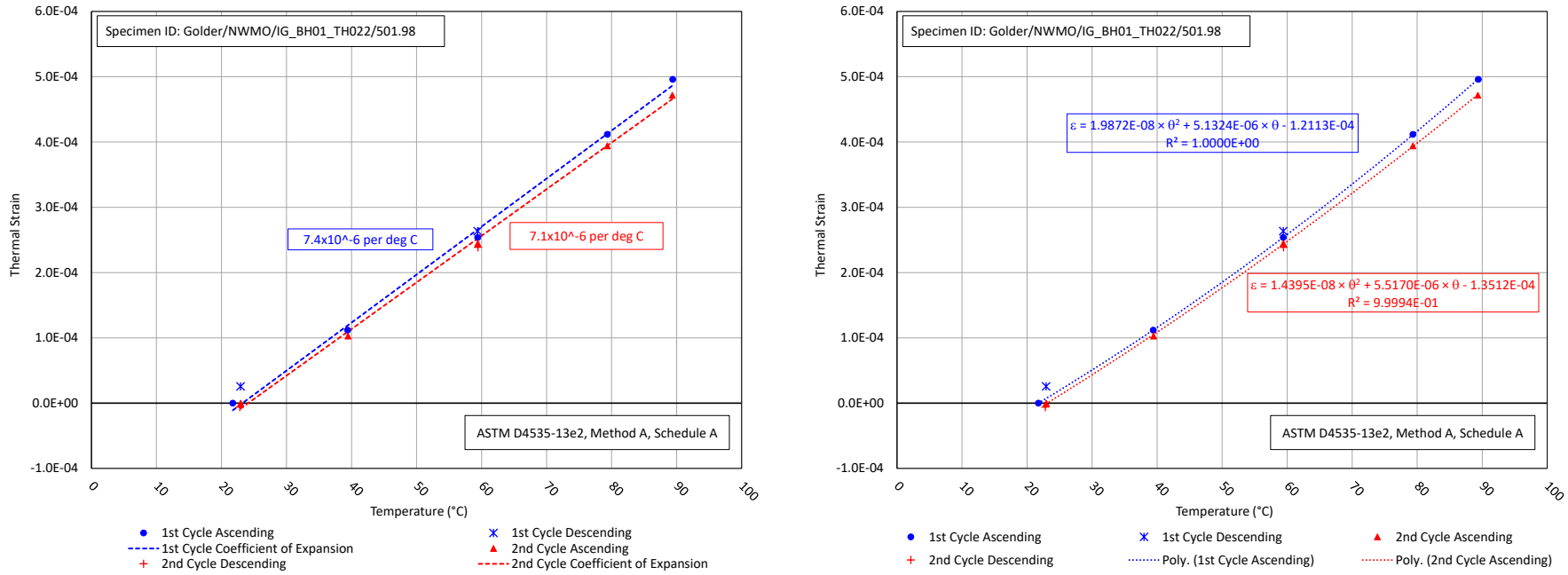
Test Specimen IG_BH01_TH021 – Depth = 457.06 m: Linear fit and quadratic fit for the thermal expansion data



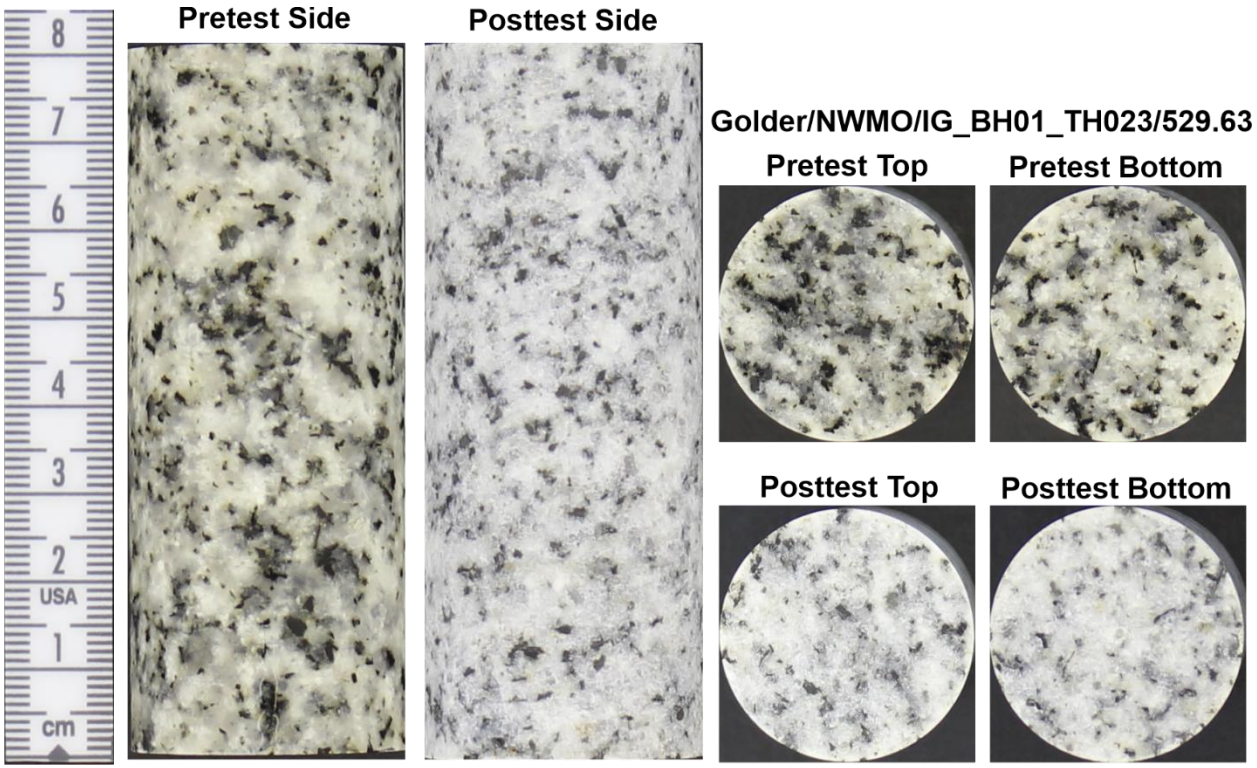
Test Specimen IG_BH01_TH022 – Depth = 501.98 m: specimen photographs

TableE-9: Thermal Expansion Results – Test Specimen IG_BH01_TH022 – Depth = 501.98 m

Average Temperature (°C)	Average Coeff. Linear Thermal Expansion – Linear (1/°K)	Coeff. Linear Thermal Expansion – Quadratic (1/°K)	Average Coeff. Linear Thermal Expansion – Linear (1/°K)	Coeff. Linear Thermal Expansion – Quadratic (1/°K)
	1st Temperature Cycle		2nd Temperature Cycle	
20	7.35E-06	5.93E-06	7.14E-06	6.09E-06
40		6.72E-06		6.67E-06
60		7.52E-06		7.24E-06
80		8.31E-06		7.82E-06
90		8.71E-06		8.11E-06



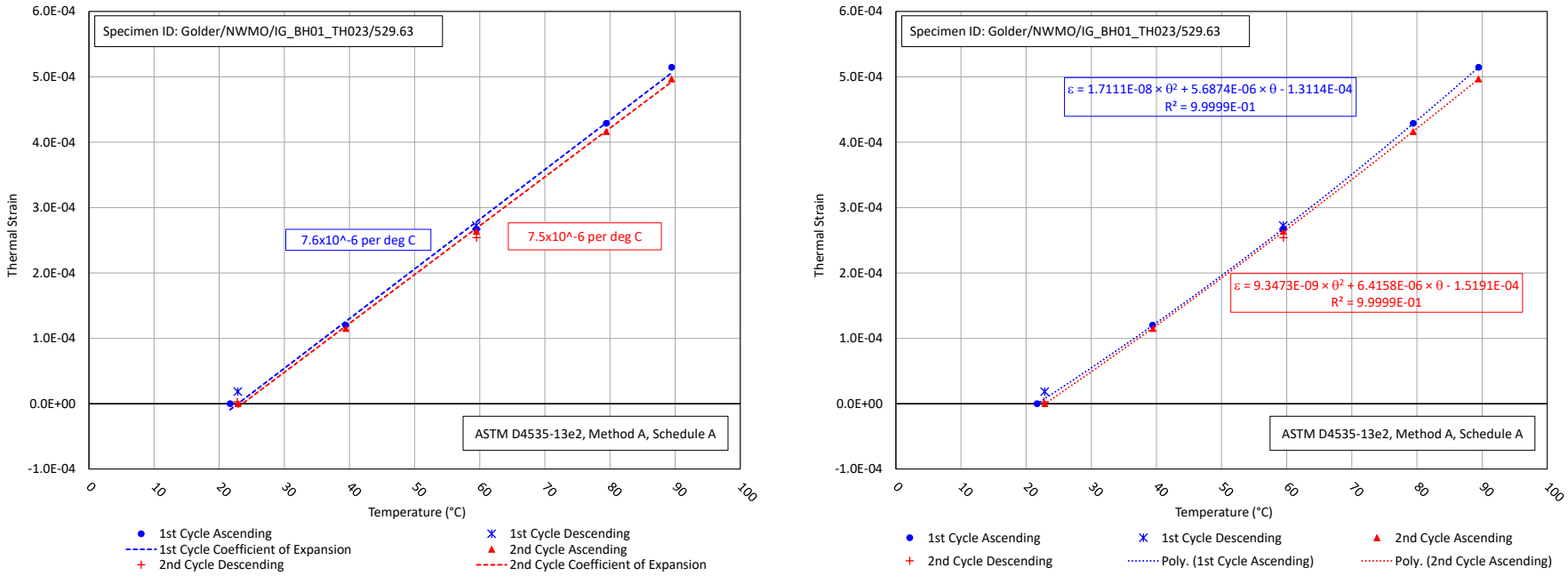
Test Specimen IG_BH01_TH022 – Depth = 501.98 m: Linear fit and quadratic fit for the thermal expansion data



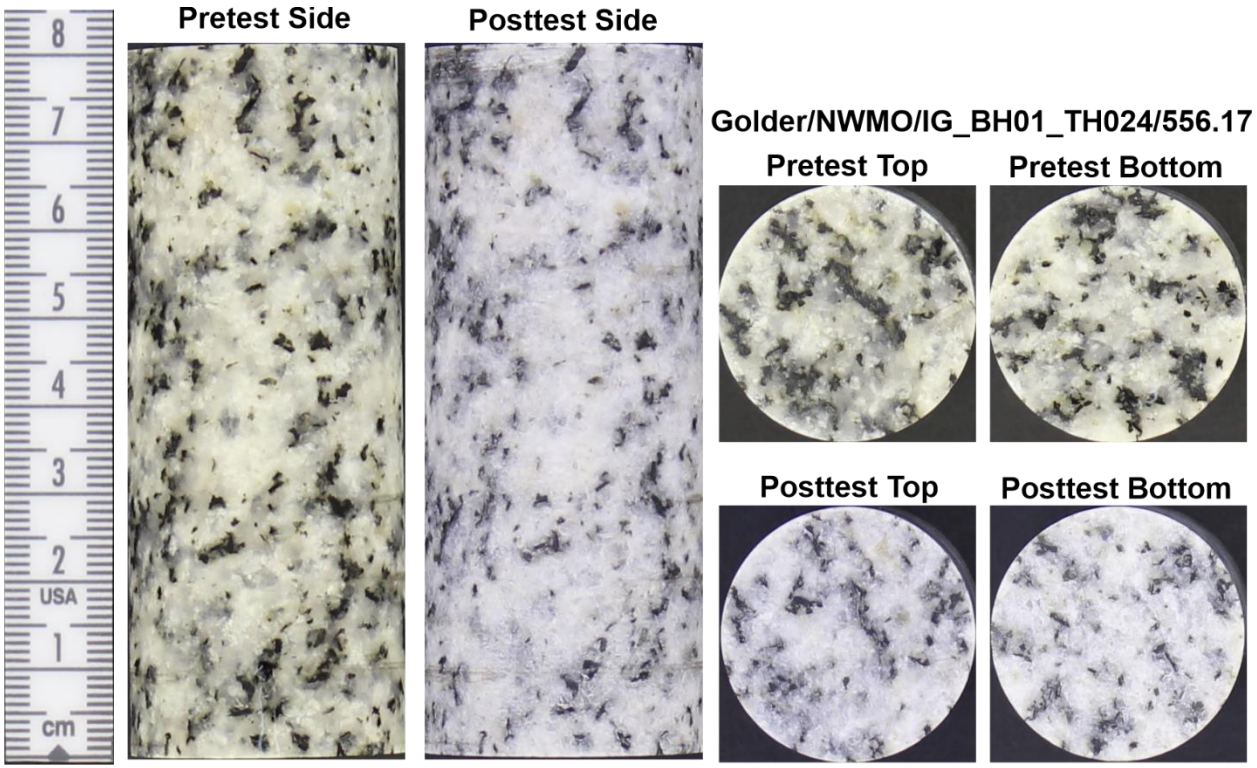
Test Specimen IG_BH01_TH023 – Depth = 529.63 m: specimen photographs

Table E-10: Thermal Expansion Results – Test Specimen IG_BH01_TH023 – Depth = 529.63 m

Average Temperature (°C)	Average Coeff. Linear Thermal Expansion – Linear (1/°K)	Coeff. Linear Thermal Expansion – Quadratic (1/°K)	Average Coeff. Linear Thermal Expansion – Linear (1/°K)	Coeff. Linear Thermal Expansion – Quadratic (1/°K)
	1st Temperature Cycle		2nd Temperature Cycle	
20	7.60E-06	6.37E-06	7.47E-06	6.79E-06
40		7.06E-06		7.16E-06
60		7.74E-06		7.54E-06
80		8.43E-06		7.91E-06
90		8.77E-06		8.10E-06



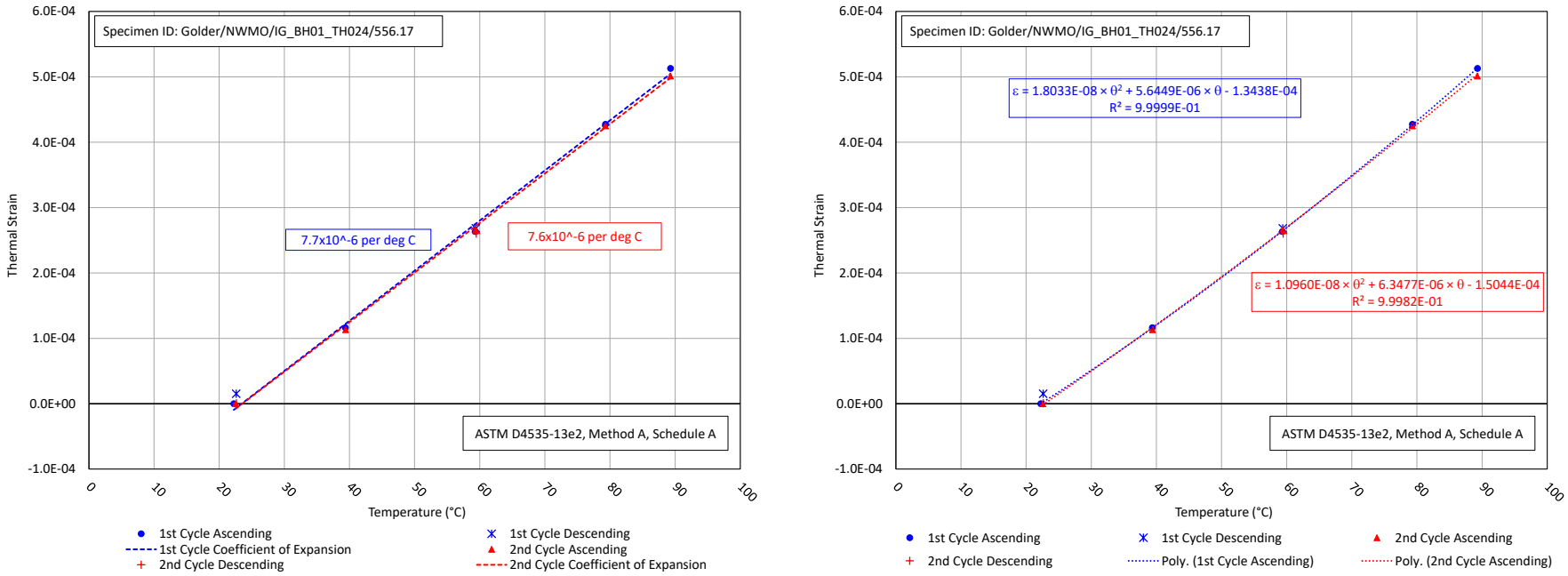
Test Specimen IG_BH01_TH023 – Depth = 529.63 m: Linear fit and quadratic fit for the thermal expansion data



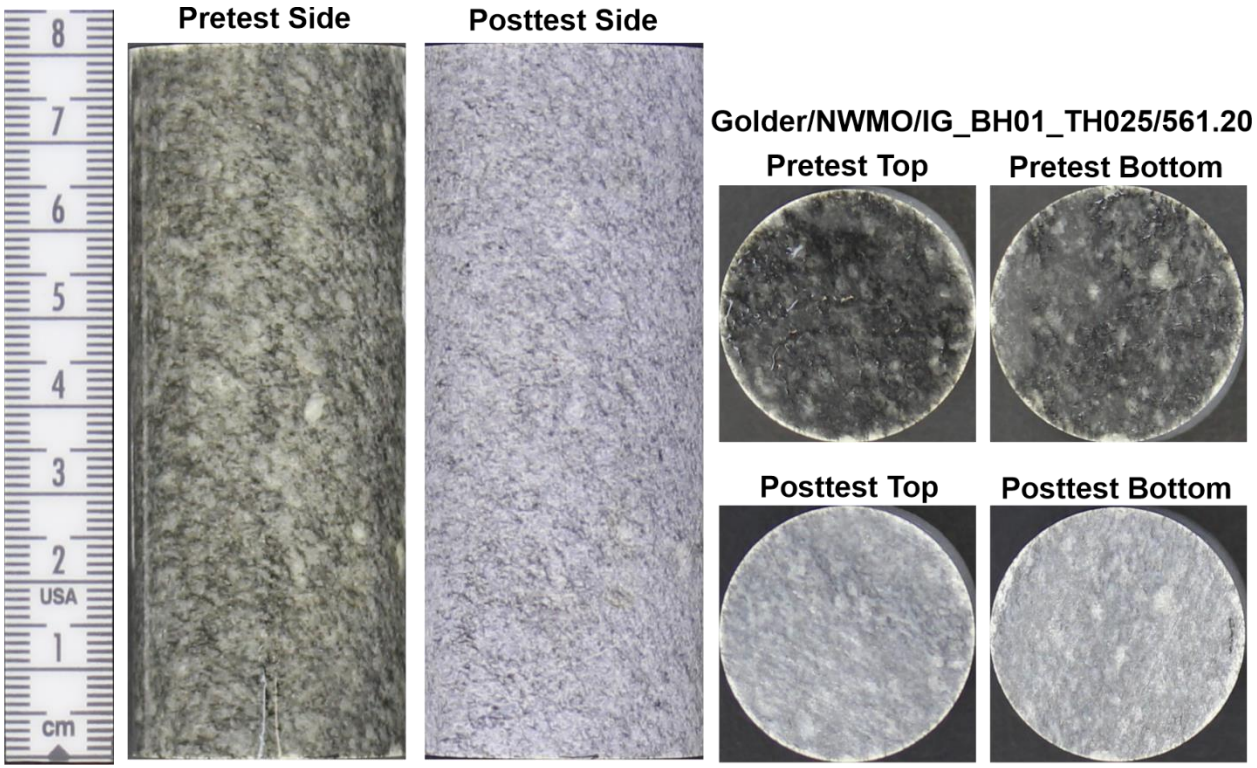
Test Specimen IG_BH01_TH024 – Depth = 556.17 m: specimen photographs

Table E-11: Thermal Expansion Results – Test Specimen IG_BH01_TH024 – Depth = 556.17 m

Average Temperature (°C)	Average Coeff. Linear Thermal Expansion – Linear (1/°K)	Coeff. Linear Thermal Expansion – Quadratic (1/°K)	Average Coeff. Linear Thermal Expansion – Linear (1/°K)	Coeff. Linear Thermal Expansion – Quadratic (1/°K)
	1st Temperature Cycle		2nd Temperature Cycle	
20	7.67E-06	6.37E-06	7.58E-06	6.79E-06
40		7.09E-06		7.22E-06
60		7.81E-06		7.66E-06
80		8.53E-06		8.10E-06
90		8.89E-06		8.32E-06



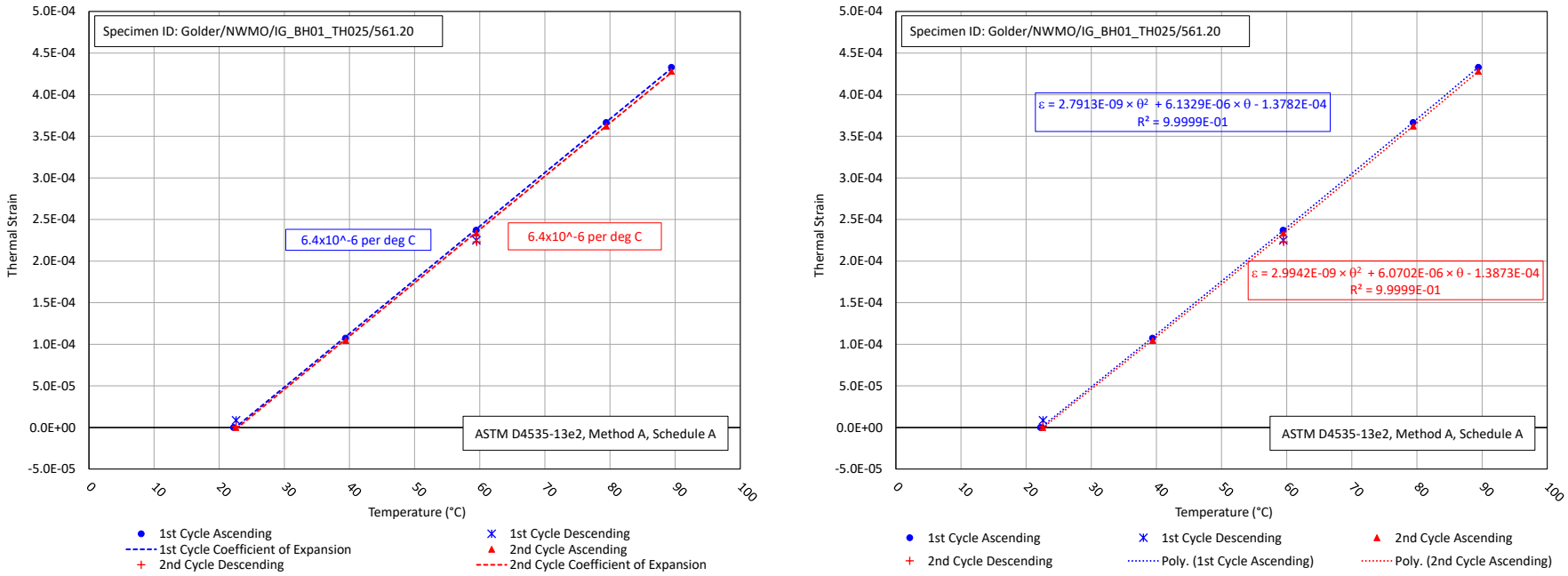
Test Specimen IG_BH01_TH024 – Depth = 556.17 m: Linear fit and quadratic fit for the thermal expansion data



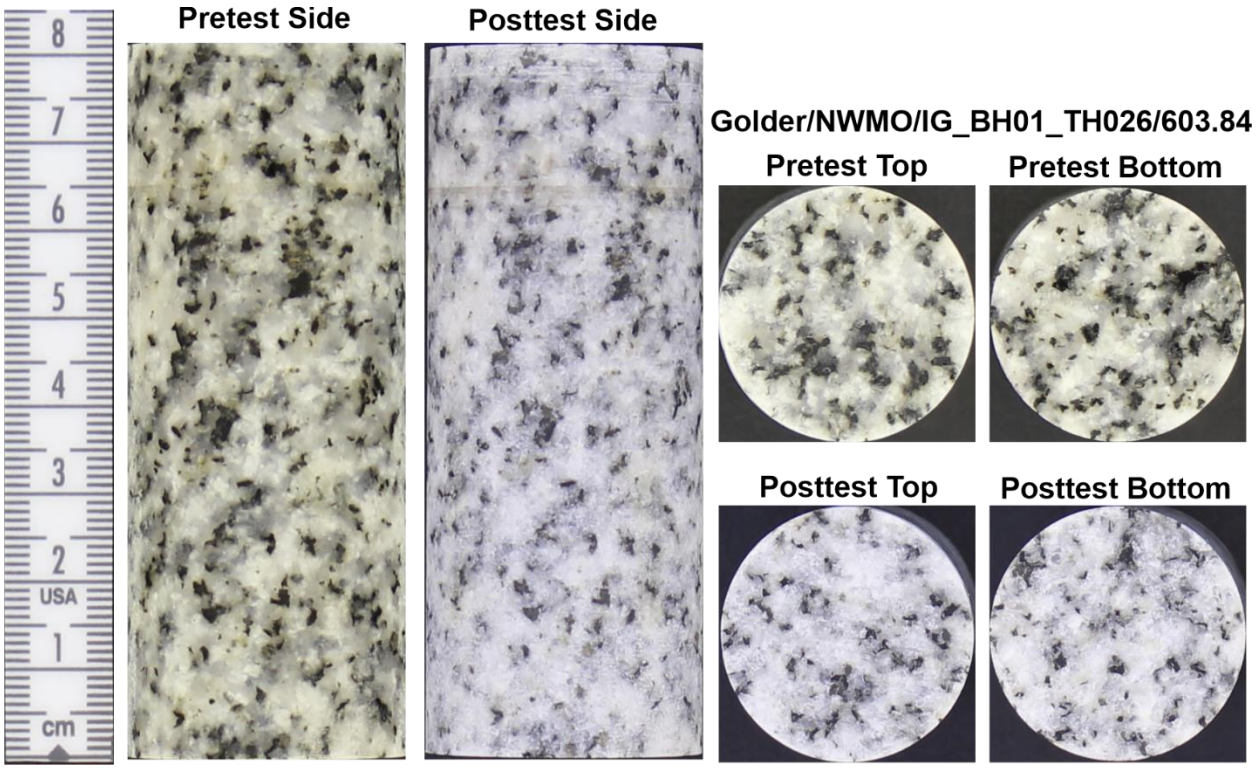
Test Specimen IG_BH01_TH025 – Depth = 561.20 m: specimen photographs

Table E-12: Thermal Expansion Results – Test Specimen IG_BH01_TH025 – Depth = 561.20 m

Average Temperature (°C)	Average Coeff. Linear Thermal Expansion – Linear (1/°K)	Coeff. Linear Thermal Expansion – Quadratic (1/°K)	Average Coeff. Linear Thermal Expansion – Linear (1/°K)	Coeff. Linear Thermal Expansion – Quadratic (1/°K)
	1st Temperature Cycle		2nd Temperature Cycle	
20	6.45E-06	6.24E-06	6.41E-06	6.19E-06
40		6.36E-06		6.31E-06
60		6.47E-06		6.43E-06
80		6.58E-06		6.55E-06
90		6.64E-06		6.61E-06



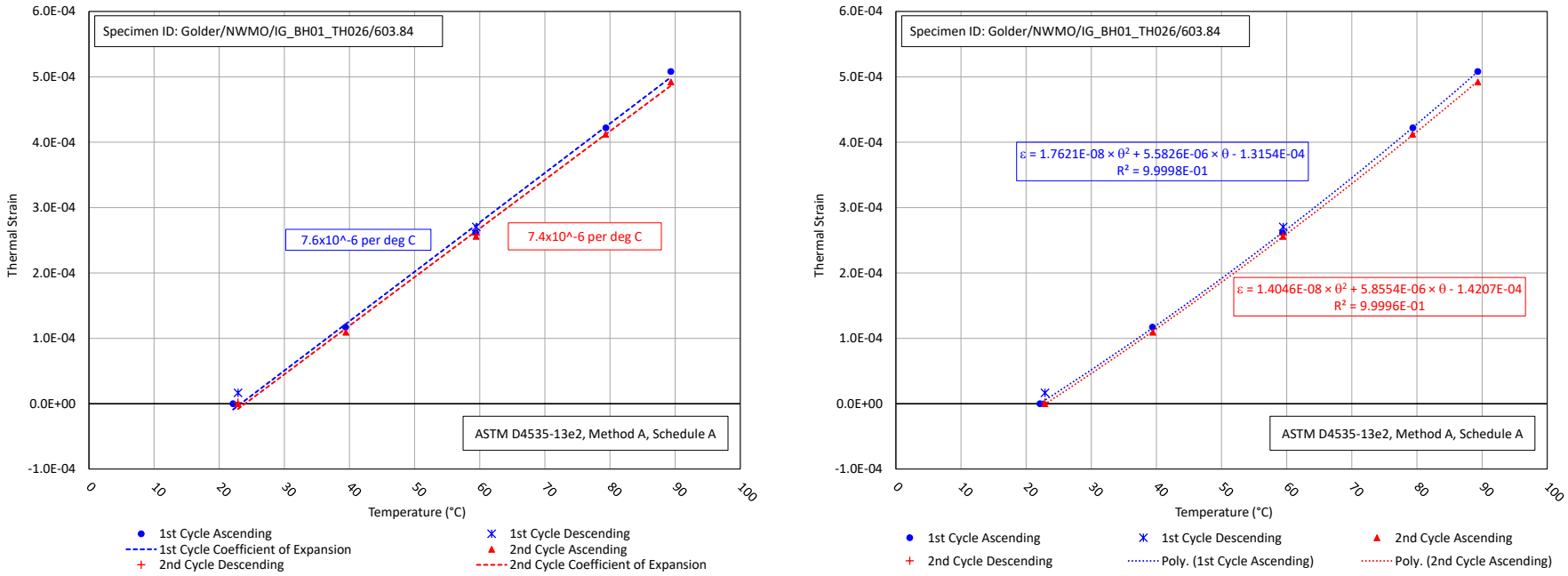
Test Specimen IG_BH01_TH025 – Depth = 561.20 m: Linear fit and quadratic fit for the thermal expansion data



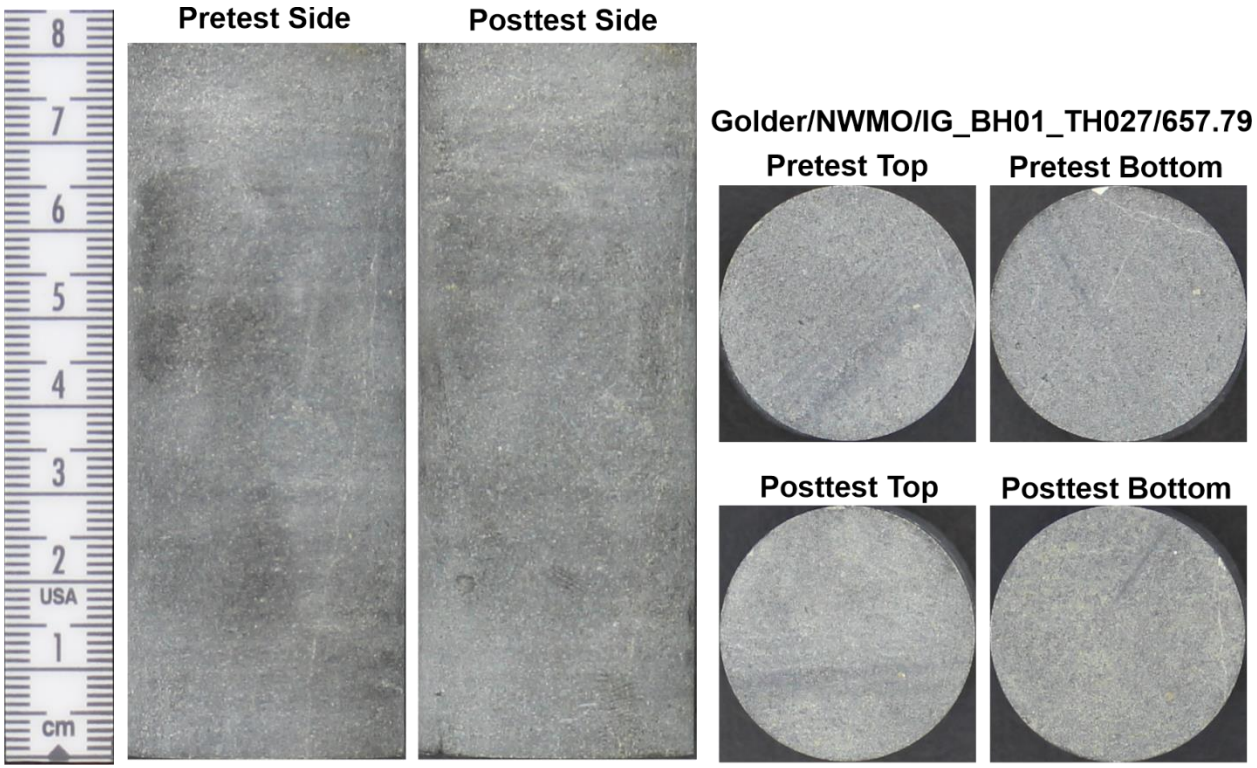
Test Specimen IG_BH01_TH026 – Depth = 603.84 m: specimen photographs

Table E-13: Thermal Expansion Results – Test Specimen IG_BH01_TH026 – Depth = 603.84 m

Average Temperature (°C)	Average Coeff. Linear Thermal Expansion – Linear (1/°K)	Coeff. Linear Thermal Expansion – Quadratic (1/°K)	Average Coeff. Linear Thermal Expansion – Linear (1/°K)	Coeff. Linear Thermal Expansion – Quadratic (1/°K)
	1st Temperature Cycle		2nd Temperature Cycle	
20	7.56E-06	6.29E-06	7.44E-06	6.42E-06
40		6.99E-06		6.98E-06
60		7.70E-06		7.54E-06
80		8.40E-06		8.10E-06
90		8.75E-06		8.38E-06



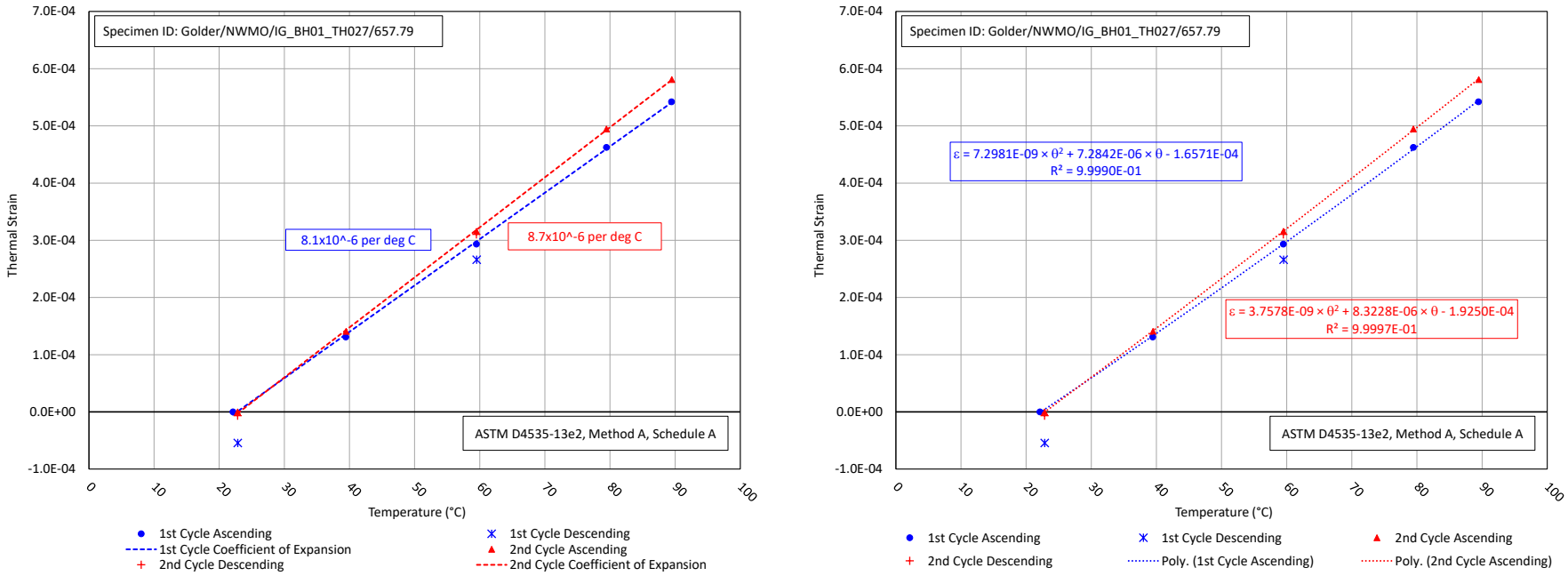
Test Specimen IG_BH01_TH026 – Depth = 603.84 m: Linear fit and quadratic fit for the thermal expansion data



Test Specimen IG_BH01_TH027 – Depth = 657.79 m: specimen photographs

Table E-14: Thermal Expansion Results – Test Specimen IG_BH01_TH027 – Depth = 657.79 m

Average Temperature (°C)	Average Coeff. Linear Thermal Expansion – Linear (1/°K)	Coeff. Linear Thermal Expansion – Quadratic (1/°K)	Average Coeff. Linear Thermal Expansion – Linear (1/°K)	Coeff. Linear Thermal Expansion – Quadratic (1/°K)
	1st Temperature Cycle		2nd Temperature Cycle	
20	8.10E-06	7.58E-06	8.75E-06	8.47E-06
40		7.87E-06		8.62E-06
60		8.16E-06		8.77E-06
80		8.45E-06		8.92E-06
90		8.60E-06		9.00E-06



Test Specimen IG_BH01_TH027 – Depth = 657.79 m: Linear fit and quadratic fit for the thermal expansion data



golder.com